

2010

Geochemical analysis of the Monturaqui Impact Crater, Chile.

Christine Marie Kloberdanz
University of Iowa

Copyright 2010 Christine Kloberdanz

This dissertation is available at Iowa Research Online: <http://ir.uiowa.edu/etd/835>

Recommended Citation

Kloberdanz, Christine Marie. "Geochemical analysis of the Monturaqui Impact Crater, Chile.." MS (Master of Science) thesis, University of Iowa, 2010.
<http://ir.uiowa.edu/etd/835>.

Follow this and additional works at: <http://ir.uiowa.edu/etd>

 Part of the [Geology Commons](#)

GEOCHEMICAL ANALYSIS OF THE
MONTURAQUI IMPACT CRATER, CHILE

by

Christine Marie Kloberdanz

A thesis submitted in partial fulfillment of the requirements for the Master of
Science degree in Geoscience in the Graduate College of The University of Iowa

December 2010

Thesis Supervisor: Assistant Professor Ingrid Ukstins Peate

Graduate College
The University of Iowa
Iowa City, Iowa

CERTIFICATE OF APPROVAL

MASTER'S THESIS

This is to certify that the Master's thesis of

Christine Marie Kloberdanz

has been approved by the Examining Committee for the thesis requirement for the Master of Science degree in Geoscience at the December 2010 graduation.

Thesis Committee: _____
Ingrid Ukstins Peate, Thesis Supervisor

David Peate

Raymond Anderson

To my family, near and far....

I am so glad you could speak enthusiastically of your visit to Iowa City. That little town means so much to me...It is almost like home. I love the people, the campus, the trees, everything about it. And it is beautiful in the spring...And I hope you strolled off across the golf course just at twilight and felt the peace and quiet of an Iowa evening, just as I used to do.

Nile Kinnick, Letter to friend Celia Peairs (May 31, 1943)

ACKNOWLEDGEMENTS

I would like to start out thanking my committee, for their many edits, suggestions, patience, and ultimately their knowledge: Ingrid Ukstins Peate, David Peate, and Raymond Anderson. The NASA grant (06-PGG06-6) for Planetary Analogs for spherule formation and funding from the NASA Education and Public Outreach Supplement for Young Women in Science to support my field work in Chile. The valuable assistance and knowledge during the 2007 Field Season in Chile: Nathalie Cabrol and Edmond Grin. The Geosciences Department Office has always been extremely helpful answering questions and helping me turn in forms and finish my thesis from out of town: Georgiana Greiner and Christine Harms. Geosciences Department funding specifically the Max and Lorraine Littlefield Fund, for supplying funds for analytical work at University of Minnesota and travel to the 2009 Spring AGU meeting in Toronto, CA. To the University of Iowa Petrographic Facilities Laboratories, Washington State University GeoAnalytical Facilities, and University of Minnesota Electron Microprobe Facilities for their assistance and help during my analytical work.

The stars/writers of *Mystery Science Theater 3000*, for being the ‘background noise’ during my many endless hours of working, and never ceasing to make me laugh so hard I cry in the wee hours of the night. To fellow graduate student Lee Falkena for his support, friendship and sound field gear shopping advice. To my furry children Stella and Jack, for keeping my company during many late night revisions, I’m sorry if you have felt ignored the past few years. And to my family, my cheerleaders: my mom Brenda, my constant sounding board, and my fiancé Bob for your support and **everything** you’ve done to help me finish this degree....and I’m sorry if you have felt ignored the past few years too.

TABLE OF CONTENTS

LIST OF TABLES	viii
LIST OF FIGURES	x
CHAPTER 1: INTRODUCTION	1
1.1 Thesis Objectives	1
1.2 Impact Craters	1
1.3 Crater Formation	5
1.4 Shock Metamorphism	7
CHAPTER 2: PREVIOUS WORK	17
2.1 Geological Setting	17
2.2 General Crater Information	17
2.3 Age	19
2.4 Geophysics	20
2.5 Target Rock	21
2.5.1 Granite	21
2.5.2 Ignimbrite	21
2.5.3 Mafic Dikes	22
2.5.4 Iron Shale	22
2.5.5 Shock Features in Target Rock	23
2.6 Impactite	23
2.6.1 Formation	23
2.6.2 Sample Description	23
2.6.3 Shocked Features in Impactite	25
2.7 Spherules	26
2.8 Chemical Data	28
2.8.1 Whole Rock Data	28
2.8.1.1 Granite	28
2.8.1.2 Ignimbrites	28
2.8.1.3 Mafic Dikes	28
2.8.1.4 Impactite	28
2.8.1.5 Iron Shale Data	28
2.8.1.6 Impact Glass	28
2.8.2 Mineral Data	29
2.8.2.1 Granite Minerals	29
2.8.2.2 Ignimbrite Minerals	29
2.8.2.3 Mafic Dike Minerals	29
2.8.2.4 Iron Shale & Oxide Minerals	30
2.8.2.5 Spherules	30
CHAPTER 3: METHODS	42

3.1 Field Work	42
3.2 Thin Sections	44
3.3 X-Ray Fluorescence.....	45
3.4 Electron Microprobe	47
3.5 Analytical Error/Standard Error	48
3.5.1 XRF Data	48
3.5.2 Electron Microprobe Data	48
3.5.2.1 Standards for October 2008	48
3.5.2.2 Samples for October 2008	49
3.5.2.3 Standards for April 2009	49
3.5.2.4 Samples for April 2009	50
3.5.3 Data Set	50
CHAPTER 4: DATA	64
4.1 Granite Data	64
4.1.1 Granite Field & Petrography Relationships	64
4.1.2 Granite Geochemical Data.....	67
4.1.2.1 Whole Rock by XRF & ICP-MS	67
4.1.2.2 Granite Mineral Compositional Data by EMP	68
4.2 Ignimbrite Data	70
4.2.1 Ignimbrite Field & Petrology Relationships	70
4.2.2 Ignimbrite Geochemical Data	73
4.2.2.1 Whole Rock by XRF & ICP-MS	73
4.2.2.2 Ignimbrite Mineral Compositional Data by EMP	73
4.3 Mafic Dikes	76
4.3.1 Mafic Dike Field & Petrology Relationships	76
4.3.2 Mafic Dike Geochemical Data	80
4.3.2.1 Whole Rock by XRF & ICP-MS	80
4.4 Impactite	80
4.4.1 Impactite Field & Petrology Relationships	80
4.4.2 Impactite Geochemical Data	85
4.4.2.1 Whole Rock by XRF & ICP-MS	85
4.4.2.2 Impactite Mineral Compositional Data by EMP	86
4.5 Iron Oxides, Meteorite, Spherules	88
4.5.1 Iron Oxides, Meteorite, Spherules Field & Petrology Relationships	88
4.5.2 Iron Oxides, Meteorite, Spherules Geochemical Data	89
4.5.2.1 Iron Oxides, Meteorite, Spherules Mineral Compositional Data by EMP	89
CHAPTER 5: DISCUSSION	117
5.1 Ignimbrite and Light Melt Impactite	117
5.2 Pressures and Temperatures in relation to the Impactite	119
5.3 Modeling	120
5.4 Meteorite	126

5.5 Spherules	126
CHAPTER 6: CONCLUSION	138
REFERENCES.....	141
APPENDIX A: SAMPLES.....	146
APPENDIX B: THIN SECTIONS	149
APPENDIX C: XRF DATA.....	170
APPENDIX D: ELECTRON MICROPROBE DATA.....	172

LIST OF TABLES

Table 1:	Electron Microprobe analyses (wt.%) of selected nickel-iron in the Monturaqui Impactite.	37
Table 2:	Electron microprobe analyses of mixed glasses and wet-chemical analyses of impactite and granite country rock.....	38
Table 3:	Electron microprobe data of shocked nonvesiculated, vitrified plagioclase from Bunch & Cassidy (1972).....	39
Table 4:	USGS standard GSP-1 from a granodiorite in Colorado used in the WSU lab publication.....	61
Table 5:	Standards Micr052 and Hbld019 were each analyzed three times before analysis begun on October 2008 electron microprobe trip.....	61
Table 6:	Ignimbrite sample CCMK07013 biotite and feldspar observed values (averages) compared to the standards and their published values.	62
Table 7:	Granite sample CCMK07016 biotite and feldspar observed values (averages) compared to the standards and their published values.	62
Table 8:	Light melt sample CCMK07046 and dark melt sample CCMK07045 observed values (averages) compared to the standards and their published values.....	62
Table 9:	Canyon Diablo polished sample analyzed as a standard to compare samples in Table 7.	63
Table 10:	Potential meteorite samples CIUP08092 and CIUP08093 with observed values.....	63
Table 11:	This table is comparing the different types of ignimbrite samples....	129
Table 12:	Least squares calculations of the granite components and ignimbrite components to determine the modal properties of phases that comprise the granite and ignimbrite.	130
Table 13:	Least squares calculations for Light Melt, Dark Melt Group 1 and Dark Melt Group 2.	131
Table 14:	Least squares calculations for Light Melt with individual mineral components.	132

Table 15:	Least squares calculations for Dark Melt Group 1 and with individual mineral components.	133
Table 16:	Least squares calculations for Dark Melt Group 2 and with individual mineral components.	134
Table 17:	Displays the Canyon Diablo (CD) averages and the iron shale averages (samples CIUP08092 and CIUP08093) from electron microprobe analysis.	135
Table A1:	Samples collected in field season 2007 in Chile.	147
Table C1:	X-Ray Fluorescence Data	171
Table D1:	Electron Microprobe Data for biotites in Granite target rock.....	173
Table D2:	Electron Microprobe Data for feldspar in Granite target rock.....	174
Table D3:	Electron Microprobe Data for hematite in Granite target rock.....	175
Table D4:	Electron Microprobe Data for biotites in Ignimbrite target rock	176
Table D5:	Electron Microprobe Data for feldspar in Ignimbrite target rock.....	177
Table D6:	Electron Microprobe Data for matrix in Ignimbrite target rock.	178
Table D7:	Electron Microprobe Data for magnetite in Ignimbrite target rock...179	
Table D8:	Electron Microprobe Data for ilmenite in Ignimbrite target rock.....	179
Table D9:	Electron Microprobe Data for Light Melt Impactite.....	180
Table D10:	Electron Microprobe Data for Melted Minerals.	182
Table D11:	Electron Microprobe Data for Dark Melt Group 1.	183
Table D12:	Electron Microprobe Data for Dark Melt Group 2.	184
Table D13:	Electron Microprobe Data for meteorite standards, meteorite and hematite samples.....	186
Table D14:	Electron Microprobe Data for metallic spherules.	187

LIST OF FIGURES

Figure 1:	Distribution of the recognized terrestrial impact structures. Red dots = entirely crystalline target rocks, blue dots = entirely sedimentary rocks, and green dots = mixed crystalline-sedimentary rocks11
Figure 2:	Cumulative size-frequency distribution of known terrestrial impact structures. The departure of $N \propto D^{-1.8}$ at the small diameters indicates a shortage of known craters due to crater recognition and retention problems (erosion, weathering, etc.)11
Figure 3:	Diagram of first stage of contact and compression12
Figure 4:	Diagram of second stage of excavation12
Figure 5:	Diagrams of ending of excavation stage and beginning of the third and final, modification stage (specifically for complex crater)12
Figure 6:	Cross-section of transient cavity, where the excavated and displaced zones are labeled above and below the impact site. The uplifted rim can be seen above the original ground level13
Figure 7:	Collapse of the transient cavity walls to form the final crater with allochthonous breccia lens13
Figure 8:	Cross-section of a simple crater showing the various depths after the transient cavity walls collapse. The transient cavity depth to diameter ratio is $\sim 1/3$. True depth and apparent depth can be figured by $d_t = 0.29D^{0.93}$, $d_a = 0.14D^{1.02}$14
Figure 9:	Pressure-Temperature diagram showing the differences between normal crust (endogenic) metamorphism and shock metamorphism. The shock metamorphic orientations that can be formed by different pressures are displayed on the right hand side. High pressure polymorphs formations are also shown15
Figure 10:	At the first pressure range ~ 7.5 -30 GPa, a quartz grain with planar deformation features from the Haughton impact structure, Canada. Field view is 2 mm in plane-polarized light16
Figure 11:	Location of the Monturaqui Impact Crater. A) Topographic Map of Chile, yellow star indicates location of Monturaqui Impact Crater, B) Satellite image of Monturaqui Impact Crater33

Figure 12:	Ugalde et al (2007)'s Geophysical Study. A) Geological map created by Ugalde et al (2007), showing topographic contours, target rock units: granite, dikes, ignimbrites, melt rocks and cross sections A-A' and B-B'. Map Scale is 1:2,000. B) Plain view of the whole 3D gravity model, colors indicate: yellow = sediments, brown = ignimbrite, purple = fractured basement (granite), and white = unfractured basement (granite). C) Cross section from geologic map along line B-B' north-south. The granite unit is also inferred while the ignimbrite unit is based off geological mapping. D) Cross section from geologic map along line A-A' east-west. The granite unit is inferred while the ignimbrite unit is based off geological mapping	34
Figure 13:	Hand sample of impactite showing inclusions of quartz, feldspar, glass and metavolcanic pebble. Width is 25cm	35
Figure 14:	Photomicrograph of Monturaqui impactite in plane-polarized transmitted light at 50x. Fractured feldspar (F) and quartz (Qz) from the granite, devitrified brown matrix glass, nickel-iron spherules and vesicles (V) are labeled. Inset shows impactite in hand sample	35
Figure 15:	Shocked features in Monturaqui Impactite. A) Weakly shocked features: cleavage in a grain of shocked quartz, width is 0.53 mm. B) Moderately to strongly shocked features: alternating band of diaplectic glass and crystalline plagioclase, width is 0.21mm. C) Intensely shocked features: vesiculated silica glass showing flow structures, width 0.53mm. D) Intensely shocked features: typical example of mixed brown and green matrix glasses with inclusions, flow lines can be seen as well as dark spots that are nickel-iron spherules, width 3.0 mm	36
Figure 16:	Semi-log plot of Fe/Ni vs. spherule size and (insert figure) P/Co vs. spherule size in nickel-iron spherules from Bunch & Cassidy (1972).....	39
Figure 17:	Canyon Diablo Meteorite.....	40
Figure 18:	Nickel-Iron contents of 100 spherules < 35µm in diameter from Monturaqui Impact Crater. Wabar Impact Crater kamacite and taenite values were used as end members since no meteorite composition of Monturaqui is known. The Monturaqui meteorite is likely similar to the Wabar meteorite	40

Figure 19:	Cobalt variation compared to the spherule diameter in 100 spherules from Monturaqui Impact Crater.....	41
Figure 20:	Cobalt-Nickel variation from 450 spherules analyzed from Henbury (100), Wabar (250) and Monturaqui (100) Impact Craters. A small number of spherules lie outside the field with more than 3% Co and 80% Ni	41
Figure 21:	Google map image with directions from Peine, Chile to the Monturaqui Impact Crater.....	51
Figure 22:	2010 Google Image of Monturaqui Impact Crater, with all samples used for analysis from field season 2007 and 2008. Also granite and ignimbrite units are shown. Contours are displayed to show elevation of crater	52
Figure 23:	Ignimbrite sample CCMK07034b, shown in the field at the rim of the crater.....	53
Figure 24:	Granite sample CCMK07042, shown in the field at the inside of the crater wall.	53
Figure 25:	Field area shown in black box, approximately 1.3 km south of the crater where samples of target rocks, granite and ignimbrite and hematite veins were collected.	54
Figure 26:	Hematite veins in granite outcrop located 1.3 km south of the crater. Sample CCMK07022, was collected from this location.	54
Figure 27:	Dark impact melt among target rock debris on the outside of the crater on the eastern side.	55
Figure 28:	Granite samples chosen for thin section and eventual XRF and electron microprobe analysis. A) CCMK07013 (located outside the crater), B) CCMK07042 (located inside the crater), C) CCMK07051 (located along the crater rim)	56
Figure 29:	Ignimbrite samples chosen for thin section and eventual XRF and electron microprobe analysis. A) CCMK07016 (located outside the crater), B) CCMK07030, C) CCMK07034b (B & C both located along the crater rim).....	57
Figure 30:	Mafic dike samples chosen for thin section and eventual XRF analysis. A) CCMK07003, B) CCMK07004, C) CCMK070029, D) CCMK07035, E) CCMK07037, F) CCMK07084, G) CCMK07085	58

Figure 31:	Hematite samples chosen for thick section and eventual electron microprobe analysis. A) CCMK07007 (located along the crater rim), B) CCMK07022 (located outside the crater), C) CCMK07086 (located outside the crater walls).....	59
Figure 32:	Impact melt samples chosen for thin section and eventual electron microprobe analysis. A) CCMK07009, B) CCMK07046, C) CCMK07047 (A-C Light melt), D) CCMK07045, E) CCMK07082 (both D and E Dark melt). Note: CCMK07A (dark) and CCMK07B (light) not shown	60
Figure 33:	Location of CCMK07013 (Ignimbrite) and CCMK07016 (Granite) samples, where visible contact (purple line) along roadside exposures of ignimbrite and granite.	92
Figure 34:	Planar Deformation Features of CCMK07042 (Granite). A) The plagioclase grain with original twinning is deformed by the multiple parallel fractures. The scale bar is 500 μ m. B) Parallel fractures running horizontally through multiple quartz and plagioclase grains. The scale bar is 2.0 mm. C) Another example of quartz and plagioclase with parallel fractures running horizontally through multiple grains. The scale bar is 500 μ m.....	93
Figure 35:	Planar deformation features in sample CCMK07051 (Granite). The scale bar for each picture is 2.0 mm. A) Parallel fractures running horizontally through multiple grains, with another set of fractures running perpendicular in the bottom left grain. B) Plagioclase grains (dark) turned into diaplectic glass (maskelynite). C) Quartz grains that exhibit decoration of fluid inclusions in multiple sets of fractures. D) Non-planar deformation features, fractures with in the sample itself are filled with smaller grains made up of quartz, feldspars and possible clay.....	94
Figure 36:	XRF whole rock major element data graphed to show individual sample concentrations and averages for each unit. Mafic dikes are in blue, ignimbrites are in pink/red and granites are in green.....	95
Figure 37:	XRF whole rock un-normalized trace elements plotted to show individual samples within the target rocks. A) Granite XRF data, B) Ignimbrite XRF data, and C) Mafic Dike XRF data.....	96
Figure 38:	Electron Microprobe analysis of feldspar grains found in granite samples inside (samples 042 and 051) and outside (sample 016) the crater. XRF whole rock data for individual granite samples also plotted.	97

Figure 39:	Electron Microprobe analysis of biotite grains found in granite samples inside (samples 042 and 051) and outside (sample 016) the crater. XRF whole rock data for individual granite samples also plotted.	98
Figure 40:	Minerals components that make up the granite unit: albite, orthoclase, biotite, quartz and hematite, with whole rock XRF data granite samples (016, 042, 051) in green.	99
Figure 41:	Sample CCMK07013 (Ignimbrite) displaying welded texture within the matrix of the sample.	100
Figure 42:	Sample CCMK07030 (Ignimbrite) displaying increased melting within the matrix of the sample. Plagioclase grains display multiple sets of planar deformation features running parallel and perpendicular to each other.	100
Figure 43:	Sample CCMK07034b (Ignimbrite) displays planar deformation features in plagioclase grains, multiple sets running parallel and perpendicular to each other like sample CCMK07030 (Ignimbrite). Increasing melting also displayed in CCMK07034b.	101
Figure 44:	Electron Microprobe analysis of feldspar grains found in ignimbrite samples inside (samples 030 and 034b) and outside (sample 016) the crater. XRF whole rock data for individual ignimbrite samples are also plotted.	102
Figure 45:	Electron Microprobe analysis of biotite grains found in ignimbrite samples inside (samples 030 and 034b) and outside (sample 016) the crater. XRF whole rock data for individual ignimbrite samples are also shown.	103
Figure 46:	Minerals components that make up the ignimbrite unit: ignimbrite matrix, albite, biotite, magnetite, ilmenite with XRF whole data granite samples (013, 030, 034b) in pink.	104
Figure 47:	Sample CCMK07003 (Mafic Dike) displaying altered olivines (lower right) altering to iddingsite.	105
Figure 48:	Sample CCMK07004 (Mafic Dike) displaying altered olivines altering to iddingsite.	105
Figure 49:	Sample CCMK07029 (Mafic Dike) displaying plagioclase crystals altered but retaining a rim.	106

Figure 50:	Sample CCMK0700A (Impactite) displaying pristine and altered spherules. A) Pristine spherules are the solid black spherules in the upper portion of the photo in PPL. The altered spherules have red and orange rims around black solid spherules. B) Photo in reflected light, the pristine spherules are silver and reflective. The altered spherules have tan, brown rims around silver spherules.....	106
Figure 51:	Sample CCMK0700A (Impactite) displaying pristine, swirled and mixed glasses. A) Clear, pristine glass shown in PPL, with red staining along fractures. The scale bar is 200 μm . B) Clear glass with silica swirls, and red staining along fractures. The scale bar is 500 μm . C) Mixed glasses, solid white areas may be lechatelierite that doesn't mix completely causing the silica swirls in the solid white areas of glass. Red staining also can be seen along fractures and alterations. The scale bar is 200 μm	107
Figure 52:	Sample CCMK07045 (Impactite) displaying planar deformation features. A) Opaque glass with transparent areas in light to dark brown. Plagioclase grains show multiple sets of fractures. The scale bar is 2.0 mm. B) Red staining in glass with small plagioclase grains with multiple sets of fractures. The scale bar is 500 μm . C) Plagioclase grains in XPL with multiple sets of fractures closely running parallel and perpendicular to each other. The scale bar is 2.0 mm.	108
Figure 53:	Sample CCMK07082 (Impactite) displaying deformation features. A) Opaque glass with transparent patches light to dark brown (similar to 045). The scale bar is 2.0 mm. B) Close up of plagioclase grains with multiple sets of fractures. The scale bar is 500 μm . C) A large clast made up of small plagioclase crystals. The scale bar is 2.0 mm. D) Plagioclase crystals with multiple sets of fractures with opaque and mixed glasses. The scale bar is 2.0 mm.	109
Figure 54:	Sample CCMK0700B (Impactite) displaying clear pristine glass with minimal red oxidation staining.	110
Figure 55:	Sample CCMK07009 (Impactite). A) Clear glass with patches of mixed glass and red staining. Also grain boundaries are present where the plagioclase is being altered to iddingsite. The scale bar is 500 μm . B) Plagioclase grain in XPL displaying multiple sets of planar deformations features fractures running parallel and perpendicular to each other. The scale bar is 2.0 mm.....	110

Figure 56:	Sample CCMK07046 (Impactite). A) Clear glass in PPL with small clusters of plagioclase crystals with red staining. The scale bar is 2.0 mm. B) Plagioclase crystal displaying PDF's of multiple sets of fractures in XPL. The scale bar is 2.0 mm.	111
Figure 57:	Sample CCMK07047 (Impactite). A) Clear glass in PPL with small clusters of plagioclase crystals with red staining. The scale bar is 2.0 mm. B) Plagioclase crystal displaying PDF's of multiple sets of fractures in XPL. The scale bar is 2.0 mm.	111
Figure 58:	Electron microprobe analysis data of light melt group (in orange) made up of samples 009, 046, and 047. XRF bulk light melt is plotted in red for comparison.	112
Figure 59:	Electron microprobe analysis data for the dark melt group. The group is made up of samples 00A, 045, and 082. The dark melt is made up of two groups of melt and melted minerals. Lechatelierite and maskelynite are circled from melted mineral data points that are mixtures between the two dark melt groups and minerals.	113
Figure 60:	Samples CIUP08092 (Meteorite) (A) and CIUP08093 (B) in reflected light of epoxy mounts of each sample.	114
Figure 61:	Electron microprobe analysis of metallic spherules, iron shale and hematite, with the Canyon Diablo sample. The major elements Ti, Al, Si, Mn, Ca, and P plotted against Fe	115
Figure 62:	Electron microprobe analysis of metallic spherules, iron shale, hematite and the Canyon Diablo sample. Metals Ni, Co, Cu, Cr and S plotted against Fe. Also Co plotted against Fe/Ni and Co plotted against Ni.	116
Figure 63:	FeO vs. SiO ₂ , all three granite and ignimbrite samples, seven dikes plotted with bulk light melt, light melt average and dark melt group 1 and group 2 averages, and iron shale averages. Plot shows that the light melt average can be derived from the ignimbrite samples but the dark melt samples cannot be derived from just the granite samples.	129

Figure 64: Graphs comparing this study’s spherules compositions with the spherules analyzed in Gibbons et al. (1976). A) Fe vs. Ni, the blue spherules (108) are from this study’s analysis, the pink field represents the spherules (100) analyzed in Gibbons et al (1976). B) Co vs. Ni, the spherules from this study (blue) fit within the field (pink) of the analysis from Gibbons et al (1976). Both graphs support the replication of spherule data. Note the spherules field in B, are made up of 450 spherules, 250 from Wabar, 100 from Henbury, and 100 from Monturaqui..136

Figure 65: Spherules size relationships. A) Plot of this study’s Fe/Ni ratios vs. width of spherules. B) Plot of this study’s P/Co ratios vs. width of spherules.137

CHAPTER 1: INTRODUCTION

1.1 Thesis Objectives

The scope of this M.Sc. project is the geochemical analysis of the target rocks, impact melt rocks and metal spherules found at the Monturaqui Impact Crater, Chile. The objectives of this analysis are to discover how the melt rock is related to the target rocks geochemically, and how much of the target rock and what mineral phases are contributing to the impact melt rock. We will use this to look at what this tell us about the melting that occurred at this impact site, and how much of the material in the spherules in the melt rock are contributions from target rock metals, sulfides, and/or the meteorite that caused the impact.

1.2 Impact Craters

Impact cratering is an established force that samples the planet's surface, from Archaean to Quaternary, and has been studied using mineralogy, geochemistry, geochronology, sedimentology and stratigraphy (Reimold, 2007). The benefits of studying impact craters include: understanding evolution of the Earth's surface, making analogues to other planets, linking them to extinctions, and understanding evolution of meteorites from asteroid parent bodies, planets, and moons from the solar system to give us more information about the origin of the solar system.

Impacts are the most fundamental process that has taken place on the terrestrial planets in our solar system. By studying impact craters, scientists can learn about aspects of planetary birth. The collision of smaller objects is how the planets were born, and the terrestrial planets would not exist without it. The geological record of the earliest impacts is

lost on the terrestrial planets, but record of the last stages of accretion is mostly preserved on the Moon, Mercury and Mars (Shoemaker, 1977). Basin sized impact events had direct and indirect effects on the Earth's early crust and lithosphere. It is not clear how long lived those effects were to affect the early crustal evolution. Preliminary modeling suggests the effects were thermal and tectonic, but there is no clear evidence (Grieve, 1987). The impact record on Earth is critical to understand the only ground-truth data we have to base interpretations of impact craters on other planets and moons (Osinski, 2006).

Impact craters can be considered "resetting events", and can result in local level changes and global scale changes. The area of the impact is sterile from the intense heat and pressure that is produced. Large scale impacts alter the global environment, with dust injected into the stratosphere, ozone depletion and acid rain. Dramatic results could produce shifts of biological evolution and extinction boundaries. These are rare events that happen every 10^7 - 10^8 years for an impact that would cause 10^6 - 10^7 Mt explosion (Cockell, 2002). Localized events stemming from smaller impacts and causing alterations in the environment would occur every 10^5 years resulting in 10^3 Mt explosions. Craters share basic ecological characteristics even in different biomes and regions. All types of catastrophic events all have their own unique recovery and the patterns of biological recovery and change at an impact site merit separate analysis. Impacts are the only event that can deliver a localized pulse of destructive energy into the ecosystem (Cockell, 2002).

Geochemical analysis of meteorites gives insight to the origin of the solar system. Thus far meteorites on Earth are found from three sources (1) the break-up of asteroidal parent bodies, (2) fragments of the Moon (found in Antarctica, Australia, North Africa,

Oman),(3) the shergottite, nakhlite, and chassigny class meteorites from Mars. The last two have never created an impact structure on Earth (McCall, 2006).

Currently there are ~178 confirmed craters according to the Earth Impact Database of the University of New Brunswick, Canada (website listed in References). Most of the craters are located in North America, Eurasia and Australia (Figure 1). Central Africa, South America and Asia have the fewest amounts of recognized impacts. This low number is contributed to by one or more reasons: regional geology with the lack of ancient stable cratons, limited access to English literature on impact cratering, lack of remote sensing and regional geophysics studies, rainforest terrains, vegetation coverage, erosion or possibly even civil strife (Reimold, 2007). The current average discovery rate is ~3-5 craters per year. Crater rates estimates come from data from the Earth and the Moon (Grieve, 1987). Over 2/3 (~96) of the craters confirmed are in sedimentary rocks. Approximately ~16 craters have been discovered due to advances in studying shallow marine environments (Osinski, 2006).

Historical controversy has been created over the lack of projectile fragments at large impact structures. This has lead many to postulate that cryptovolcanic explosions of gas were the mechanism for formation of those particular craters. Small young craters tend to have projectile fragments remaining since small projectiles impact with reduced velocities due to atmospheric retardation or breakup (Grieve, 1987). The Earth's atmosphere stops most stony bodies that are < 150 m in diameter that would have energy < 200 Mt. But smaller bodies of high density iron can make it to the Earth's surface. Small craters are generally from iron bodies, due to the Earth's atmosphere stopping most stony bodies and more likely to disintegrate from stresses during atmospheric entry unlike iron meteorite. The suggested fall frequency is one to several times a century, thus numerous small impacts are produced.

Craters especially in semi-arid to arid regions could survive for thousands to tens of thousands of years. There are 13 known localities of prehistoric impact craters with recovered fragments of an iron or stony iron meteorite, most of these are in semiarid and arid regions. Eight craters with associated iron meteorites ≥ 100 m in diameter have been found. Shoemaker estimates that roughly 1000 should have been formed in the last 20,000 years. Discovery rates of craters below ~ 0.5 km in diameter drops rapidly (Shoemaker, 1983).

If the projectile is destroyed or vaporized during impact, composition detection is possible from material that is mixed with the melt rock. Generally the projectile material will make up 1% or less of the melted rock. Siderophile elements are abundant at the ppb level. Fractionation of siderophile elements can occur directly through vaporization and melt phases or indirectly through weathering and alteration. This can hinder projectile identification. Chondritic bodies have easily identifiable geochemical signature with high abundances of siderophile elements and Cr. Non-chondritic identification is usually a negative result that the projectile is not chondritic rather than a firm indication that it is an iron body (Grieve & Shoemaker, 1994).

Identified craters with large diameters have cumulative size-frequency distribution similar to those on other planets. For craters below ~ 20 km in diameter, the distribution falls off (Figure 2). This gives an increasing deficit of craters of small diameters. It indicates resurfacing processes like erosion and burial are at work (Grieve & Shoemaker, 1994).

Spatial and temporal distribution of known craters are both biased towards young craters. Sixty percent are younger than 200 Myr; this is a function of erosion and sedimentation, not an increase in the cratering rate. Very few known craters occur outside cratonic areas, these are the most suitable for crater preservation. Cratonic areas expose older

rocks, and presumably a longer record cratering. But not all craters are on the surface of the Earth, some have been discovered through geophysical anomalies and then explored through drilling. Forty percent of confirmed craters have isotopic ages (K-Ar and ^{40}Ar - ^{39}Ar) from melt rock. The remainder have biostratigraphic or stratigraphic ages from the sediments filling the crater together with estimates of degree of erosion (Grieve & Shoemaker, 1994).

Impacts are characterized by the circular form, evidence for intense, localized, near-surface structural disturbance and brecciation. Geophysical modeling indicates that craters have no deep-seated roots, disruption and brecciation is associated with low seismic velocities and residual negative gravity anomalies. Impact structures have a magnetic signature that disrupts the magnetic trend in the target rock and shows a magnetic low (Grieve, 1987).

1.3 Crater Formation

There are three main stages to crater formation, and since Monturaqui Impact Crater, the field area for this project, is a simple crater the discussion of formation stages will stick to simple crater formation.

(1) Contact & Compression Stage (Figure 3) is the contact of the projectile with the surface of the Earth. It will penetrate no more than 1-2 times its diameter before transferring kinetic energy into the surface via shock waves. These shock waves are created between the boundary of the compressed and uncompressed target material. The shock waves propagate into the surface and back into the projectile as a reflected shock wave. The reflected shock wave reaches the upper surface of the projectile and reflects back into the projectile as a tension wave. As this tension wave travels through the projectile it causes it to unload from

the high shock pressures, completely melting and/or vaporizing the projectile. The internal energy from the compression and tension wave instantaneously melts and or vaporizes the target material at the point of the impact producing melt rocks and glass bearing breccias. The melt rocks and breccias are the impactites that fill the crater in most impact structures. When the projectile is completely unloaded from the high shock pressure the contact and compression stage ends. The duration of the stage depends on the projectile size, composition and velocity, but usually lasts no more than a few seconds (Osinski, 2006).

(2) The Excavation Stage (Figure 4) is continuous after the contact and compression stage, and occurs when the actual crater is exposed by interactions of the expanding shock wave and the surface. The hemispherical shock wave propagates out into the target material, which sets it into an outward radial trajectory. Shock waves that are traveling upward intersect with the surface generating tension waves that propagate downward into the target sequence. Excavation flow is produced and creates the transient cavity. Different trajectories of material in different regions of the excavation flow field partition the transient cavity into the excavated zone, where the material is ejected beyond the crater rim, and the displaced zone which remains in the transient crater where a portion of the melt and rock debris remains (Figure 6). Each zone will contain different levels of shock melted target lithologies from the excavation flow, which transects the hemispherical pressure contours. A mixture of rock and melt debris forms the lining of the transient crater. The ending point of the excavation stage is when the shock and tension waves no longer excavate or displace target rock and melt (Osinski, 2006).

(3) The Modification Stage (Figure 5) is the third stage of crater formation. The effects of this stage are governed by size of transient cavity and the target rock lithologies. If

the transient cavity is $< 2-4$ km it undergoes minor modification creating a simple bowl shaped crater. If the transient cavity is $> 2-4$ km it undergoes unstable modification controlled by gravity creating a complex impact crater (Osinski, 2006).

Also, the impact generates pressures and temperatures that melt and/or heat the target material. This interaction with groundwater or surface water can produce an impact-generated hydrothermal system. This will occur with the majority of impacts with the exception of small craters in arid environments (Osinski, 2006).

This paper will focus on the aspects of simple craters. Simple craters are bowl-shaped depression similar to the initial transient cavity, with an uplifted rim area (Figure 6). In fresh impact examples the crater rim is overlain by the overturned flap of near surface target rocks with inverted stratigraphy, which is then overlain by fallout ejecta. The cavity walls collapse inward to form an allochthonous breccias lens that is observed in simple crater structures (Figure 7). The breccia lens is overlain by a thin deposit of fallback breccias from the ejecta cloud (Grieve, 1987).

1.4 Shock Metamorphism

Osinski (2006) defines the keys of indentifying an impact crater with shock metamorphism, using indicators such as: megascopic shatter cones, microscopic planar deformation features, diaplectic glass, and high pressure polymorphs (stishovite, coesvite). Breccias, melt rocks and pseudotachtylyte are not characteristic enough to be evidence on their own. This opposes Grieve (1987)'s earlier mentioned idea of impact classification. Shock metamorphism is different than endogenic metamorphism due to the differing scales of pressure, temperature and time (Figure 9). The differences between impact events and

other geological events are: extreme physical conditions, concentrated nature of energy release at a single point on Earth's surface, instantaneous nature of the impact process, high strain rates vs. low strain rates for tectonic and metamorphic processes (Osinski, 2006).

When the pressure increases, shock metamorphism occurs as fracturing, cataclasis, plastic deformation, vaporization, phase transitions, thermal decompositions, and melting (Grieve, 1987).

The typical terrestrial impact velocity for the projectile is $15\text{-}25 \text{ km s}^{-1}$, penetrating the target rock at 2-3 times its radius. The peak pressures close to the point of impact, are up to several hundreds of gigapascals. Shock compression is not completely recovered by tension waves and some is trapped as waste heat. At the point of contact this can raise the temperature several thousands of degrees Celsius. Compressed material results in permanent changes in target materials, the best documentation of this is in quartz and feldspar grains. Planar deformation features (or PDFs) develop along specific crystallographic orientations and have strict geometric constraints. The spacing between individual features is $1\text{-}2 \text{ }\mu\text{m}$ and they are parallel to the crystal structure orientations. The width of the actual individual planar deformation feature is $1\text{-}2 \text{ }\mu\text{m}$ also. Single sets of PDFs can be created by other tectonic events. A sub-planar to planar single set does not constitute diagnostic shock deformation (Reimold, 1997).

Certain orientations can develop with particular pressure ranges (Figure 9):

- At $\sim 7.5\text{-}30 \text{ GPa}$ - planar features in tectosilicates develop, the exact threshold pressure depends on mineral composition, structural state, exsolution lamellae and alteration. Further planar feature development and increasing pressures increase mosaicism, asterism, loss of birefringence, and glass formation (Figure 10).

- At ~30-45 GPa the crystals are converted to diaplectic glass. They exhibit the original habit of the unshocked mineral and are known as theomorphic glass. High-pressure polymorphs are stishovite, diamond, coesite.
- At ~45-55 GPa evidence of flow is present in melted rocks. There is inhomogenous glass with mixed mineral composition.
- Above 60 GPa whole rock melting occurs producing impact melt. There is a high degree of correlation in composition of impact melt rocks that corresponds with the mixture of the target rocks. Textural inhomogeneity occurs particularly in melt sheets. Unlike igneous melts, impact melts are super heated.

Other silicates show a progressive series of subsolidus shock-metamorphism with planar features and mechanical twins. The pressures are not as well documented as they are for the tectosilicates. Observations of the shock features of the autochthonous rocks indicate recorded shock pressures at max ~25 GPa with a decrease with depth beneath the surface (Grieve 1987).

The melt rocks can have higher K_2O/NaO ratio than the target rocks. Explanations for this could be selective elemental vaporization and condensation during melt and vapor formation, or hydrothermal alteration. Excesses of trace elements Cr, Ni, Co (ppm) and Ir (ppb) can be from the impacting projectile and can help identify it (Grieve 1987).

This project will examine the whole rock and mineralogical major and trace element composition variations in the target rocks and impact melt from the Monturaqui Impact Crater, Chile. I hope to use these data to understand the process of impact melting of the target rocks and the relative contributions of different target rocks, and different mineral phases from each target rock, to the impact melt found there. I will use these data to construct

geochemical models of different phase contributions in order to better constrain impact processes and the formation impact craters.

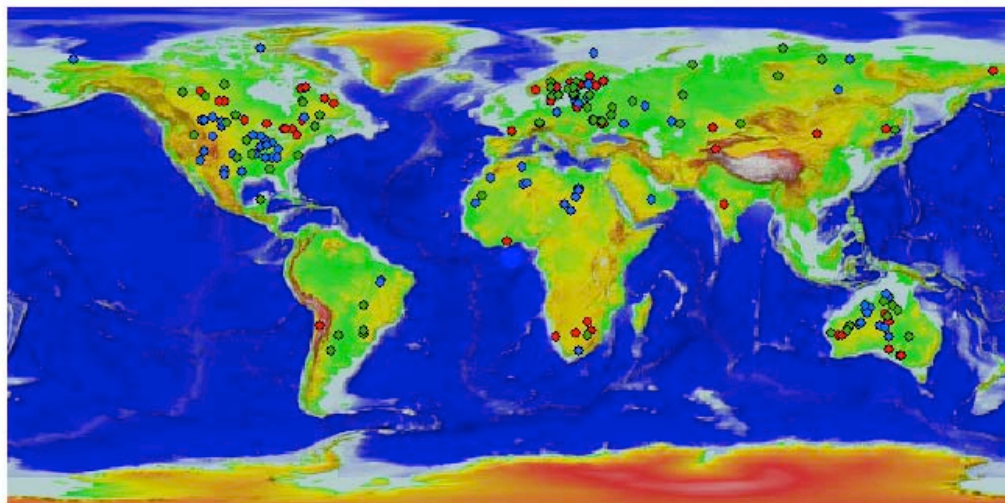


Figure 1: Distribution of the recognized terrestrial impact structures. Red dots = entirely crystalline target rocks, blue dots = entirely sedimentary rocks, and green dots = mixed crystalline-sedimentary rocks (Osinski, 2006).

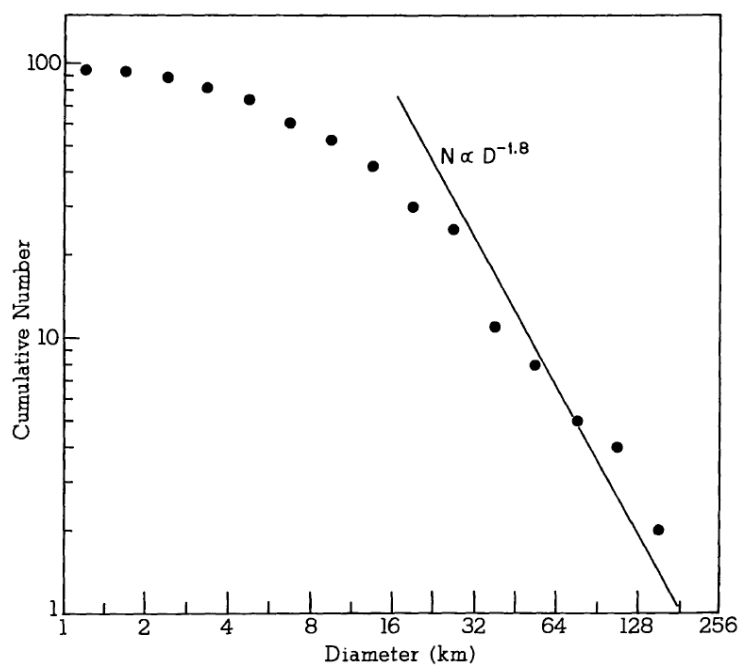


Figure 2: Cumulative size-frequency distribution of known terrestrial impact structures. The departure of $N \propto D^{-1.8}$ at the small diameters indicates a shortage of known craters due to issues with crater recognition and retention problems (erosion, weathering, etc.) (Grieve, 1987).

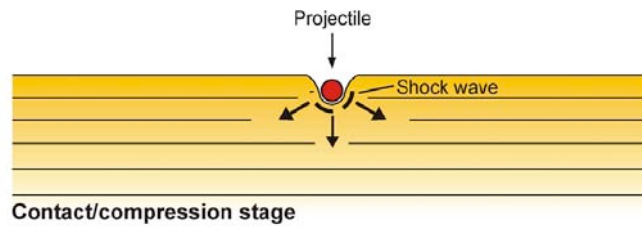


Figure 3: Diagram of first stage of contact and compression (Osinski, 2006).

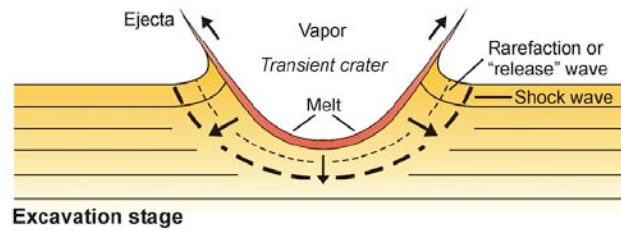


Figure 4: Diagram of second stage of excavation (Osinski, 2006).

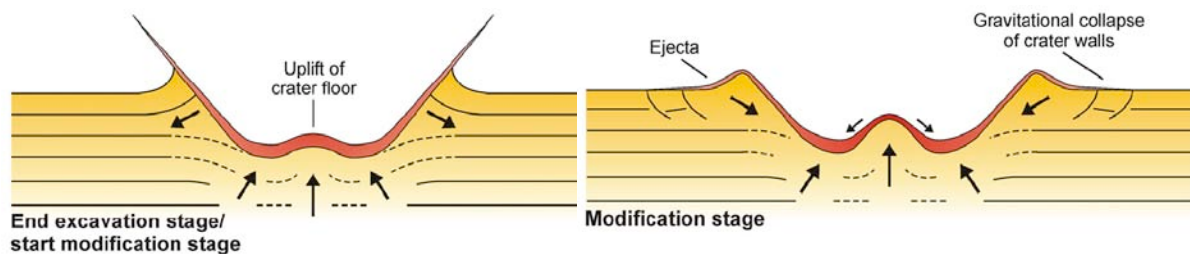


Figure 5: Diagrams of ending of excavation stage and beginning of the third and final, modification stage (specifically for complex crater) (Osinski, 2006).

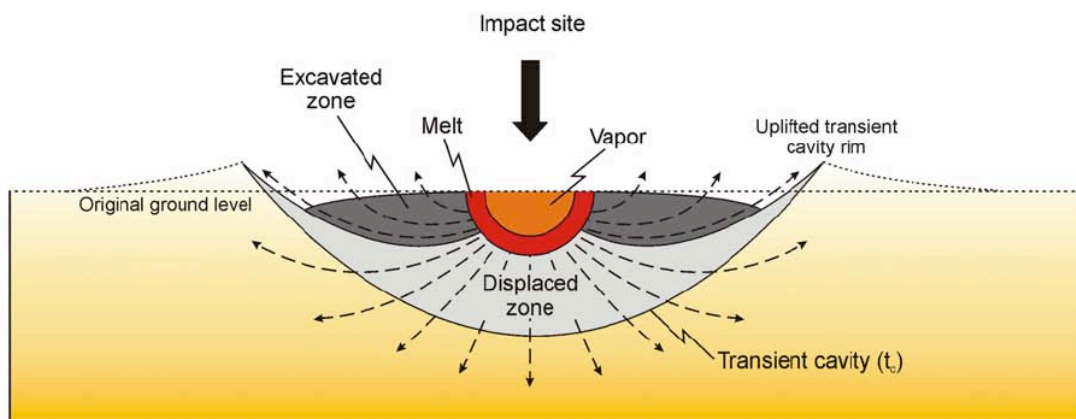


Figure 6: Cross-section of transient cavity, where the excavated and displaced zones are labeled above and below the impact site. The uplifted rim can be seen above the original ground level (Osinski, 2006).

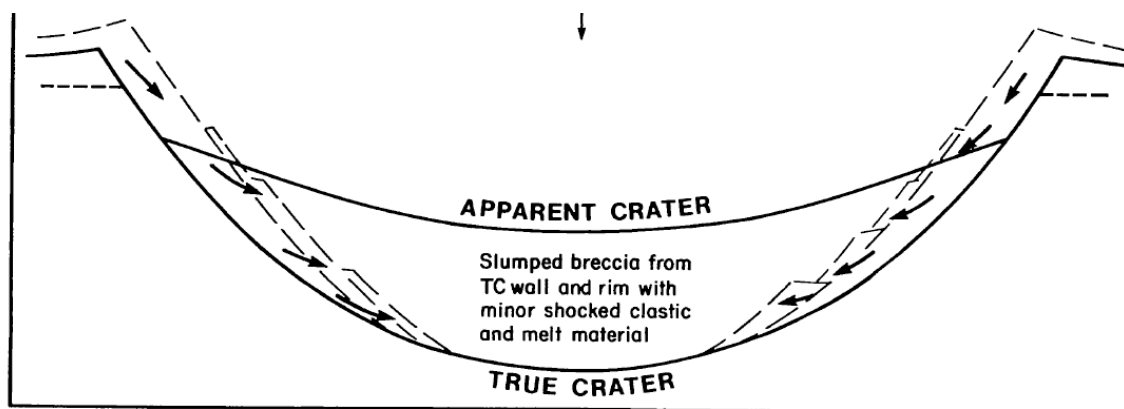


Figure 7: Collapse of the transient cavity walls to form the final simple crater with allochthonous breccia lens (Grieve, 1987).

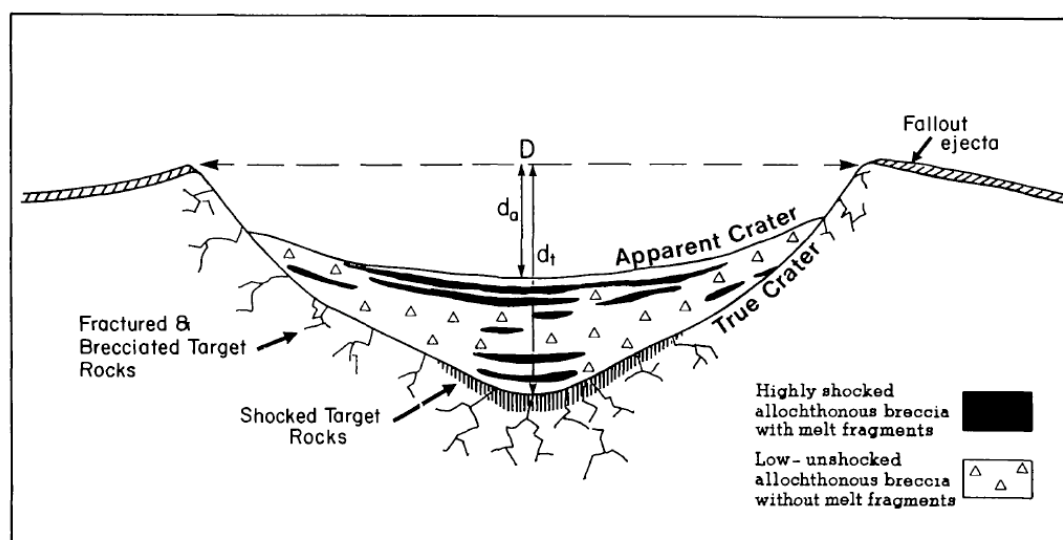


Figure 8: Cross-section of a simple crater showing the various depths after the transient cavity walls collapse. The transient cavity depth to diameter ratio is $\sim 1/3$. True depth and apparent depth can be figured by $d_t = 0.29D^{0.93}$, $d_a = 0.14D^{1.02}$ (Grieve, 1987).

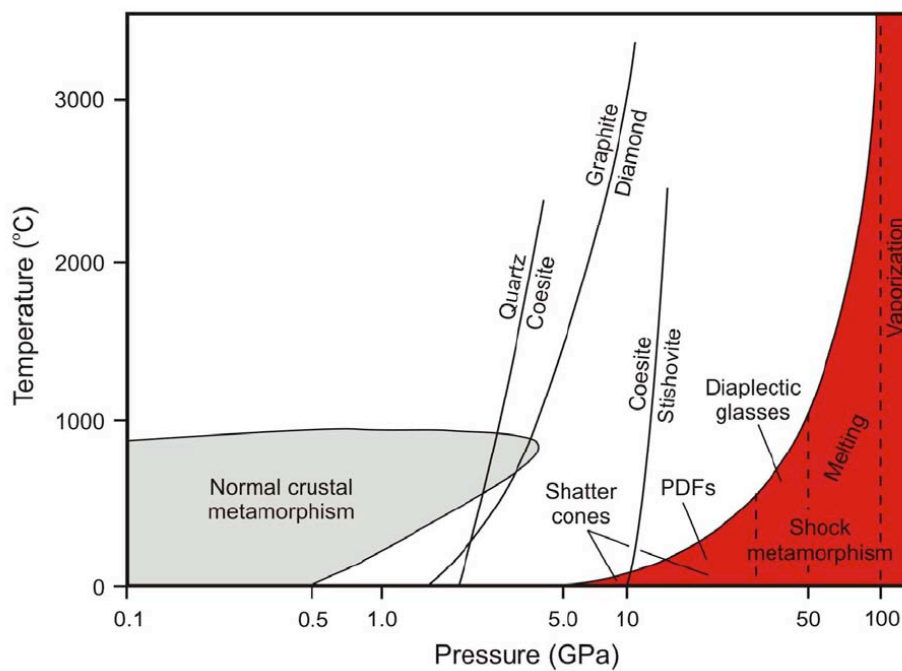


Figure 9: Pressure-Temperature diagram showing the differences between normal crust (endogenic) metamorphism and shock metamorphism. The shock metamorphic orientations that can be formed by different pressures are displayed on the right hand side. High pressure polymorphs formations are also shown (Osinski, 2006).



Figure 10: At the first pressure range $\sim 7.5\text{-}30$ GPa, a quartz grain with planar deformation features from the Houghton impact structure, Canada. Field view is 2 mm in plane-polarized light (Osinski, 2006).

CHAPTER 2: PREVIOUS WORK

2.1 Geological Setting

The Atacama Desert is the driest subtropical desert in the Southern Hemisphere. It covers a 966 km long strip on the Pacific coast of South America, from Peru to Northern Chile. The elevation reaches up to 5000 m. The Salar de Atacama is 2300 m in elevation and a 120 km long, 60-90 km wide depression trending N-S in the Atacama Desert. It is a flat plain in the bottom of a drainage basin that is bounded by the Domeyko Range to the west and the Western Cordillera on the eastern side of the Altiplano (Moreno, 2007).

Extreme hyperaridity existed in the Atacama Desert as early as 25-22 Ma and is due to a combination of three factors: (1) the extreme rainshadow effect of the Andes Mountains, (2) limited influence of winter storm tracks from the presence of the semi-permanent South Pacific Anticyclone and (3) generation of temperature inversion at 1000 m by the Humboldt Current, a cold north flowing current that constrains inland penetration of Pacific moisture (Moreno, 2007).

2.2 General Crater Information

The Monturaqui Impact Crater (Figure 11) is located in the Atacama Desert in northern Chile at the southern end of Salar de Atacama (S23°55'5.5" W068°15'0.2") at an altitude of 3000 m. The crater has a diameter of 0.46 km and was formed in bedrock of Jurassic granite, overlain by a thin Tertiary-Quaternary ignimbrite sheet (Sanchez & Cassidy, 1966).

Monturaqui was first recognized as an impact crater in publication by Sanchez and Cassidy in 1966. The geometry of the crater has a preferred northwest - southeast elongation with dimensions of the crater at 470 m (east to west) by 440 m (north to south) (Sanchez & Cassidy, 1966). The wall height ranges from 16 to 48 m above the lowest point. The variation is contributed to by pre-existing topographic irregularities in the surface before the formation of the impact crater (Sanchez & Cassidy, 1966). The northern portion of the floor is a deposit of white to yellow lime approximately 40 m² and 1-2 m thick, slightly off center, originating from sediment deposition from ponding by possible summer precipitation. Ugalde et al (2007) recognized a north-south trend affecting the granite units and a north-east trend affecting the ignimbrite units, and both were measured within the units. No evidence of isostatic rebound or inverse faulting that would have caused uplift of the crater has been found (Ugalde, 2007).

A mathematical model for the formation of the Monturaqui Impact Crater was calculated using the parameters of a circular shape, diameter of 460 meters, and basement composition of granite (Echaurren, 2005). The model produced an asteroid diameter of ~14.92 m with a density of ~6.31 g/cm³. The calculated asteroid had a model velocity of ~17.82 km/s with an impact angle of 41.12°. This created ~4.77 x 10²² Ergs (~1.14 megatons) of energy at impact. The calculated hydrothermal zone is ~14.92 to 113.21 m from the nucleus of the impact, with a lifetime estimated at ~2244 ± 22 to 3503 ± 96 years. The temperatures created in the hydrothermal zone range from ~97.95 to 21.79 °C, lasting 0.25 to 1,400 years (Echaurren, 2005).

The model estimated the melt volume to be ~6,763,699 m³ or 0.0068 km³, with a density for ejected fragments of 2.63 g/cm³. The fragments of the impact were ejected to

~11.49 km from the impact center, at a velocity of 1.12 km/s at an angle of $\sim 2.58^\circ$ with a maximum height of 129.59 m. The number of fragments ejected are estimated at ~ 7401.1 with an average size of ~ 0.77 m and a cloud of dust with a diameter of ~ 23.61 km (Echaurren, 2005).

2.3 Age

In the Ugalde et al (2007) geological study, the granite unit is described as being part of the Paleozoic granites from the Tucucar Pluton outcropping in the area, dated at 441 ± 8 Ma. The ignimbrite is overlain the granite and is part of the Pliocene ignimbrite units from the Tucucaro Ignimbrite at 3.2 ± 0.3 Ma (Ugalde, 2007).

The emplacement of the crater interrupted the drainage patterns in the ignimbrite and diverted the well-established watercourses. This shows that the age of the formation of the crater is younger than the erosion of the ignimbrites. The diverted watercourses also show that there was a significant period of erosion after the formation of the crater (Sanchez & Cassidy, 1966; Bunch & Cassidy, 1972).

Buchwald (1975) lists Monturaqui as $>100,000$ years old. This age was noted as obtained by thermoluminescence analysis with an appreciable error by Ugalde et al (2007). In July 1998, an expedition conducted to collect impactite from the Monturaqui Impact Crater produced a thermoluminescence (TL) age of $590,000 \pm 28,700$ years (Verdugo & Cartes, 2000).

The first absolute ages of the Monturaqui Impact Crater were calculated by measuring the residual activities of ^{10}Be , ^{26}Al , ^{36}Cl , ^{41}Ca , ^{59}Ni , ^{60}Fe , and ^{53}Mn from iron shale samples that correspond to altered fragments of the impactor. Ages were also calculated using in-situ

ages from long-lived terrestrial cosmogenic radionuclides ^{10}Be and ^{26}Al in the granite outcrops exposed to cosmic radiation assumed to have started from the time of impact (Valenzuela, 2009). The best fit from the measured shortest-lived radionuclide ^{36}Cl was with a terrestrial age of 500-600 Ka. The calculated age from ^{26}Al ($t_{1/2} = 0.7\text{Ma}$) agrees with this ^{36}Cl data. The ^{10}Be concentrations in quartz calculated an age of 200-250 Ka, but the ^{26}Al ages (not given) were determined to be erroneous. Paleomagnetic measurements were conducted on samples of the granite inside the crater that revealed a reverse magnetic field polarity. This suggested an age of 780 Ka for the remagnetization of the granite. It is unclear if this remagnetization is related to the impact or the emplacement of the ignimbrite pre-impact. The authors concluded that the most likely terrestrial age of the Monturaqui Impact Crater is 500-780 Ka (Valenzuela, 2009).

A more recent study (Ukstins Peate et al 2010) used U/Th-He dating of zircon and apatite grains picked from samples from the 2008 field season at Monturaqui Impact Crater. Many of the grains were partially reset, which required an analysis of a large number of grains. The success of the apatite grains was low due to undetected inclusions and low He contents. The data yielded a mean age of 633 ± 90 Ka (Ukstins Peate et al, 2010).

2.4 Geophysics

A geophysical study from a field expedition carried out in December 2003 collected densely spaced gravity, magnetic and topographic data along with detailed geologic mapping (Figure 12a, 12b, 12c) with the purpose of building a 3D model of the structure (Figure 12d) (Ugalde, 2007). A high-resolution digital elevation model was created, and the crater dimensions of 350 x 370 x 34 m confirmed those found by a Danish expedition from 1973,

which were never published (Ugalde, 2007). For the 3D gravity model four basic layers were used: post-impact sediments (center of crater), volcanic tuff (ignimbrites), fractured basement, and unfractured basement as a background. The final calculated geometry is composed of ignimbrites 13-20 m thick at the center, 0 to 5-7 m thick at the sides of the crater; fractured basement < 35-40 m thick at the center, 5-7 m thick at the sides; and a thin < 2 m layer of sediments at the center (Ugalde, 2007). The negative gravity anomaly of ~1 mGal at the center is best explained by fracturing and brecciations of the target rocks. The 3D model (Figure 12d) of the structure supports the predictions of a fracturing induced low-density granitic layer on top of the unfractured basement (Ugalde, 2007). Ugalde et al (2007) estimated that the impact pressures exerted by the impact, range from 8 to 40 GPa and are similar to the results of Bunch and Cassidy (1972).

2.5 Target Rock

2.5.1 Granite

The oldest target rock of the Monturaqui Impact Crater is the Jurassic granite (Sanchez & Cassidy, 1966; Bunch & Cassidy, 1972), which is cross-cut by mafic and felsic dikes (Ugalde, 2007). The granite (Figure 12b & 12c) is highly eroded and crops out in the walls and the rim crest of the crater (Sanchez & Cassidy, 1966). In hand sample the granite is coarse-grained, grey-white to pink color showing red oxidation surfaces where fractured (Ugalde, 2007).

2.5.2 Ignimbrite

The next youngest target rock in the Monturaqui Impact Structure is the Upper Tertiary or Pleistocene ignimbrite (Sanchez & Cassidy, 1966) varying in thickness from 0-

5m (Bunch & Cassidy, 1972). The ignimbrite (Figure 12b & 2c) is also highly eroded and crops out in the walls and rim crest of the crater with the granite. The rim crest is almost completely mantled with ignimbrite (Sanchez & Cassidy, 1966). The high erosion of both the granite and ignimbrite give a soft relief to the crater rim and cavity to the north-west, but preserve the steep slope to the south-east (Ugalde, 2007). Ugalde et al (2007) notes the ignimbrite does not appear in outcrops, but as a regolith cap (debris) filling the crater and its surroundings. The clasts of ignimbrite are of irregular angular shape and sizes that vary from a few centimeters at the base of the crater to 50-60 cm at the rim of the crater. The ignimbrite unit consists of mainly ash and lapilli tuffs, ranging in color from grey to white. Crystals of plagioclase and biotite are common with a smaller proportion of quartz and flat pumice fragments (Ugalde, 2007).

2.5.3 Mafic Dikes

Sanchez and Cassidy (1966) do not describe the dikes in their overview of the Monturaqui Impact Crater. Bunch and Cassidy (1972) describe the igneous dikes as relatively common green-gray with phaneritic texture and probable basic composition, 3-10 cm thick. Ugalde et al (2007) states that the granite is cross-cut by mafic and felsic dikes but do not give a petrographical description.

2.5.4 Iron Shale

'Iron shale' was found originally by Sanchez & Cassidy (1966), and identified as highly weathered and oxidized fragments of meteorite. Ugalde et al (2007) found fragments distributed all around the crater walls, but preferentially to the south. The size ranged from a few millimeters to centimeters. Samples had extreme magnetism but were too small and

randomly distributed to have a noticeable effect on the overall magmatic signature of the crater as a whole (Ugalde, 2007).

2.5.5 Shock Features in Target Rock

Shock features in the target rock are only addressed by Ugalde et al (2007). The granite unit shows shock metamorphism that is inferred from the presence of impact melt rocks containing fragments of the main minerals of the granite. At a microscopic level, quartz and to a lesser extent feldspar and biotite grains exhibit different degrees of shock, ranging from planar microdeformation and cleavage to the development of intense planar deformation features and diaplectic glasses in some grains (Ugalde, 2007).

There are no shock features found in the ignimbrite samples. Other shock effects were detected in surface rock samples, and Ugalde et al (2007) concluded this indicates that most of the shocked material lies beneath the regolith of ignimbrite or that the release of energy associated with the melting rocks was very constrained and restricted to the granite unit (Ugalde, 2007).

2.6 Impactite

2.6.1 Formation

The conditions by which the impactite formed are an interaction of an Ni-Fe meteorite traveling at orbital velocity with the target rocks (a granite mass overlain by ignimbrite). Bunch & Cassidy (1972) concluded that the impactite glass resulted from preferential melting of the lower-temperature granitic components and is contaminated with Fe from the melted meteorite. This is supported by petrographic observations that biotite and chlorite have melted preferentially compared to feldspar and quartz. The impactites would

have still been plastic upon falling to the ground after impact. There are no ignimbrite inclusions present which indicates they originated at some depth within the crater. The deepest point inside the crater was probably the point of the most stressful physical conditions (Bunch & Cassidy, 1972).

2.6.2 Sample Description

The impactite is also described as cindery with a twisted, ropy appearance, from distortion during flight while components were still hot. There are unshocked single grains, grain fragments, and rock fragments found in the impactites enclosed in completely vitrified material, others are fused at their borders. A typical impactite specimen (Figure 13) contains white inclusions that are made up of quartz and feldspar, glass, nickel-iron spherules, iron oxides, vesicles, and several metavolcanic pebbles. The glasses in transmitted light range in color from dark brown to reddish brown to green. The vesicles are commonly lined with glass and or oxides and are a maximum of 4 cm in diameter. The pebbles are only on the outside of the sample and suggest that the impactites were very hot and still viscous when hitting the ground. Magnetite droplets may also be found in the glasses (Bunch & Cassidy, 1972).

Impactites also contain shocked and unshocked granite fragments that range from several microns to 4 cm. Bunch and Cassidy (1972) described the unshocked granite in impactite as hypidiomorphic-granular in texture and consisting of zoned oligoclase-andesine, quartz, microcline, chlorite, biotite, magnetite (some exsolved ilmenite grains), apatite and zircon with sericite and other alteration minerals. The oxide minerals found in the granite are not well represented in hand samples of impactite, this may be due to magnetite oxidizing to

hematite during the impact shock and may be undistinguishable from post-impact oxidation and weathering products (Bunch & Cassidy, 1972).

In the Ugalde et al (2007) study the impactites have been found on the southeast edge of the crater where there are the steepest slopes ($\sim 35^\circ$), ranging in size from a few millimeters to ~ 10 cm. As shown in Figure 14, Ugalde (2007) states impactite is made of 40% brown and green glass present, 30% fractured feldspar and quartz crystals, and 30% vesicles. The vesicles are empty (70%) and the rest are filled with either Fe-oxides (hematite, magnetite, goethite) or metal spherules, which are relicts of the meteorite impactor (Ugalde, 2007).

2.6.3 Shocked Features in Impactite

A range of shock effects in the impactite were determined by Bunch & Cassidy (1972): weakly to moderately shocked quartz and feldspar that exhibit microdeformation structures, moderately to strongly shocked minerals that exhibit solid-state phase transformations, intensely shocked minerals exhibit complete melting.

The parameters for weakly shocked features are < 100 to 250kb and < 100 to 300°C . These features are found in quartz, plagioclase, biotite, and apatite. Figure 15a shows an example by Bunch & Cassidy (1972) in which the quartz has microdeformation features (as well as the plagioclase to a lesser extent). Grains with planar features are partly vitrified. Also in this stage, small biotite grains have kinked cleavages (Bunch & Cassidy, 1972).

The parameters for moderately to strongly shocked features are defined as occurring at 250 to 500kb , 300 to 1500°C . These features are found in quartz, plagioclase, and potassium feldspar also. In quartz grains, coesite is identified. It is sparsely present as very fine-grained and partly to completely vitrified with preserved boundaries. Plagioclase (Figure

15b) and potassium feldspar are diaplectic, and partially to totally transformed in solid-state amorphous phases without the loss of grain morphology. They are intermediate in degree of structural disorder and are not true glass (not totally disordered by fusion) (Bunch & Cassidy, 1972).

The parameters for intensely shocked features occur at 500 to 650kb, 1500° to 3000°C. These features are found in quartz, plagioclase, biotite, and the impactite matrix. The vesiculated quartz and feldspar glasses are common in impactites and show flow structures (Figure 15c). They are partially or fully recrystallized with a few showing growth of needle or lath-like crystals into surrounding green or brown glass matrix. The impactite matrix is made up of devitrified brown glass and isotropic green glass shown in Figure 15d. Blebbly brown glass is fairly common as inclusions within the colorless or green glass. The relict biotites are opaque indicating breakdown under shock-loading to iron oxides and red-brown glass (Bunch & Cassidy, 1972).

2.7 Spherules

The iron mineralogy of the impactite was investigated with a Mössbauer study. The interpretations of the Mössbauer spectra revealed the molten glass is enriched in Fe (ferrous iron) relative to the granite as Fe was transferred from the molten droplets of Fe-Ni alloy. Quenching allowed the alloy droplets to become embedded in the newly formed glass. The Fe-Ni alloy spherules lying close to the cracks in the glass have later weathered into a complex mixture of Ni-containing iron oxides (Lipka, 1992 & 1994).

The Ni-Fe spherules are dispersed throughout the glass in the Monturaqui impactite. Many have been oxidized by weathering and range in size from submicron to 2 mm. They

consist of single-phase nickel-iron alloy with interstitial, interlocking troilite and small isolated grains of schreibersite and glass. Nital etching of several spherules showed circular to polygonal grain boundaries of kamacite. Larger spherules have irregular boundaries and are surrounded by wide zones of secondary iron oxide (Bunch & Cassidy, 1972).

The spherules are fairly homogenous in Fe, Ni, Co, and P compositions with no enrichment or depletion near the spherule-matrix boundary. The variable compositions show a correlation with spherule size and amount of oxidation (Table 1). The smaller spherules are always free of enveloping oxidation crust and contain the highest Ni and Co. There is enrichment in Fe and P in the largest spherules but not in the surrounding glass of any of the spherules (Bunch & Cassidy, 1972).

The metallic spherules vary in Fe/Ni and P/Co ratios according to size shown in Figure 16. The larger the spherule, the less it is affected by chemical fractionation and the closer it remains in composition to the parent projectile. This suggests the parent projectile could have been an octahedrite, with a composition of less than 7.8 wt.% Ni (this is the lowest Ni content in one of the largest spherules analyzed) (Bunch & Cassidy, 1972). According to Gibbons et al (1976) this implies a relatively low sulfur content. Since the country rocks are sulfide-free, this leads the authors to the conclusion that the impactor must be the source of sulfur (Gibbons, 1976).

2.8 Chemical Data

2.8.1 Whole Rock Data

2.8.1.1 Granite

Whole rock data was collected for the granite through wet-chemical analyses and is only discussed in comparison to individual minerals in Bunch & Cassidy (1972) and will be discussed further in this chapter.

2.8.1.2 Ignimbrites

No whole rock data has been collected or discussed on the ignimbrite in previous works.

2.8.1.3 Mafic Dikes

No whole rock data has been collected or discussed on the dikes found cross-cutting the granite in previous works.

2.8.1.4 Impactite

Bulk analyses of the impactite material have similar SiO₂ content for both brown and green glasses, and FeO, CaO, MgO and Na₂O, and K₂O are different in composition from the granite country rock, as shown in Table 2. The high 5.32% Fe₂O₃ found in impactites is probably due to post-impact oxidation by weathering processes (Bunch & Cassidy, 1972).

2.8.1.5 Iron Shale Data

No whole rock data has been collected or discussed for the iron shale in previous works.

2.8.1.6 Impact Glass

The glasses in the impactite formed under the highest degree of shock possible without complete vaporization. In most cases the colorless glass is pure SiO₂. There are very

few chemical differences between the green and devitrified brown mixed glasses, except that the brown glass has lower Al_2O_3 and the higher FeO . This may have resulted from diffusion of Fe from nickel-iron spherules into the glass and/or higher initial Fe content. The heterogeneous texture may be influenced by high melting and quenching rates that allow selective melting of individual minerals or mineral grain associations, but restrict the mixing and homogenization of melted material (Bunch & Cassidy, 1972).

2.8.2 Mineral Data

2.8.2.1 Granite Minerals

The range of major elements in Table 3 and corresponds very closely to plagioclase found in unshocked granite country rock in Table 2. This is an indication of little to no loss of constituents during shock melting. For shock-formed vesicular feldspar glasses this is not true, there is a loss of SiO_2 , Na_2O and K_2O in all cases (Bunch & Cassidy, 1972). The electron microprobe results (Table 2) also show the granite contains ~ 1.5% normative magnetite (mg + il in Table 2) and 0.4% hematite. This agrees with the petrographic estimates of 1-3 wt% magnetite-ilmenite intergrowth (Bunch & Cassidy, 1972).

2.8.2.2 Ignimbrite Minerals

No data was collected for the minerals found in the ignimbrites or discussed in previous works.

2.8.2.3 Mafic Dike Minerals

No data was collected or discussed for the minerals found in the dikes in previous works.

2.8.2.4 Iron Shale & Oxide Minerals

Fourteen fragments of iron shale were examined to determine the corrosion products of the entirely disintegrated iron meteorite by Koch & Buchwald (1994). The overall morphology of the iron shales is a coarse octahedrite, probably Group IA (similar to the Canyon Diablo meteorite (Figure 17)). Polished sections of the iron shale display vugs and microporosities and are >99.9% oxidic. Fe/Ni oxides formed from weathering of metal spherules along the cracks and lining of vesicles. The average composition of the oxides is 90 wt.% Fe₂O₃ and 10 wt.% NiO (Koch, 1991).

The non-oxidized parts are minute particles of taenite (38-42 wt.% Ni) and cohenite. X-ray diffractometry on powdered samples showed goethite, maghemite and lepidocrocite and reevesite. Magnetite, akaganeite and hematite were not found. The oxidation state of Fe was investigated by ⁵⁷Fe Mössbauer spectroscopy. The dominant components in the sample are goethite and maghemite. The Fe is portioned between maghemite and goethite in the ratio 55:45 (Koch & Buchwald, 1994). A relative loss in Ni in all the oxide phases is also noted by Koch & Buchwald (1994).

2.8.2.5 Spherules

The average composition of the Ni-Fe phase spherules can be seen in Table 1. There are correlations between composition, spherule size and oxidation. The brown glass that surrounds the largest spherules is enriched in Fe and P, but is not the same for smaller spherules. The smallest spherules had the highest Ni and Co and the lowest Fe and P. Several spherules contained a core of troilite surrounded by pentlandite (Table 1) and were concluded to be sulfide spherules (Bunch & Cassidy, 1972).

Gibbons et al (1976) analyzed 100 spherules $< 35\mu\text{m}$ in diameter, with the assumption that the spherules could not represent a mixture of taenite and kamacite from the original meteorites, but had to go through fractionation of the original bulk meteorite composition during the impacting process. The spherules generally consist of a homogenous, single-phase iron-nickel alloy, but some consisted of a metal alloy core with a sulfide shell. Intricate intergrowths of metal and sulfide are also present. The Ni content varied from 13 to 74% and Fe content from 85 to 24% as shown in Figure 18 (Gibbons, 1976).

In Figure 19 variations in Co are shown relative to spherule size, but the Co concentrations appear to be independent of the grain size for spherules that were $< 35\mu\text{m}$. In Figure 20 a variation between Co and Ni is shown, at less than 50% Ni there is an increase of Co content, above 50% Ni, the Co content decreases. Relative to Fe there is an enrichment of Ni and Co, and above 50% Ni there is enrichment in Ni relative to Co. This is true not only for Monturaqui but other craters with metal spherules. In this case the Wabar and Henbury crater data is also shown in Figure 20 demonstrating these relationships (Gibbons, 1976).

Gibbons (1976) suggested selective oxidation of Fe as the major process affecting the Ni-enrichment of spherules in terrestrial impact glasses. The meteorite materials were subjected to a range of pressure and temperature conditions, which makes various degrees of fractionation possible. Spherules only microns apart have drastically different Ni content, and this variation in Ni content must represent very different degrees of oxidation that occurred over a short time. Small spherules have greater surface areas for oxidation, which might explain the Ni and Co enrichments with decreasing size.

A lack of chemical gradients indicates strongly that the spherules have not reacted at all with the glass. There was no enrichment or depletion of constituent elements near the

spherules/glass contact, either as variations in the spherule compositions or in the composition of the glass. The fractionation of the metal into unique chemical spherules must have occurred before the final emplacement into the still viscous glass (Gibbons, 1976).

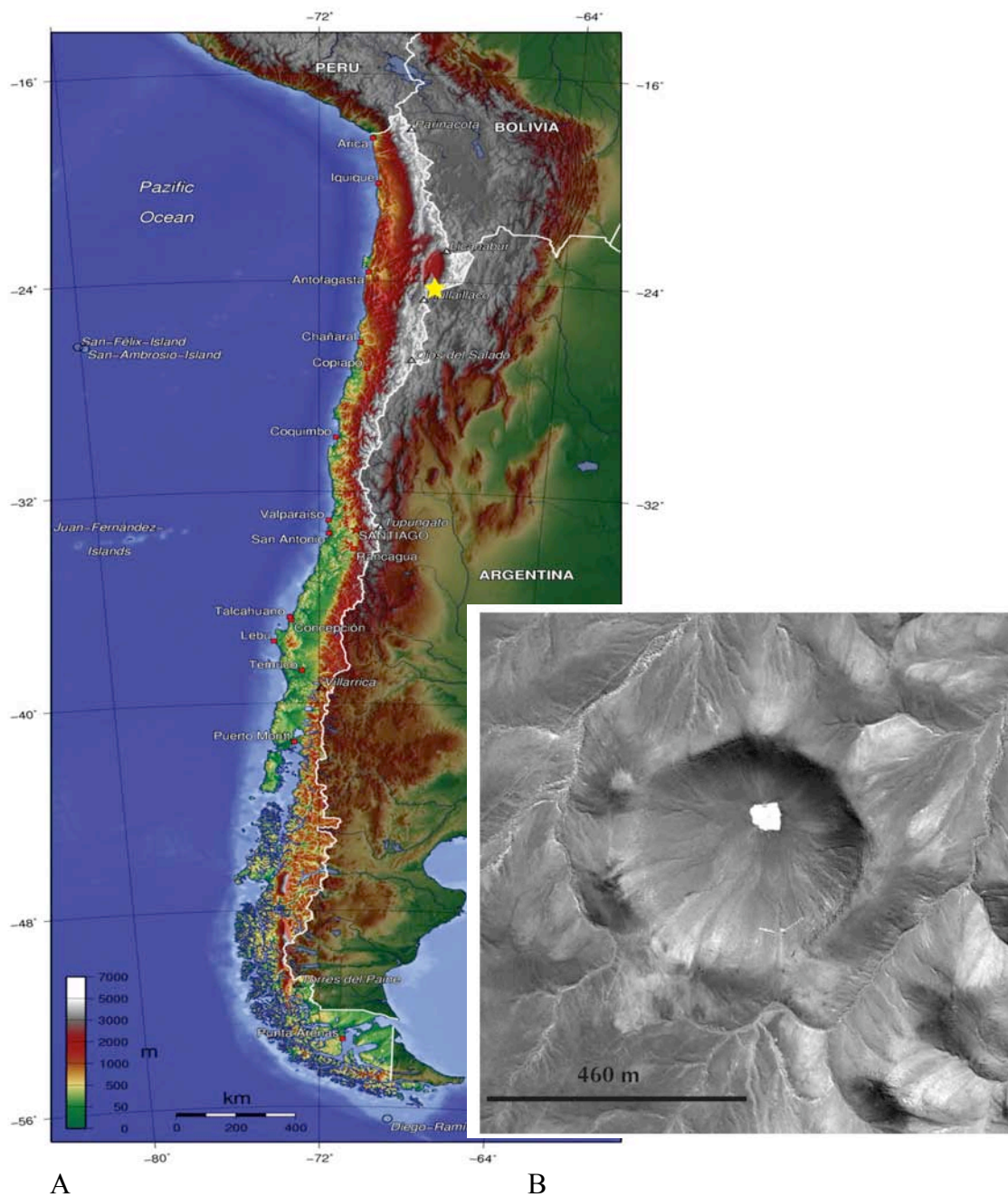


Figure 11: Location of the Monturaqui Impact Crater. A) Topographic Map of Chile, yellow star indicates location of Monturaqui Impact Crater, B) Satellite image of Monturaqui Impact Crater.

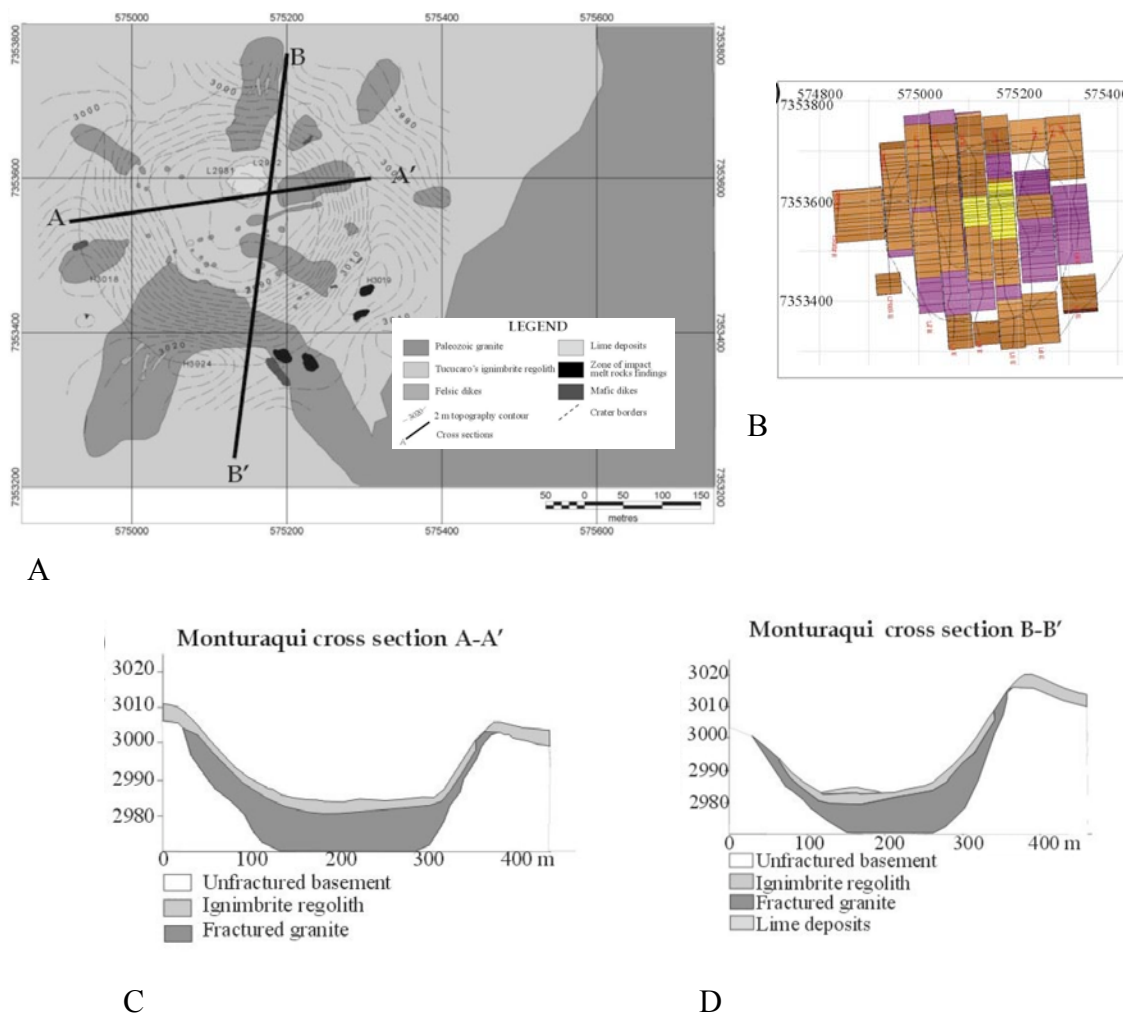


Figure 12: Ugalde et al (2007)'s Geophysical Study. A) Geological map created by Ugalde et al (2007), showing topographic contours, target rock units: granite, dikes, ignimbrites, melt rocks and cross sections A-A' and B-B'. Map Scale is 1:2,000. B) Plain view of the whole 3D gravity model, colors indicate: yellow = sediments, brown = ignimbrite, purple = fractured basement (granite), and white = unfractured basement (granite). C) Cross section from geologic map along line B-B' north-south. The granite unit is also inferred while the ignimbrite unit is based off geological mapping. D) Cross section from geologic map along line A-A' east-west. The granite unit is inferred while the ignimbrite unit is based off geological mapping (Ugalde, 2007).

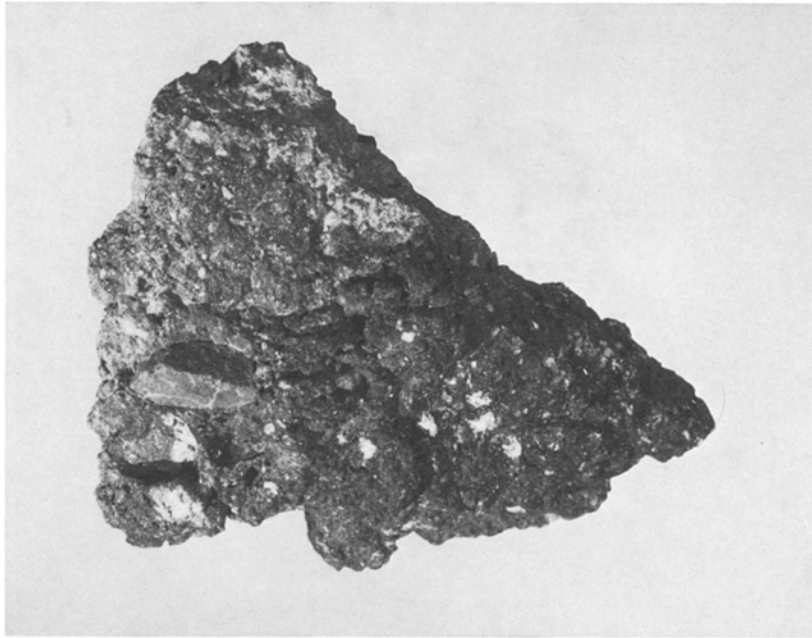


Figure 13: Hand sample of impactite showing inclusions of quartz, feldspar, glass and metavolcanic pebble. Width is 25cm (Bunch & Cassidy, 1972).

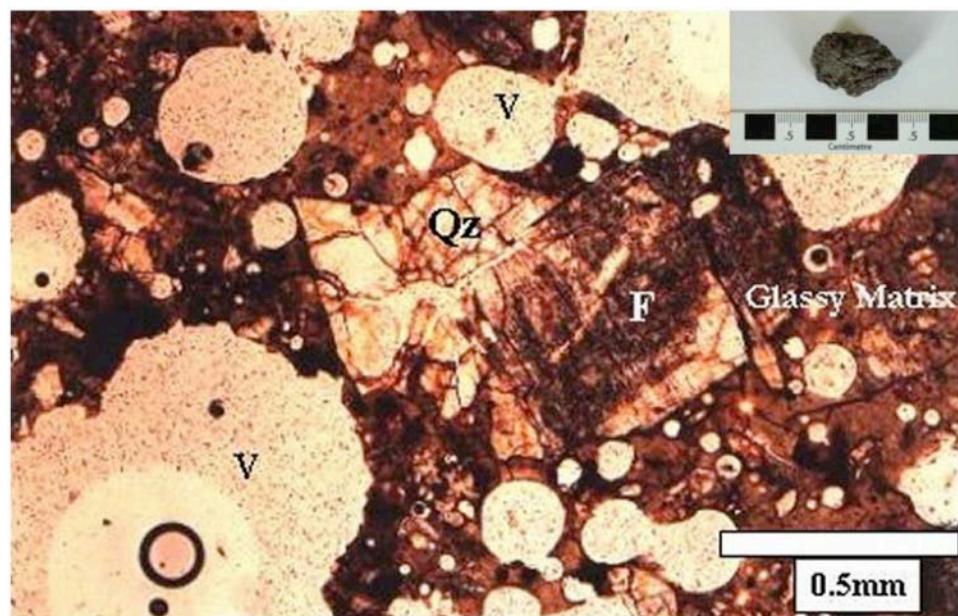


Figure 14: Photomicrograph of Monturaqui impactite in plane-polarized transmitted light at 50x. Fractured feldspar (F) and quartz (Qz) from the granite, devitrified brown matrix glass, nickel-iron spherules and vesicles (V) are labeled. Inset shows impactite in hand sample (Ugalde, 2007).

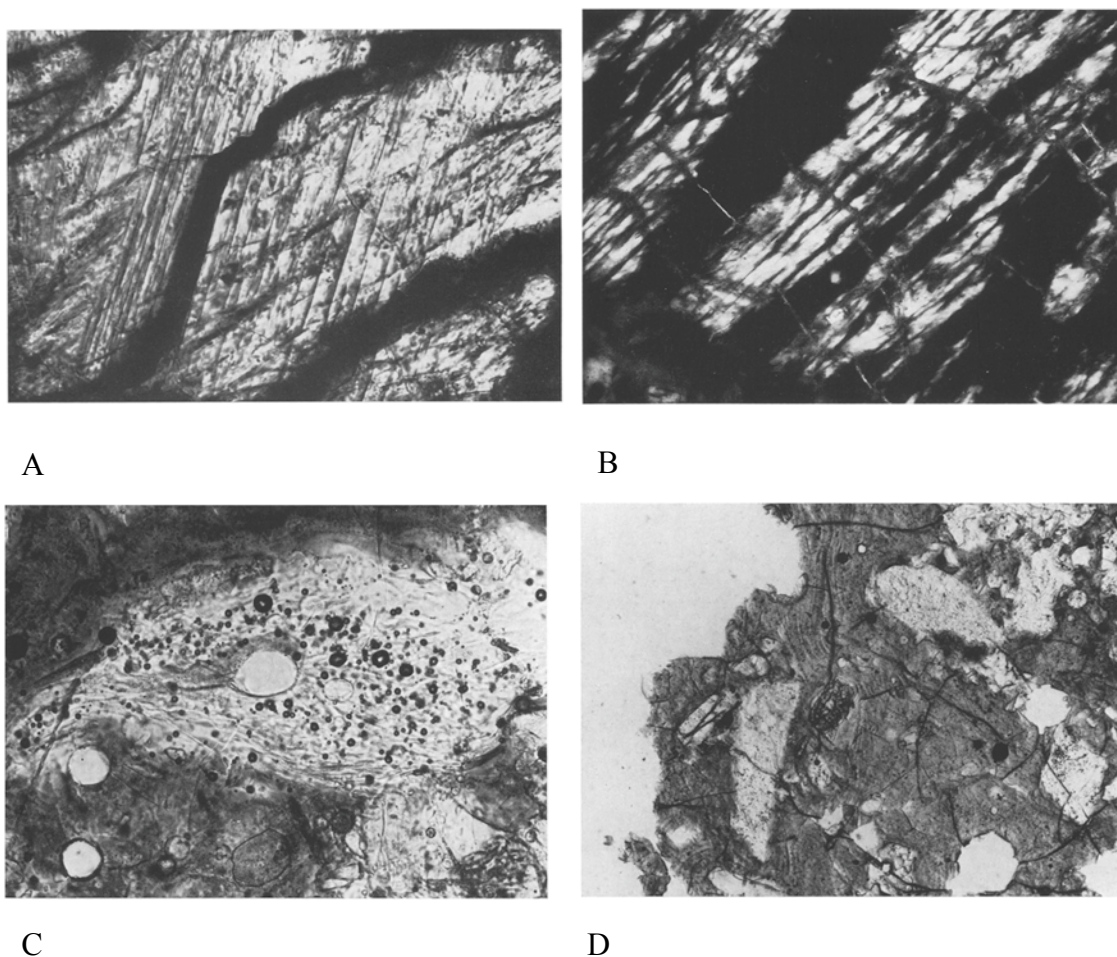


Figure 15: Shocked features in Monturaqui Impactite. A) Weakly shocked features: cleavage in a grain of shocked quartz, width is 0.53 mm (Bunch & Cassidy, 1972). B) Moderately to strongly shocked features: alternating band of diaplectic glass and crystalline plagioclase, width is 0.21mm (Bunch & Cassidy, 1972). C) Intensely shocked features: vesiculated silica glass showing flow structures, width 0.53mm (Bunch & Cassidy, 1972). D) Intensely shocked features: typical example of mixed brown and green matrix glasses with inclusions, flow lines can be seen as well as dark spots that are nickel-iron spherules, width 3.0 mm (Bunch & Cassidy, 1972).

Table 1: Electron Microprobe analyses (wt.%) of selected nickel-iron in the Monturaqui Impactite.

Apparent Diameter	1.5 mm- 350 μm	350 -150 μm	150-40 μm	40-10 μm	$\leq 10\mu\text{m}$	Ni-Fe spherules	Sulfide Spherules	
							troilite	pentlandite
Fe	90.3	89.9	87.2	66.1	65.4	77.1	61.7	42.5
Ni	8.5	9.1	12.1	31.8	32.5	21.4	2.39	23.6
Co	0.51	0.69	0.74	1.43	1.56	1.17	0.32	0.75
S	--	--	--	--	--	--	35.5	32.6
P	0.42	0.36	0.16	0.15	0.05	0.16	--	--
Totals	99.73	100.35	100.2	99.48	99.51	99.83	99.91	99.45
Number of grains analyzed	9	8	9	7	8	--	--	--

Note: Based on Table 2 from Bunch & Cassidy, (1972). Also included are average compositions of Ni-Fe spherules and troilite and pentlandite compositions of sulfide spherules.

Table 2: Electron microprobe analyses of mixed glasses and wet-chemical analyses of impactite and granite country rock.

Apparent Diameter	A. Green Glass		B. Brown Glass		C. Synthetic Glass		D. Impactite	E. Granite country rock		F. Oxides (Koch)
	Average	range	average	range	average	range		a	b	
SiO ₂	53.90	51.5-54.8	52.30	51.2-54.0	54.00	53-56	56.32	72.06	74.64	0-4.0
Al ₂ O ₃	17.60	15.0-18.8	13.20	13.1-14.8	21.50	15-25	11.77	15.01	13.81	0.02
TiO ₂	n.d.	--	n.d.	--	--	--	0.31	0.20	0.14	--
FeO	15.50	13.8-17.7	24.30	22.5-25.1	12.20	6.2-22.8	13.51	0.59	0.55	--
Fe ₂ O ₃	--	--	n.d.	--	--	--	5.52	1.54	1.17	--
CaO	4.60	4.1-5.2	1.00	3.6-4.5	4.90	3.6-6.1	3.14	1.10	1.65	--
MgO	2.41	2.13-2.93	1.55	1.19-1.80	1.80	1.4-2.2	1.35	0.78	0.51	--
MnO	n.d.	--	n.d.	--	--	--	0.06	0.05	0.04	--
Na ₂ O	2.81	1.95-3.41	2.89	1.83-3.30	2.70	1.9-4.1	2.28	4.13	3.49	--
K ₂ O	2.36	1.90-2.75	2.54	2.27-2.73	2.20	1.6-2.5	2.25	3.43	3.31	--
H ₂ O ⁺	--	--	--	--	--	--	2.77	1.11	0.76	--
H ₂ O ⁻	--	--	--	--	--	--	0.10	0.37	0.47	--
P ₂ O ₃	n.d.	--	n.d.	--	--	--	0.08	0.02	0.02	--
S	n.d.	--	n.d.	--	--	--	0.23	--	--	--
NiO	n.d.	--	n.d.	--	--	--	1.04	0.01	0.05	1.7-5.3
CoO	n.d.	--	n.d.	--	--	--	0.07	--	--	0.2-0.8
Cl	--	--	--	--	--	--	--	--	--	0-0.2
SO ₃	--	--	--	--	--	--	--	--	--	0-0.3
Totals	99.18		100.78		99.3		100.80	100.39	100.59	--

Note: Analyses from Bunch & Cassidy, 1972 and oxides from Koch & Buchwald (1994).

Table 3: Electron microprobe data of shocked nonvesiculated, vitrified plagioclase from Bunch & Cassidy (1972).

	SiO ₂	Na ₂ O	Al ₂ O ₃	CaO	K ₂ O
Plagioclase (Nonvesiculated, vitrified)	60.6-63.5	7.7-9.3	24.0-22.2	5.3-2.87	1.22-1.10

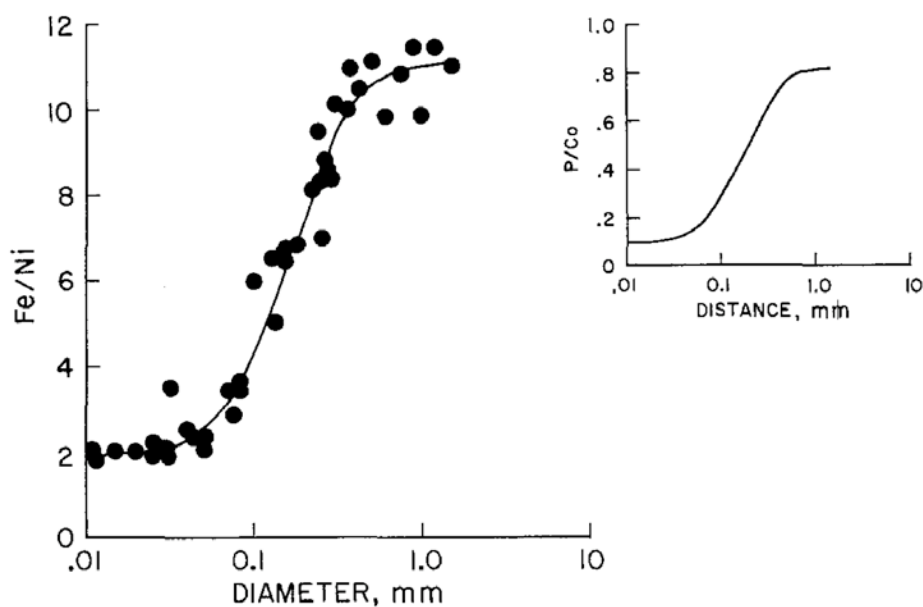


Figure 16: Semi-log plot of Fe/Ni vs. spherule size and (insert figure) P/Co vs. spherule size in nickel-iron spherules from Bunch & Cassidy (1972).

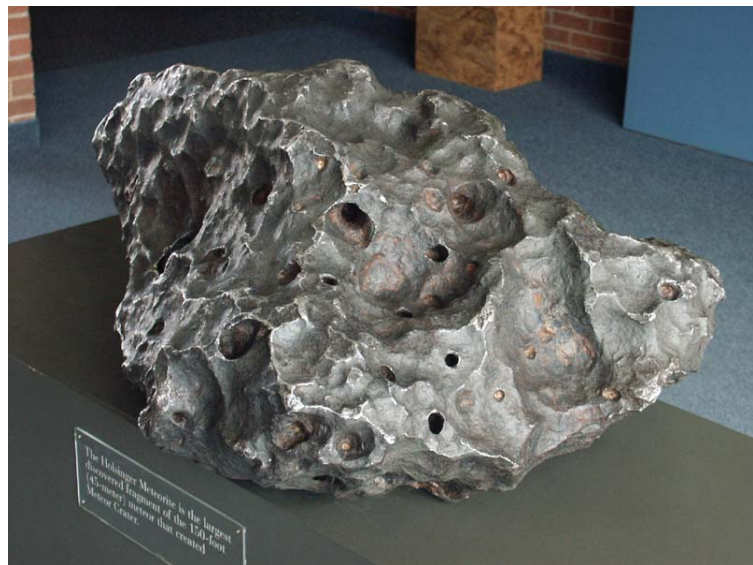


Figure 17: Canyon Diablo Meteorite.

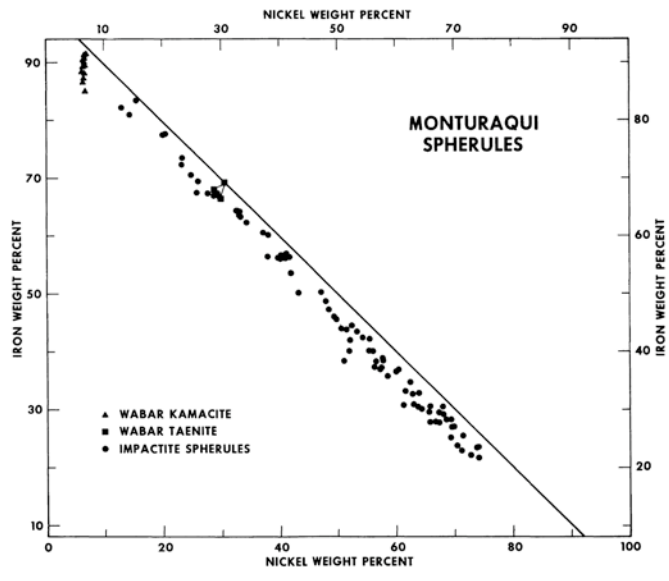


Figure 18: Nickel-Iron contents of 100 spherules < 35µm in diameter from Monturaqui Impact Crater. Wabar Impact Crater kamacite and taenite values were used as end members since no meteorite composition of Monturaqui is known. The Monturaqui meteorite is likely similar to the Wabar meteorite (Gibbons, 1976).

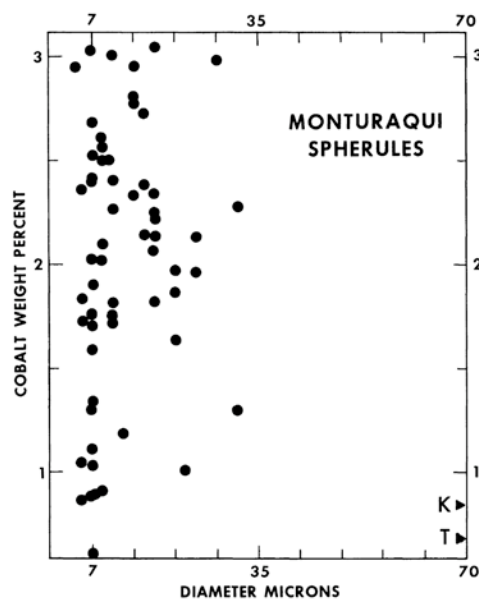


Figure 19: Cobalt variation compared to the spherule diameter in 100 spherules from Monturaqui Impact Crater (Gibbons, 1976).

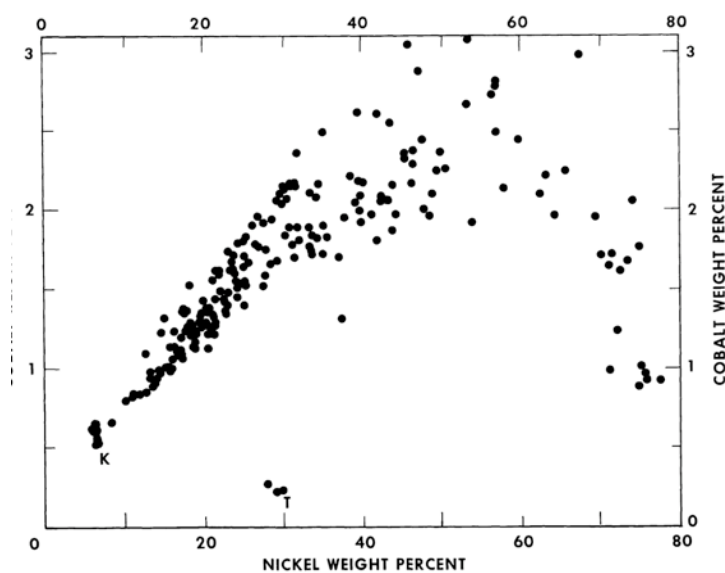


Figure 20: Cobalt-Nickel variation from 450 spherules analyzed from Henbury (100), Wabar (250) and Monturaqui (100) Impact Craters. A small number of spherules lie outside the field with more than 3% Co and 80% Ni (Gibbons, 1976).

CHAPTER 3: METHODS

3.1 Field Work

Fieldwork was conducted in the Atacama Desert, Chile, at the Monturaqui Impact Crater on December 4-8, 2007. Figure 21 shows the route taken from San Pedro to the crater. The location given by Sanchez & Cassidy (1966), $23^{\circ} 55.6'S$, $68^{\circ} 16.7'W$ was not accurate and the crater is located at $S23^{\circ} 55' 37.5''$, $W068^{\circ} 15' 48.1''$. The mislocation might be due to Sanchez & Cassidy using less accurate base maps, which were not as accurate as using current GPS location systems.

The Ugalde et al (2007) geologic map (Figure 12a) was used as a guide to investigate areas of impact melt and target rocks during the sampling. Samples collected from the crater include (Figure 22) target rocks of ignimbrite (Figure 23), granite (Figure 24), and mafic dikes, along with light and dark impact melt. The target rocks (Figure 25) were collected from 1.3 km south outside the crater along a roadside outcrops, outcrops exposed along the rim of the crater, and the inner walls of the crater. The purpose of collecting target rock outside the crater was to evaluate the changes due to impact shock through petrological differences between shocked and unshocked samples. The ignimbrite overlies the granite and was abundant along the rim of the crater and as fragments on inner walls of the crater. The granite was less frequently outcropping on the rim of the crater and found as less abundant fragments on the inner walls of the crater.

Hematite veins (Figure 26) were found outcropping in the unaltered granite outside of the crater along the roadside outcrops that were sampled. The hematite is a significant find

since it was not identified by previous studies (example: Bunch and Cassidy 1972) and might be a source for iron in the impact melts.

Ugalde's map showed 6 mafic and felsic dikes (Figure 12a) radially cutting the rim of Monturaqui crater. We identified 7 mafic dikes and no felsic dikes, and used measuring tape and Brunton compass measurements to constrain the width and orientations of the dikes (from 150° to 240° and ranging from 1 to 3 m thick).

One of the main targets of sampling was impactite material from the crater. In previous work the impactite was described as dark cindery aggregate up to 7 cm in diameter (Sanchez & Cassidy, 1966). The first day of fieldwork no dark cindery pieces were apparent, but there were fragments of light grey to clear vesicular and fluidal glassy fragments which we termed light impact melt and samples. After careful examination, the small pieces of dark aggregate material were identified. The impact melt did not form an ejecta blanket, but was generally patchy and widely dispersed and, where present, was mixed with fragments of granite, ignimbrite and light impact melt that covered the crater rim and flanks. The impact melt was collected along the rim of the crater, as well as the eastern and western flanks immediately outside the crater (Figure 22). The impact melt (Figure 27) ranges in sizes: length \leq 0.50 cm to 6.50 cm; width \leq 0.50 cm to 3.50 cm; height 0.25 cm to 4.50 cm; with the average of 1.95 cm length, 1.30 cm width, and 0.90 cm height. Approximately 15-20% of the impact melt found was light impact melt vs. 80-85% dark impact melt based on the number of melt fragments collected.

3.2 Thin Sections

Samples chosen for thin sections represent the full variability of the rock units inside and outside of the crater, in order to distinguish petrographic differences and impact features. Samples include (Figure 28): one granite from outside the crater that contained potassium and sodium feldspar, and two samples from inside the crater where the granite appeared to be bimodal with either potassium or sodium feldspar in hand sample to outcrop scale, but not both. Three ignimbrites (Figure 29) all exhibited a range in texture, from unwelded outside the crater to two samples from the crater rim that appeared to be re-melted to varying degrees. Seven mafic dikes (Figure 30), from within the crater, had a range in petrography and were eventually placed into three distinct groups. Three hematite samples (Figure 31) from outside the crater were chosen because they were found in the granite, but no hematite veins were observed in the granite outcrop within the crater. Four light impact melt clasts (Figure 32) from the crater rim showed a range in texture from ropy to vesicular. Three dark impact melt clasts (Figure 32) one from the crater rim and two from the flanks, ranged in iron amounts. Two metallic fragments that resembled the descriptions of iron shale (Sanchez & Cassidy, 1966; Ugalde et al, 2007) and were potential meteorite samples were also made into thin sections.

The samples were processed for thin sections in the Petrographic Facilities Laboratory at the University of Iowa, Geoscience Department in multiple rounds during January 2008-April 2008, July 2008 and September 2008. The samples were cut with a rock saw down to a 1 x 2 inch slab. Samples of friable or delicate material such as ignimbrite, or small samples such as potential iron shale, were mounted in epoxy for stability. Samples sit in an epoxy mixture overnight to fill in any vesicles, veins, or fractures. This is important to

help preserve sample texture during grinding. Samples are ground down to a flat, smooth surface using the lap wheel and grit plates. A few samples of small fragments were mounted in 1-inch epoxy pucks that can easily be used in the electron microprobe. The 1 x 2 inch bullets are glued to glass thin section slides using UV glue. Precise rock saws are used to saw most of the rock slab portion off the glass, then an Ingram Grinder and the grit plates are used again to polish the rock slab on the glass down to 30 microns. A few samples- such as the hematite slides- are kept thicker for possible future laser ablation work. For microprobing the thin sections are polished with micro-polishing cloths on the lap wheel instead of a cover slip.

Each thin section was examined on the petrographic microscope in transmitted and reflected light to identify minerals and textures. Petrographic descriptions were written for each thin section (see Appendix B) as well as photomicrographs of important textures and minerals. The electron microprobe analysis of the thin sections and 1-inch rounds will be discussed later in this chapter.

3.3 X-Ray Fluorescence

Monturaqui Crater target rocks were analyzed by XRF for major and trace element compositions. No whole rock data were collected for the dark melt impactite because it contained abundant lithic clasts and in hand samples were heterogeneous, this heterogeneity would impact the impact melt composition. The light melt impactite was analyzed for bulk composition, because it appeared to be more homogeneous than the dark melt impactite.

In April 2008 samples were cut down with rock saws, dried overnight, and crushed into smaller manageable 1-2 inch chunks with a rock hammer. A Brahn 'chipmunk' jaw

crusher was used to crush the pieces into smaller chips. The cleanest chips were then crushed to a powder using a Spex8505 Alumina shatterbox with an alumina puck. Cross-contamination was an issue and meticulous cleaning before and between samples tried to minimize this risk. Acetone was used to clean all machine parts and work areas after each sample was processed. A dry-vac was used to suction any unreachable dust within the machines and surrounding area. Plain sheets of paper were used to line the work area and transport samples from machine to machine and finally the plastic sample bags.

The powders were sent to Washington State University in May 2008 for XRF analysis. The machine used for trace and major element analysis is the ThermoARL Advant'XP+ sequential X-ray fluorescence spectrometer. For analysis, 3.5 grams of powdered sample is mixed with 7.0 grams of dilithium tetraborate ($\text{Li}_2\text{B}_4\text{O}_7$) and the mixture is put into a graphite crucible and fused into a glass twice. Glass beads are then run through the XRF using a Rhodium target run at 50kV and 50mA at full vacuum and a 25 mm mask for all samples and elements. For a more detailed description of sample processing see Washington State University Geoanalytical website (website listed in References). The major elements analyzed are: Si, Ti, Al, Fe, Mn, Mg, Ca, Na, K, P, SO_3 , Cl, and trace elements analyzed by ICP-MS are: Ni, Cr, Sc, V, Ba, Rb, Sr, Zr, Y, Nb, Ga, Cu, Zn, Pb, La, Ce, Th, Nd, U, Cs, As. The facility website states the standards used are USGS standard samples (PCC-1, BCR-1, BIR-1, DNC-1, W-2, AGV-1, GSP-1, G-2, and STM -1, using the values recommended by Govindaraju (1994).

3.4 Electron Microprobe

Thin section and epoxy pucks were analyzed at the University of Minnesota's Electron Microprobe Facilities on two trips in October 2008 and April 2009. The JEOL 8900 "Super Probe" Electron Probe Microanalyzer has five wavelength-dispersive, one energy-dispersive spectrometers and secondary and backscattered electron imaging capabilities. The samples were carbon coated with a JEOL JEE-420 Vacuum Evaporator. The target rocks of ignimbrite and granite were analyzed for oxides and mineral phases of biotite and feldspars. Impact melt was analyzed for glass composition. Metals were also analyzed, which included spherules in dark impact melt, hematite veins from the granite, and potential iron shale pieces.

The October 2008 trip: target rocks of ignimbrite and granite were analyzed for mineral phases of biotite and feldspars. Impact melt was analyzed for glass composition along with mineral phases of biotite and feldspars. Conditions for analysis included 15 kV accelerating voltage with a 20 nA beam and the diffusing beam was set to 5 microns. Each measurement was counted for 2 minutes. Analyses within individual minerals typically contained 4-5 points per grain. Line scans of 10 points were used for glass analysis to look for heterogeneous sections of the impact melt. Elements analyzed for this trip were: Na, Mg, Al, Si, Ca, K, Fe, S, Ni, Mn, F, Cl, Ti, and P. Standards used: hbl019, tek017, micro052, PbS, Ni metal, MnHa051, apatit003, and scapo031.

The April 2009 trip: the target rocks of ignimbrite and granite were analyzed for oxides. Spherules and oxides were also analyzed in the impact melt both light and dark. Hematite and meteorite samples for analyzed for metal content. Conditions for analysis included 15 kV accelerating voltage with a 20 nA beam and the diffusing beam was set to 1

micron. Each measurement was counted for 10 seconds. Typically oxide grains and spherules had one point set to gain as many data points as possible. Bigger spherules and metal phases had multiple points for analysis data of different phases. Elements analyzed for this trip were: S, P, Ti, Ca, Si, Al, Ni, Co Fe, Cu, Mn, and Cr, Standards used: FeS₂, apatit003, hbld19, Ni metal, Co metal, Cu metal, Mn metal, Cr metal, and CD and NA meteorites

3.5 Analytical Error/ Standard Error

3.5.1 XRF Data

The accuracy for the XRF data and precision of replicated analyses of the samples at Washington State University can be found in the publication by Johnson et al (1999) (<http://www.sees.wsu.edu/Geolab/note/xrf.html>). The USGS standard sample GSP-1 (Table 4) is used for comparison to the Monturaqui target rock XRF data. The material for GSP-1 was collected from a granodiorite in Colorado.

For ICP-MS trace element data the WSU website states “Long term precision for the method is typically better than 5% (RSD) for the REEs and 10% for the remaining trace elements. Analyses of USGS and international rock standards show good agreement with consensus values.”

3.5.2 Electron Microprobe Data

3.5.2.1. Standards for October 2008

The following standards were used for the October 2008 trip: hbld019, tek017, micr052, PbS, Ni Metal, apatit003, scapo31, and MnHor051. For hbld019 and micr052, three analyses each were performed before beginning the analysis on the Monturaqui samples. The

average values can be seen in (Table 5), the relative standard deviation is < 1% for SiO₂, MgO, and Al₂O₃, < 2% for Na₂O, TiO₂, and FeO, and < 3% for CaO and K₂O.

3.5.2.2 Samples for October 2008

The samples for the October 2008 trip included: biotite and feldspar phases for target rocks units granite and ignimbrite, the glass material in the ignimbrite, the glass material from the dark and light melt. In Table 6 the biotites and albite feldspar are shown from sample CCMK07013, an ignimbrite samples located outside the crater (Figure 22). The relative standard deviation for the biotites was < 3% for Si, Mg, and Fe, and < 4% for Al and K. The relative standard deviation for the feldspars was < 5% for Si, < 10% for Na and Al.

The biotites and albite feldspars are shown for sample CCMK0016 in Table 7, the granite sample located outside the crater (Figure 22). The relative standard deviation for the biotites was < 9% for Si, Mg, and Fe, and < 6% for Al. The relative standard deviation for the feldspars was < 1% for Si, < 2.5% for Na and Al.

The impact melt samples displayed in Table 8 are CCMK07046 for light impact melt and CCMK07045 for dark impact melt. The relative standard deviation for the light impact melt was < 4% for Si and Al, < 6% Fe and K. The relative standard deviation for the dark impact melt was < 4% for Al, < 5% for Si and < 15% for Fe.

3.5.2.3 Standards for April 2009

The metal and oxide analysis performed during the April 2009 trip used standards of pure metal and compounds from MicroAnalytical Consultants, that included Ni metal, Co metal, Cu metal, Mn metal, and Cr metal. Other standards were FeS₂, hlbd019, and apatit003. For the iron shale samples, a portion of the Canyon Diablo meteorite (Table 9) was analyzed for comparison.

3.5.2.4 Samples for April 2009

The CIUP08092 and CIUP08093 (Table 10) samples were analyzed and the relative standard deviation for Ni was < 3%, P was < 75.5%, Co < 26.5% and Fe < 16% for 092 and < 3% for 093.

3.5.3 Data Set

After each microprobe trip the data was filtered for analysis points that had low totals because the beam was not on the correct phase or was on the edge a crystal. The totals that were generally low (sum < 95% total weight) also tended to have totals off for individual elements and were discarded. Analysis points that stood out from the rest of the points of that phase could likely be the result of the beam hitting the edge of the crystal or another nearby phase which in turn threw off that analysis points numbers. The stoichiometry of the calculated mineral compositions was checked using the cation sum method as a means to check the robustness of each analysis. The cation sum is calculated using the formula $X * \text{moles of oxygen} / Y = \text{cation}$, where $X = \text{sum of cations}$ and $Y = \text{sum of oxygens}$. For example the number 8 is used to represent the number of moles of oxygen in the feldspar version of the formula. 'Sum of cations' is calculated by the data in wt.% /molecular weight of the oxide. This is divided by the 'sum of the oxygens' which was calculated by # of moles x # of oxygen. The cation sum for the feldspar structure should equal 5 ± 0.05 . Any data points that did not fit into this could be thrown out as bad data. The remaining data is normalized to 100 and is the data that will be used in the rest of the thesis.



Figure 21: Google map image with directions from Peine, Chile to the Monturaqui Impact Crater.

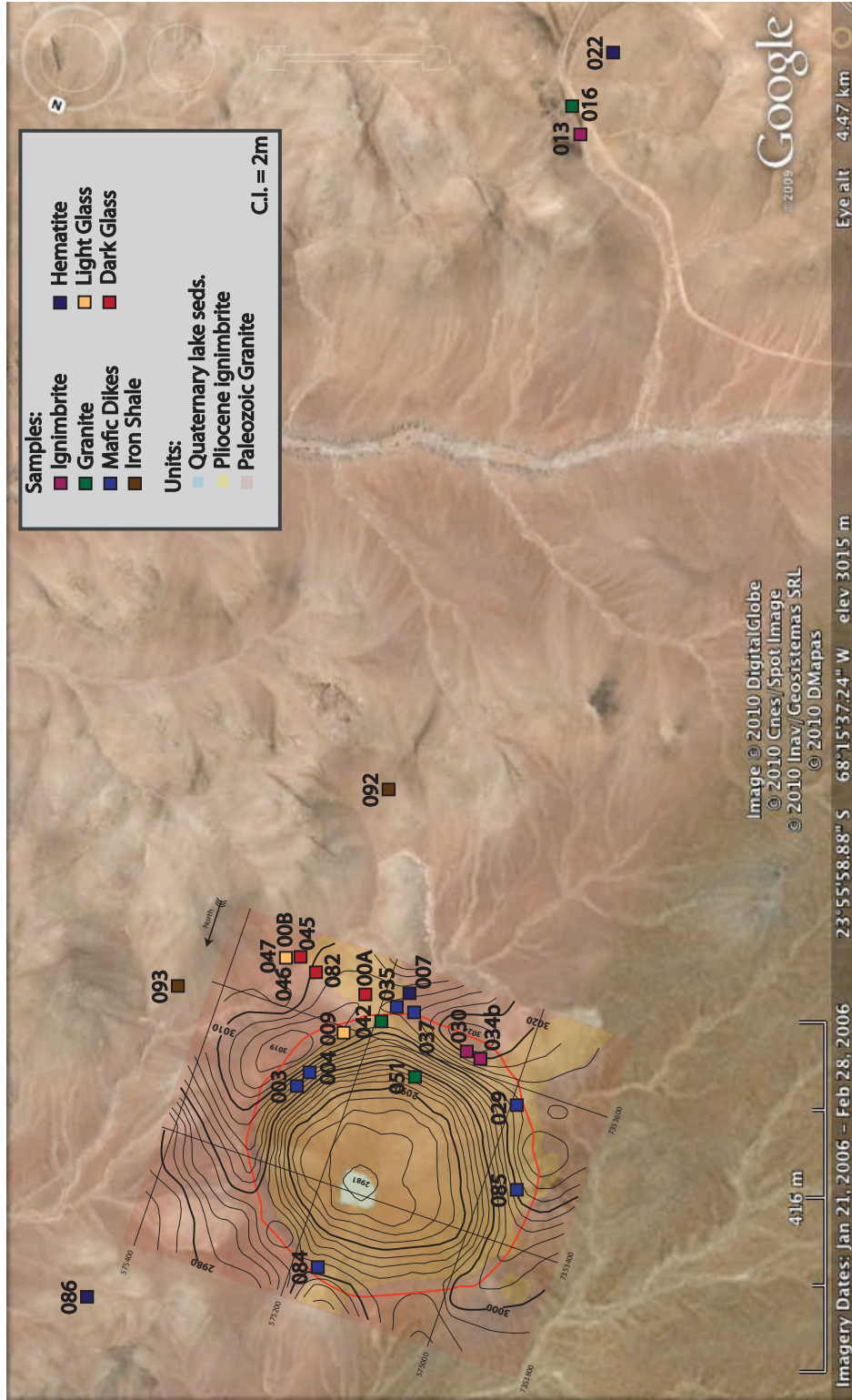


Figure 22: 2010 Google Image of Monturaqui Impact Crater, with all samples used for analysis from field season 2007 and 2008. Also granite and ignimbrite units are displayed to show elevation of crater.



Figure 23: Ignimbrite sample CCMK07034b, shown in the field at the rim of the crater.



Figure 24: Granite sample CCMK07042, shown in the field at the inside of the crater wall.



Figure 25: Field area shown in black box, approximately 1.3 km south of the crater where samples of target rocks, granite and ignimbrite and hematite veins were collected.



Figure 26: Hematite veins in granite outcrop located 1.3 km south of the crater. Sample CCMK07022, was collected from this location.

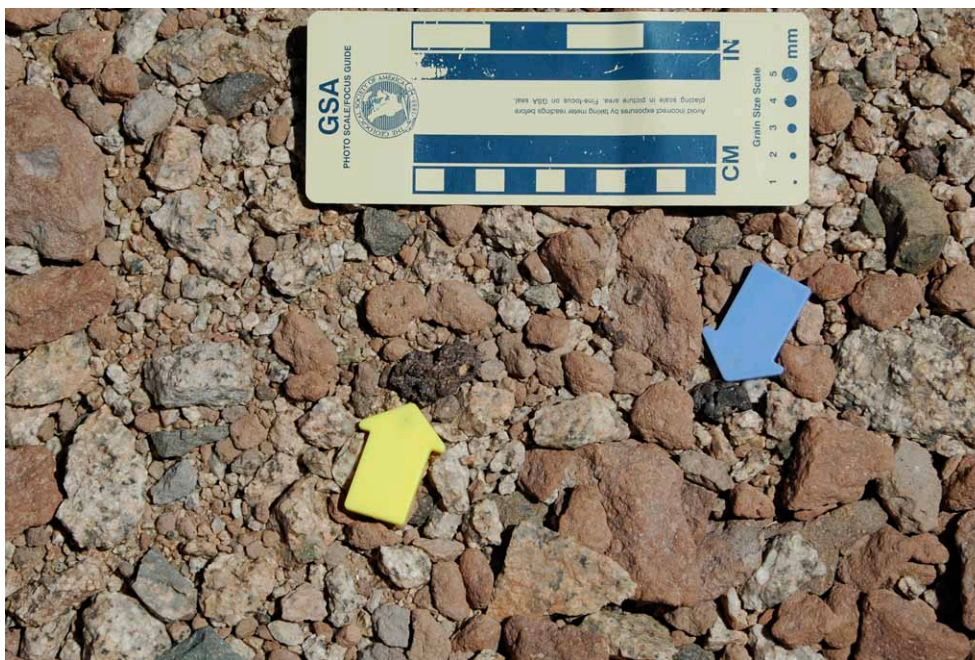
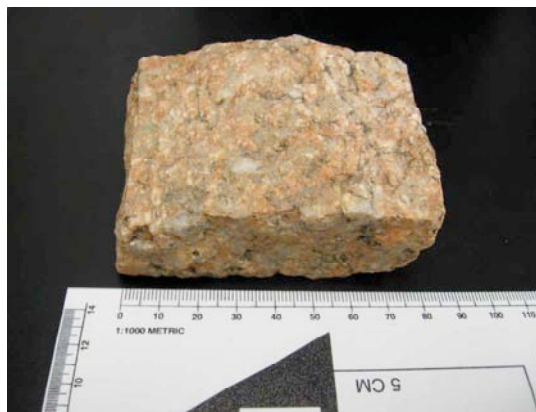


Figure 27: Dark impact melt among target rock debris on the outside of the crater on the eastern side.



A



B



C

Figure 28: Granite samples chosen for thin section and eventual XRF and electron microprobe analysis. A) CCMK07013 (located outside the crater), B) CCMK07042 (located inside the crater), C) CCMK07051 (located along the crater rim).



A



B



C

Figure 29: Ignimbrite samples chosen for thin section and eventual XRF and electron microprobe analysis. A) CCMK07016 (located outside the crater), B) CCMK07030, C) CCMK07034b (B & C both located along the crater rim.)

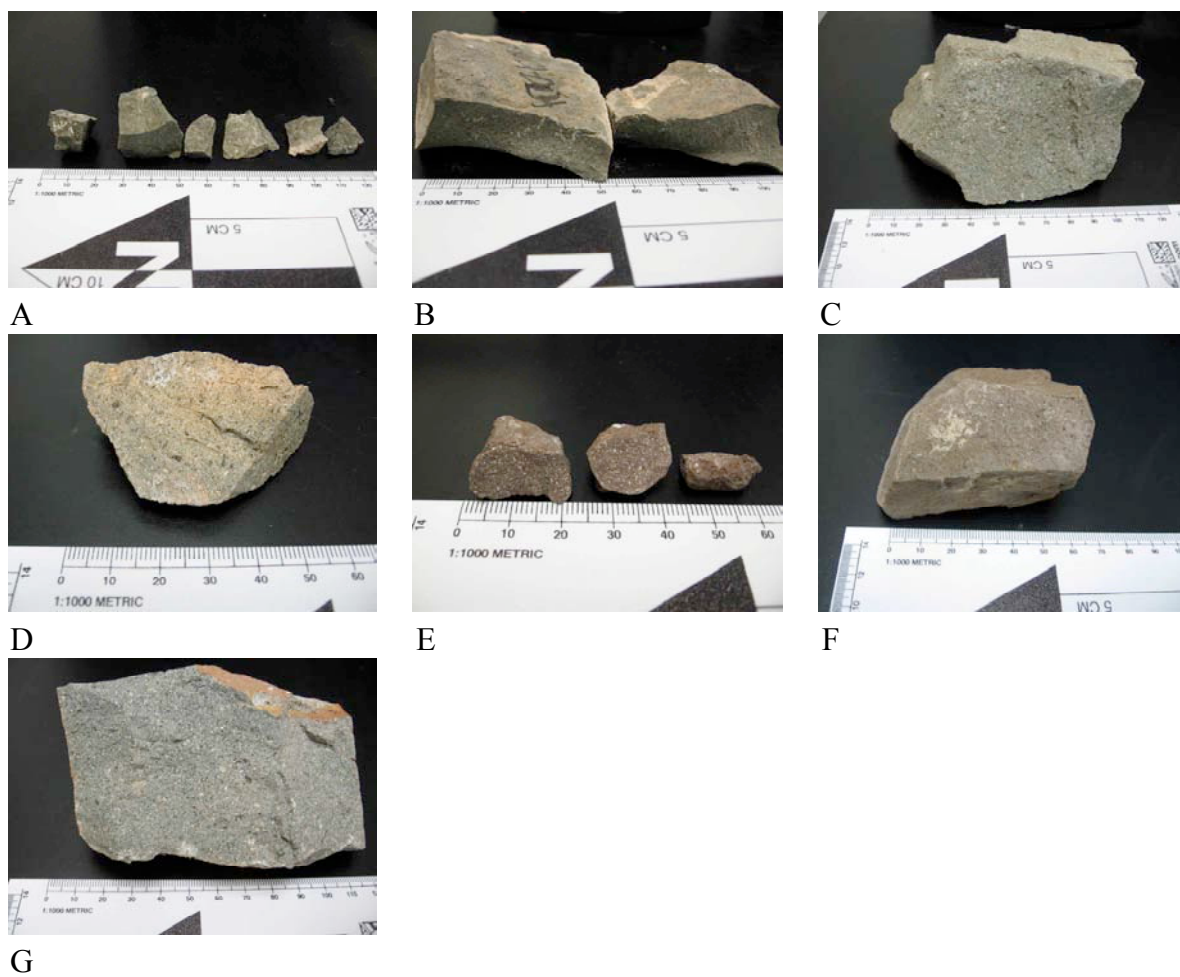
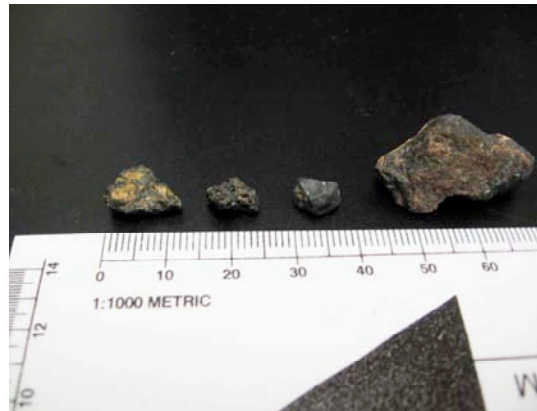


Figure 30: Mafic dike samples chosen for thin section and eventual XRF analysis. A) CCMK07003, B) CCMK07004, C) CCMK070029, D) CCMK07035, E) CCMK07037, F) CCMK07084, G) CCMK07085.



A



B



C

Figure 31: Hematite samples chosen for thick section and eventual electron microprobe analysis. A) CCMK07007 (located along the crater rim), B) CCMK07022 (located outside the crater), C) CCMK07086 (located outside the crater walls).

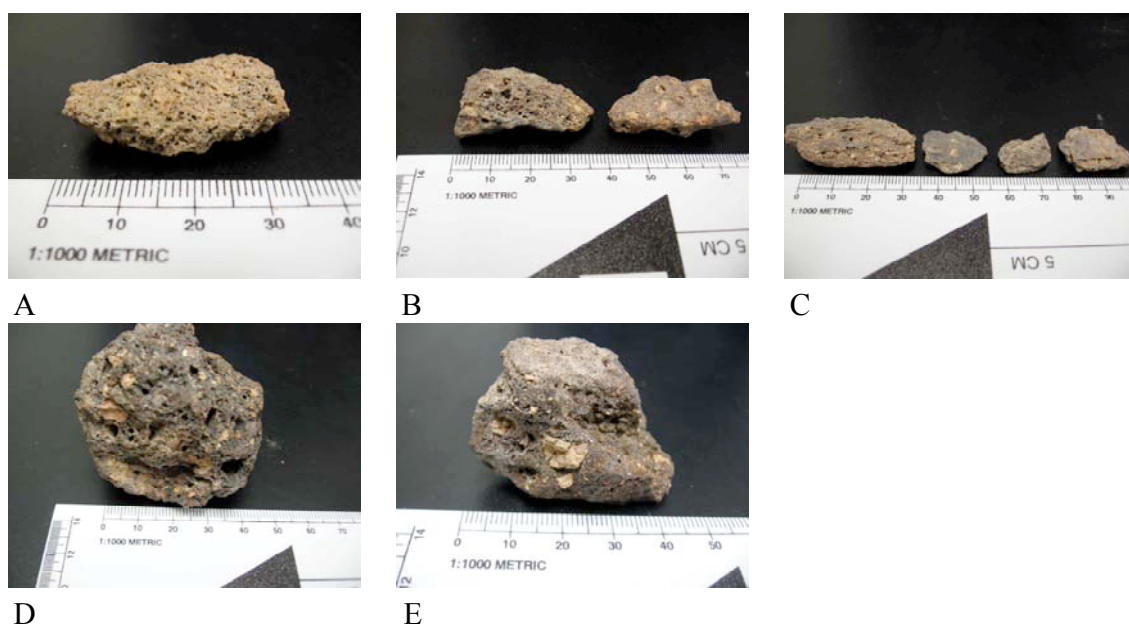


Figure 32: Impact melt samples chosen for thin section and eventual electron microprobe analysis. A) CCMK07009, B) CCMK07046, C) CCMK07047 (A-C Light melt), D) CCMK07045, E) CCMK07082 (both D and E Dark melt). Note: CCMK07A (dark) and CCMK07B (light) not shown.

Table 4: USGS standard GSP-1 from a granodiorite in Colorado used in the WSU lab publication.

	GSP-1			
	observed value	std. dev.	relative std. dev.	2σ std. dev.
SiO₂	68.45	0.18	0.26	0.36
Na₂O	2.91	0.05	1.72	0.1
TiO₂	0.667	0.004	0.60	0.008
NiO	16 ppm	1 ppm	--	--
MgO	1.1	0.1	9.09	0.2
CaO	2.02	0.01	0.50	0.02
Al₂O₃	15.35	0.11	0.72	0.22
FeO	3.86	0.01	0.26	0.02
K₂O	5.56	0.09	1.62	0.18
P₂O₅	0.287	0.003	1.05	0.006
MnO	0.038	0.001	2.63	0.002

Note: Observed and standard deviation data from Table 4 in Johnson et al (1999).

Table 5: Standards Micr052 and Hbld019 were each analyzed three times before analysis began on October 2008 electron microprobe trip.

		Electron Microprobe Standards					
		accepted value	observed value	std. dev.	relative std. dev.	% deviation	2σ std. dev.
SiO₂	micr052	64.69	63.78	0.43	0.68	-1.41	0.86
Na₂O	hbld019	2.60	2.75	0.05	1.75	5.84	0.10
TiO₂	hbld019	4.72	4.64	0.05	1.04	-1.71	0.10
NiO							
MgO	hbld019	12.80	12.85	0.02	0.13	0.43	0.03
CaO	hbld019	10.30	10.51	0.22	2.09	2.02	0.44
Al₂O₃	micr052	18.38	18.77	0.12	0.66	2.14	0.25
FeO	hbld019	7.95	10.98	0.19	1.73	38.05	0.38
K₂O	micr052	16.57	16.24	0.42	2.59	-1.97	0.84
P₂O₅							
MnO							

Table 6: Ignimbrite sample CCMK07013 biotite and feldspar observed values (averages) compared to the standards and their published values.

	Sample CCMK07013			Biotites			Sample CCMK07013			Albite Feldspar		
	accepted value	standard	observed value	std. dev.	relative std. dev.	% deviation	2 σ std. dev.	observed value	std. dev.	relative std. dev.	% deviation	2 σ std. dev.
SiO ₂	64.69	micr052	37.52	0.96	2.56	-41.99	1.92	60.35	2.46	4.08	-6.70	4.93
Na ₂ O	2.6	hbld019	0.75	0.06	8.57	-71.33	0.13	7.50	0.74	9.85	188.27	1.48
TiO ₂	4.72	hbld019	4.83	0.21	4.34	2.43	0.42	0.01	0.02	404.60	-99.89	0.04
NiO		Nimetal	0.00	0.05	-2260.85		0.09	0.01	0.04	525.54		0.08
MgO	12.8	hbld019	16.19	0.47	2.89	26.51	0.94	0.02	0.02	91.38	-99.84	0.04
CaO	10.3	hbld019	0.07	0.09	134.37	-99.36	0.18	6.29	1.96	31.15	-38.89	3.92
Al ₂ O ₃	18.38	micr052	13.63	0.54	3.96	-25.84	1.08	25.53	1.69	6.61	38.91	3.37
FeO	7.95	hbld019	13.54	0.34	2.49	70.33	0.67	0.31	0.05	15.49	-96.10	0.10
K ₂ O	16.57	micr052	8.90	0.27	3.01	-46.27	0.54	0.99	0.46	46.40	-94.02	0.92
P ₂ O ₅	40.78	apatite003	0.03	0.05	155.70	-99.92	0.10	0.00	0.02	436.08	-99.99	0.04
MnO	5.12	MNHoro51	0.24	0.06	23.24	-95.31	0.11	0.00	0.02	-819.65	-100.05	0.04

Table 7: Granite sample CCMK07016 biotite and feldspar observed values (averages) compared to the standards and their published values.

	Sample CCMK07016			Biotites			Sample CCMK07016			Albite Feldspar		
	accepted value	standard	observed value	std. dev.	relative std. dev.	% deviation	2 σ std. dev.	observed value	std. dev.	relative std. dev.	% deviation	2 σ std. dev.
SiO ₂	64.69	micr052	25.60	1.87	7.32	-60.42	3.75	66.95	0.50	0.75	3.49	1.01
Na ₂ O	2.6	hbld019	0.02	0.02	81.12	-99.08	0.04	11.25	0.26	2.31	332.68	0.52
TiO ₂	4.72	hbld019	0.12	0.09	76.93	-97.40	0.19	-0.01	0.03	-258.29	-100.21	0.05
NiO		Nimetal	-0.02	0.05	-235.41		0.09	0.01	0.03	376.11		0.05
MgO	12.8	hbld019	6.55	0.56	8.57	-48.83	1.12	0.01	0.02	178.65	-99.92	0.03
CaO	10.3	hbld019	0.07	0.05	72.52	-99.28	0.11	0.75	0.15	19.60	-92.70	0.29
Al ₂ O ₃	18.38	micr052	21.05	1.23	5.85	14.53	2.46	20.96	0.29	1.40	14.02	0.59
FeO	7.95	hbld019	33.30	2.71	8.13	318.81	5.41	0.05	0.06	138.74	-99.42	0.13
K ₂ O	16.57	micr052	0.71	0.91	129.04	-95.74	1.82	0.23	0.18	77.71	-98.63	0.35
P ₂ O ₅	40.78	apatite003	0.02	0.03	114.25	-99.94	0.05	0.01	0.02	392.01	-99.99	0.04
MnO	5.12	MNHoro51	2.05	0.34	16.77	-59.97	0.69	0.01	0.02	298.01	-99.85	0.05

Table 8: Light melt sample CCMK07046 and dark melt sample CCMK07045 observed values (averages) compared to the standards and their published values.

	Sample CCMK07046			Light Impact Melt			Sample CCMK07045			Dark Impact Melt		
	accepted value	standard	observed value	std. dev.	relative std. dev.	% deviation	2 σ std. dev.	observed value	std. dev.	relative std. dev.	% deviation	2 σ std. dev.
SiO ₂	64.69	micr052	71.95	2.22	3.08	11.22	4.44	53.21	2.63	4.94	-17.75	5.26
Na ₂ O	2.6	hbld019	2.40	0.31	12.82	-7.67	0.62	1.40	0.66	46.79	-46.01	1.31
TiO ₂	4.72	hbld019	0.18	0.04	19.57	-96.13	0.07	0.43	0.06	13.26	-90.93	0.11
NiO		Nimetal	0.01	0.03	278.91		0.07	0.04	0.09	245.46		0.18
MgO	12.8	hbld019	0.05	0.02	32.00	-99.61	0.03	1.54	0.35	22.36	-87.94	0.69
CaO	10.3	hbld019	0.27	0.04	15.83	-97.36	0.09	3.99	0.47	11.73	-61.26	0.94
Al ₂ O ₃	18.38	micr052	11.97	0.45	3.72	-34.88	0.89	12.64	0.47	3.73	-31.26	0.94
FeO	7.95	hbld019	0.90	0.05	5.69	-88.66	0.10	22.27	3.05	13.68	180.18	6.09
K ₂ O	16.57	micr052	5.58	0.31	5.53	-66.35	0.62	2.15	0.35	16.35	-87.01	0.70
P ₂ O ₅	40.78	apatite003	0.01	0.03	179.17	-99.97	0.05	0.09	0.07	73.97	-99.78	0.13
MnO	5.12	MNHoro51	0.04	0.03	75.10	-99.26	0.06	0.08	0.03	36.40	-98.44	0.06

Table 9: Canyon Diablo polished sample analyzed as a standard to compare samples in Table 7.

Canyon Diablo					
	accepted value	observed value	std. dev.	relative std. dev.	2 σ std. dev.
S					
Ti					
Si					
Ni	70.1 ug/g	6.25	0.50	7.93	0.99
Cu					
P		0.08	0.03	33.90	0.06
Ca					
Al					
Co		0.65	0.08	12.20	0.16
Mn					
Fe	922 mg/g	90.23	1.26	1.40	2.52
Cr					

Table 10: Potential meteorite samples CIUP08092 and CIUP08093 with observed values.

	Sample CIUP08092		Iron Shale		Sample CIUP08093		Iron Shale	
	observed value	std. dev.	relative std. dev.	2 σ std. dev.	observed value	std. dev.	relative std. dev.	2 σ std. dev.
S	0.00	0.00	47.14	0.00	0.03	0.01	31.55	0.02
Ti	-0.03	0.01	-43.80	0.02	0.00	0.03	-1156.27	0.06
Si	0.26	0.35	135.44	0.70	0.07	0.06	76.84	0.11
Ni	5.21	0.13	2.47	0.26	7.11	0.21	2.99	0.43
Cu	0.01	0.03	462.26	0.06	0.02	0.02	104.80	0.05
P	0.07	0.05	75.12	0.10	0.60	0.39	65.61	0.79
Ca	0.06	0.08	129.02	0.15	0.11	0.10	86.55	0.19
Al	0.14	0.19	140.91	0.39	0.09	0.09	100.73	0.18
Co	0.47	0.12	26.27	0.25	0.55	0.09	16.80	0.18
Mn	-0.04	0.04	-114.80	0.09	0.01	0.02	221.57	0.04
Fe	80.40	12.86	16.00	25.73	86.36	2.23	2.58	4.46
Cr	0.02	0.02	117.85	0.04	0.00	0.01	172.95	0.02

CHAPTER 4: DATA

4.1 Granite Data

4.1.1 Granite Field & Petrology Relationships

The granite forms the main basement unit in this area, and it is dated at 441 ± 8 Ma (Ugalde, 2007). It was sampled in three places both inside and outside the crater in order to assess any compositional heterogeneity and the impact of shock metamorphism. The sample localities (Figure 22) include 1.3 km south from the center of the crater (sample CCMK07016), along the crater rim (sample CCMK07042) and inside the crater (sample CCMK07051). There was minor variation in the granite mineralogy over the 1.3 km sampled, which is discussed below.

CCMK07016

The locality for sample CCMK07016 is 1.3 km south of the center of the crater. Granite outcrops appear along the roadside and through the surrounding small hills. Along the roadside a basalt dike intrudes granite, with the contact trending N-S. The contact is seen along the roadside in Figure 33 where sample CCMK07016 was taken. Brecciated hematite and quartz veins are present in the outcrops on the hillside to the west of the CCMK07016 sample site (see CCMK07022 on Figure 22 for hematite vein location). A mafic dike trending N-S is also found on this hillside. To the southeast of the CCMK07016 sample site, two parallel dikes are trending NW-SE (Figure 22). These mafic dikes range from 1 to 3 m in width.

The fresh surface of the hand sample CCMK07016 is pink, and on the surface is a rusty orange color from the weathering of oxides. The grains are medium to coarse in size.

The estimated modal mineral abundances of this hand sample are: 40% subhedral-anhedral plagioclase (2-4 mm), 25% anhedral quartz (2-4 mm), 20% subhedral potassium feldspar (< 2 mm), 10% subhedral biotite (0.5-2 mm), \leq 5% anhedral oxides (< 0.2 mm). Based on these modal estimates, this sample is a coarse-grained biotite granite.

Fractures are present in the outcrop along the fault and also in hand sample. In the thin section random fractures are seen through plagioclase and quartz grains. The fractures are not parallel sets of planar deformation features (Figure 34 & 35) like those that will be discussed in CCMK07042 and CCMK07051.

CCMK07042

The locality for sample CCMK07042 is along the southern portion of the crater rim, where the exposures of granite increase. To the west of the location are two parallel mafic dikes that are trending NW-SE, and further south over the crater rim is another NW-SE trending mafic dike. No hematite veins are observed at these outcrops.

The fresh surface of hand sample CCMK07042 is white, but most of the surface is weathered a rusty orange color. The grains are medium to coarse in size. The estimated modal mineral abundances of the hand sample collected along the southern rim of the crater are: 35% subhedral-anhedral plagioclase (0.10-2 mm), 25% anhedral quartz (2-4 mm), 20% subhedral-anhedral potassium feldspar (< 1 mm), 15% subhedral biotite (1-2.5 mm), and < 5% anhedral oxides (< 0.10 mm). Based on the modal estimates, this sample is a medium-grained biotite granite.

Planar deformation features are present in plagioclase grains. The original twinning in the feldspar is deformed and faulted along multiple parallel fractures (Figure 34a). The plagioclase in Figure 34b have many more parallel fractures that are much closer together

running through multiple grains. Quartz also shows PDF's, in Figure 34c, the plagioclase and quartz grains have parallel fractures running through multiple grains.

CCMK07051

The locality of sample CCMK07051 is on the inside of the south wall of the crater. The closest mafic dikes to this location are the same as described above for sample CCMK07042. No hematite veins are observed at this locality. The outcrops of granite inside the crater are weathered and rounded compared to those along the rim. The hand sample of CCMK07051 is freshly pink and has weathering of a rusty orange color. The grains are medium to coarse in size. The estimated modal mineral abundances of the hand sample from inside the crater wall are: 20% subhedral plagioclase (0.5-4 mm), 30% anhedral quartz (< 1-5 mm), 30% subhedral potassium feldspar (2-4 mm), 10% subhedral biotite (< 2 mm) and 10% anhedral oxides (< 0.10 mm). Based on these modal estimates, this sample is a coarse-grained biotite granite.

Planar deformation features are present within the plagioclase crystals, similar to CCMK07042. Figure 35a, has one set of fractures that are close together running parallel through the grains, and another set running perpendicular to the first set. Figure 35b has potential conversion of the plagioclase crystals to diaplectic glass or maskelynite. Also the plagioclase shows signs of alteration to sericite. The quartz grains exhibit multiple parallel deformation features decorated with fluid inclusions in Figure 35c. Non-planar deformation feature fractures are present through the hand sample and thin section, and are filled with components of quartz, feldspars and possible clay (Figure 35d).

The field locations of the granite samples have mafic dikes that are either trending N-S or NW-SE, there are also mafic dikes that run parallel to each other, both outside the crater

and along the rim. The hematite veins were observed at the locality 1.3 km outside the crater and not seen at either of the other two localities at the crater rim or inside wall.

The estimated modal abundances of the granites in hand sample differ from those seen in thin section samples. This is most likely a result of the coarse-grained nature of the granite and as a result the small area taken for thin section sample is not a completely accurate representation of the larger sample. The planar deformation features are found in quartz and plagioclase grains from samples CCMK07042 and CCMK07051, along the rim and inside the crater. The fracturing seen within the plagioclase grains increased in samples closer to the center of the crater. Potassium feldspars were identified with plaid twinning in thin section and were frequently located near biotite grains. The modal abundance of potassium feldspars in hand sample was larger than in thin section (20% vs. < 5%).

Approximately 50% of the biotites in each sample were altering to chlorite while the other 50% were unaltered. Biotites in CCMK07051 are altering to chlorite to a lesser degree than CCMK07016 and CCMK07042. The oxides in the granite samples were concluded to be hematite grains and will be further discussed in the geochemical section.

4.1.2 Granite Geochemical Data

4.1.2.1 Whole Rock by XRF & ICP-MS

XRF whole rock data showing major and trace element variations in the three granite samples that were analyzed are shown in Figure 36 and 37b. They are plotted with the XRF whole rock data of the ignimbrites and mafic dikes along with the averages. Based on the XRF whole rock data, the granite as a whole unit is a quartz-rich granitoid, using the IUGS classification scheme of phaneritic igneous rocks (Winter, 2001).

There are notable variations in compositional data for granite whole rock analyses (Figure 1): The SiO_2 content for granites lies at a range of 74.6-77.8 wt.% with the average at 76 wt.%. The granites as a whole have an Al_2O_3 content with a range of 12.9-13.8 wt.% with an average of 13.4 wt.%. The granites varied in Na_2O content (range 4.1-5 wt.%, average 4.4 wt.%), CaO content (range 0.3-2.3, average 1.2 wt.%), and in K_2O content (range 2.7-3.9 wt.%, average 3.2 wt.%).

Individual samples show differences based on location: CCMK07051 inside the crater has the lowest SiO_2 (74.6 wt.%) and the highest CaO (2.3 wt.%). This sample also has the highest Al_2O_3 (13.8 wt.%) and lowest Na_2O (4.1 wt.%). Sample CCMK07016 outside the crater has the highest SiO_2 (77.3 wt.%) and the lowest CaO (0.3 wt.%), and the lowest Al_2O_3 (12.9 wt.%). Sample CCMK07042 along the crater rim has the highest Na_2O (5 wt.%).

The un-normalized trace element data of the three granite samples on a log scale are plotted Figure 37a. The granite, ignimbrite and mafic dikes have many similar peaks but the granite show defined peaks in Ba from 363-718 ppm, and smaller peaks with Rb (79-121 ppm), Sr (48-142 ppm), Zr (57-86 ppm), Zn (17-45 ppm), and Ce (39-52 ppm).

4.1.2.2 Granite Mineral Compositional Data by EMP

Individual grains were analyzed by electron microprobe at the University of Minnesota Microprobe Lab as discussed in the Methods section. Feldspars, biotites and oxides were analyzed in each granite sample, and compositional variations are shown in Figures 38, 39, and 40.

Feldspar minerals were analyzed in all three granite thin sections, to assess any compositional heterogeneity among samples, as well as within individual samples and mineral grains. Four mineral grains were analyzed in each of the three thin sections, and five

points were analyzed in each mineral grain, for a total of 60 data points. Of these, 52 were deemed 'good data' and graphed in Figure 38.

Plagioclase compositional variations in the granite had little heterogeneity irrespective of sample location either outside or inside the crater. The plagioclase compositions range from anorthosite 0.6 to 5.2 and orthoclase 0.5 to 3.7, with albite of all plagioclase minerals ranging from 88.4 to 98.7. These feldspar grains classify as albite. The potassium feldspar was identified in only one sample of the 12 mineral grains analyzed. The potassium feldspar compositions from granite sample CCMK07042, range from anorthosite 0.0 to 0.1, orthoclase 92.6 to 97.8, and albite 2.1 to 7.2.

Biotite minerals were analyzed in all three granite thin sections and to assess any compositional heterogeneity among the samples as well as within the individual samples and mineral grains. Four mineral grains were analyzed in each of the three thin sections, and five points were analyzed in each mineral grain for a total of 60 data points. Of these, 56 were deemed 'good data' and graphed in Figure 39.

The biotite grains from CCMK07016 range in Mg# from 22.4 to 29 (Fe# 71 to 76.1), the biotite grains in CCMK07042 range in Mg# from 37.5 to 41 (Fe# 59 to 62.5), and biotite grains in CCMK07051 range in Mg# from 38.2 to 43 (Fe# 57 to 62). Although CCMK07016 has lower Mg# and higher Fe# than CCMK07042 and CCMK07051, all three samples are classified as having Fe-rich biotites with an average ratio of Mg# to Fe# of 29.6 to 70.4.

The oxides of the granite were analyzed in all three granite samples. Ten grains were analyzed for each of the three thin sections, with one point analyzed for each mineral grain, for a total of 30 points. The oxides have a high content of FeO (93-98 wt.%), and were determined to be hematite grains.

The major element compositional data for all the mineral phases that make up the granite along with the whole rock XRF granite sample average analysis are displayed in Figure 40. The individual phases demonstrate how they contribute to the whole rock composition. Quartz is a large contributor to the whole rock unit, as reflected by the SiO₂ content of the granites of 75-78 wt.%. The high Na₂O and K₂O contents in the whole rock granite samples show that the feldspars make a significant contribution to the unit also. The percentages found in hand samples agree (30-50% plagioclase and 5-30% potassium feldspar). The low (< 5 wt.%) MgO and FeO content in the whole rock granite samples show that the biotites do not make up as large a population as the feldspars, which agrees with the amounts found in hand sample (10 to 20%). The hematite is not abundant enough to affect the FeO content in the granites, and so is an accessory mineral.

4.2 Ignimbrite Data

4.2.1 Ignimbrite Field & Petrology Relationships

The ignimbrite unit was emplaced on the granite basement rock unit and is dated at 3.2 ± 0.3 Ma (Ugalde, 2007). It was sampled in three places both inside and outside the crater in order to assess any compositional heterogeneity and the impact of shock metamorphism. The sample localities include 1.3 km south from the center of the crater (sample CCMK07013) near the granite sample CCMK07016, and along the crater rim (samples CCMK07030 and CCMK07034b) southwest of the granite samples CCMK07042 and CCMK07051 collected in the crater (Figure 22). The ignimbrite samples are heterogeneous in hand sample with varying amounts of matrix and phenocrysts from each site. The variation in the ignimbrite mineralogy over the 1.3 km sampled is discussed below.

CCMK07013

The locality for sample CCMK07013 is 1.3 km south of the center of the crater. Fractures are present in the ignimbrite outcrops along the contact running between the granite and ignimbrite. This is the site where granite sample CCMK07016 was also collected (Figure 22). The fresh surface of the hand sample CCMK07013 is gray with fine-grained phenocrysts in a matrix of glass. In thin section the matrix is a gray brown color with vesicles. Portions of the glassy matrix display a welded texture with discernable ash shards (Figure 41). The biotite phenocrysts displayed pleochroism from green to light to dark brown. The plagioclase phenocrysts showed intergrowth between the grains. The estimated modal mineral abundances from the hand sample south of the crater are: 85% glassy matrix, phenocrysts of 10% euhedral-subhedral plagioclase (0.5-2 mm), 5% euhedral-subhedral biotite (0.25-1mm), and <1% anhedral oxides (< 0.25 mm). Based on these modal estimates, this sample is a fine-grained biotite, plagioclase rhyolitic vitric tuff.

CCMK07030

The locality of the sample CCMK07030 is along the southern portion of the crater rim (Figure 22). Generally the ignimbrite outcrops around the crater rim and does not appear inside the crater like the granite exposures. The fresh hand sample surface of CCMK07030 is gray, and weathers to a light tan on the surface. The phenocryst grain size is medium with a glassy matrix. The glassy matrix displays increased melting and vesicles compared to CCMK07013 that is likely impact generated (Figure 42). The phenocrysts of biotite show the same pleochroism as CCMK07013. The estimated modal mineral abundances of the hand sample along the southern portion of the crater rim are: 71% glassy matrix, phenocrysts of 20% euhedral-subhedral plagioclase (0.25-1.5 mm), 7% euhedral-subhedral biotites (0.25-1

mm), 1 % subhedral pyroxenes (≤ 0.25 mm), 1% anhedral oxides (< 0.05 - 0.25 mm). Based on these modal estimates, this sample is medium-grained biotite, plagioclase rhyolitic vitric tuff.

The plagioclase grains show distinct planar features that were not seen in the sample from outside the crater. The planar deformation features found in CCMK07030 are multiple sets of fractures that run parallel and perpendicular to each other (Figure 42).

CCMK07034b

The locality of sample CCMK07034b is from the southern portion of the crater rim south of CCMK07030 (Figure 22). The fresh surface of CCMK07034b is pink, with an outer orange weathered surface. The phenocryst grains are fine to medium, the matrix displays gradation of melting with more vesicles than the previous two samples. The modal mineral abundances are: 88% glassy matrix, 7% euhedral-subhedral plagioclase (0.25-1.75 mm, 8-9 mm), 3% subhedral biotites (≤ 0.50 mm), 1% subhedral pyroxenes (≤ 0.25 mm), and $<1\%$ anhedral oxides (< 0.20 mm). Based on these modal estimates, this sample is medium-grained biotite, plagioclase rhyolitic vitric tuff.

The vesicles are larger than in samples CCMK07013 and CCMK07030 and have irregular shapes and sizes (up to 1 mm) throughout the matrix (Figure 43). The planar deformation features in CCMK07034b show multiple parallel fractures throughout the plagioclase grains in Figure 43 like the grains in CCMK07030.

The estimated modal abundances of the ignimbrites in hand sample matched closely with those found in thin section samples. CCMK07034b shows increased welding on the ignimbrite outcrops both from the center of the massive outcrops on the crater rim towards

outer surfaces, as well as from the base of the massive outcrops towards the uppermost surfaces.

4.2.2 Ignimbrite Geochemical Data

4.2.2.1 Whole Rock by XRF & ICP-MS

XRF whole rock data showing major and trace element variations in the three ignimbrite samples that were analyzed are shown in Figure 36 and 37a. They are plotted with the major element data of the granites and dikes along with the averages of each rock type. Based on the XRF whole rock data, the ignimbrite is classified as a rhyolite using the IUGS classification scheme of volcanic and pyroclastic rocks (Winter, 2001). The ignimbrite samples show a limited compositional range of SiO₂ of 73.7-74.5 wt.% (average at 74.2 wt.%), Al₂O₃ of 13.1-13.8 wt.% (average of 13.38 wt.%), Na₂O of 3.7-4.0 wt.% (average 3.8 wt.%), CaO of 1-1.2 wt.% (average 1.1 wt.%), and K₂O of 4.9-5.3 wt.% (average 5 wt.%). The ignimbrite has higher Al₂O₃, CaO, K₂O and lower SiO₂ and Na₂O than the granite.

The un-normalized trace element data for the three ignimbrite samples are plotted on a log scale in Figure 37b. The ignimbrite showed defined peaks in Ba from 635-718 ppm, and smaller peaks with Rb (182-191 ppm), Sr (97-129 ppm), Zr (230-249 ppm), and Ce (89-93 ppm). The ignimbrite has higher Ba, Rb, Zn, Zr, Ce, La, Th, and Nd, with only lower Sr than the granite.

4.2.2.2 Ignimbrite Mineral Compositional Data by EMP

Compositions of feldspars, biotites and oxides were analyzed by electron microprobe in each ignimbrite sample, and are graphed in Figures 44, 45, and 46.

Feldspar minerals were analyzed in all three ignimbrite thin sections to assess any compositional heterogeneity among samples, as well as within individual samples and

mineral grains. Four to five mineral grains were analyzed in each of the three thin sections, and five points were analyzed in each mineral grain, for a total of 65 data points. Of these, 61 were deemed 'good data' and graphed in Figure 44.

Plagioclase compositional variations in the ignimbrite were less heterogeneous than the plagioclase compositions in the granite. The plagioclase compositions range from anorthosite 18.2 to 48.1, orthoclase 1.9 to 10.2, and albite 50 to 72.6. The ranges show all three ignimbrite samples are dominated by albite feldspars like the granite, although the albite content in the ignimbrites is lower than the granite albite content.

Biotite minerals were analyzed in all three ignimbrite thin sections and were analyzed to assess any compositional heterogeneity among the samples as well as within the individual samples and mineral grains. Four mineral grains were analyzed in each of the three thin sections, and five points were analyzed in each mineral grain for a total of 60 data points. Of these, 57 were deemed 'good data' and graphed in Figure 45.

The biotite grains in CCMK07013 have a range of Mg# from 66.1 to 69.5 (Fe# 30.1 to 34), in CCMK07030 the biotite grains range in Mg# from 67.3 to 70 (Fe# 30 to 33.7), and the biotite grains in CCMK07034b range in Mg# from 67.5 to 70 (Fe# 30.2 to 32.5). The Mg# and Fe# composition in all three samples are generally the same, these biotites differ from the granite biotites because they are more Mg rich. The average ratio of Mg# to Fe# is 62.3 to 32.8.

The oxides of the ignimbrite were analyzed in all three ignimbrite samples. Ten grains were analyzed for each of the three thin sections, with one point analyzed for each mineral grain, for a total of 30 points.

The oxides of the ignimbrite were chemically identified to be magnetite and ilmenite grains. The FeO content in both minerals (43-53 wt.% in ilmenites and 83-92 wt.% in magnetites) does not seem to influence the whole rock chemically in Figure 46. These confirm the small percentages found in hand samples indicating oxides are accessory minerals.

The ignimbrite glassy matrix was analyzed in all three ignimbrite samples. Each sample had two lines of ten data points through the glassy matrix, for a total of 60 data points, 34 were deemed 'good data' and graphed with the ignimbrite components in Figure 46.

The glassy matrix that makes up a large percentage of the ignimbrite is high in SiO₂ (64-76 wt.%), which influences the SiO₂ content of the whole rock ignimbrite data shown in Figure 36. The Al₂O₃ range of 12-23 wt.%, Na₂O (2-5.5 wt.%) and K₂O (5.5-9 wt.%) also influence the whole rock data. The higher amounts of Na₂O and K₂O (as opposed to MgO and FeO) would indicate that feldspars, particularly albite make a bigger contribution to the whole rock composition than the biotites do.

The major element compositional data for all the mineral phases that make up the ignimbrite unit along with the whole rock ignimbrite averages are displayed in Figure 46. The individual minerals in Figure 46 demonstrate how they contribute to the whole rock unit. SiO₂ is a large contributor to the whole rock composition, which is reflected by the SiO₂ content of the ignimbrites to of 75-78 wt.%. This SiO₂ is most likely coming from the glassy matrix, SiO₂ (64-76 wt.%). The Na₂O content in the whole rock ignimbrite samples is influenced by the higher amount of Na₂O in the feldspars. The percentages found in hand samples agree with this (7-20% plagioclase). The high K₂O contents (8-9.5 wt.%) from the

biotites influence the whole rock unit as well. The matrix also contributes to the Na₂O and K₂O content in the whole rock ignimbrite unit. The low (< 2 wt.%) MgO and FeO content in the whole rock ignimbrite samples show that the biotites do not make up as large of a volumetric component in the ignimbrite as the feldspars, which agrees with the amounts found in hand sample (3-7%). Therefore the feldspars and glassy matrix are in greater modal abundances than the biotites. As mentioned before the oxides that were determined to be magnetite and ilmenites do not directly affect the chemical abundances of the whole rock ignimbrite samples.

4.3 Mafic Dikes

4.3.1 Mafic Dike Field & Petrology Relationships

Mafic dikes were sampled around and inside the crater, orientation of trends were taken for each location. Six dikes were previously mapped by Ugalde (2007). During the 2007 field season we discovered a new mafic dike within the vicinity of the crater that was not on previous maps (CCMK07035). All of the mafic dikes are from 1-3 meters in width.

Mafic Dike Group 1:

Three of the mafic dikes are grouped together based on similar SiO₂ values (average 52 wt.%) and similar bearings. These mafic dikes are located on the north and eastern sides of the crater. According to the chemical classification of volcanics from Winter (2001) group 1 of the mafic dikes are categorized as olivine-phyric basaltic andesite.

CCMK07003

This mafic dike is located along the eastern rim of the crater, and it trends NW-SE (Figure 22). In hand sample, the surface is dark to light gray with greenish hues. The

estimated modal mineral abundances are: 90% groundmass, which is made up of inter-granular subhedral plagioclase crystals (≤ 0.25 - 0.5 mm), black anhedral oxides (< 0.25 - 0.10 mm) and 10% phenocrysts of euhedral to subhedral olivines (0.25 - 0.50 mm). The groundmass has a significant amount of brown oxidation from the oxides. The olivine phenocrysts are very altered with a pockmarked appearance (Figure 47) and have a yellowish green hue. Some olivines phenocrysts have been weathered out of the sample, but the groundmass still retains the euhedral void space of the former olivine crystal. Weathered olivines are altered to iddingsite (Figure 47).

CCMK07004

This mafic dike is located parallel to and slightly southwest of sample CCMK07003, trending NW-SE (Figure 22). The hand sample has a dark gray surface with visible light gray weathering. The estimated modal mineral abundances are similar to CCMK07003 with 90% groundmass, with inter-granular subhedral plagioclase crystals, black anhedral oxides (≤ 0.10 mm), subhedral olivines (≤ 0.15 - 0.25 mm); 10% phenocrysts of euhedral-subhedral olivines (≤ 0.5 - 1 mm). There is less brown oxidation in the groundmass compared to CCMK07003. The olivine phenocrysts are very altered and the weathered crystals are not as easily identifiable in the hand sample as for CCMK07003 (Figure 48).

CCMK07084

This mafic dike is located to the north of CCMK07003 and CCMK07004 trending slightly NE-SW (Figure 22). The hand sample is weathered to a red brown color. The estimated modal abundances are: 70% groundmass, which is made up of inter-granular subhedral-anhedral plagioclase crystals (≤ 0.25 mm); 20% phenocrysts of subhedral plagioclase (0.75 - 1 mm); 5% phenocrysts of subhedral olivines (≤ 1 mm); 5% black anhedral

oxides (≤ 0.25 mm). There is brown to orange weathering around the plagioclase crystals, both in the groundmass and phenocrysts. This mafic dike is classified in the same group as the olivine-phyric samples based on silica content and has a similar trend. This sample has olivine + plagioclase phenocrysts, and therefore based on mineralogy could be considered different from CCMK07003 and CMMK07004.

Mafic Dike Group 2:

The next three mafic dikes are classified together with similar SiO₂ contents, with an average of 59 wt.%. They are located on the western and southern sides of the crater rim. The chemical classification for group 2 of the mafic dikes are classified as hornblende-olivine andesite (Winter, 2001).

CCMK07029

This mafic dike is located is southwestern rim of the crater trending slightly NE-SW (Figure 22). The hand sample has a gray fresh surface and is weathered to a brown color. The estimated modal mineral abundances are: 50% groundmass, which is made up of subhedral-anhedral plagioclase (< 0.10 mm) and black anhedral oxides (≤ 0.10 mm); 25% phenocrysts of subhedral hornblendes (0.25-1.5 mm), 15% phenocrysts of euhedral-subhedral olivines (0.25-0.75 mm), and 10% phenocrysts of euhedral to subhedral plagioclase (≤ 1 mm). The groundmass has red brown oxidation along fractures and gray to light brown alteration. The hornblendes display pleochroism from light green to green. The plagioclase crystals are weathered out but retain a grain-shaped void (Figure 49).

CCMK07035

This mafic dike is located along the south rim of the crater trending NW- SE (Figure 22). The hand sample is gray on the fresh surface and light brown on weathered surfaces. The

estimated modal mineral abundances are: 60% groundmass, which is made up of microcrystalline gray and brown crystals and black anhedral oxides (< 0.10 mm); 20% phenocrysts of subhedral hornblendes ($\leq 1-2.5$ mm); 10% phenocrysts of euhedral-subhedral olivines (≤ 0.75 mm); and 10% phenocrysts of euhedral-subhedral plagioclases (0.5 mm). The plagioclase phenocrysts altered to sericite, but the shape of the original grain boundary is preserved.

CCMK07085

This mafic dike is located along the western rim of the crater trending slightly NE-SW (Figure 22). The hand sample is gray on fresh surfaces and brown on weathered surfaces. The estimated modal mineral abundances are very similar to CCMK07029: 45% groundmass, which is made up of microcrystalline brown-gray crystals and black anhedral oxides (0.25 mm); 30% phenocrysts of subhedral hornblende (4 mm); 15% phenocrysts of euhedral olivine (1 mm); 10% phenocrysts of anhedral plagioclase (≤ 1 mm). The phenocrysts are very similar to those of CCMK07029, the hornblendes are pleochroic, the plagioclases crystals are weathered away with boundaries left intact. The olivines are more altered than those found in CCMK07029.

Mafic Dike Group 3:

CCMK07037

This mafic dike is located parallel to the east of sample CCMK07035, also trending NW-SE (Figure 22). The hand sample is dark red likely due to oxidation. The estimated modal mineral abundances are: 60% groundmass, which is made up of orange to red, brown and gray microcrystalline crystals and black microcrystalline oxides; 40% phenocrysts of euhedral olivines (≤ 0.50 mm). The majority of the olivines have been altered to iddingsite

and retain a grain boundary. Group 3 falls under the chemical classification of olivine-phyric trachy-basalt (Winter, 2001).

4.3.2 Mafic Dike Geochemical Data

4.3.2.1 Whole Rock by XRF & ICP-MS

XRF whole rock data showing major and trace element variations in the seven dikes samples that were analyzed are shown in Figure 1 and 2c. They are plotted with the XRF whole rock data of the granites and ignimbrites along with the averages. The dikes have a large range of SiO₂ content from 47-58 wt.%. This is a significantly lower SiO₂ content compared to granite and ignimbrite (~15 wt.%). The dikes have significantly higher abundances of FeO (range 5.9-10.7 ppm, average: 6 ppm), MgO (range: 3.7-7 ppm, average: 3.8 ppm), CaO (range: 5-8.8 ppm, average: 5 ppm), TiO₂ (range: 0.7-3 ppm, average 1.6 ppm) and P₂O₅ (range: 0.2-0.6 ppm, average: 0.2 ppm) than the ignimbrites and granites. The Na₂O (3-5 ppm) and Al₂O₃ (17.2-18.6 ppm) content is similar to the ignimbrites and granites.

The un-normalized trace element data of the seven dike samples are plotted on a log scale in Figure 37c. The units have many similar peaks but the dikes showed defined peaks in Ba from 506-1173 ppm, and smaller peaks with Ni (28-134 ppm), Cr (23-174 ppm), V (127-193 ppm), Sr (348-1024 ppm), Zr (102-303 ppm), and Zn (68-208 ppm), all of which are higher than the ignimbrite or granite.

4.4 Impactite

4.4.1 Impactite Field and Petrology Relationships

The impactite unit is comprised of a mixture of target rock material and meteoritic material. The impactite was sampled along the eastern side of the crater rim and down the

flanks of the crater to assess any heterogeneity (Figure 22). The impactite is divided up into two groups; light melt and dark melt, each is distinct in hand sample and geochemistry. The variation of the impactite mineralogy is discussed below.

Dark Melt:

CCMK0700A

The sample CCMK0700A is located along the crater rim on the southeastern side. The hand sample is a dark brown cindery texture and vesicular, with glassy melt and visible angular grains of plagioclase and metallic spherules. The glassy melt is visible in hand sample and dark brown, altered with oxidation. The plagioclase grains and metallic spherules are barely visible to the naked eye at ≤ 1 mm. The metallic spherules range from perfectly spherical to irregular in shape, Figure 50a and 50b show examples of the metallic and oxidized spherules with rims in plain polar light and reflected light. The estimated modal mineral abundances are: 50-65% glass, 20-30% subhedral plagioclase (≤ 1 mm), and 15-20% metallic and oxidized spherules (≤ 1 mm). The impactite classification scheme of Stöffler and Grieve (2007) for this sample is identified as an iron-rich proximal hypocrySTALLINE impact melt rock. CCMK0700A in thin section has pristine glass seen in Figure 51a, glass with schlieren in Figure 51b and the mixed glasses in Figure 51c show the presence of lechatelierite that mixes incompletely and produces the schlieren of silica in the glass.

CCMK07045

The sample CCMK07045 is located on the flanks to the southeast of the crater, on the eastern side of the gully. CCMK07045 was the largest sample collected at this site (4.5 cm long by 3.5 cm in width by 4.5 cm in height). The hand sample is dark brown to black cindery texture and vesicular, with glassy melt and visible angular grains of plagioclase and

metallic spherules. The glassy melt is visible in hand sample, dark brown to black and altered with oxidation. The plagioclase grains are visible and are fine grained (≤ 2 mm) and very altered. The metallic spherules are barely visible with a hand lens (≤ 10 mm), and weathered with red and orange stains. Not many spherules are perfectly spherical like those in CCMK0700A, most are irregular in shape. The estimated modal mineral abundances are: 55-60% glass, 35-40% subhedral plagioclase (≤ 2 mm), and 5% spherules metallic and oxidized spherules (≤ 10 mm). The impactite classification of Stöffler and Grieve (2007) identifies as an iron-rich distal hypocrySTALLINE impact melt rock. The glass is almost opaque in thin section, other patches are transparent and light to dark brown, most likely from oxidation staining (Figure 52a and 52b). The plagioclase grains in Figure 52 a,b,c all show multiple planar deformation features of multiple sets of fractures parallel and perpendicular to each other.

CCMK07082

The sample CCMK07082 is also located on the flanks of the southeastern side of the crater, closer to the crater rim than CCMK07045 on the western side of the gully. In hand sample it dark brown to black cindery texture and vesicular, with glassy melt and visible angular grains of plagioclase and metallic spherules. The glassy melt is visible in hand sample, dark brown to black and altered with oxidation. The plagioclase crystals are visible, fine-grained and stained from oxidation. The metallic spherules are similar to those in CCMK07045, they are not perfectly spherical, irregular in shape and are approximately ≤ 10 mm. The estimated modal mineral abundances: 50-60% glass, 40% subhedral plagioclase (0.5-1.5 mm), and $\leq 10\%$ altered spherules (≤ 10 mm). The impactite classification of Stöffler and Grieve (2007) identifies as an iron-rich distal hypocrySTALLINE impact melt rock.

The glass in thin section, like sample CCMK07045, is almost opaque but there are patches that are transparent and light to dark brown (Figure 53a). The plagioclase grains also show multiple planar deformation features of multiple sets of fractures parallel and perpendicular to each other (Figure 53b and 53d).

Light Melt:

CCMK0700B

The sample CCMK0700B is located on the southeastern flanks of the crater with samples CCMK07046 and CCMK07047 on the eastern side of the gully. In hand sample it is weathered tan to red purple color with visible angular grains of plagioclase and biotite. The sample has a glassy fluidal surface crust and internally vesicular. This would indicate that the sample was molten during transport and aerodynamically shaped. There are no spherules present in this sample. The estimated modal mineral abundances: 85% glass, (50-60% of the clear glass mixed with plagioclase grains (< 0.10 mm), and 20-25% of the glass has red staining from oxidation), < 10% euhedral to subhedral plagioclase (0.25-2.5 mm) and < 5% euhedral to subhedral biotite (0.25-1 mm). The impactite classification of Stöffler and Grieve (2007) identifies as distal hypocrySTALLINE ignimbrite impact melt rock. The glass in thin section is clear and mostly pristine with few patches of red staining (Figure 54). The plagioclase minerals did not have visible planar deformation features, which might be due to the small size of the sample and few grains present.

CCMK07009

The sample CCMK07009 is located on the southeastern edge of the crater rim. In hand sample it is tan, no surface crust like CCMK0700B and highly vesicular. The glassy melt is visible in hand sample with angular grains of plagioclase. There are no spherules

present in this sample. The estimated modal mineral abundances: 70% glass (clear with patches of plagioclase crystals (<0.10 mm)), 20% subhedral plagioclase (0.5-1.5 mm), and 10% grains of plagioclase altering to clay. The impactite classification of Stöffler and Grieve (2007) identifies as a proximal hypocrySTALLINE ignimbrite impact melt rock. The glass is mostly clear in thin section with patches of red staining (Figure 55a). The plagioclase grains show planar deformation features with multiple sets of features parallel and perpendicular to each other (Figure 55b).

CCMK07046

The sample CCMK07046 is located on the flank to the southeast of the crater rim, in the vicinity of CCMK07047 and CCMK0700B on the eastern side of the gully. In hand sample it is weathered tan to purple with visible angular grains of plagioclase and biotites. The sample, like CCMK0700B, has glassy fluidal surface crust and is internally vesicular, this again would indicate that the sample was molten during transport and aerodynamically shaped. There are no spherules present in this sample. The estimated modal mineral abundances: 70-60% glass (clear with patches of plagioclase crystals (< 0.10 mm)), 25-30% euhedral to subhedral plagioclase (0.25-2.5 mm), and 5-10% euhedral to subhedral biotites (0.75-1 mm) with some alteration to chlorite. The impactite classification of Stöffler and Grieve (2007) identifies as a distal hypocrySTALLINE ignimbrite impact melt rock. The glass in thin section is clear with clusters of small plagioclase clusters and red brown staining (Figure 56a). The plagioclase grains show planar deformation features like CCMK07009 and CCMK0700B, with multiple sets of features parallel and perpendicular to each other (Figure 56b).

CCMK07047

The sample CCMK07047 is located on flanks to the southeast of the crater, with samples CCMK07047 and CCMK0700B on the eastern side of the gully. In hand sample it is weathered tan to purple with visible angular grains of plagioclase and biotites. The sample is like CCMK0700B and CCMK07046 and has the glassy fluidal surface crust and internally vesicular, but exhibits more of a ropy surface texture than the other two. There are no spherules present in this sample. The estimated modal mineral abundances: 70% glass (40% clear and 30% oxidized patches with anhedral plagioclase crystals (< 0.10 mm)), 15-20% subhedral plagioclase (0.5-2.5 mm), and 5-10% subhedral to euhedral biotites (0.5-2 mm). The impactite classification of Stöffler and Grieve (2007) identifies as a light distal glassy hypocrySTALLINE impact melt rock. The glass in thin section is clear with clusters of small plagioclase clusters and red brown staining (Figure 57a). The plagioclase grains show planar deformation features like CCMK07009, CCMK0700B, and CCMK07046 with multiple sets of features parallel and perpendicular to each other (Figure 57b).

4.4.2 Impactite Geochemical Data

4.4.2.1 Whole Rock by XRF & ICP-MS

The XRF whole rock data for the bulk light melt is plotted with the electron microprobe data for the light melt group in Figure 58. The bulk light melt is an average of multiple samples of the analyzed light melt. The bulk light melt has a composition of SiO₂ of 75.6 wt.%, Al₂O₃ of 12.3 wt.%, Na₂O of 3.3%, CaO of 1.2 wt.% and K₂O of 4.6 wt.%. Geochemically, the bulk light melt is similar to the XRF average ignimbrite target rock compositions SiO₂ of 74.2 wt.%, Al₂O₃ of 13.4 wt.%, Na₂O of 3.8%, CaO of 1.1 wt.% and K₂O of 5 wt.%. The un-normalized trace element data for the bulk light melt is also very

similar to the trace element data for the ignimbrite target rock except for higher Rb concentration of 496 ppm. XRF whole rock and trace element data was not conducted for the dark melt.

4.4.2.2. Impactite Compositional Data by EMP

Compositions for light and dark melt groups were analyzed by electron microprobe in each sample, and are graphed in Figures 58 and 59. A line of ten to twenty points was set up for each area analyzed on the thin sections. The sites of analysis were selected prior to analysis with the main target areas as pristine glass, showing color variations that could potentially reflect compositional variations.

Dark Melt

The samples, CCMK0700A, CCMK07045, and CCMK07082 were originally grouped together as dark melt, based on hand sample and thin section observations. The electron microprobe data illustrates that these samples are geochemically similar with distinct groups making up the melt (melted minerals with distinct maskelynite and lechatelierite, dark melt group 1- high FeO, and dark melt group 2- low FeO). The groups (Figure 59) within the dark melt support that the melt is heterogeneous.

Sample CCMK0700A had three lines of 10 test points and four lines of twenty points analyzed through out the thin section for a total of 110 data points. Of these, 60 points were deemed 'good data'. Sample CCMK07045 had four lines of twenty points analyzed through the thin section for a total of 80 points, and 38 were deemed 'good data.' Sample CCMK07082 had four lines of 10 points analyzed through the thin section for a total of forty points, and 18 were deemed 'good data'.

The data was identified based on the SiO₂ and FeO contents were identified as dark melt groups. Group 1 showed a range of SiO₂ from 50 to 51.8 wt.%, and FeO of 24.5 to 27 wt.%. Group 2 had a range of SiO₂ of 54 to 60.4 wt. % and FeO 18.7 to 21.9 wt.%. The SO₃ content in the dark melt is high with 0.64 wt.%, The NiO content is high with 0.93 wt.%, which may also be related to a meteorite component.

The remaining data was contributed to melted minerals that combined with the dark melt group 1 and dark melt group 2 as well as distinct maskelynite and lechatelierite. The maskelynite and lechatelierite points were identified by SiO₂ and Al₂O₃ ranges. The maskelynite group had SiO₂ from 66.2 to 77.6 wt.% with Al₂O₃ from 10.9-20.6 wt.%. The lechatelierite group had SiO₂ ranging from 90.5-99.8 wt.%. Data points were taken across the schlieren in the glass, which supports the SiO₂ range of lechatelierite mixing incompletely.

Light Melt

Samples CCMK0700B, CCMK07009, CCMK07046, CCMK07047 are classified as light melt due to thin section observations. The hand sample observations showed different textures for the samples, which indicated different results of projectile molten melt that was aerodynamically shaped. The electron microprobe data illustrates that these samples, along with the XRF bulk light melt, are all from the same group of melt geochemically.

Sample CCMK07009 had four lines of twenty points each for a total of 80 data points analyzed. Of these, 60 were deemed 'good data.' Sample CCMK07046 has two lines of ten points each for a total of 20 data points analyzed, and 19 points were deemed 'good data.' Sample CCMK07047 had two lines of 10 points each for a total of 20 data points analyzed, and 4 points were deemed 'good data'.

The SiO₂ content range for the light melt samples is from 76 to 78.5 wt.%, which is much higher than the SiO₂ ranges of the dark melts groups. The significant difference geochemically between the dark and light melt is the FeO content. The range in the light melt is 0.8 to 1.2 wt.%, much lower than the FeO ranges of the dark melts groups. The highest SO₃ and NiO contents in the light melt are 0.06 wt.% and 0.05 wt.%, much lower than the dark melt groups.

The average content of Al₂O₃ of 12.8 wt.%, Na₂O of 2.5 wt.%, CaO of 0.2 wt.%, and K₂O of 5.5 wt.% is similar to the XRF bulk light melt contents (SiO₂ of 75.6 wt.% Al₂O₃ of 12.3 wt.%, Na₂O of 3.3%, CaO of 1.2 wt.% and K₂O of 4.6 wt.%). The XRF bulk light melt data is graphed with the light melt electron microprobe data in Figure 58, showing that the bulk light melt is more closely related to the light melt than dark melt.

4.5 Iron Oxides, Meteorite, Spherules

4.5.1 Iron Oxides, Meteorite, Spherules Field and Petrology Relationships

The oxides at Monturaqui Impact Crater were sampled outside the crater 1.3 km to the south, along the crater rim, and outside the crater to the northeast during the 2007 field season. The meteorite samples were collected to the east and to the south of the crater rim during the 2008 field season.

Iron Oxides

CCMK07007

Sample CCMK07007 was collected along the crater rim (Figure 22) with other small dark oxides samples that had weak magnetism. CCMK07007 was less than a centimeter in diameter and had a dark black surface in hand sample.

CCMK07022

Sample CCMK07022 was collected 1.3 km south of the crater (Figure 22), west of the samples CCMK07013 and CCMK07016. The sample is 10 cm long by 3 cm wide and 3 cm in height, and was found near a granite exposure, which contained a vein of hematite and has quartz bands from 1-2cm in width layered throughout the sample.

CCMK07086

Sample CCMK07086 was collected to the northeast of the crater (Figure 22). The sample is 6.5 cm long by 3 cm wide and 3.5 cm in height. The hand sample is dark gray to black with orange weathering and quartz inclusions that range from 1-2 cm in width.

Meteorite**CIUP08092 and CIUP08093**

The term 'iron shale' was identified by Sanchez and Cassidy (1966) as previously stated, as weathered and oxidized fragments of meteorite. From this point forward the samples of CIUP08092 and CIUP08093 will be referred to as meteorite samples. The samples CIUP08092 and CIUP08093 (Figure 60a and 60b) were collected to the south and east of the crater respectively. The samples are each 2-3 cm in length and in hand sample are oxidized dark brown to red.

4.5.2 Iron Oxides, Meteorite, Spherules Geochemical Data**4.5.2.1 Iron Oxides, Meteorite, Spherules Mineral Compositional Data by EMP****Iron Oxides**

Samples CCMK07007, CCMK07022, and CCMK07086 were each sampled at 10 analysis points, for a total of 30 data points. Of these, 20 points were deemed 'good data'.

The average Fe composition for the metals was 97.2 wt.% and are identified as hematite. The average hematite composition is plotted in Figure 61 & 62 with the iron shale and spherules.

Meteorite

Samples CIUP08092 and CIUP08093 were each analyzed for at 10 analysis points for a total of 20 data points. Of these, 5 were deemed 'good data'. The average compositions are Ni 6.9 wt.%, Co 0.6 wt.%, Fe 91.7 wt.%, and S 0.02 wt.%. The Ni and S contents are important to identify possible meteoritic components. The average meteorite composition is plotted in Figure 61 & 62 with the hematite and spherules.

Spherules

The spherules in samples CCMK0700A and CCMK07045 were analyzed with a total of 210 points, average of one point per spherule. Of these, 108 were deemed 'good data'. The data used was chosen based off the totals of any samples > 90 wt.%.

The spherules in CCMK0700A were a mixture of perfectly spherical and altered shaped spherules. The widths of the spherules used ranged from 10-45 μm . The spherules in CCMK07045 were mainly altered spherules that were not perfectly spherical. The widths of the spherules used ranged from 10-100 μm . Over 75 of the spherules had some kind of alteration whether in shape or metallic appearance in reflected light. Twenty of the data points used were perfectly whole spherules. Approximately 16 of the total data points were spherules with elongated shapes creating a tail off the spherule. Only five of the data points that were used were taken from the rims of altered spherules.

The major elements of the spherules are graphed (Figure 61 and 62) with the meteorite samples, hematite samples and the meteorite standard Canyon Diablo. The spherules at > 90 wt.% totals have the average composition of Fe 76.1 wt.%, Ni 21.8 wt.%,

Co 1.5 wt.%, and S 0.2 wt. %. The spherules Ni and Fe compositions are seen to have a wide range in Figure 61 and 62, Fe ranges from 49 to 89 wt.% and the Ni content ranges from 9 to 49 wt.%. Explanations for these wide ranges are discussed in the next chapter.

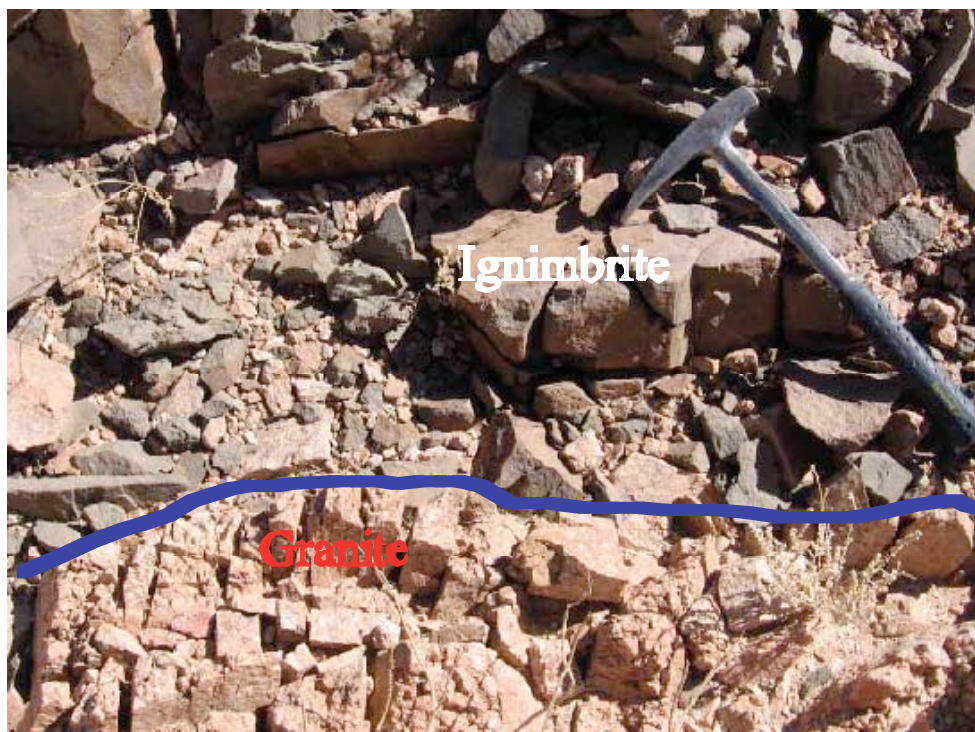
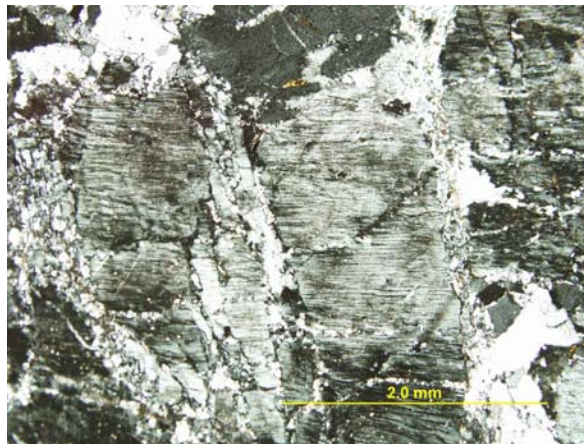


Figure 33: Location of CCMK07013 (Ignimbrite) and CCMK07016 (Granite) samples, where visible contact (purple line) along roadside exposures of ignimbrite and granite.



A



B



C

Figure 34: Planar Deformation Features of CCMK07042 (Granite). A) The plagioclase grain with original twinning is deformed by the multiple parallel fractures. The scale bar is 500 μm . B) Parallel fractures running horizontally through multiple quartz and plagioclase grains. The scale bar is 2.0 mm. C) Another example of quartz and plagioclase with parallel fractures running horizontally through multiple grains. The scale bar is 500 μm .

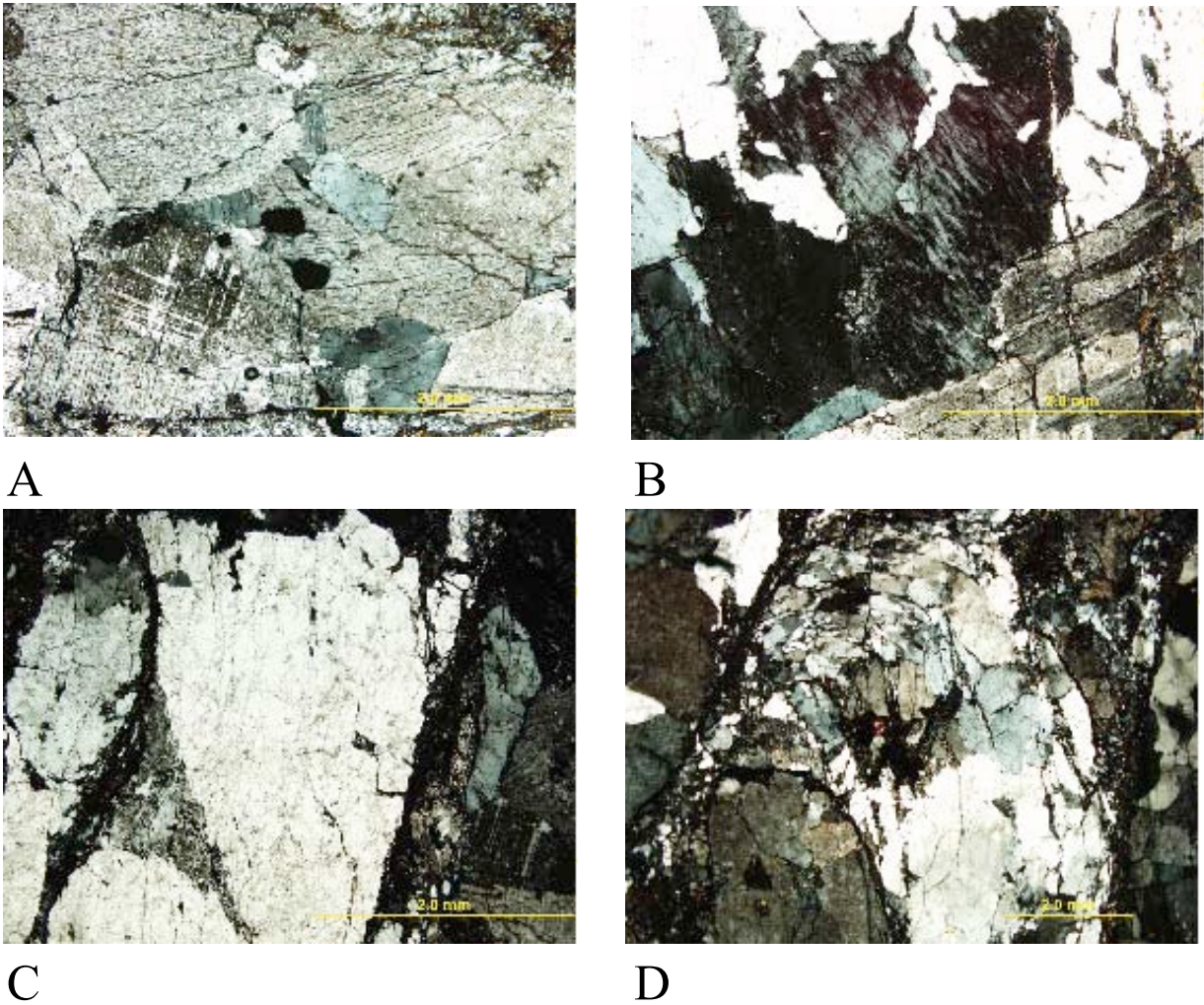


Figure 35: Planar deformation features in sample CCMK07051 (Granite). The scale bar for each picture is 2.0 mm. A) Parallel fractures running horizontally through multiple grains, with another set of fractures running perpendicular in the bottom left grain. B) Plagioclase grains (dark) turned into diaplectic glass (maskelynite). C) Quartz grains that exhibit decoration of fluid inclusions in multiple sets of fractures. D) Non-planar deformation features, fractures with in the sample itself are filled with smaller grains made up of quartz, feldspars and possible clay.

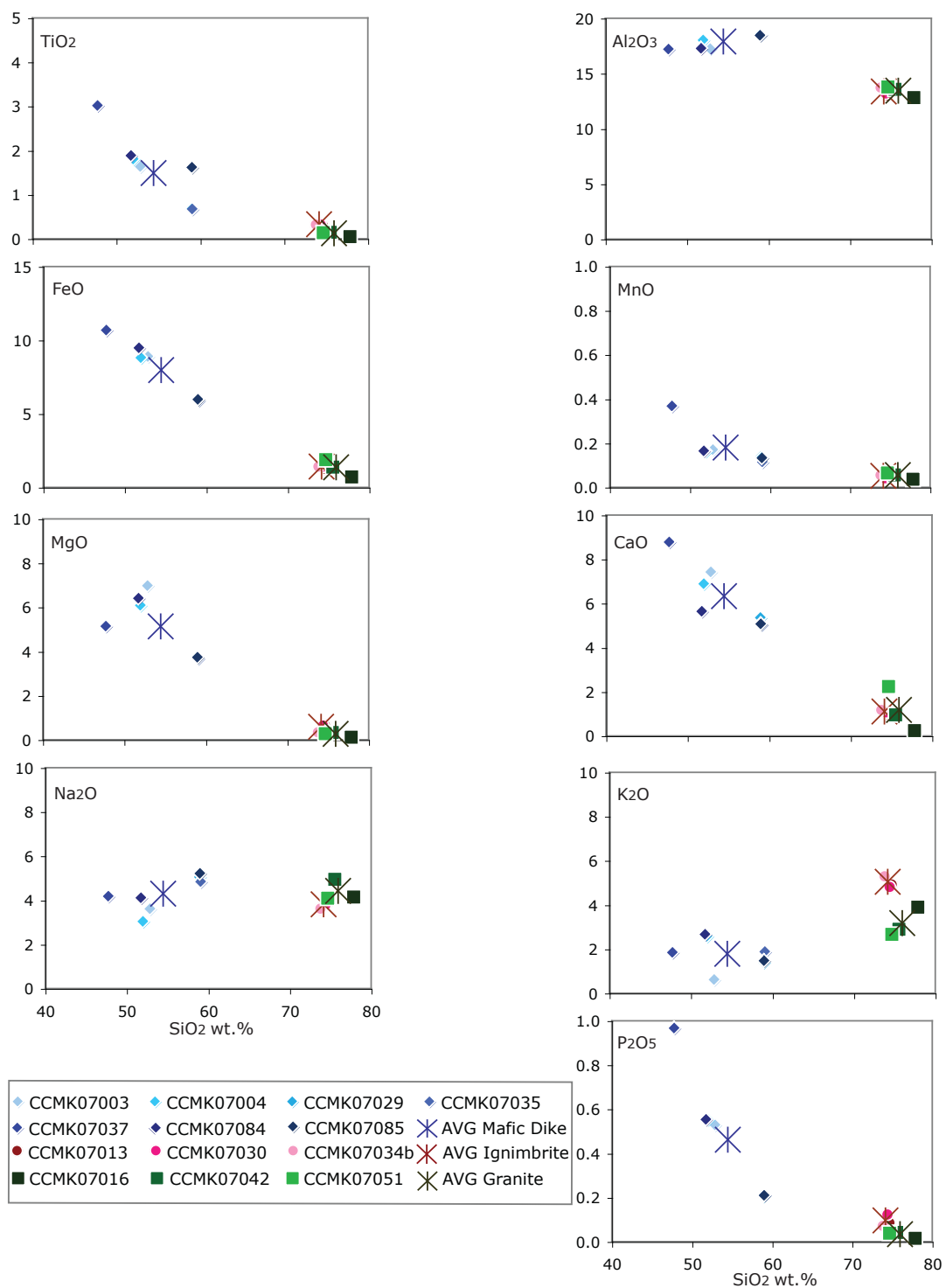


Figure 36: XRF whole rock major element data graphed to show individual sample concentrations and averages for each unit. Mafic dikes are in blue, ignimbrites are in pink/red and granites are in green.

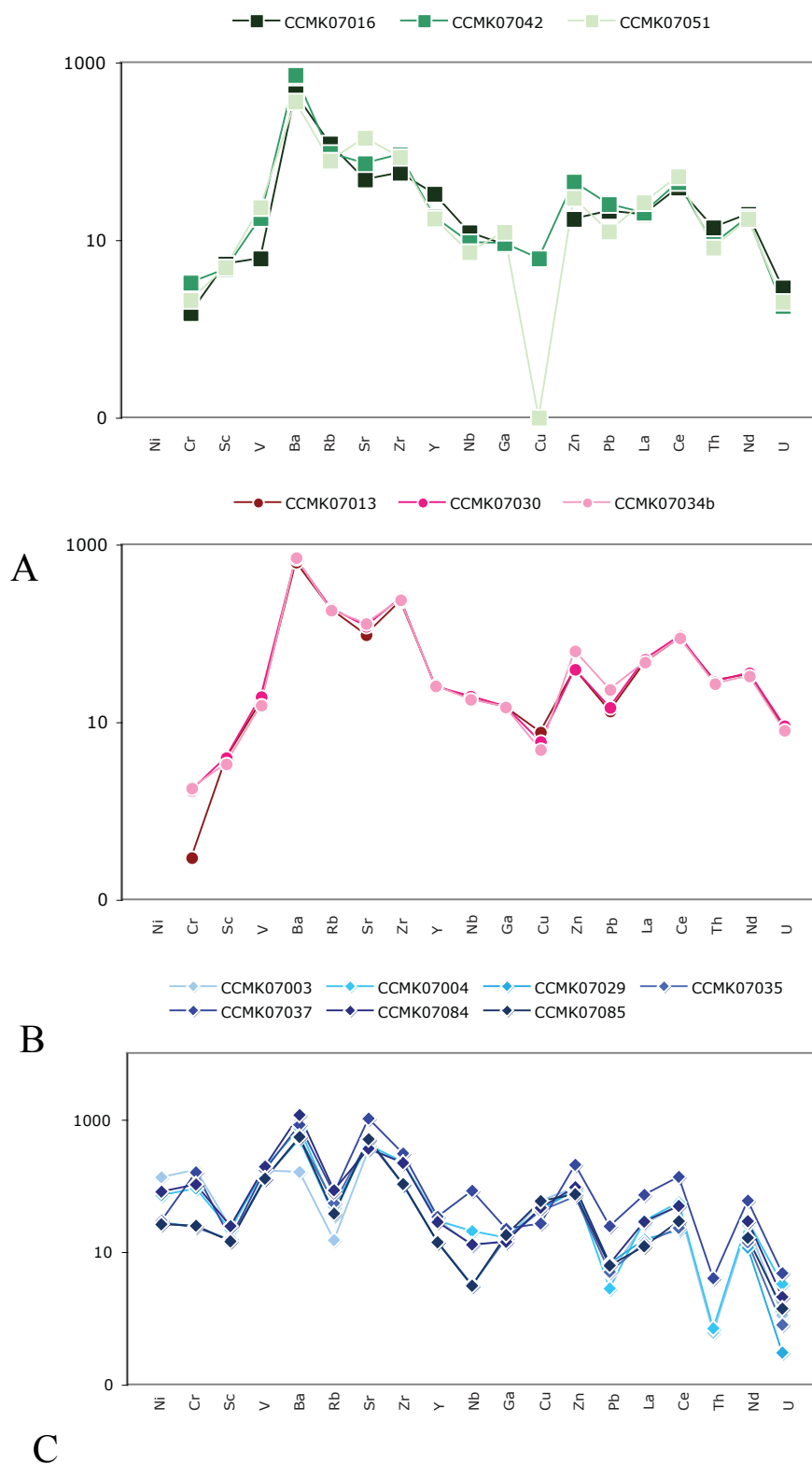


Figure 37: XRF whole rock un-normalized trace elements plotted to show individual samples within the target rocks. A) Granite XRF data, B) Ignimbrite XRF data, and C) Mafic Dike XRF data.

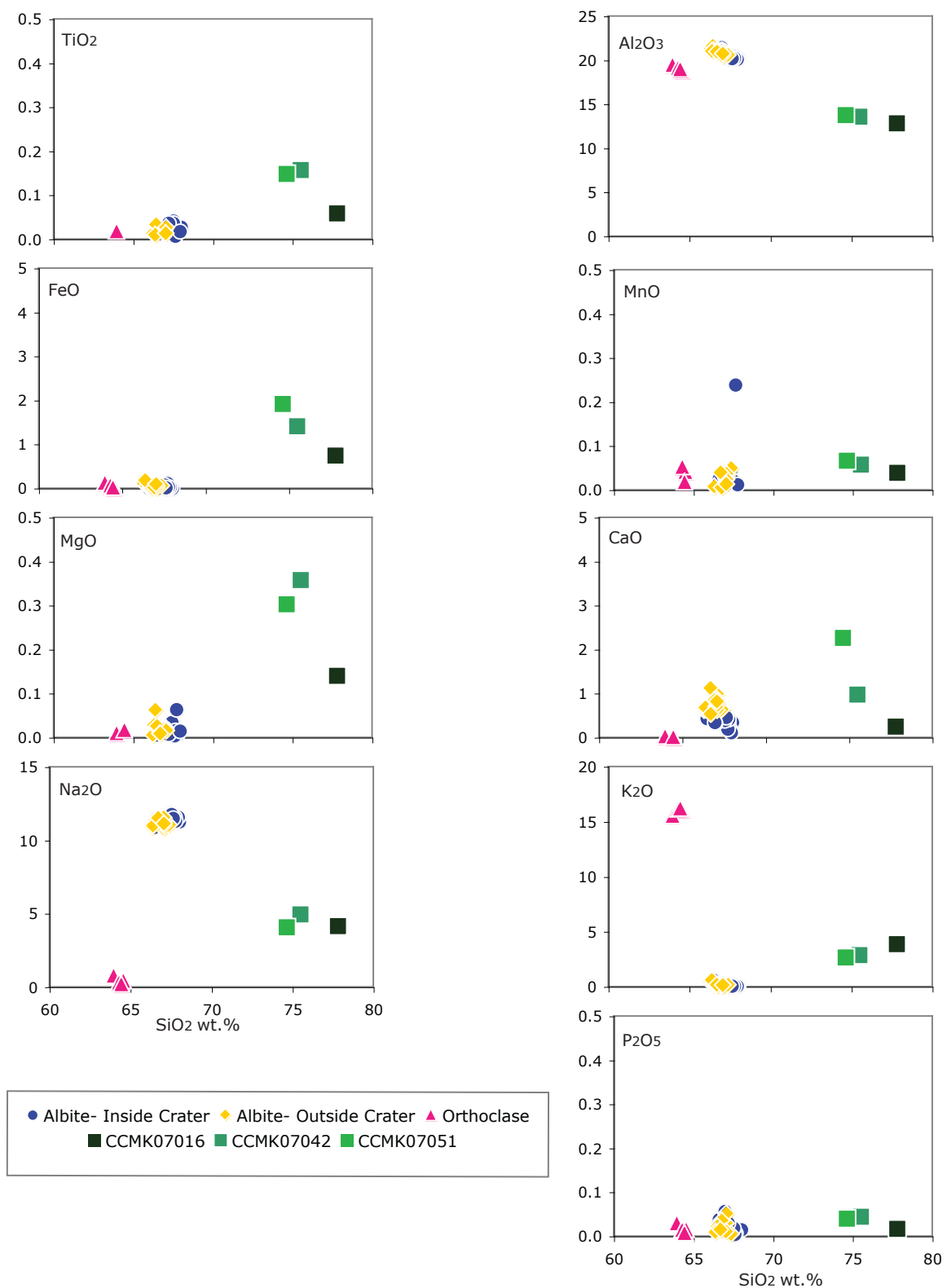


Figure 38: Electron Microprobe analysis of feldspar grains found in granite samples inside (samples 042 and 051) and outside (sample 016) the crater. XRF whole rock data for individual granite samples also plotted.

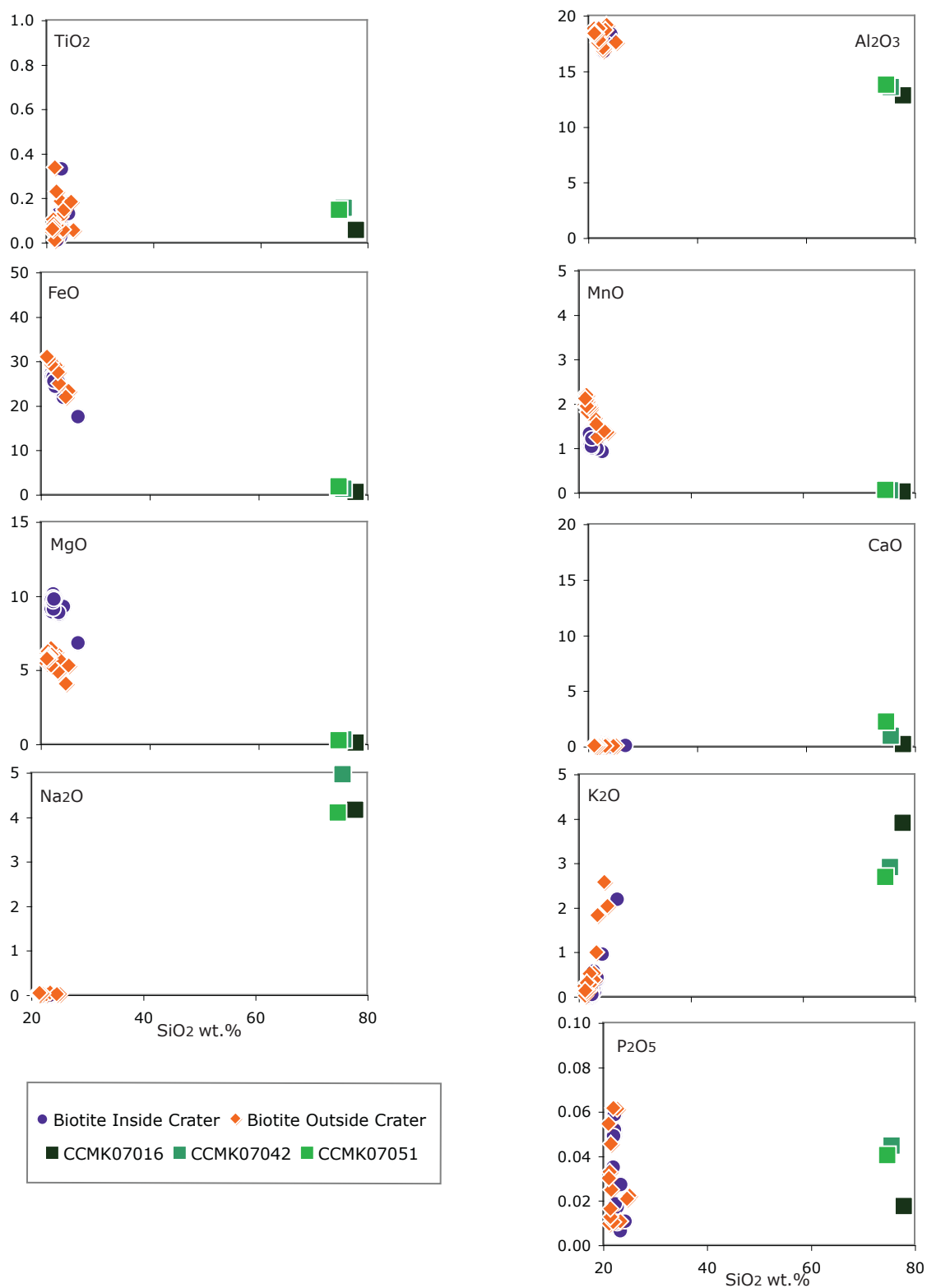


Figure 39: Electron Microprobe analysis of biotite grains found in granite samples inside (samples 042 and 051) and outside (sample 016) the crater. XRF whole rock data for individual granite samples also plotted.

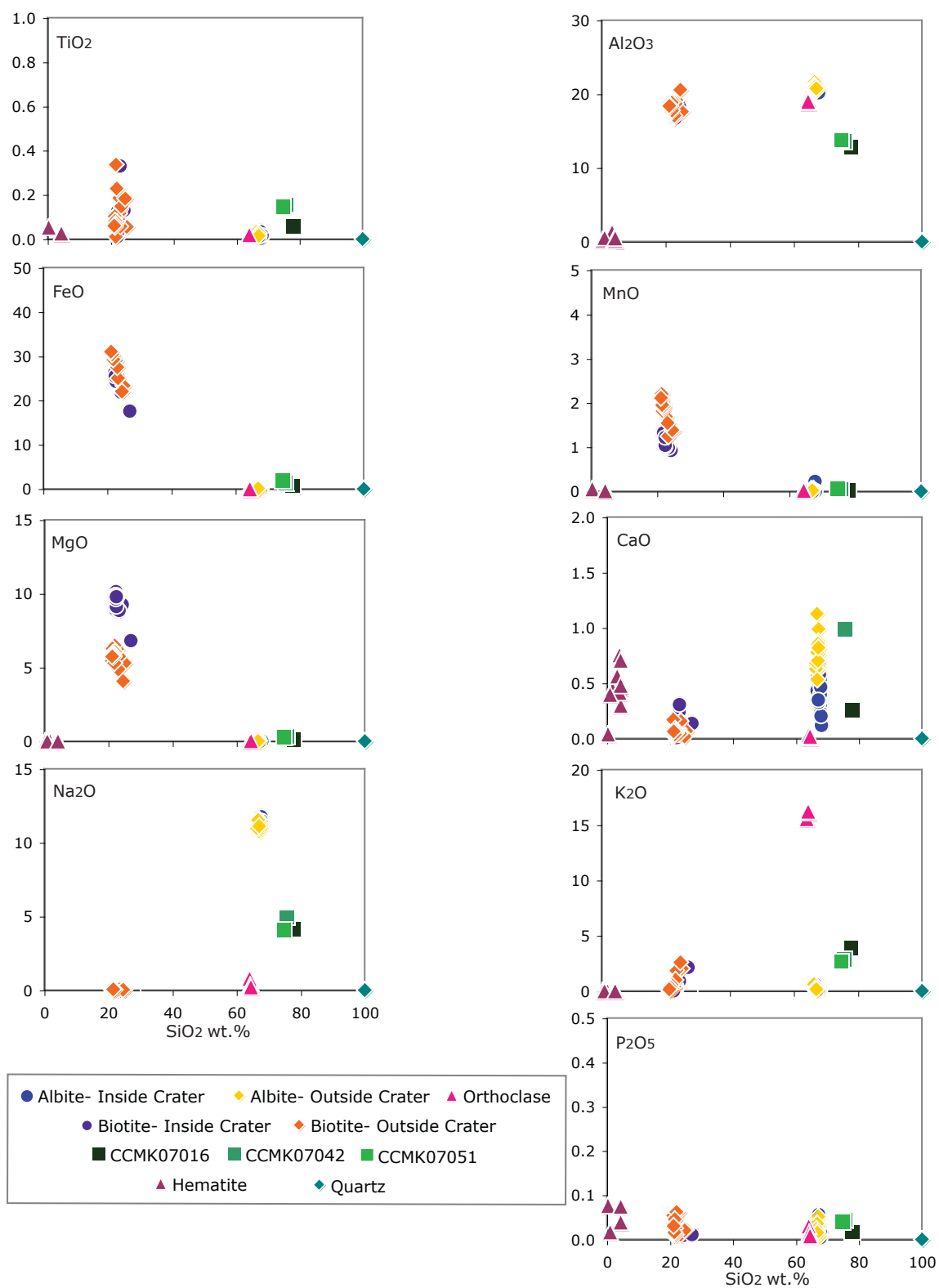


Figure 40: Minerals components that make up the granite unit: albite, orthoclase, biotite, quartz and hematite, with whole rock XRF data granite samples (016, 042, 051) in green.

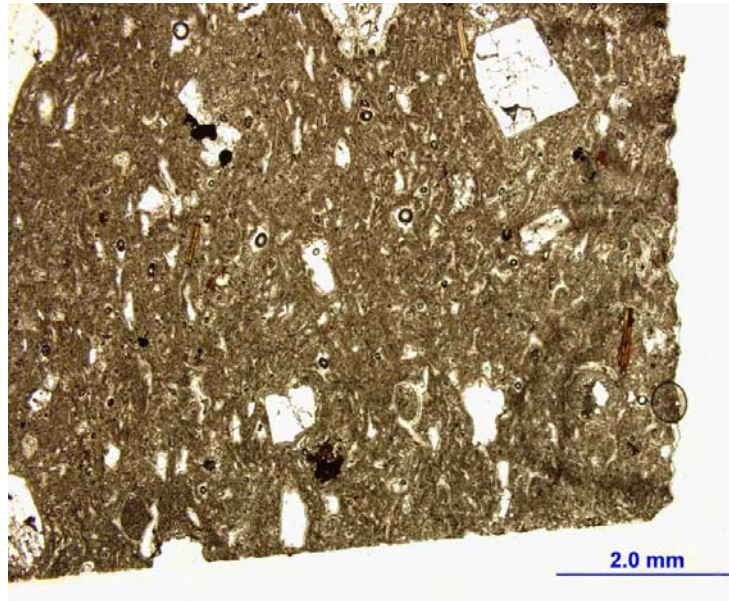


Figure 41: Sample CCMK07013 (Ignimbrite) displaying welded texture within the matrix of the sample.

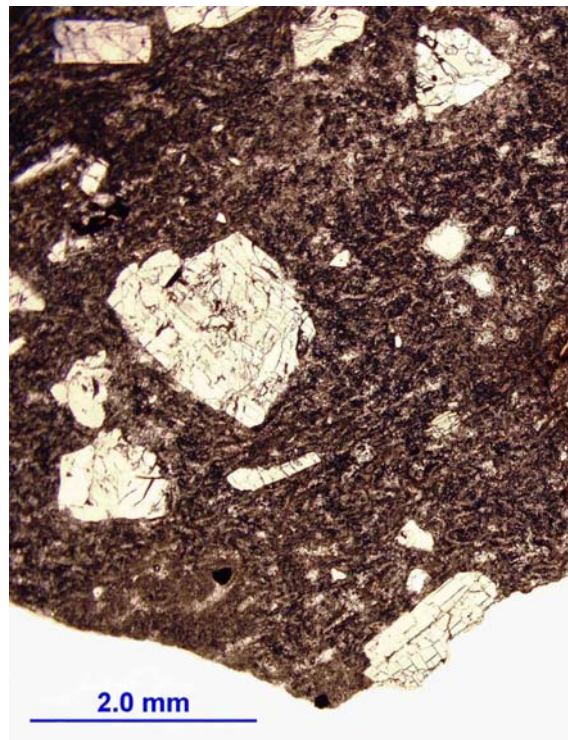


Figure 42: Sample CCMK07030 (Ignimbrite) displaying increased melting within the matrix of the sample. Plagioclase grains display multiple sets of planar deformation features running parallel and perpendicular to each other.

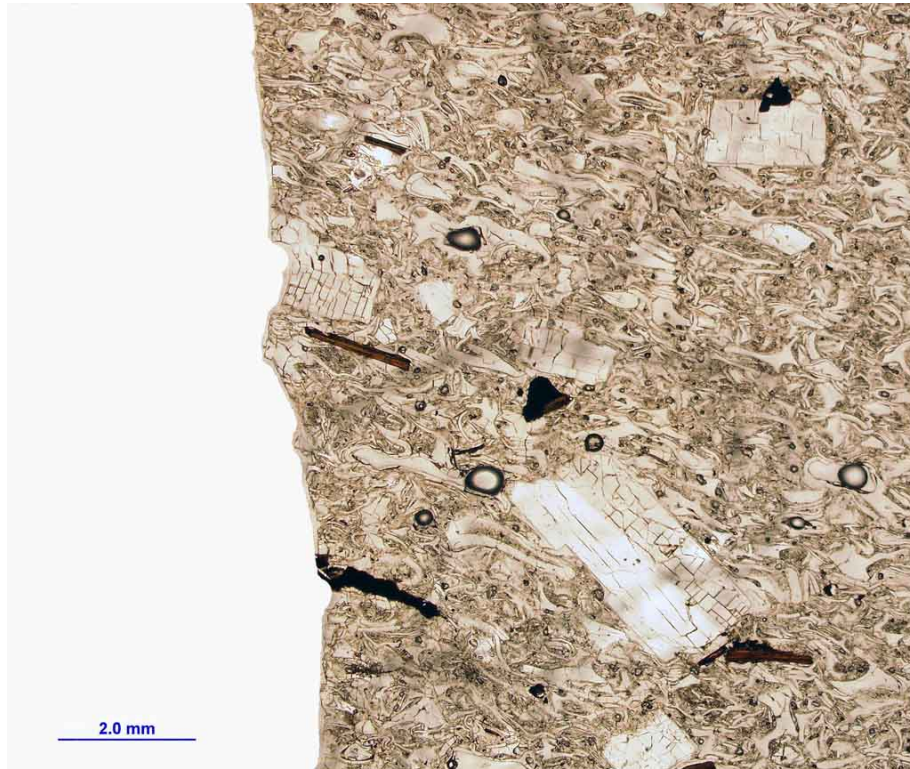


Figure 43: Sample CCMK07034b (Ignimbrite) displays planar deformation features in plagioclase grains, multiple sets running parallel and perpendicular to each other like sample CCMK07030 (Ignimbrite). Increasing melting also displayed in CCMK07034b.

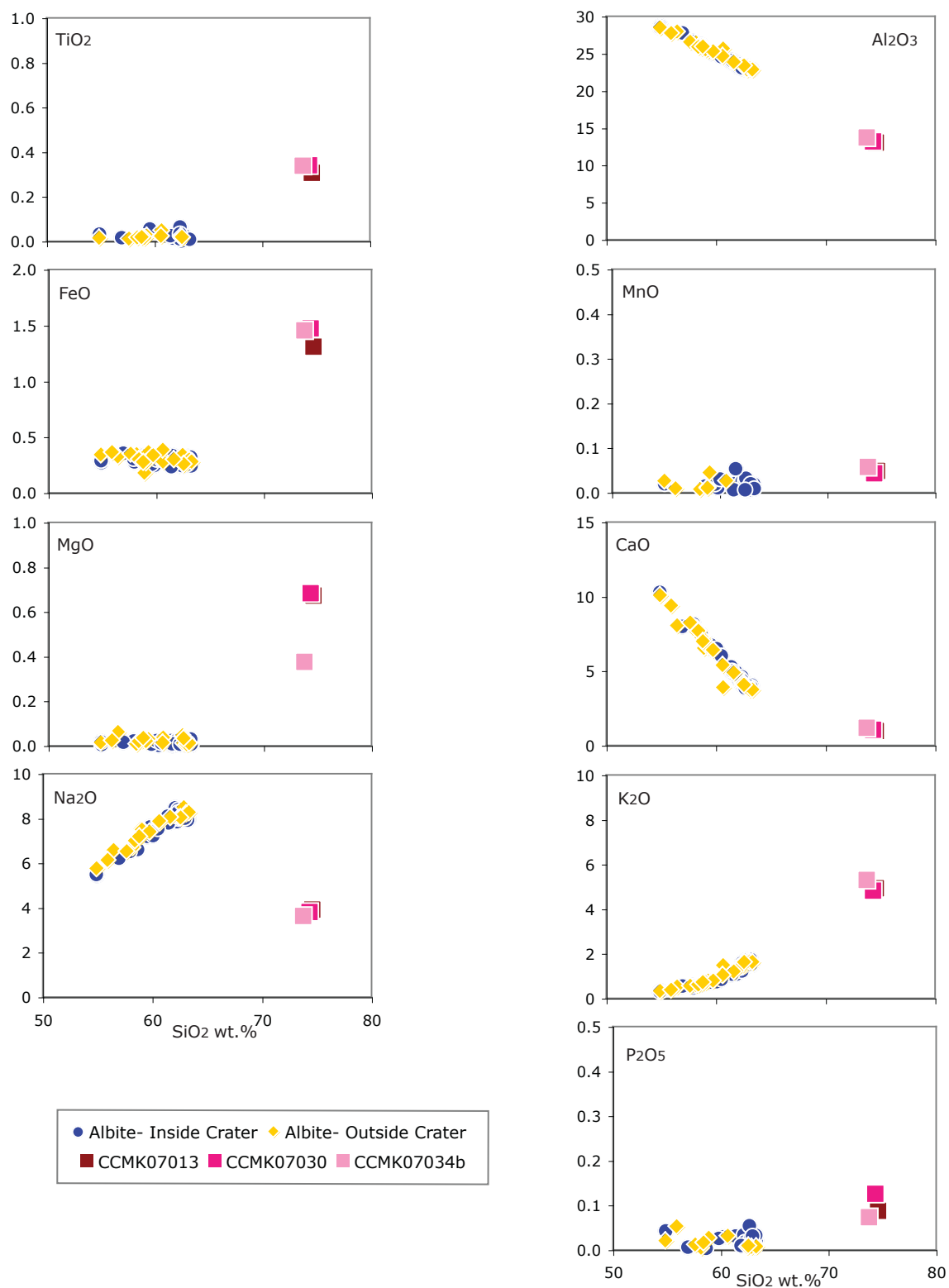


Figure 44: Electron Microprobe analysis of feldspar grains found in ignimbrite samples inside (samples 030 and 034b) and outside (sample 016) the crater. XRF whole rock data for individual ignimbrite samples are also plotted.

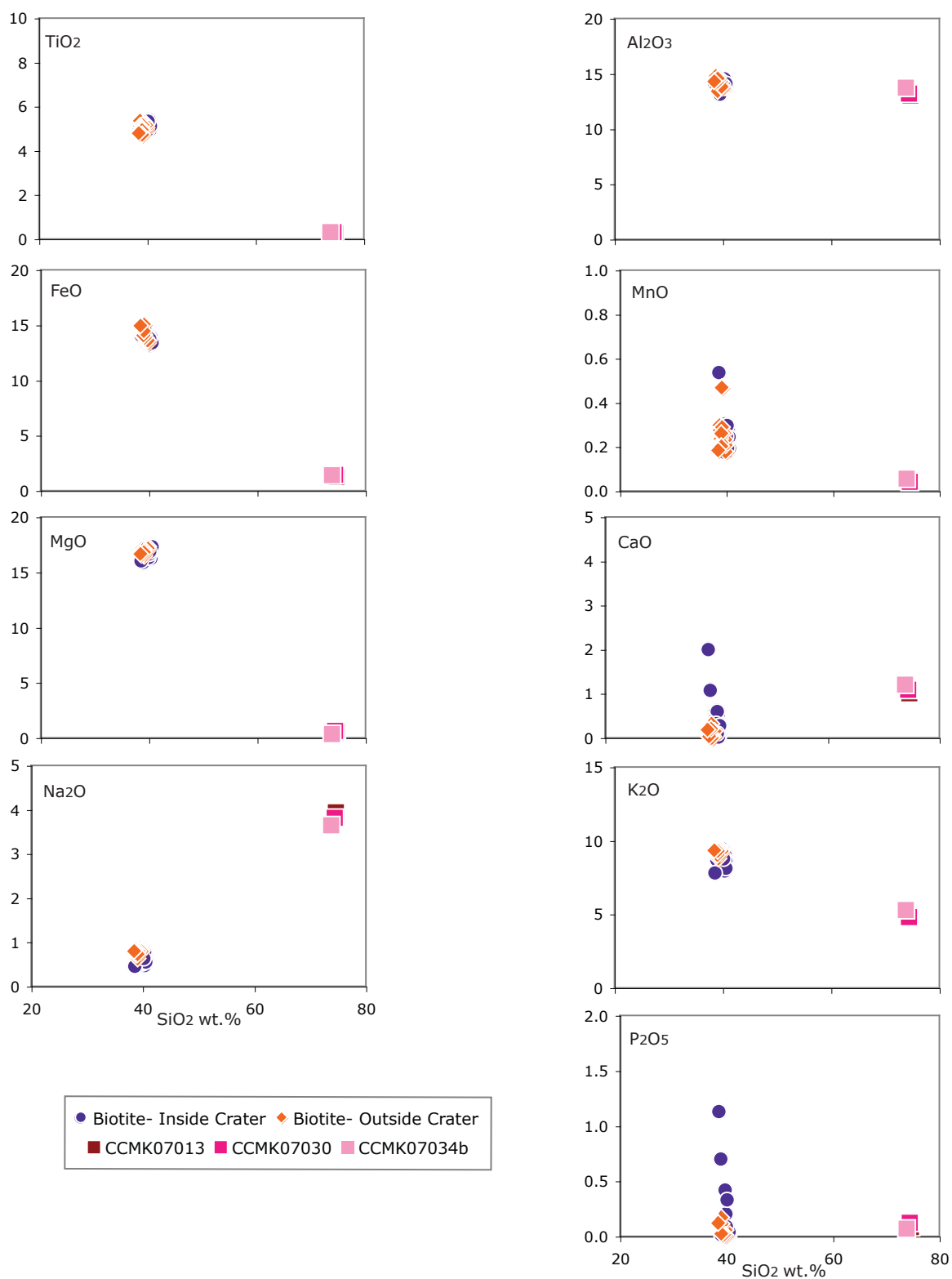


Figure 45: Electron Microprobe analysis of biotite grains found in ignimbrite samples inside (samples 030 and 034b) and outside (sample 016) the crater. XRF whole rock data for individual ignimbrite samples are also shown.

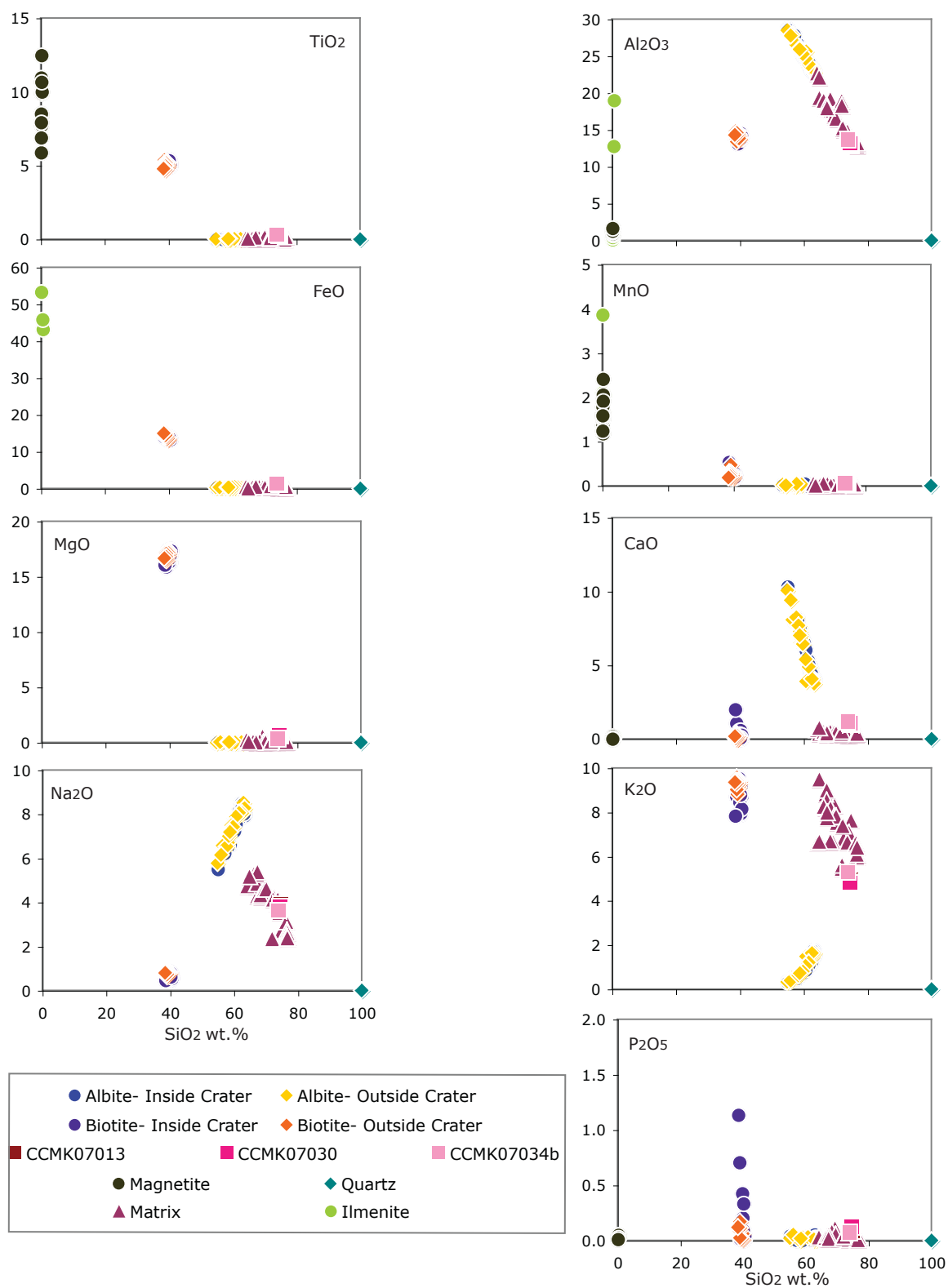


Figure 46: Minerals components that make up the ignimbrite unit: ignimbrite matrix, albite, biotite, magnetite, ilmenite with XRF whole data granite samples (013, 030, 034b) in pink.



Figure 47: Sample CCMK07003 (Mafic Dike) displaying altered olivines (lower right) altering to iddingsite.

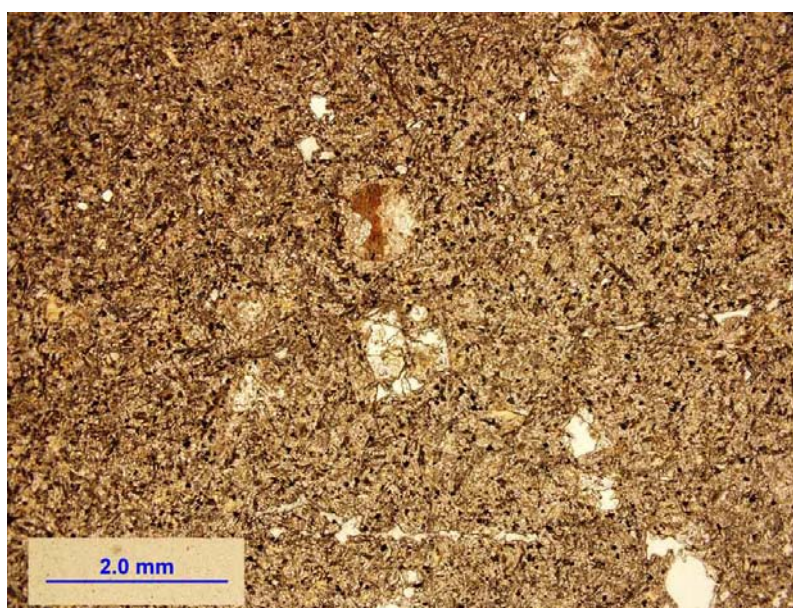


Figure 48: Sample CCMK07004 (Mafic Dike) displaying altered olivines altering to iddingsite.

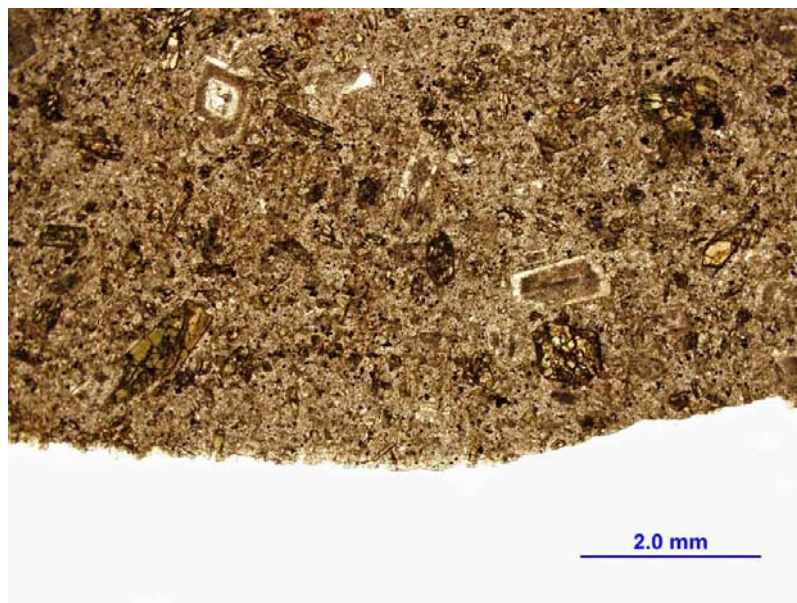
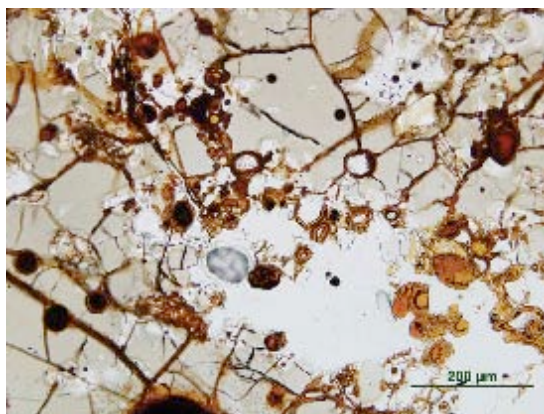
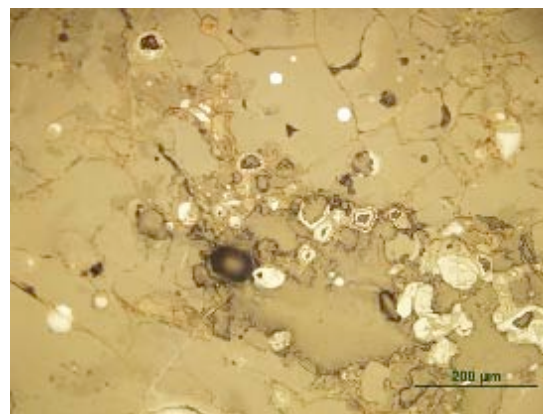


Figure 49: Sample CCMK07029 (Mafic Dike) displaying plagioclase crystals altered but retaining a rim.

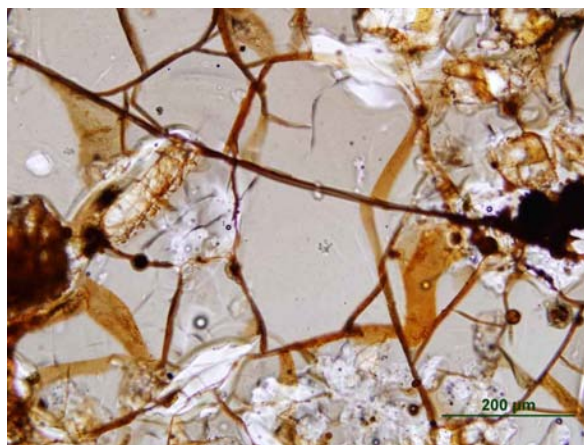


A

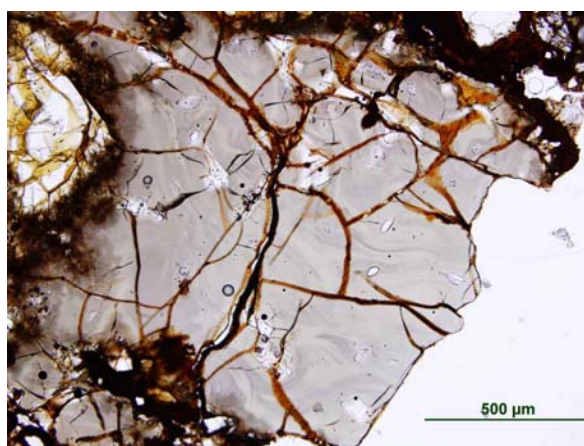


B

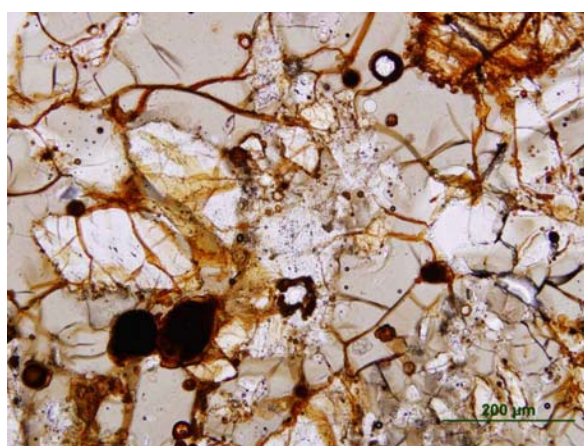
Figure 50: Sample CCMK0700A (Impactite) displaying pristine and altered spherules. A) Pristine spherules are the solid black spherules in the upper portion of the photo in PPL. The altered spherules have red and orange rims around black solid spherules. B) Photo in reflected light, the pristine spherules are silver and reflective. The altered spherules have tan, brown rims around silver spherules.



A

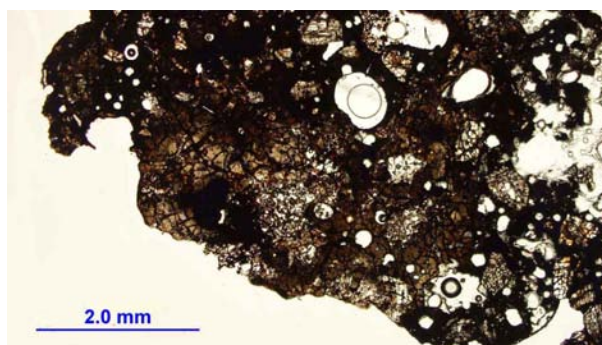


B

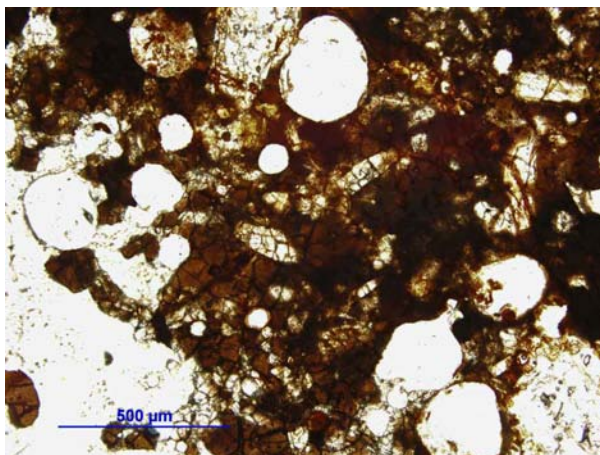


C

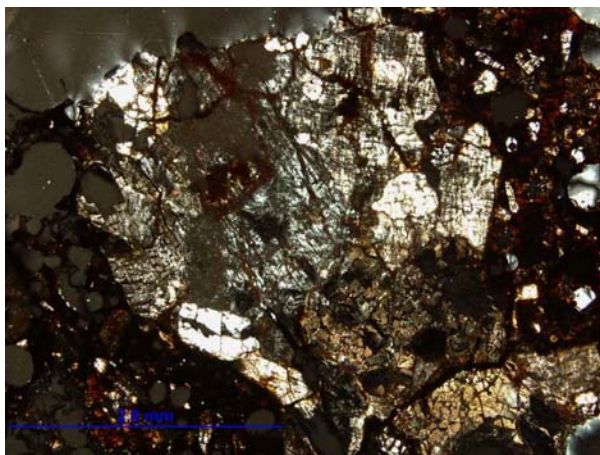
Figure 51: Sample CCMK0700A (Impactite) displaying pristine, swirled and mixed glasses. A) Clear, pristine glass shown in PPL, with red staining along fractures. The scale bar is 200 μm. B) Clear glass with silica swirls, and red staining along fractures. The scale bar is 500 μm. C) Mixed glasses, solid white areas may be lechatelierite that doesn't mix completely causing the silica swirls in the solid white areas of glass. Red staining also can be seen along fractures and alterations. The scale bar is 200 μm.



A



B



C

Figure 52: Sample CCMK07045 (Impactite) displaying planar deformation features. A) Opaque glass with transparent areas in light to dark brown. Plagioclase grains show multiple sets of fractures. The scale bar is 2.0 mm. B) Red staining in glass with small plagioclase grains with multiple sets of fractures. The scale bar is 500 μm . C) Plagioclase grains in XPL with multiple sets of fractures closely running parallel and perpendicular to each other. The scale bar is 2.0 mm.

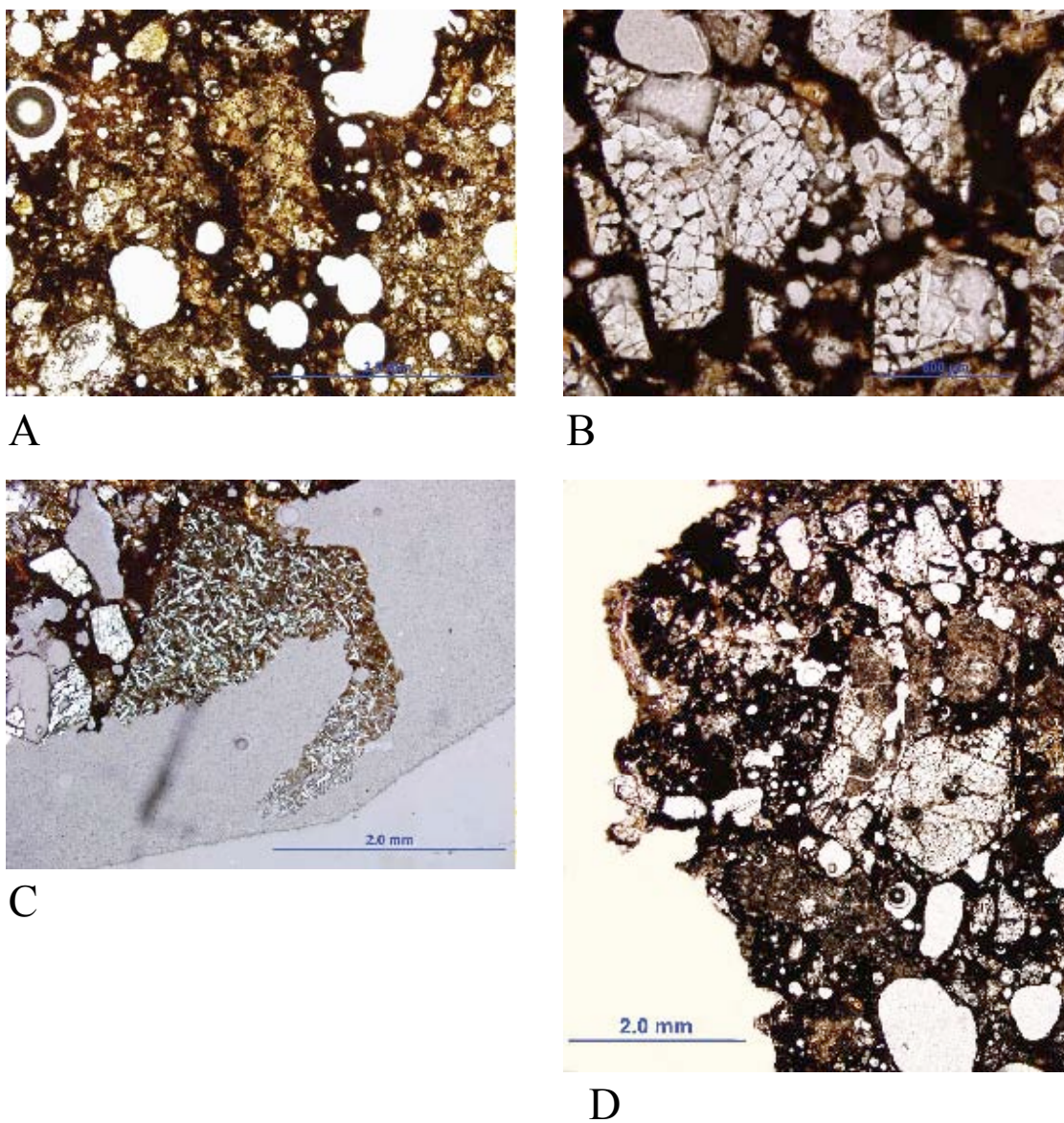


Figure 53: Sample CCMK07082 (Impactite) displaying deformation features. A) Opaque glass with transparent patches light to dark brown (similar to 045). The scale bar is 2.0 mm. B) Close up of plagioclase grains with multiple sets of fractures. The scale bar is 500 μm . C) A large clast made up of small plagioclase crystals. The scale bar is 2.0 mm. D) Plagioclase crystals with multiple sets of fractures with opaque and mixed glasses. The scale bar is 2.0 mm.

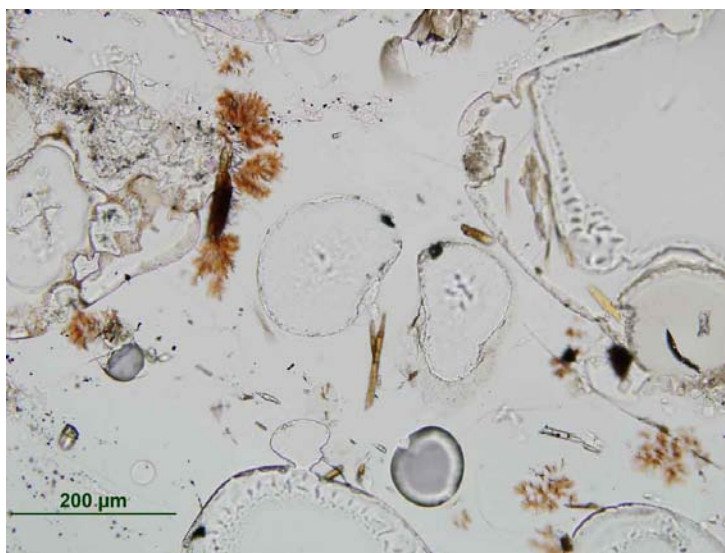


Figure 54: Sample CCMK0700B (Impactite) displaying clear pristine glass with minimal red oxidation staining.

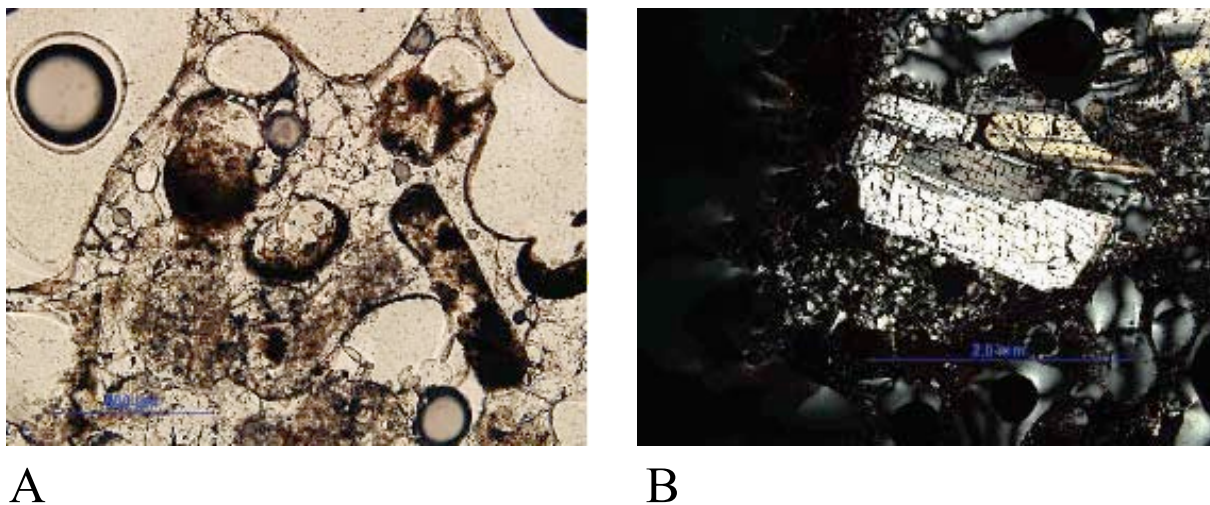


Figure 55: Sample CCMK07009 (Impactite). A) Clear glass with patches of mixed glass and red staining. Also grain boundaries are present where the plagioclase is being altered to iddingsite. The scale bar is 500 μm . B) Plagioclase grain in XPL displaying multiple sets of planar deformation features fractures running parallel and perpendicular to each other. The scale bar is 2.0 mm.

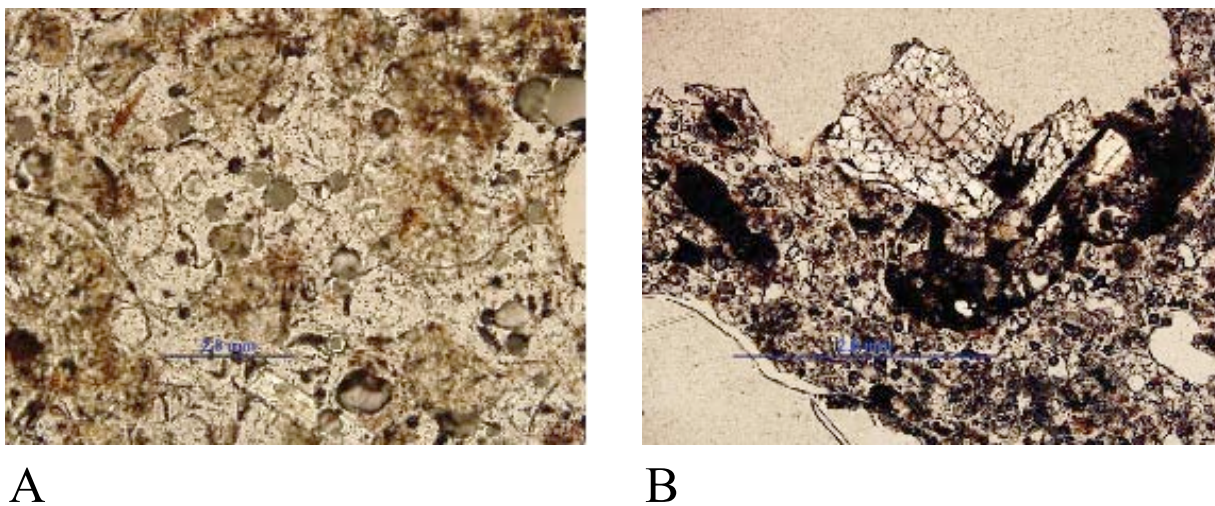


Figure 56: Sample CCMK07046 (Impactite). A) Clear glass in PPL with small clusters of plagioclase crystals with red staining. The scale bar is 2.0 mm. B) Plagioclase crystal displaying PDF's of multiple sets of fractures in XPL. The scale bar is 2.0 mm.

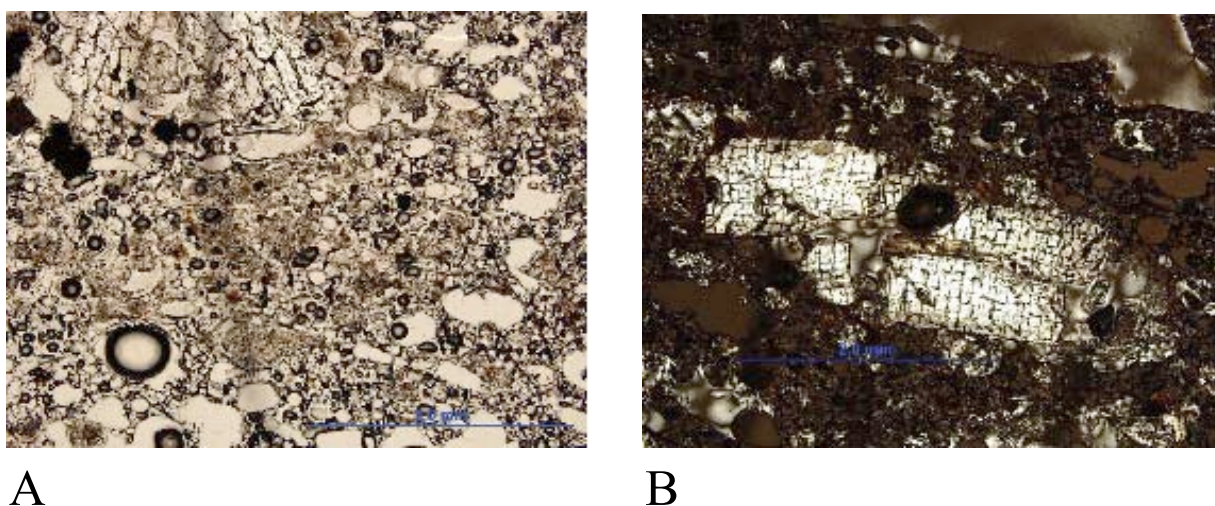


Figure 57: Sample CCMK07047 (Impactite). A) Clear glass in PPL with small clusters of plagioclase crystals with red staining. The scale bar is 2.0 mm. B) Plagioclase crystal displaying PDF's of multiple sets of fractures in XPL. The scale bar is 2.0 mm.

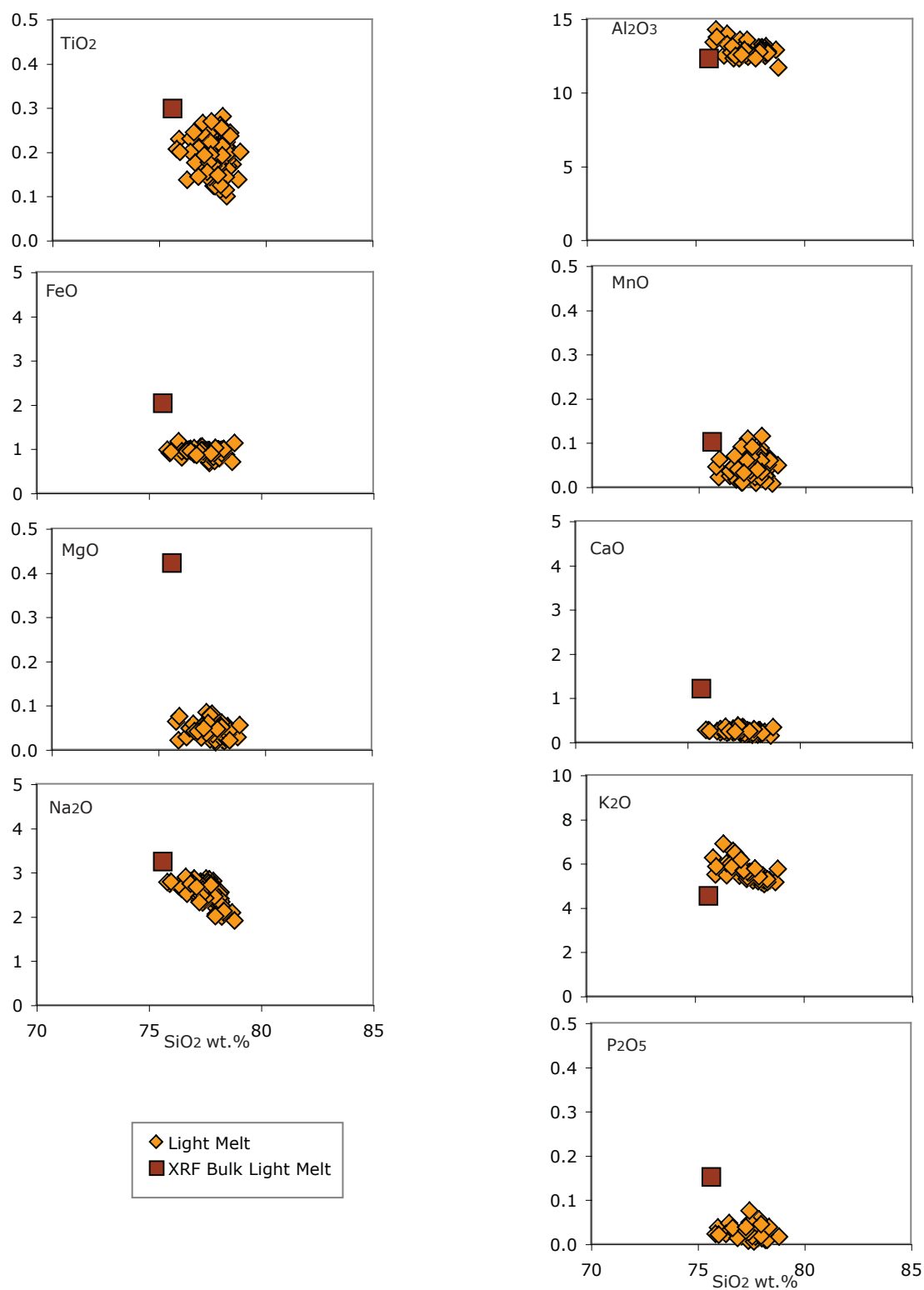


Figure 58: Electron microprobe analysis data of light melt group (in orange) made up of samples 009, 046, and 047. XRF bulk light melt is plotted in red for comparison.

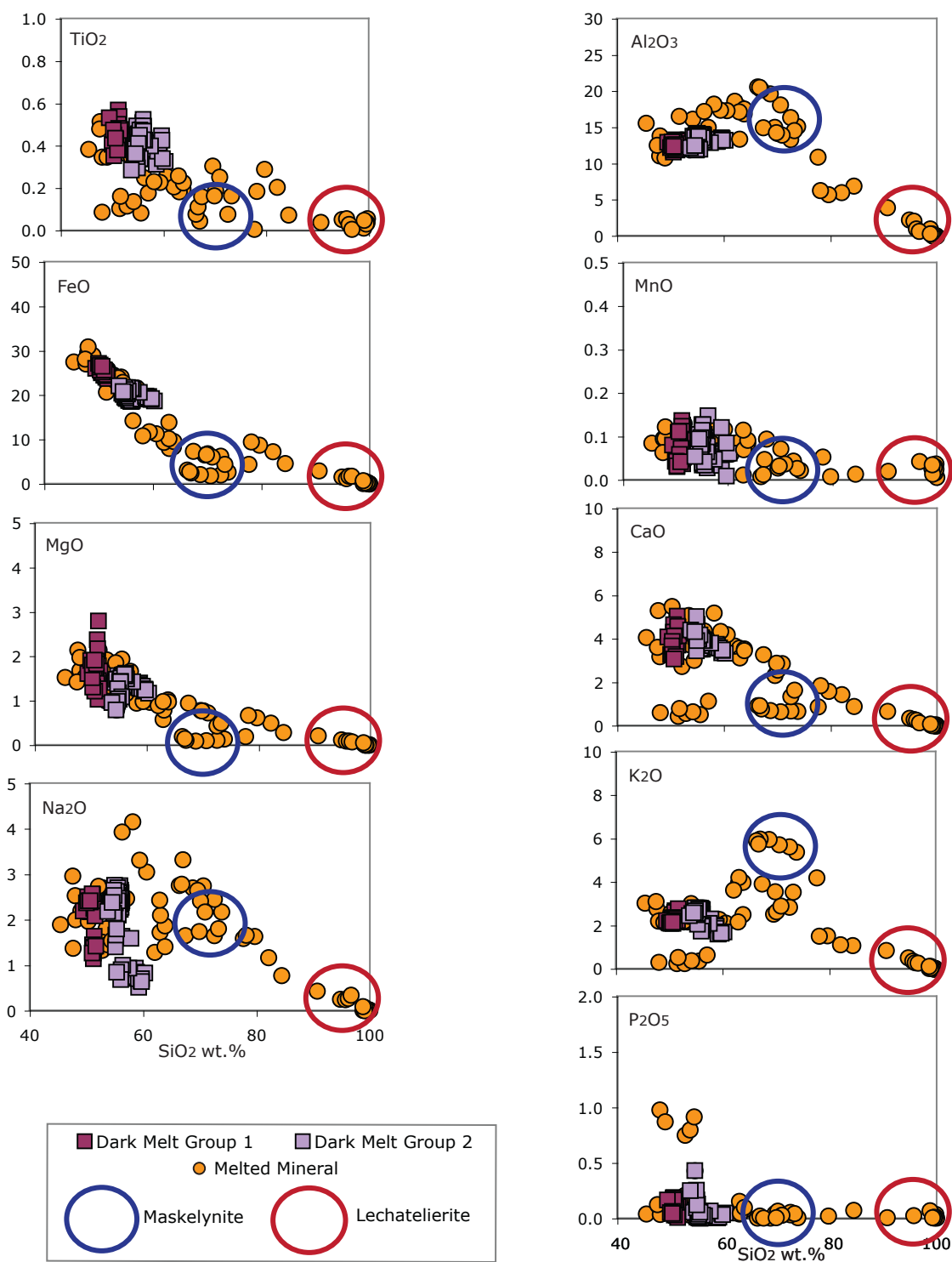


Figure 59: Electron microprobe analysis data for the dark melt group. The group is made up of samples 00A, 045, and 082. The dark melt is made up of two groups of melt and melted minerals. Lechatelierite and maskelynite are circled from melted mineral data points that are mixtures between the two dark melt groups and minerals.



A



B

Figure 60: Samples CIUP08092 (Meteorite) (A) and CIUP08093 (B) in reflected light of epoxy mounts of each sample.

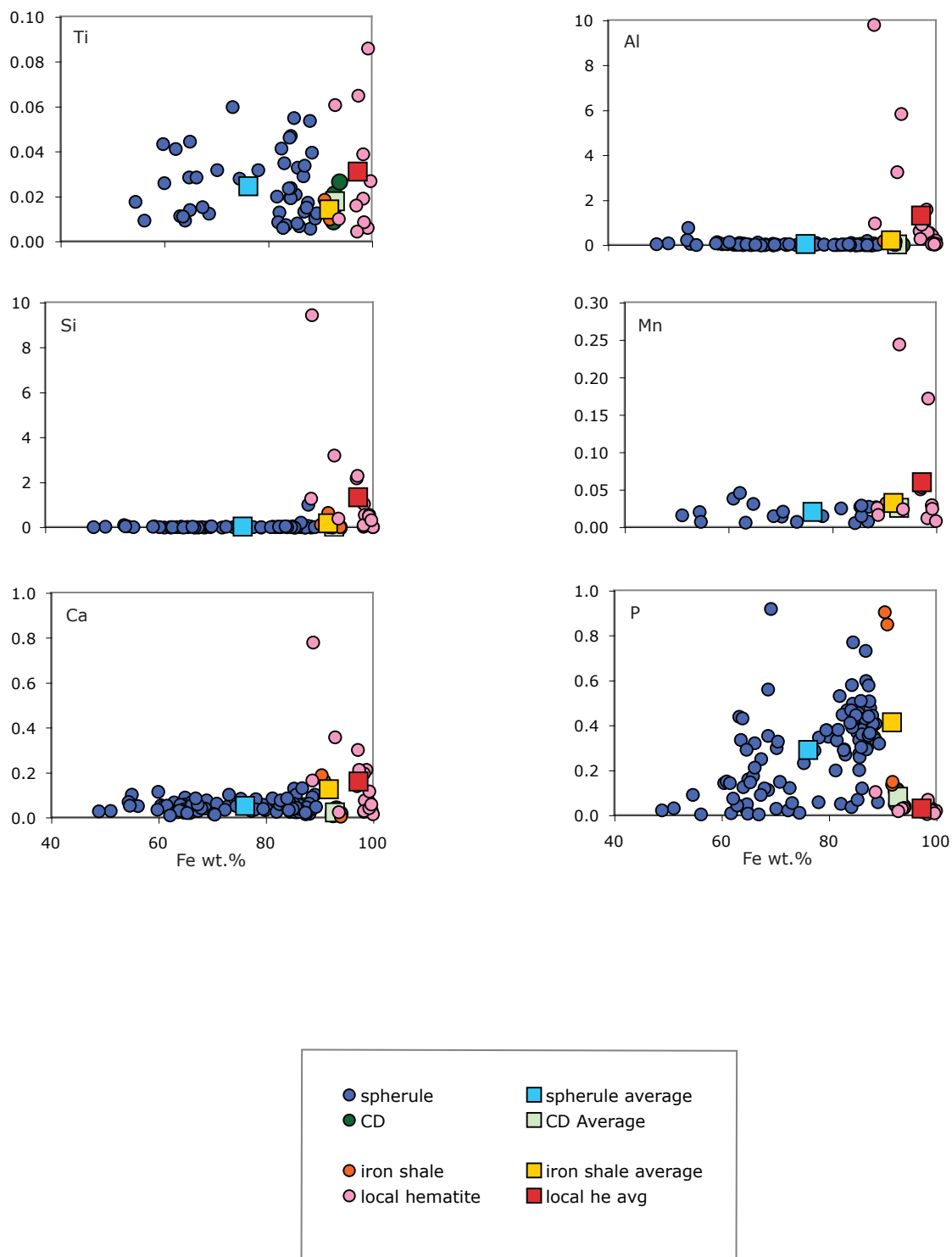


Figure 61: Electron microprobe analysis of metallic spherules, iron shale and hematite, with the Canyon Diablo sample. The major elements Ti, Al, Si, Mn, Ca, and P plotted against Fe.

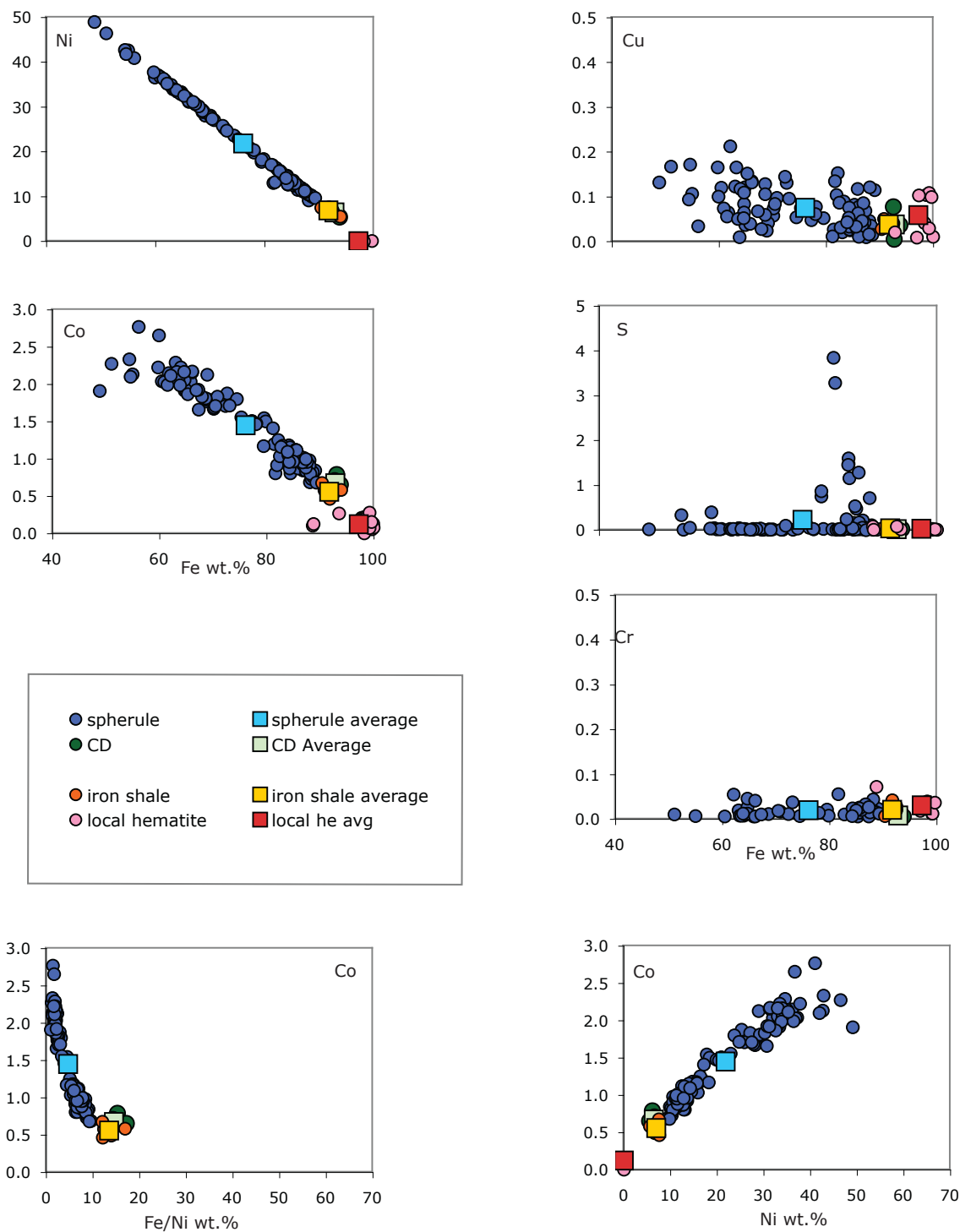


Figure 62: Electron microprobe analysis of metallic spherules, iron shale, hematite and the Canyon Diablo sample. Metals Ni, Co, Cu, Cr and S plotted against Fe. Also Co plotted against Fe/Ni and Co plotted against Ni.

CHAPTER 5: DISCUSSION

5.1 Ignimbrite and Light Melt Impactite

The ignimbrite unit is observed as the youngest target rock that overlays the granite, and melting of the ignimbrite formed the light melt group of the impactite at Monturaqui Impact Crater. I will present data that links the petrography and geochemistry of the target rock ignimbrite to the light melt found at Monturaqui Crater. In the following discussion ignimbrite refers to the target rock and light melt refers to the clear, low-Fe impactite described in the data chapter.

Petrographically the ignimbrite has a vesicular glassy matrix with a welded texture made up of visible ash shards. The ignimbrite target rock samples at the crater rim (CCMK07030 and CCMK07034b) show in hand sample observations, increased melting and more vesicles compared to the sample 1.3 km away from the crater (CCMK07013). All of the samples have visible grains of plagioclase and biotite crystals. The plagioclase grains found at the crater rim (CCMK07030 and CCMK07034b) exhibit planar deformation features, with multiple sets of fractures. The planar deformation features of the plagioclase grains indicate that the ignimbrite layer underwent shock metamorphism at pressures < 10 GPa and temperatures of < 100° C (French, 1988). The light melt samples (CCMK07009, CCMK07046, and CCMK07047) exhibit similar petrographic features as the ignimbrite target rock. The light melt samples have a glassy fluidal surface crust, internally vesicular with visible crystals of plagioclase and biotite. Sample CCMK07009 is vesicular while CCMK0700B, CCMK07046, and CCMK07047 have a ropy surface texture, which is indicative of the liquid melt being aerodynamically shaped before solidifying. The plagioclase grains in three of the four samples exhibit similar planar deformation features as

the ignimbrite target rock samples. The red staining found within the glass may be due to the formation of hematite (French, 1988).

Features of the light melt impactite that are indicative of an impact event are:

- glassy fluidal surface crust
- ropy surface texture- indicating the samples were aerodynamically shaped before solidifying
- rounded clasts
- clear glass replacing the melted matrix

If the ignimbrite target rock had been weathered we would not see the surface crust on the light melt samples or the ropy surface textures, and we would expect the clasts in the light melt to be angular from fracturing off the ignimbrite. The melted matrix from the ignimbrite target rock would not have resulted into clear glass (seen in the light melt) unless melting had occurred.

Geochemically the ignimbrite target rock and the light melt group are similar. The table in Table 11 shows the XRF data analysis of all three ignimbrite samples (1.3 km away from the crater, and at the crater rim), with the total average ignimbrite, bulk light melt, and light melt average. The bulk light melt compared to the average ignimbrite target rock was discussed in the Data Chapter as being virtually the same. The light melt composition has a SiO₂ of 77.6 wt.%, Al₂O₃ of 12.8 wt.%, Na₂O of 2.5 wt.%, CaO of 0.2 wt.%, K₂O of 5.5 wt.%. This shows that the light melt has slightly higher SiO₂ and K₂O, and lower Al₂O₃, Na₂O, and CaO than the bulk light melt and total ignimbrite target rock compositions. This is similar enough to indicate that the light melt is melted ignimbrite. The minor differences can

be explained by the presence of plagioclase crystals (with high Al_2O_3 , Na_2O , and CaO) in the bulk ignimbrite samples.

5.2 Pressures and Temperatures in relation to the Impactite

The impact melt of the Monturaqui Impact Crater is divided up into two groups: the first as discussed above is the light melt that is composed of melted ignimbrite target rock, the second group is the dark melt. The dark melt is not homogenous due to multiple groups identified within the electron microprobe analyses, melted minerals with defined data points of maskelynite (glass from plagioclase feldspar) and lechatelierite (glass from quartz), dark melt group 1 (SiO_2 of 50.8 wt. % and FeO of 25.4 wt.%) and dark melt group 2 (SiO_2 of 55.8 wt.%, and FeO of 19.7 wt.%). In some shocked rocks, post-shock temperatures may exceed the melting points of the minerals present and will melt to a mixture of heterogeneous glasses (French, 1988). French (1988) indicates that this selective melting is relatively uncommon in rocks from impact structures and that the region of pressure for this process is $\sim 45\text{-}55$ GPa. Anything at pressures ≥ 55 GPa would create more chemically homogeneous bodies of impact melt (French, 1988).

For the light melt, some of the analyses of impactite glass that had high silica concentrations (79.8- 80.6 wt.%) were interpreted to be dominated by melted quartz. These points were most likely melted quartz crystals within the impactite glass from minerals found in the ignimbrite. For the dark melt, the extra data points during the analysis were identified as melted minerals with defined maskelynite and lechatelierite. The mixed minerals within the dark melt were likely a result of melted target rock minerals mixed with the dark melt impactite glass. This indicates that the impactite reached pressures > 35 GPa and

temperatures $> 300^{\circ}\text{C}$. The shock phases reached at these conditions are likely responsible for the conversion of the mineral grains into diaplectic glasses, and in the case of plagioclase into maskelynite. The original textures and fabric of the mineral grains are retained in diaplectic glasses, but they are optically isotropic in thin section and the reddening is produced from the formation of hematite. The lechatelierite indicates high temperature shock melting of quartz. The temperature of formation for lechatelierite is $> 1700^{\circ}\text{C}$, and does not always mix completely with the other melt before it cools (French, 1988). This can create schlieren or clear streaks of pure silica throughout the glass. The schlieren can range from 50-200 μm in length.

5.3 Modeling

The light melt group is clearly derived from the ignimbrite target rock unit as the petrological characteristics and geochemical compositions display. Least square calculations can also determine if the light melt is solely derived from the ignimbrite target rock or if other components such as impactor or granite have been mixed in. Bunch and Cassidy (1972) suggest that the impact melt (dark melt groups) are from the minerals of the granite only. However dark melt groups are not clearly derived just from the granite (Figure 63), based on petrological and geochemical observations. The dark melt samples contain metallic spherules, which cannot be explained by only melting the granite. Geochemically the dark melt groups have lower SiO_2 (group 1: 50.8 wt.%, group 2: 55.9 wt.%, and granite 76 wt.%), Na_2O (group 1: 2.1 wt.%, group 2: 2.2 wt.%, and granite 4.4 wt.%), and higher MgO (group 1: 1.7 wt.%, group 2: 1.4 wt.%, and granite 0.3 wt.%), CaO (group 1: 4.1 wt.%, group 2: 3.9 wt.%, and granite 1.2 wt.%), and FeO (group 1: 25.4 wt.%, group 2: 19.7 wt.%, and granite

1.4 wt.%). Least square calculations can help to determine whether mixtures of varying proportions of the different source components (granite, ignimbrite, mafic dikes, hematite, and minerals in these rocks) can explain the composition of the dark impactite melt.

The least squares calculations can be made using the Solver function in Microsoft Excel. For example, the mineral mode of the granite target rock can be estimated by mixing the average compositions of the different mineral phases (determined by electron microprobe) in different proportions to try to match the whole rock granite composition as determined by XRF analysis. The averages of the all the mineral component analyses are used as the acceptable composition of that component. For example, all of the biotite analyses from the granite samples (CCMK07016, CCMK07042, CCMK07051) are averaged together to use as the estimated average biotite component for calculating granite. This is done for each component used to make up the granite unit: orthoclase, plagioclase, biotite, hematite, and quartz. The average composition of the granite is taken from the XRF whole rock data. The calculated composition of the bulk granite sample is then formed by multiplying the composition of a particular element in each mineral component by the estimated percentage of that phase, and repeating for each element. The percentage cells are set in the Solver window to vary with the condition that they sum to 100%. Another cell is set as the sum of the percentage cells is used as a condition to equal to 1. A residual calculation is made by subtracting the calculated composition of granite from the average composition of granite. Then the residual values for each element are taken to the second power and added together to reach the sum of squares. The sum of squares is the third cell set in the Solver window. The Solver function will vary the percentage of the different mineral components in order to minimize the sum of the squares of the residuals.

The first calculations (Table 12) are done to determine the modal composition of the ignimbrite and granite target rocks. The percentages of the minerals that make up the least-square average granite unit are: 40% plagioclase, 35% quartz, 20% orthoclase, 5% biotite and < 0.5% hematite. The sum of the squares for this modal estimate is 1.02. The percentages of the minerals that make up the average ignimbrite unit are: 62% glass matrix, 22% quartz, 12% plagioclase, 3% biotite, 1% magnetite and almost < 0.5% ilmenite. The sum of the squares for this estimate is 0.39. Note that all of these components were identified in electron microprobe analysis in each unit, except for quartz, which was assumed to have a composition of 100 wt.% SiO₂.

The calculation for the impactite light melt group (Table 13) used the average XRF composition for the ignimbrite target rock, a generic iron meteorite at 92.1 wt.% Fe and 7.9 wt.% Ni (the average Ni was taken from Buchwald, 1977), and the average light melt composition from electron microprobe analysis, the percentages are 102% ignimbrite, and -2% iron meteorite. The sum of the squares for this estimate is 9.36. The high least-square calculation supports the petrological observation that no metal was found in the light melt, and that the light melt is solely derived from the ignimbrite target rock. A second least squares calculation was made using individual mineral components of ignimbrite (Table 14) to see if any phases in the ignimbrite were preferentially contributing to the light impactite melt. The light melt mineral components were ignimbrite matrix average, biotite, plagioclase, and quartz. The accessory minerals magnetite and ilmenites, were not used due to not being of significance proportion in the ignimbrite and they were creating large negative percentages.

Similarly the previous model had shown that the iron meteorite was not an important contributor to the light melt. The percentages that make up the least-squares calculation for light melt: 75% ignimbrite matrix, 25% quartz, 1% biotite, and 1% plagioclase. The sum of the squares for this estimation is 0.51. This calculation does not agree with petrological or geochemical observations for the modal amount of plagioclase and biotite (62% glass matrix, 22% quartz, 12% plagioclase, 3% biotite).

The calculations for dark melt groups (Table 13) used the average XRF data calculation for the granite target rock, the averages for the three mafic dikes groups, a generic iron meteorite at 92.1 wt.% Fe and 7.9 wt% Ni (the average Ni was taken from Buchwald 1977), and the average compositions for Group 1 and Group 2 of the dark melts. The percentages of different components contributing to dark melt group 1 are: 44% granite, 23% iron meteorite, 16% mafic dike group 3, 15% mafic dike group 1, 2% mafic dike group 2. The sum of the squares for this modal estimate is 7.30. The percentages for group 2 are: 51 % granite, 32% mafic dike group 3, 17% iron meteorite, 4% mafic dike group 1, and 0% mafic dike group 2. The sum of the squares for this modal estimate is 5.17. For the dark melt groups the process of determining the components began with just the average granite component, which gave a sum of squares of over 750, consistent with the observed significant compositional differences between the dark melt and the average granite composition. The average ignimbrite was added with the average granite and the percentage of average ignimbrite was negative indicating it was not a component that was incorporated based on the chemical data. The average granite plus the mafic dike groups gave a sum of squares of 185, but the metallic spherules could not be explained with just these components.

Hematite would not work because it would not contribute the nickel content needed. So the components that worked with the lowest sum of square became the average granite, mafic dike groups, and iron meteorite.

To investigate whether some of the mineral phases in the granite were melting preferentially (in non-modal proportions), the least squares modeling was repeated, this time using the average mineral compositions rather than the granite whole rock compositions, to see if these could better match the composition of the dark melts. The granite mineral components used were orthoclase, plagioclase, biotite and quartz in addition to iron meteorite and mafic dike group 1 and group 3. Hematite and mafic dike group 2 were not included due to creating large negative calculations.

The first calculation in Table 15 is only the granite mineral compositions, the percentages for dark melt group 1: 73% biotite, 41% quartz, -5% orthoclase and -9% plagioclase. The percentages for dark melt group 2 in Table 16 are: 57% biotite, 37% quartz, 3% orthoclase, and 3% plagioclase. The sum of squares for this estimation is 97.54 and 58.49 respectively. Not only are the sum of square estimations high, but using only the granite contributes large percents of biotite and quartz, which were not seen in hand sample. The second calculation includes the ignimbrite target rock in addition to the granite minerals, the percentages for the dark melt group 1: 193% ignimbrite, 6% biotite, -20% quartz, -64% orthoclase, and -70% plagioclase. The percentages for dark melt group 2 are: 200% ignimbrite, 46% biotite, -27% quartz, -59% orthoclase, and -60% plagioclase. The sum of squares estimations were 94.39 for group 1 and 16.64 for group 2. The ignimbrite is not a logical component to the dark melt impactite as its percentage was over 100%. The third calculation in Table 15 and Table 16 is the granite mineral compositions with the iron

meteorite. For dark melt group 1: 22% plagioclase, 22% biotite, 21% iron meteorite, 21% quartz and 14% orthoclase with a sum of squares estimation at 18.72. For dark melt 2: 26% plagioclase, 23% quartz, 20% biotite, 16% orthoclase, and 15% iron meteorite with sum of squares at 16.64. The biotite percentages are high for not observing any in hand sample and thin sections. The final calculations in Table 15 and Table 16 are including the mafic dike groups 1 and 3. The percentages that make up the least-squares calculation for the dark melt group 1: 34% mafic dike group 1, 24% iron meteorite, 15% mafic dike group 3, 13% quartz, 11% orthoclase, 10% plagioclase, and -7% biotite. The percentages for dark melt group 2: 36% mafic dike group 1, 18% iron meteorite, 15% quartz, 14% orthoclase, 14% plagioclase, 9% mafic dike group 3, and -7% biotite. The sum of squares for each group: group 1 at 7.39 and group 2 at 7.22. The final calculations in Table 15 and Table 16 seem to be the most logical in comparison to the dark melt impactite observations.

The dark melt groups model estimates that 17-23 wt.% of iron meteorite is needed to explain the enrichment of Fe in the dark melt compositions (Group 1 has FeO of 25.4 wt.% and Group 2 has FeO of 19.7 wt.%). In order for the meteorite to contribute 17-23 wt.% to the dark melt, the meteorite would need approximately 92.1 wt.% Fe (with approximately 7.9 wt.% Ni). The Fe enrichment is unlikely to be from local sources such as hematite alone, since this would not account for the high Ni content. Also neither main target rock, granite or ignimbrite contains a significant amount of Ni. Is 17-23 wt.% a realistic amount of iron contribution from an iron meteorite? Tagle & Hecht (2008) indicate that more than 5 wt.% of the impactor is not realistic. The question then becomes where the rest of the Fe enrichment is coming from- this could perhaps be a combination of meteorite and hematite contributions.

Further analysis of the metal contents (especially Fe, Ni, S, Cr), of the impact melt, and terrestrial hematite would be beneficial to answering this problem.

5.4 Meteorite

The averages of the meteorite samples CIUP08092 and CIUP08093 compare closely to the Canyon Diablo averages (Table 15). The average nickel in the samples was higher than Canyon Diablo, 6.9 wt.% versus 6.4 wt.%. The average iron in the samples was lower at 91.7 wt.% versus the Canyon Diablo iron content at 92.8 wt.%. Buchwald (1977) states that > 5% nickel is indicative of iron being of meteoritic rather than terrestrial origin, and the average Ni content for CIUP08092 and CIUP08093 at 6.9 wt.% would indicate it is an iron meteorite. Also Buchwald (1977) gives the range of 0.02-12% bulk sulfur as indicative of meteorite components, and these samples' average sulfur content is 0.02 wt.% and ranges up to 0.04 wt.%. Further analysis of these iron shale samples particularly for trace elements (such as Ga, Ir, Ge, and Platinum Group Elements) would also be beneficial in determining more specifically the composition of the meteorite that hit Monturaqui Crater and assigning to a specific iron meteorite group (determine if it agrees with the group assigned by Bunch & Cassidy (1972) as an octahedrite IAB).

5.5 Spherules

Gibbons et al (1976) analyzed metallic spherules from Monturaqui by electron microprobe with compositions of Fe 24-85%, Ni 13-75%, and up to 4.1% Co. (This study found average compositions of Fe 76.1 wt.%, Ni 21.8 wt.%, Co 1.5 wt.%) Gibbons et al (1976) found compositional variation in the spherules for Fe, Ni and Co. In Figure 18 the

nickel-iron contents of the Monturaqui spherules is displayed as high iron corresponding to low nickel, creating an inversely proportional relationship between the nickel and iron content. Figure 20 displays the direct proportional relationship between nickel and cobalt. Figure 64a and 64b show this study's spherules plotted in blue with the pink field representing the spherules from Gibbons et al (1976). Also plotted are the iron shale samples and the Canyon Diablo meteorite. This study's spherules generally fall within the field of the spherules from Gibbons et al (1976). Figure 64a and 64b exhibit the inverse proportional relationship between the nickel and iron content, and the directly proportional relationship between the nickel and cobalt. This correlation supports the quality of the spherule data replicated within this study. The spherules' Fe/Ni range is from 1.0 to 9.6, while the iron shale samples Fe/Ni range from 10-16.9 and the Canyon Diablo Fe/Ni range is 10.7-17.1.

Bunch and Cassidy (1972) analyzed the metallic spherules and plotted the diameters with Fe/Ni and P/Co (Figure 16). As the diameter of the spherule increases the Fe/Ni and P/Co increases as well. The metallic spherules in this study were measured and plotted with the electron microprobe data for Fe/Ni and P/Co. The graphs do not show the same data pattern as Bunch and Cassidy (1972) achieved. The widths of the spherules have varying ranges of Fe/Ni, creating vertical lines of data. For example for 10 μm the Fe/Ni ranges from 1 to 9. The spherules in Figure 65a and 65b are not the true size of the spherules as they were measured in thin section. This may have resulted in larger diameter spherules only being exposed at the thin section surface with less than maximum diameter, which does not reflect the true size of the spherule.

Many of the spherules in samples CCMK0700A and CCMK07045 show color differences in the reflected light that were assumed to be alteration. Twelve spherules of the

108 (with totals above 90 wt.%) have high sulfur contents < 0.5-4 wt.%, all of which appear to have color differences (alteration) inside the spherule. Preliminary SEM work supported the high sulfur contents on spherules with rims and alteration. The source of this sulfur may be from the impactor or a terrestrial source such as regional caliche from gypsum. The spherules with low totals might be due to barium (recognized by undergoing SEM element mapping), which was not analyzed for in the electron microprobe studies. The barium could be barite, which is a sulfide. Further analysis on the altered spherules would be beneficial to determine the stage at which the alteration occurred.

Table 11: This table is comparing the different types of ignimbrite samples.

	CCMK07013	CCMK07030	CCMK07034b	Total Sample Average	Bulk Melt	Light Melt Average
	XRF Analysis	XRF Analysis	XRF Analysis		XRF Analysis	Electron Microprobe
SiO ₂	74.54	74.29	73.70	74.18	75.61	77.60
Na ₂ O	3.95	3.83	3.65	3.81	3.26	2.53
TiO ₂	0.31	0.34	0.34	0.33	0.30	0.19
MgO	0.67	0.69	0.38	0.58	0.42	0.04
CaO	1.02	1.10	1.22	1.11	1.22	0.23
Al ₂ O ₃	13.09	13.25	13.79	13.38	12.34	12.80
FeO	1.31	1.48	1.46	1.42	2.04	0.91
K ₂ O	4.96	4.85	5.32	5.04	4.56	5.54
P ₂ O ₅	0.09	0.13	0.07	0.10	0.15	0.03
MnO	0.05	0.04	0.06	0.05	0.10	0.05
Total Sum	100.00	100.00	100.00	100.00	100.00	100.00

Note: CCMK07013, CCMK07030, CCMK07034b are ignimbrite target rock samples with XRF major element normalized data shown. The Total Sample Average is the average of all three ignimbrite target rock samples. Bulk Melt major element data is from XRF analysis, of multiple samples of light melt crushed together. The Light Melt average is from the data of samples CCMK07009, CCMK07046, and CCMK07047 collected with electron microprobe analysis.

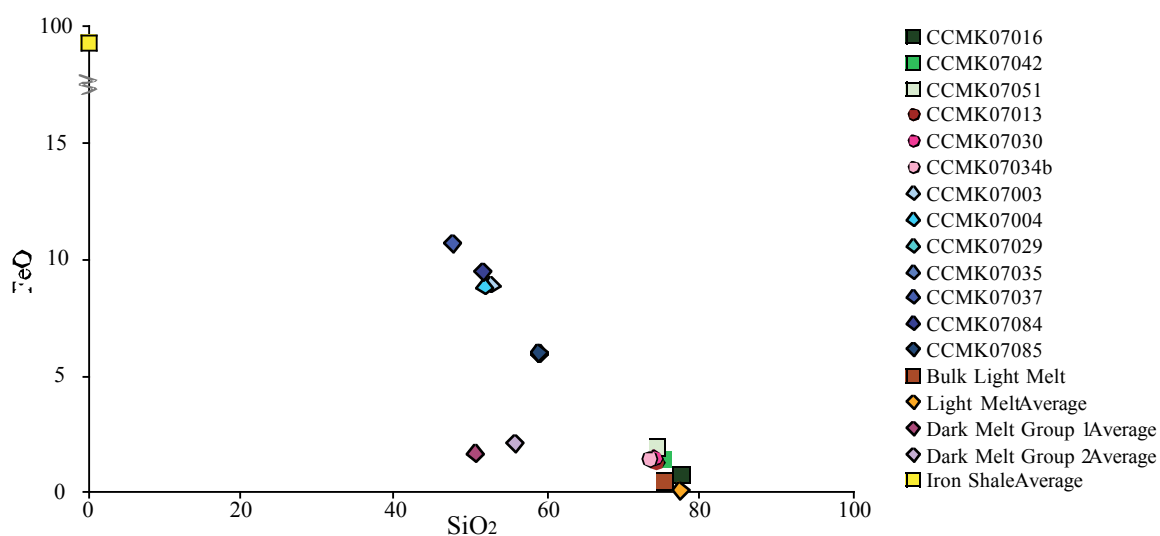


Figure 63: FeO vs. SiO₂, all three granite and ignimbrite samples, seven dikes plotted with bulk light melt, light melt average and dark melt group 1 and group 2 averages, and iron shale averages. Plot shows that the light melt average can be derived from the ignimbrite samples but the dark melt samples cannot be derived from just the granite samples.

Table 12: Least squares calculations of the granite components and ignimbrite components to determine the modal properties of phases that comprise the granite and ignimbrite.

	Percentage	%	SiO ₂	Na ₂ O	TiO ₂	MgO	CaO	Al ₂ O ₃	FeO	K ₂ O	P ₂ O ₅	MnO
Granite Components												
Orthoclase	20%	0.1997	64.35	0.45	0.02	0.01	0.02	19.07	0.05	16.04	0.02	0.04
Plagioclase	40%	0.4055	67.17	11.39	0.02	0.02	0.54	20.67	0.05	0.17	0.02	0.04
Biotite	5%	0.0493	22.84	0.02	0.09	7.37	1.77	18.15	25.41	0.33	0.03	1.30
Hematite	0%	-0.0005	3.18	0.00	0.03	0.00	0.46	0.37	95.49	0.00	0.05	0.03
Quartz	35%	0.3461	100.00	0.00	0.00	0.00	0.00	0.00	0.00	0.00	0.00	0.00
	100%	1.00										
Calculated Composition			75.82	4.71	0.02	0.37	0.31	13.08	1.23	3.29	0.01	0.09
Average Granite Comp (XRF Data)			75.95	4.42	0.12	0.27	1.17	13.43	1.36	3.18	0.03	0.06
Residual			0.13	-0.29	0.10	-0.11	0.86	0.35	0.13	-0.11	0.02	-0.03
Sum of Squares			1.02									
Ignimbrite Components												
Ignimbrite Matrix Average	62%	0.6205	70.57	4.08	0.10	0.12	0.41	16.81	0.46	7.32	0.04	0.03
Biotite	3%	0.0281	39.50	0.72	5.13	16.95	0.20	14.07	13.88	9.06	0.12	0.25
Plagioclase	12%	0.1170	60.61	7.61	0.02	0.02	5.70	24.63	0.30	1.11	0.02	0.02
Magnetite	1%	0.0069	0.07	0.00	8.57	18.73	0.06	1.28	88.20	0.00	0.04	1.72
Ilmenite	0%	0.0043	0.22	0.00	40.03	5.22	0.08	8.11	48.99	0.00	0.04	2.41
Quartz	22%	0.2232	100.00	0.00	0.00	0.00	0.00	0.00	0.00	0.00	0.00	0.00
	100%	1.00										
Calculated Composition			74.31	3.44	0.44	0.70	0.93	13.75	1.53	4.93	0.03	0.05
Average Ignimbrite Comp (XRF Data)			74.18	3.81	0.33	0.58	1.11	13.38	1.42	5.04	0.10	0.05
Residual			-0.13	0.37	-0.11	-0.13	0.18	-0.38	-0.11	0.12	0.07	0.00
Sum of Squares			0.39									

Note: The calculations use the Solver function in Microsoft Excel. The granite components include 10% plagioclase, 20% orthoclase, 35% quartz, 5% biotite, and 0% (<0.5) hematite. A sum of squares equaled 1.02 for the granite calculation. The ignimbrite components include 62% ignimbrite matrix, 22% quartz, 12% plagioclase, 3% biotite, 1% magnetite, and 0% (<0.5) ilmenite. A sum of squares equaled 0.39. Note all components were analyzed via electron microprobe except for quartz, which was calculated at 100 wt.% SiO₂.

Table 13: Least squares calculations for Light Melt, Dark Melt Group 1 and Dark Melt Group 2.

	Percentage	%	SiO ₂	Na ₂ O	TiO ₂	MgO	CaO	Al ₂ O ₃	FeO	K ₂ O	P ₂ O ₅	MnO	NiO
Light Melt Components													
Ignimbrite Average (XRF Data)	102%	1.0205	74.18	3.81	0.33	0.58	1.11	13.38	1.42	5.04	0.10	0.05	0.00
Iron Meteorite	-2%	-0.0205	0.00	0.00	0.00	0.00	0.00	0.00	92.10	0.00	0.00	0.00	7.90
Calculated Composition	100%	1.00	75.70	3.89	0.34	0.59	1.14	13.65	-0.45	5.15	0.10	0.05	-0.16
Total Light Melt Average			77.60	2.53	0.19	0.04	0.23	12.80	0.91	5.54	0.03	0.05	0.03
Residual			1.90	-1.36	-0.15	-0.55	-0.90	-0.86	1.36	0.39	-0.07	-0.01	0.19
Sum of Squares			9.36										
Group 1 Dark Melt Components													
Mafic Dike Group 1 (XRF Data)	15%	0.1473	52.18	3.60	1.78	6.50	6.66	17.52	9.08	1.96	0.55	0.17	0.00
Mafic Dike Group 2 (XRF Data)	2%	0.0220	58.98	5.05	0.69	3.74	5.16	18.50	5.95	1.59	0.21	0.13	0.00
Mafic Dike Group 3 (XRF Data)	16%	0.1623	47.73	4.19	3.02	5.15	8.79	17.23	10.69	1.85	0.97	0.37	0.00
Granite Average (XRF Data)	44%	0.4414	75.95	4.42	0.12	0.27	1.17	13.43	1.36	3.18	0.03	0.06	0.00
Iron Meteorite	23%	0.2270	0.00	0.00	0.00	0.00	0.00	0.00	92.10	0.00	0.00	0.00	7.90
Calculated Composition	100%	1.00	50.26	3.27	0.82	1.99	3.04	11.71	24.71	2.03	0.26	0.11	1.79
Total Group 1 Average			50.78	2.06	0.46	1.69	4.14	12.50	25.38	2.33	0.12	0.08	0.08
Residual			0.52	-1.22	-0.37	-0.31	1.10	0.78	0.67	0.30	-0.14	-0.03	-1.71
Sum of Squares			7.30										
Group 2 Dark Melt Components													
Mafic Dike Group 1 (XRF Data)	4%	0.0359	52.18	3.60	1.78	6.50	6.66	17.52	9.08	1.96	0.55	0.17	0.00
Mafic Dike Group 2 (XRF Data)	0%	-0.0042	58.98	5.05	0.69	3.74	5.16	18.50	5.95	1.59	0.21	0.13	0.00
Mafic Dike Group 3 (XRF Data)	32%	0.3241	47.73	4.19	3.02	5.15	8.79	17.23	10.69	1.85	0.97	0.37	0.00
Granite Average (XRF Data)	51%	0.5111	75.95	4.42	0.12	0.27	1.17	13.43	1.36	3.18	0.03	0.06	0.00
Iron Meteorite	17%	0.1648	0.00	0.00	0.00	0.00	0.00	0.00	92.10	0.00	0.00	0.00	7.90
Calculated Composition	100%	1.00	55.91	3.73	1.10	2.02	3.67	13.00	19.64	2.29	0.35	0.15	1.30
Total Group 2 Average			55.88	2.15	0.41	1.40	3.86	13.57	19.73	2.53	0.05	0.07	0.17
Residual			-0.03	-1.58	-0.69	-0.63	0.20	0.57	0.09	0.24	-0.30	-0.08	-1.13
Sum of Squares			5.17										

Note: Light Melt components included 102% ignimbrite average and -2% iron meteorite. The sum of squares equaled 9.32. The Dark Melt Group 1 components included 44% granite average, 23% iron meteorite, 15% mafic dike group 1, 16% mafic dike group 3, and 2% mafic dike group 2. The sum of squares equaled 7.30. The Dark Melt Group 2 components included 51% granite average, 17% iron meteorite, 32% mafic dike group 3, 4% mafic dike group 1, 0% mafic dike group 2. The sum of squares equaled 5.17. Note the iron meteorite values were determined from Buchwald (1977), which gives the average Ni content for an iron meteorite as 7.9 wt.%.

Table 15: Least squares calculations for Dark Melt Group 1 and with individual mineral components.

	Percentage	%	SiO ₂	Na ₂ O	TiO ₂	MgO	CaO	Al ₂ O ₃	FeO	K ₂ O	P ₂ O ₅	MnO	NiO
Group 1 Dark Melt Components													
Orthoclase	-5%	-0.0484	64.35	0.45	0.02	0.01	0.02	19.07	0.05	16.04	0.02	0.04	0.02
Plagioclase	-9%	-0.0916	67.17	11.39	0.02	0.02	0.54	20.67	0.05	0.17	0.02	0.04	0.01
Biotite	73%	0.7308	22.84	0.02	0.09	7.37	1.77	18.15	25.41	0.33	0.03	1.30	0.01
Quartz	41%	0.4091	100.00	0.00	0.00	0.00	0.00	0.00	0.00	0.00	0.00	0.00	0.00
	100%	1.00											
Calculated Composition			48.34	-1.05	0.06	5.38	1.25	10.45	18.56	-0.55	0.02	0.95	0.01
Total Group 1 Average			50.78	2.06	0.46	1.69	4.14	12.50	25.38	2.33	0.12	0.08	0.08
Residual			2.44	3.11	0.40	-3.69	2.90	2.05	6.82	2.88	0.10	-0.87	0.07
Sum of Squares			97.54										
Group 1 Dark Melt Components													
Orthoclase	-64%	-0.6399	64.35	0.45	0.02	0.01	0.02	19.07	0.05	16.04	0.02	0.04	0.02
Plagioclase	-70%	-0.7044	67.17	11.39	0.02	0.02	0.54	20.67	0.05	0.17	0.02	0.04	0.01
Biotite	6%	0.6191	22.84	0.02	0.09	7.37	1.77	18.15	25.41	0.33	0.03	1.30	0.01
Quartz	-20%	-0.2054	100.00	0.00	0.00	0.00	0.00	0.00	0.00	0.00	0.00	0.00	0.00
Ignimbrite Average (XRF Data)	193%	1.9307	74.18	3.81	0.33	0.58	1.11	13.38	1.42	5.04	0.10	0.05	0.00
	45%	1.00											
Calculated Composition			48.31	-0.94	0.66	5.66	2.86	10.30	18.40	-0.44	0.18	0.85	-0.01
Total Group 1 Average			50.78	2.06	0.46	1.69	4.14	12.50	25.38	2.33	0.12	0.08	0.08
Residual			2.47	3.00	-0.21	-3.97	1.28	2.20	6.98	2.77	-0.06	-0.77	0.09
Sum of Squares			94.39										
Group 1 Dark Melt Components													
Orthoclase	14%	0.1388	64.35	0.45	0.02	0.01	0.02	19.07	0.05	16.04	0.02	0.04	0.02
Plagioclase	22%	0.2219	67.17	11.39	0.02	0.02	0.54	20.67	0.05	0.17	0.02	0.04	0.01
Biotite	22%	0.2221	22.84	0.02	0.09	7.37	1.77	18.15	25.41	0.33	0.03	1.30	0.01
Quartz	21%	0.2122	100.00	0.00	0.00	0.00	0.00	0.00	0.00	0.00	0.00	0.00	0.00
Iron Meteorite	21%	0.2050	0.00	0.00	0.00	0.00	0.00	0.00	92.10	0.00	0.00	0.00	7.90
	100%	1.00											
Calculated Composition			50.13	2.59	0.03	1.64	0.52	11.26	24.54	2.34	0.01	0.30	1.63
Total Group 1 Average			50.78	2.06	0.46	1.69	4.14	12.50	25.38	2.33	0.12	0.08	0.08
Residual			0.65	-0.54	0.43	0.05	3.63	1.23	0.84	-0.01	0.11	-0.22	-1.55
Sum of Squares			18.72										
Group 1 Dark Melt Components													
Mafic Dike Group 1 (XRF Data)	34%	0.3418	52.18	3.60	1.78	6.50	6.66	17.52	9.08	1.96	0.55	0.17	0.00
Mafic Dike Group 3 (XRF Data)	15%	0.1463	47.73	4.19	3.02	5.15	8.79	17.23	10.69	1.85	0.97	0.37	0.00
Orthoclase	11%	0.1135	64.35	0.45	0.02	0.01	0.02	19.07	0.05	16.04	0.02	0.04	0.02
Plagioclase	10%	0.0947	67.17	11.39	0.02	0.02	0.54	20.67	0.05	0.17	0.02	0.04	0.01
Biotite	-7%	-0.0685	22.84	0.02	0.09	7.37	1.77	18.15	25.41	0.33	0.03	1.30	0.01
Quartz	13%	0.1347	100.00	0.00	0.00	0.00	0.00	0.00	0.00	0.00	0.00	0.00	0.00
Iron Meteorite	24%	0.2374	0.00	0.00	0.00	0.00	0.00	0.00	92.10	0.00	0.00	0.00	7.90
	100%	1.00											
Calculated Composition			50.39	2.97	1.05	2.47	3.50	11.39	24.81	2.76	0.33	0.03	1.88
Total Group 1 Average			50.78	2.06	0.46	1.69	4.14	12.50	25.38	2.33	0.12	0.08	0.08
Residual			0.39	-0.91	-0.59	-0.79	0.65	1.11	0.57	-0.43	-0.21	0.05	-1.80
Sum of Squares			7.39										

Note: First the granite mineral compositions are used as components of the dark melt, then granite + ignimbrite, then granite minerals + iron meteorite, finally granite minerals, mafic dike groups 1 & 3 and iron meteorite.

Table 16: Least squares calculations for and Dark Melt Group 2 with individual mineral components.

	Percentage	%	SiO ₂	Na ₂ O	TiO ₂	MgO	CaO	Al ₂ O ₃	FeO	K ₂ O	P ₂ O ₅	MnO	NiO
Group 2 Dark Melt Components													
Orthoclase	3%	0.0276	64.35	0.45	0.02	0.01	0.02	19.07	0.05	16.04	0.02	0.04	0.02
Plagioclase	3%	0.0288	67.17	11.39	0.02	0.02	0.54	20.67	0.05	0.17	0.02	0.04	0.01
Biotite	57%	0.5725	22.84	0.02	0.09	7.37	1.77	18.15	25.41	0.33	0.03	1.30	0.01
Quartz	37%	0.3711	100.00	0.00	0.00	0.00	0.00	0.00	0.00	0.00	0.00	0.00	0.00
	100%	1.00											
Calculated Composition			53.90	0.35	0.05	4.22	1.03	11.51	14.55	0.63	0.02	0.75	0.01
Total Group 2 Average			55.88	2.15	0.41	1.40	3.86	13.57	19.73	2.53	0.05	0.07	0.17
Residual			1.99	1.80	0.36	-2.82	2.83	2.06	5.18	1.89	0.04	-0.68	0.16
Sum of Squares			58.49										

	Percentage	%	SiO ₂	Na ₂ O	TiO ₂	MgO	CaO	Al ₂ O ₃	FeO	K ₂ O	P ₂ O ₅	MnO	NiO
Group 2 Dark Melt Components													
Orthoclase	-59%	-0.5852	64.35	0.45	0.02	0.01	0.02	19.07	0.05	16.04	0.02	0.04	0.02
Plagioclase	-60%	-0.6061	67.17	11.39	0.02	0.02	0.54	20.67	0.05	0.17	0.02	0.04	0.01
Biotite	46%	0.4567	22.84	0.02	0.09	7.37	1.77	18.15	25.41	0.33	0.03	1.30	0.01
Quartz	-27%	-0.2656	100.00	0.00	0.00	0.00	0.00	0.00	0.00	0.00	0.00	0.00	0.00
Ignimbrite Average (XRF Data)	200%	2.0002	74.18	3.81	0.33	0.58	1.11	13.38	1.42	5.04	0.10	0.05	0.00
	100%	1.00											
Calculated Composition			53.87	0.47	0.68	4.50	2.70	11.36	14.38	0.75	0.18	0.65	-0.01
Total Group 2 Average			55.88	2.15	0.41	1.40	3.86	13.57	19.73	2.53	0.05	0.07	0.17
Residual			2.01	1.68	-0.27	-3.11	1.16	2.22	5.36	1.78	-0.13	-0.58	0.18
Sum of Squares			55.11										

	Percentage	%	SiO ₂	Na ₂ O	TiO ₂	MgO	CaO	Al ₂ O ₃	FeO	K ₂ O	P ₂ O ₅	MnO	NiO
Group 1 Dark Melt Components													
Orthoclase	16%	0.1640	64.35	0.45	0.02	0.01	0.02	19.07	0.05	16.04	0.02	0.04	0.02
Plagioclase	26%	0.2572	67.17	11.39	0.02	0.02	0.54	20.67	0.05	0.17	0.02	0.04	0.01
Biotite	20%	0.2018	22.84	0.02	0.09	7.37	1.77	18.15	25.41	0.33	0.03	1.30	0.01
Quartz	23%	0.2276	100.00	0.00	0.00	0.00	0.00	0.00	0.00	0.00	0.00	0.00	0.00
Iron Meteorite	15%	0.1494	0.00	0.00	0.00	0.00	0.00	0.00	92.10	0.00	0.00	0.00	7.90
	100%	1.00											
Calculated Composition			55.20	3.01	0.03	1.49	0.50	12.11	18.91	2.74	0.01	0.28	1.19
Total Group 2 Average			55.88	2.15	0.41	1.40	3.86	13.57	19.73	2.53	0.05	0.07	0.17
Residual			0.68	-0.86	0.39	-0.10	3.37	1.47	0.83	-0.21	0.04	-0.21	-1.02
Sum of Squares			16.64										

	Percentage	%	SiO ₂	Na ₂ O	TiO ₂	MgO	CaO	Al ₂ O ₃	FeO	K ₂ O	P ₂ O ₅	MnO	NiO
Group 2 Dark Melt Components													
Mafic Dike Group 1 (XRF Data)	36%	0.3639	52.18	3.60	1.78	6.50	6.66	17.52	9.08	1.96	0.55	0.17	0.00
Mafic Dike Group 3 (XRF Data)	9%	0.0924	47.73	4.19	3.02	5.15	8.79	17.23	10.69	1.85	0.97	0.37	0.00
Orthoclase	14%	0.1398	64.35	0.45	0.02	0.01	0.02	19.07	0.05	16.04	0.02	0.04	0.02
Plagioclase	14%	0.1395	67.17	11.39	0.02	0.02	0.54	20.67	0.05	0.17	0.02	0.04	0.01
Biotite	-7%	-0.0688	22.84	0.02	0.09	7.37	1.77	18.15	25.41	0.33	0.03	1.30	0.01
Quartz	15%	0.1528	100.00	0.00	0.00	0.00	0.00	0.00	0.00	0.00	0.00	0.00	0.00
Iron Meteorite	18%	0.1805	0.00	0.00	0.00	0.00	0.00	0.00	92.10	0.00	0.00	0.00	7.90
	99%	1.00											
Calculated Composition			55.47	3.35	0.93	2.34	3.19	12.27	19.18	3.13	0.29	0.02	1.43
Total Group 2 Average			55.88	2.15	0.41	1.40	3.86	13.57	19.73	2.53	0.05	0.07	0.17
Residual			0.41	-1.20	-0.52	-0.94	0.67	1.30	0.56	-0.60	-0.24	0.06	-1.26
Sum of Squares			7.22										

Note: First the granite mineral compositions are used as components of the dark melt, then granite + ignimbrite, then granite minerals + iron meteorite, finally granite minerals, mafic dike groups 1 & 3 and iron meteorite.

Table 17: Displays the Canyon Diablo (CD) averages and the iron shale averages (samples CIUP08092 and CIUP08093) from electron microprobe analysis.

	CD average	Iron Shale average
Si	0.00	0.18
Ti	0.00	-0.01
Al	0.02	0.13
Fe	92.78	91.67
Mn	-0.01	-0.01
Ca	0.01	0.10
P	0.08	0.42
Ni	6.43	6.92
Cu	0.01	0.02
Co	0.67	0.56
Cr	-0.01	0.01
S	0.01	0.02
Total	100.00	100.00

Note: Canyon Diablo meteorite is a type IAB iron meteorite, which is the same group Bunch and Cassidy (1972) and Buchwald (1977) concluded that the Monturaqui meteorite was.

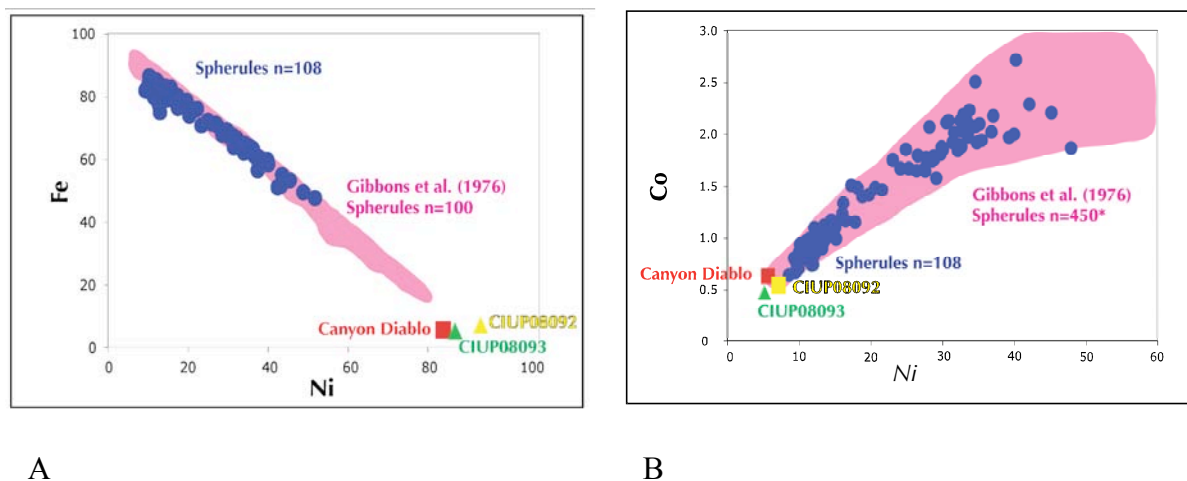


Figure 64: Graphs comparing this study's spherules compositions with the spherules analyzed in Gibbons et al. (1976). A) Fe vs. Ni, the blue spherules (108) are from this study's analysis, the pink field represents the spherules (100) analyzed in Gibbons et al (1976). B) Co vs. Ni, the spherules from this study (blue) fit within the field (pink) of the analysis from Gibbons et al (1976). Both graphs support the replication of spherule data. Note the spherules field in B, are made up of 450 spherules, 250 from Wabar, 100 from Henbury, and 100 from Monturaqui.

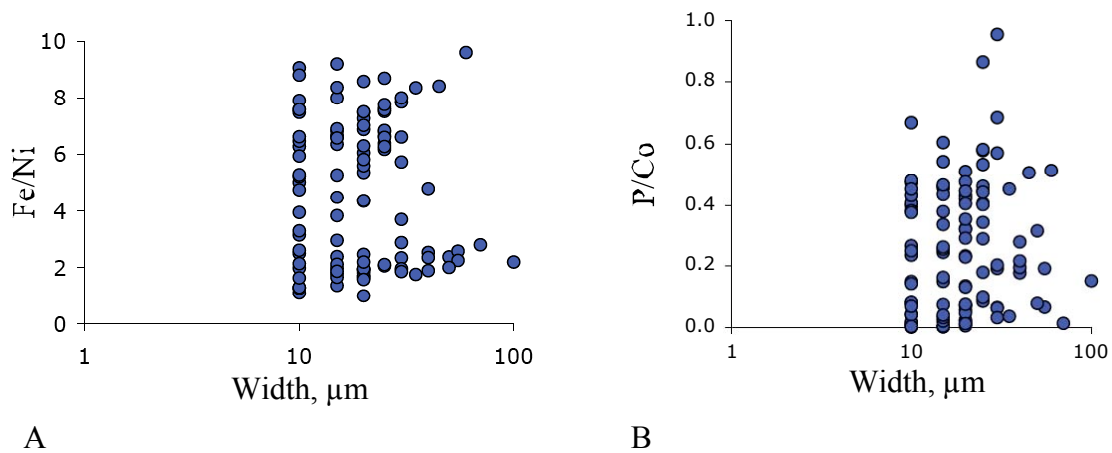


Figure 65: Spherules size relationships. A) Plot of this study's Fe/Ni ratios vs. width of spherules. B) Plot of this study's P/Co ratios vs. width of spherules.

CHAPTER 6: CONCLUSIONS

The scope of this M.Sc. project was to perform geochemical analysis of the target rocks, impact melt rocks and metal spherules found at Monturaqui Impact Crater, Chile. The fieldwork was performed in December 2007 and 2008 to collect the samples of target rocks and impact melt rocks. Steps were taken to make thin sections and prep samples for XRF analysis out of key samples of granite, ignimbrite, mafic dikes, impact melt rocks, metals, and iron shale samples. XRF and ICP-MS analysis was conducted by Washington State University for major and trace elements. Electron microprobe analysis was conducted at the University of Minnesota for the mineral phases of the granite and ignimbrite target rocks, glass composition for the impact melt clasts and metal spherules, local metals and meteorite samples.

The objectives of the project were to discover how the melt rock is related to the target rocks geochemically by quantifying how much of the target rock and what specific mineral phases are contributing to the impact melt rock. The target rock components were determined from the electron microprobe and XRF data, which was then used to perform least squares calculations. For the granite target rock the components are: 40% plagioclase, 35% quartz, 20% orthoclase, 5% biotite and 0% (< 0.5%) hematite. For the ignimbrite target rock the components are: 62% matrix, 22% quartz, 12% plagioclase, 3% biotite, 1% magnetite and almost 0% (< 0.5%) ilmenite. The impact melt was then calculated. The light melt group was determined to be from the ignimbrite target rock determined from petrological and geochemical similarities. Also the least squares calculations determined the components of the light melt to be 100% ignimbrite. The dark melt group was multiple

groups, including melted minerals with determined maskelynite and lechatelierite and dark melt group 1 made up of the components of 44% granite, 23% iron meteorite, 16% mafic dike group 3, 15% mafic dike group 1, and 2% mafic dike group 2. Group 2 is made up of the components of 51% granite, 32% mafic dike group 3, 17% iron meteorite, 4% mafic dike group 1, and 0% mafic dike group 2. The dark melt impactite is located on the southeast side of the crater where the mafic dike group 1 and group 3 are located, so it is more likely that these groups are components in the dark melt than mafic dike group 2 (located on the western side of the crater). Based on the components calculated, the impact melt is heterogeneous. The pressures and temperatures are concluded from the data points of melted minerals with maskelynite and lechatelierite, and planar deformation features found in plagioclase and quartz grains, to be ~45-55 GPa, and < 1700°C.

Studies of large impact craters typically assume the target rock contributes to one type of melt. The two types of melt at Monturaqui were created from each separate target rock in addition to the mafic dikes and iron meteorite. This was not previously discovered at Monturaqui or at any other impact crater that we know of. Monturaqui can be used a valuable analogue for impact craters on Earth and other planets and moons, because of the simple target rock lithology and multiple impact melts with preferentially melted minerals, it is a rarity in the impact world.

The iron shale and metallic spherules were also analyzed in this project. The iron shale fit within Buchwald (1977) statement that > 5% nickel is indicative of meteorite nickel. The Ni content for the iron shale samples was 6.9 wt.%. Also Buchwald (1977) gave the range of sulfur content indicative of a meteorite at a range of 0.02-12%. The range of sulfur in the iron shale is 0.02-0.04%. The analysis of the spherules confirmed the Fe, Ni, Co

content that was found by Gibbons et al (1976). The size distribution vs. Fe/Ni and P/Co did not agree with the data from Bunch and Cassidy (1972). This is due to the measuring the spherules in thin section, the spherules are not at their true size due to cutting and polishing of the clast.

In-depth study of the trace elements of the iron shale sample especially Ga, Ir, Ge and Platinum Group Elements would further support the samples as derived from of the impactor at Monturaqui. Additional analysis of the altered metal spherules especially Fe, Ni, S, and Ba would help to understand the alteration effects the spherules went through and when during the impact they occurred.

Monturaqui can also be used an analogue for craters on Earth, other planets and moons with metal spherules. Future studies on the spherules will help compare to other spherule craters by showing the relationship of the Fe, Ni, Co and P due to the size of spherule. Formation and alteration of spherules is important mechanisms to understand to compare and contrast to other craters. Also the emplacement of the spherules in the impact melt and how it may contribute to the glass can help the understanding of the heterogeneous state of the impact melt at Monturaqui.

REFERENCES

- Benedix, G.K., McCoy, T.J., and K. Keil. "A Petrologic study of the IAB iron meteorites: Constraints on the formation of the IAB-Winonaite parent body." *Meteoritics & Planetary Science*, Vol. 35, No. 6 (November 2000): 1127-1141.
- Blau, P. J., Axon, H.J., and J. I. Goldstein. "Investigation of the Canyon Diablo Metallic Spheroids and their relationship to the breakup of the Canyon Diablo Meteorite." *Journal of Geophysical Research*, Vol. 78, No. 2 (January 1973): 363-374.
- Buchwald, W.F. "The Mineralogy of Iron Meteorites." *Philosophical Transactions of the Royal Society of London*, Vol. 286, No. 1336 (September 1977): 453-491.
- Buchwald, W.F. *Handbook of Iron Meteorites: Their History, Distribution, Composition, and Structure*, Vol 1, University of California Press, 1975.
- Bunch, T.E., and W.A. Cassidy. "Petrographic and Electron Microprobe Study of the Monturaqui Impactite." *Contributions to Mineralogy and Petrology*, Vol 36, No. 2 (1972): 95-112.
- Cabrol, N.A., Chong, G., Grin, E.A., Piatek, J.L. and I. Ukestins Peate "Formation and Evolution of Spherules and Possible Planetary Analogy."
- Canyon Diablo Meteorite. Remote Sensing Tutorial Page 18-1.
http://rst.gsfc.nasa.gov/Sect18/Sect18_1.html.
- Carter, N. L. "Basal quartz deformation lamellae; a criterion for recognition of impactites." *American Journal of Science*, Vol 263, (November 1965): 786-806.
- Cassidy, W.A. "A small meteorite crater; structural details." *Journal of Geophysical Research*, Vol.76, no. 17 (1971): 3896-3912.
- Cockell, C.S., and P. Lee. "The biology of impact craters – a review." *Biological Reviews*, Vol. 77, No. 03 (September 2002): 279-310.
- Deutsch, A, and U. Schaerer. "Dating terrestrial impact events." *Meteoritics*, Vol. 29, No. 3 (1994): 301-322.
- Dressler, B.O., and W.U. Reimold. "Terrestrial impact melt rocks and glasses." *Earth-Science Reviews*, Vol. 56, No. 1 - 4 (December 2001): 205- 285.
- Dunlap, R.A., and J.D. McGraw. "A Mössbauer effect study of Fe environments in impact glasses." *Journal of Non-Crystalline Solids*, Vol. 353, No. 22 - 23 (July 2007): 2201-2205.

Earth Impact Database. UNB | Planetary and Space Science Centre.
<http://www.unb.ca/passc/>.

Echaurren, A., Ocampo, C., and M.C.L. Rocca "A Mathematical model for the Monturaqui Impact Crater, Chile, South America." 68th Annual Meteoritical Society Meeting (2005).

French, B.M. *Traces of Catastrophe: A handbook of shock-metamorphic effects in terrestrial meteorite impact structures*. LPI Contribution No. 954, Lunar and Planetary Institute, Houston (1998).

Gibbons, R.V., Hörz, F., Thompson, T.D., and D.E. Brownlee. "Metal spherules in Wabar, Monturaqui, and Henbury impactites." *Lunar Science Conference 7th*, (March 1976): 863-880.

Grieve, Richard A.F. "Terrestrial Impact Structures." *Annual Review of Earth and Planetary Sciences*, Vol. 15 (May 1987): 245-275.

Grieve, Richard A.F., and E. M. Shoemaker. "The record of past impacts on Earth." *Hazards Due to Comets and Asteroids*, (1994): 417-462.

Hörz, Friedrich, Mittlefehldt, D.W., See, T.H., and C. Galindo. "Petrographic studies of the impact melts from Meteor Crater, Arizona, USA." *Meteoritics & Planetary Science*, Vol. 37, No. 4 (April 2002): 501-531.

Johnson, D.M., Hooper, P.R., and R.M. Conrey. "XRF Analysis of rocks and minerals for major and trace elements on a single low dilution Li-tetraborate fused bead." *Advances in X-ray Analysis*, Vol. 41 (1999): 843-867.

Kelly, W.R., Holdsworth, E., and C.B. Moore. "The chemical composition of metallic spheroids and metallic particles within impactite from Barringer Meteorite Crater, Arizona." *The Geochimica et Cosmochimica Acta*, Vol. 38, No. 4 (April 1974): 533-543.

Koeberl, C. "Geochemistry of tektites and impact glasses." *Annual Review of Earth and Planetary Sciences*, Vol. 14 (1986): 323-350.

Koeberl, C., "Identification of meteoritic components in impactites." *Geological Society of London Special Publication*, (1998): 133-153.

Koeberl, C., "Impact cratering: The mineralogical and geochemical evidence." *Oklahoma Geological Survey Circular*, Vol. 100 (1997): 30-54.

Koeberl, C., "Mineralogical and geochemical aspects of impact craters." *Mineralogical Magazine*, Vol. 66, No. 5 (October 2002): 745-768.

- Koch, C.B. "Weathering of impactite from Monturaqui." Abstract, *Program and Abstracts for Clay Minerals Society* (1991): 91.
- Koch, C., and V.F. Buchwald, "Weathering of Iron Meteorites from Monturaqui, Chile." Abstract, *Meteoritics*, Vol. 29, No. 4 (July 1994): 443.
- Lipka, J., Madsen, M.B., Koch, C.B., Miglierini, M., Knudsen, J.M., Morup, S., and M.B. Bentson. "The Monturaqui impactite and the iron in it." *Meteoritics*, Vol. 29, No. 4 (July 1994): 492.
- Lipka, J., Jensen, H.G., Knudsen, J.M., Madsen, M.B., Bentson, M.D., Koch, C.B., and S. Mørup. "A Mössbauer study of an impactite from the Monturaqui crater." *Hyperfine Interactions*, Vol. 70, No. 1-4 (1992): 965-968.
- Location of Monturaqui Impact Crater. Topographic Map of Chile | Mapsorama.com
<http://www.mapsorama.com/topographic-map-of-chile/>.
- McCall, G.J.H., Bowden, A.J., and R.J. Howarth. "Meteorite cratering; Hooke, Gilbert, Barringer and beyond." *Geological Society of London Special Publication*, Vol. 256 (2006): 443-469.
- McPherson, D., Pye, L.D., and V.D. Fréchet. "Microstructure of natural glasses." *Journal of Non-Crystalline Solids*, Vol. 67, No. 1-3 (September 1984): 61-79.
- Mittlefehldt, D.W., Hörz, F. See, T.H., Scott, E.R.D., Mertzman, S.A. "Geochemistry of target rocks, impact-melt particles, and metallic spherules from Meteor Crater, Arizona: Empirical Evidence on the impact process." *Large meteorite impacts III: Geological Society of America Special Paper 384*, (2005): 367-390.
- Mittlefehld, D.W., Varley, L.R., Mertzmann, S.A., Roddy, D.J., and F. Hörz, "Major element composition of the target rocks at Meteor Crater, AZ." *Lunar and Planetary Science XXXI*, 1720.
- Moon, H.K., Min, B.H., Fletcher, A.B., Kim, B.G., Han, W., Chun, M.Y. Jeon, Y.B., and W.B. Lee. "Terrestrial impact cratering chronology: a preliminary analysis." *Journal of Astronomy and Space Science*, Vol. 18, No. 3 (2001): 191-208.
- Moreno, Teresa, and Wes Gibbons. *The Geology of Chile*. London: Geological Society of London, 2007.
- Osinski, G.R., Grieve, R.A.F., Collins, G.S., Marion, C. and P. Sylvester. "The effect of target lithology on the products of impact melting." *Meteoritics & Planetary Science*, Vol. 43, No. 12 (2008): 1939-1954.

Osinski, Gordon R. "Hypervelocity impacts into sedimentary targets: processes and products." PhD diss., University of New Brunswick, 2004.

Parfenova, O.V., and O.I. Yakolev. "Some peculiarities of selective evaporation in target rocks after meteoritic impact." *Impact and Explosion Cratering*, (1977): 843-859.

Park, F.R., "A comparative study of some metallic spherules." *Annals of the New York Academy of Sciences*, Vol. 119 (1964): 250-281.

Poelchaup, M.H., and T. Kenkmann. "Asymmetric signatures in simple craters as an indicator for an oblique impact direction." *Meteoritics & Planetary Science*, Vol. 43, No. 12 (December 2008): 2059–2072.

Reimold, W.U. "The Impact Crater Bandwagon (Some problems with the terrestrial impact cratering record)." *Meteoritics & Planetary Science*, Vol. 42, No. 9 (2007): 1467-1472.

Reimold, W.U., Horton, W., and R.T. Schmitt, "Debate about impactite nomenclature-recent problems." *Large Meteorite Impact and Planetary Evolution IV*, (2008): 3033.

Sanchez, J., and W. Cassidy. "A previously undescribed meteorite crater in Chile." *Journal of Geophysical Research*, Vol. 71, No. 20 (October 1966): 4891-4895.

Schrand, C. and A. Deutsch, "Formation of lechatelierite and impact melt glasses in experimentally shocked rocks." *Lunar and Planetary Science XXIX*, 1671.

See, T.H., Höra, F., Mittlefehldt, D.W., Varley, L., Mertzman, S., and D. Roddy, "Major element analyses of the target rocks at Meteor Crater, Arizona. NASA/TM-2002-210787.

Shoemaker, E.M., "Asteroid and comet bombardment of the earth." *Annual Review of Earth and Planetary Sciences*. Vol. 11 (1983): 464-494.

Shoemaker, E.M. "Why study impact craters?" *Impact and Explosion Cratering; Planetary and Terrestrial Implications; Proceedings of the Symposium on Planetary Cratering Mechanics*, (1977): 1-10.

Smith, T., and P. Hodge, "Microscopic meteoritic material surrounding meteorite craters." *Meteoritics & Planetary Science*, Vol. 29 (1993): 439.

Stöffler, D., and R.A.F. Grieve, "11. Impactites." www.bgs.ac.uk/scmr/home.html.

Tagle, R., and L. Hecht. "Geochemical identification of projectiles in impact rocks." *Meteoritics & Planetary Science*, Vol. 41, No. 11 (November 2006): 1721-1735.

Ugalde, H., Valenzuela, M., and Milkereit, B., "An integrated geophysical and geological study of the Monturaqui impact crater, Chile." *Meteoritics & Planetary Science*, Vol. 42, No. 12 (December 2007): 2153-2163.

Ukstins Peate, I., Klobberdanz, C., Peate, D.W., Chung Wan, L., Cabrol, N., Grin, E., Piatek, J., and G. Chong, "Non-modal melting of target rocks to produce impactite at Monturaqui Crater, Chile." 41st Lunar and Planetary Science Conference, 1-5 March 2010, Houston, Texas.

Ukstins Peate, I., Van Soest, M.C., Wartho, J.A., Cabrol, N., Grin, E., Piatek, J., and G. Chong, "A novel application of (U-Th)/He geochronology to constrain the age of small, young meteorite impact craters: A case study of the Monturaqui crater, Chile." 41st Lunar and Planetary Science Conference, 1-5 March 2010, Houston, Texas.

Valenzuela, M., Bland, P.A., Russell, S.S., Roeschmann, C., and D. Morata, "Chondrites from the Atacama Desert." 68th Annual Meteoritical Society Meeting (2005): 5096.

University of Minnesota Electron Microprobe Facilities. Electron Microprobe.
<http://probelab.geo.umn.edu/>.

Valenzuela, M., Rochette, P., Bournès, D.L., Braucher, R., Faestermann, T., Finkel, R.C., Gattacceca, J., Poutivtsev, M., Riegel, G., Suavet, C., Korschinek, G., Merchel, S., Morata, D., and M. Poutivtsev. "The Age of the Monturaqui Impact Crater." *Meteoritics and Planetary Science*, Vol. 44, 7 Suppl. (September 2009): 5185.

Verdugo, M. and C. Cartes, "Establecimiento de la edad del Crater Monturaqui por el metodo de termoluminiscencia en solidos." Facultad de Física, Pontificia Universidad Católica de Chile, (2000).

Washington State University Geoanalytical Facilities. WSU SEES: GeoAnalytical Lab.
<http://www.sees.wsu.edu/Geolab/index2.html>.

APPENDIX A
SAMPLES

Table A1: Samples collected in field season 2007 in Chile.

Sample ID	GPS		Elevation	Elevation Error (m)	Description
	Easting	Northing			
CCMK07001	S23° 55' 35.5"	W068° 15' 40.2"			ignimbrite pumice
CCMK07002	S23° 55' 39.4"	W068° 15' 39.3"	2984m	3.66	ignimbrite pumice
CCMK07003	S23° 55' 43.2"	W068° 15' 37.7"	2998m	5.49	basalt dyke~ 5m long
CCMK07004	S23° 55' 43.9"	W068° 15' 38.3"	3002m	5.79	basalt dyke~ 30m long
CCMK07005	S23° 55' 40"	W068° 15' 36"	3005m		ignimbrite melt rock
CCMK07006	S23° 55' 43"	W068° 15' 36"	3014m		ignimbrite melt rock
CCMK07007	S23° 55' 46.9"	W068° 15' 36"	3010m		8 magnetic rocks (iron shale?)
CCMK07008	S23° 55' 39.4"	W068° 15' 39.3"	2984m	3.66	darker ignimbrite
CCMK07009	S23° 55' 45.3"	W068° 15' 38.8"	3005m		7 light colored vesicular melt
CCMK07010	S23° 55' 44.1"	W068° 15' 37.2"	3004m		11 ignimbrite melt rock
CCMK07011	S23° 55' 37.3"	W068° 15' 48.1"			magnetic, iron shale?, ignimbrite?
CCMK07012	S23° 56' 21.9"	W068° 15' 34.9"	3001m		basalt dyke, contact with granite
CCMK07013	S23° 56' 21.0"	W068° 15' 35.5"	3029m	4.88	unaltered ignimbrite
CCMK07014	S23° 56' 38.3"	W068° 15' 54.9"			unaltered granite with hematite vien
CCMK07015	S23° 56' 38.3"	W068° 15' 54.9"			hematite
CCMK07016	S23° 56' 21.9"	W068° 15' 34.9"	3001m		unaltered granite, contact with basalt dyke
CCMK07017	S23° 56' 23.9"	W068° 15' 34.6"	3039m	6.71	massive hematite
CCMK07018	S23° 56' 23.9"	W068° 15' 34.6"	3039m	6.71	plagioclase-phyric basalt dyke
CCMK07019	S23° 56' 24.8"	W068° 15'35.4"	3050m	5.49	unaltered granite with hematite vien
CCMK07020	S23° 56' 24.8"	W068° 15'35.4"	3050m	5.49	massive brecciated hematite veins
CCMK07021	S23° 56' 24.8"	W068° 15'35.4"	3050m	5.49	brecciated quartz weathering out of hematite
CCMK07022	S23° 56' 24.1"	W068° 15' 35.5"	3045m	7.92	brecciated quartz outcrop/vein with hematite
CCMK07023	S23° 56' 24.8"	W068° 15' 32.3"	3051m	6.40	basalt dyke~3.5m across, stops at gully
CCMK07024	S23° 56' 24.8"	W068° 15' 32.3"	3051m	6.40	basalt dyke- middle of, plag. Crxls
CCMK07025	S23° 56' 25.6"	W068° 15' 31.6"	3048m	5.18	basalt dyke, parallel to previous one
CCMK07026	S23° 56' 22.3"	W068° 15' 32.7"	3045m	5.18	magnetic basalt dyke
CCMK07027	S23° 55' 45.2"	W068° 15' 47.4"	3014m		10 dark ferric ignimbrite- larger vesicules
CCMK07028	S23° 55' 45.2"	W068° 15' 47.4"	3014m		10 dark ferric ignimbrite-vesicules
CCMK07029	S23° 55' 45.1"	W068° 15' 47.1"	3014m		9 basalt with amphibole dyke
CCMK07030	S23° 55' 46.6"	W068° 15' 44.5"	3024m		22 ignimbrite w/ biotite flakes
CCMK07031	S23° 55' 46.0"	W068° 15' 45.1"	3020m		12 ignimbrite with black glass, shows gradation
CCMK07032	S23° 55' 46.0"	W068° 15' 45.1"	3020m		12 ignimbrite with black glass, even throughout
CCMK07033	S23° 55' 46.5"	W068° 15' 45.2"	3020m		11 ignimbrite with brown glass, lighter matrix
CCMK07034a	S23° 55' 46.5"	W068° 15' 44.9"	3022m		8 ignimbrite with glass- darker, more glass
CCMK07034b	S23° 55' 46.5"	W068° 15' 44.9"	3022m		8 ignimbrite with glass-lighter, larger pieces of glass
CCMK07034c	S23° 55' 46.5"	W068° 15' 44.9"	3022m		8 ignimbrite with glass-lighter, larger pieces of glass
CCMK07035	S23° 55' 46.7"	W068° 15' 40.3"	3010m		8 mafic dyke- previously mapped
CCMK07036	S23° 55' 46.9"	W068° 15' 41.4"	3013m		15 anorthosite?? Very hard
CCMK07037	S23° 55' 46.9"	W068° 15' 41.4"	3013m		15 mafic dyke with mustard yellow spherules
CCMK07038	S23° 55' 46.7"	W068° 15' 41.5"	3013m		15 calcite with floating ignimbrite(?)
CCMK07039	S23° 55' 46.7"	W068° 15' 41.5"	3013m		15 black vesicular glass melt
CCMK07040a	S23° 55' 46.6"	W068° 15' 41.4"	3002m		9 black vesicular glass melt
CCMK07040b	S23° 55' 46.6"	W068° 15' 41.4"	3002m		9 black vesicular glass melt
CCMK07041a	S23° 55' 46.6"	W068° 15' 41.4"	3002m		9 black vesicular glass melt
CCMK07041b	S23° 55' 46.6"	W068° 15' 41.4"	3002m		9 black vesicular glass melt
CCMK07041c	S23° 55' 46.6"	W068° 15' 41.4"	3002m		9 black vesicular glass melt
CCMK07041d	S23° 55' 46.6"	W068° 15' 41.4"	3002m		9 black vesicular glass melt
CCMK07041e	S23° 55' 46.6"	W068° 15' 41.4"	3002m		9 black vesicular glass melt
CCMK07041f	S23° 55' 46.6"	W068° 15' 41.4"	3002m		9 black vesicular glass melt
CCMK07042	S23° 55' 46.4"	W068° 15' 40.1"	3005m		10 white granite
CCMK07043a	S23° 55' 47"	W068° 15' 35"	3000m		light colored vesicular melt
CCMK07043b	S23° 55' 47"	W068° 15' 35"	3000m		light colored vesicular melt
CCMK07043c	S23° 55' 47"	W068° 15' 35"	3000m		light colored vesicular melt
CCMK07043d	S23° 55' 47"	W068° 15' 35"	3000m		light colored vesicular melt
CCMK07043e	S23° 55' 47"	W068° 15' 35"	3000m		light colored vesicular melt
CCMK07043f	S23° 55' 47"	W068° 15' 35"	3000m		light colored vesicular melt
CCMK07044	S23° 55' 47"	W068° 15' 35"	3000m		amphibole basalt
CCMK07045	S23° 55' 47"	W068° 15' 35"	3000m		large black vesicular melt
CCMK07046	S23° 55' 47"	W068° 15' 35"	3000m		ignimbrite melt rock- vesicular texture
CCMK07047	S23° 55' 47"	W068° 15' 35"	3000m		ignimbrite melt rock- ropy texture
CCMK07048a	S23° 55' 47"	W068° 15' 35"	3000m		very black vesicular melt
CCMK07048b	S23° 55' 47"	W068° 15' 35"	3000m		very black vesicular melt
CCMK07049	S23° 55' 44.9"	W068° 15' 41.9"	2995m		13 from diggings-white granite with kspar & qtz
CCMK07050	S23° 55' 44.9"	W068° 15' 41.9"	2995m		13 from diggings-white granite with gypsum(?)

Note: Samples CIUP08092 and CIUP08093 were collected in the 2008 field season.

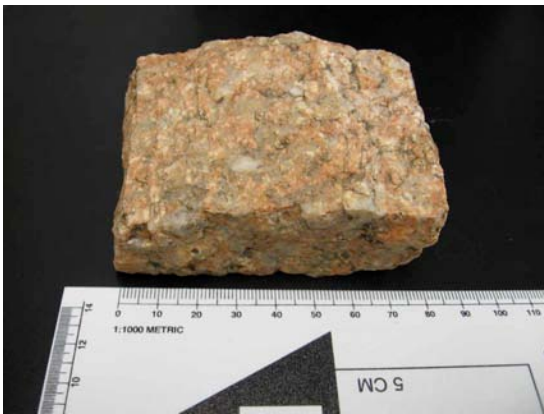
Table A1: Continued.

Sample ID	GPS		Elevation	Error (m)	Description
	Easting	Northing			
CCMK07051	S23° 55' 44.5"	W068° 15' 42.1"	2993m		8 pink kspar granite
CCMK07052	S23° 55' 44.3"	W068° 15' 39.5"	2997m		22 from diggings-white granite with gypsum(?)
CCMK07053	S23° 55' 44.3"	W068° 15' 39.5"	2997m		22 from diggings-white granite encased in breccia
CCMK07054	S23° 55' 44.3"	W068° 15' 39.5"	2997m		22 from diggings-breccia with granite and gypsum pieces
CCMK07055	S23° 55' 44.3"	W068° 15' 39.5"	2997m		22 from diggings-breccia with granite and gypsum pieces
CCMK07056	S23° 55' 44.3"	W068° 15' 39.5"	2997m		22 from diggings-large breccia with granite and gypsum pieces
CCMK07057	S23° 55' 44.3"	W068° 15' 39.5"	2997m		22 from diggings-breccia with granite and gypsum pieces
CCMK07058	S23° 55' 45.6"	W068° 15' 36.5"	3008m		3.96 light colored vesicular melt
CCMK07059	S23° 55' 46.8"	W068° 15' 37.0"	3009m		27 black vesicular glass melt
CCMK07060	S23° 55' 46.8"	W068° 15' 37.0"	3009m		27 black vesicular glass melt
CCMK07061	S23° 55' 46.8"	W068° 15' 37.0"	3009m		27 black vesicular glass melt
CCMK07062	S23° 55' 46.8"	W068° 15' 37.0"	3009m		27 black vesicular glass melt
CCMK07063	S23° 55' 46.8"	W068° 15' 37.0"	3009m		27 black vesicular glass melt
CCMK07064	S23° 55' 46.8"	W068° 15' 37.0"	3009m		27 black vesicular glass melt
CCMK07065	S23° 55' 46.8"	W068° 15' 37.0"	3009m		27 black vesicular glass melt
CCMK07066	S23° 55' 46.8"	W068° 15' 37.0"	3009m		27 black vesicular glass melt
CCMK07067	S23° 55' 46.8"	W068° 15' 37.0"	3009m		27 black vesicular glass melt
CCMK07068	S23° 55' 46.8"	W068° 15' 37.0"	3009m		27 black vesicular glass melt
CCMK07069	S23° 55' 46.8"	W068° 15' 37.0"	3009m		27 black vesicular glass melt
CCMK07070	S23° 55' 46.8"	W068° 15' 37.0"	3009m		27 black vesicular glass melt
CCMK07071	S23° 55' 46.8"	W068° 15' 37.0"	3009m		27 black vesicular glass melt
CCMK07072	S23° 55' 46.8"	W068° 15' 37.0"	3009m		27 black vesicular glass melt
CCMK07073	S23° 55' 46.8"	W068° 15' 37.0"	3009m		27 black vesicular glass melt- 2 pieces
CCMK07074	S23° 55' 46.8"	W068° 15' 37.0"	3009m		27 black vesicular glass melt- ropy texture
CCMK07075	S23° 55' 46.4"	W068° 15' 36.7"	3006m		6.10 black vesicular glass melt
CCMK07076	S23° 55' 46.4"	W068° 15' 36.7"	3006m		6.10 brown vesicular glass melt
CCMK07077	S23° 55' 46.4"	W068° 15' 36.7"	3006m		6.10 black vesicular glass melt
CCMK07078	S23° 55' 46.4"	W068° 15' 36.7"	3006m		6.10 brown vesicular glass melt
CCMK07079	S23° 55' 46.4"	W068° 15' 36.7"	3006m		6.10 black vesicular glass melt
CCMK07080	S23° 55' 47"	W068° 15' 35"			black vesicular with hematite(?)
CCMK07081	S23° 55' 46.7"	W068° 15' 35.7"	2994m		12 light colored vesicular melt
CCMK07082	S23° 55' 47.1"	W068° 15' 36.3"	3003m		30 black vesicular glass melt
CCMK07083	S23° 55' 47.1"	W068° 15' 36.3"	3003m		30 black vesicular glass melt
CCMK07084	S23° 55' 35.9"	W068° 15' 41.2"	2997m		14 mafic dyke- white spots (altered)
CCMK07085	S23° 55' 42.2"	W068° 15' 49.1"	3015m		10 mafic dyke- increase of plagioclase
CCMK07086	S23° 55' 31.3"	W068° 15' 31.8"	2986m		25 hematite with possible iron (?) heavy
CCMK07087	S23° 55' 36.8"	W068° 15' 52.2"	2995m		16 brown vesicular glass melt
CCMK07088	S23° 55' 34.5"	W068° 16' 02.8"	3007m		4.88 sampled soil (for magnetic material)-4in below surface
CCMK07089	S23° 55' 18.1"	W068° 16' 03.9"	2996m		3.96 sampled soil ~2in below surface
CCMK07090	S23° 55' 14.9"	W068° 16' 06.1"	2979m		4.57 sampled soil in gully ~2in below surface
CCMK07091	S23° 55' 06.5"	W068° 16' 10.5"	2996m		10 sampled soil at top of ridge near end of eject field ~2in below
CCMK07092	S23° 55' 18.6"	W068° 15' 49.9"	2963m		4.27 sampled soil to NW of crater ~2-4in below
CCMK07093	S23° 55' 45.5"	W068° 15' 37.5"	3007m		3.05 sampled soil at southern rim ~2-4in below
CCMK07094	S23° 55' 46.3"	W068° 15' 36.4"	3000m		3.35 sampled soil further down crater wall ~2-4in below
CCMK07095	S23° 55' 45.9"	W068° 15' 36.2"	3004m		3.35 sampled soil under surface ~2-4in below
CIUP08092	S 23° 55' 54.8"	W068° 15' 36.8"			8 iron shale?
CIUP08093	S 23° 55' 44.3"	W068° 15' 31.0"			8 black oxide

APPENDIX B
THIN SECTION DESCRIPTIONS

Appendix B-1: Granites

CCMK07016 (S23° 56' 21.9", W068° 15' 34.9")



Hand Sample



Thin Section in PPL

Igneous: Paleozoic Granite**Name:** Coarse-grained biotite granite**Texture:** medium to coarse grained, fracturing present**Color:** dominantly pink on fresh surface, rusty orange on weathered surface**Mineral Abundances:**

Plagioclase: 40%, 2 to 4mm, subhedral to anhedral

Quartz: 25%, 2 to 4mm, anhedral

Fractures seen in thin section

K-spar: 20%, < 2 mm, subhedral

More is typically seen in hand sample than thin section.

Biotite: 10%, 0.5 to 2mm, anhedral

Approximately 5% is altering into chlorite

Oxides: $\leq 5\%$, ≤ 0.20 mm, anhedral

Appendix B-2: Granites

CCMK07042 (S23° 55' 46.4", W068° 15' 40.1")



Hand Sample



Thin Section in PPL

Igneous: Paleozoic Granite**Name:** Medium grained biotite granite**Texture:** medium to coarse grained, fracturing present**Color:** dominantly white on fresh surface, rusty orange on weathered surface**Mineral Abundances:**

Plagioclase: 35%, 0.10 to 2 mm, subhedral to anhedral

Planar Deformation Features present, multiple parallel fractures

Quartz: 25%, 2 to 4mm, anhedral

PDFs present, multiple parallel fractures

K-spar: 20%, < 1 mm, subhedral to anhedral

More is typically seen in hand sample.

Biotite: 15%, 1 to 2.5 mm, subhedral

Approximately half is altering into chlorite

Oxides: < 5%, < 0.10 mm, anhedral

Appendix B-3: Granites

CCMK07051 (S23° 55' 44.5", W068° 15' 42.1")



Hand Sample



Thin Section in PPL

Igneous: Paleozoic Granite**Name:** Coarse-grained feldspar granite**Texture:** medium to coarse grained, fracturing present**Color:** dominantly pink on fresh surface, rusty orange on weathered surface**Mineral Abundances:**

- Plagioclase: 20%, 0.5 to 4mm, subhedral
 - PDFs, multiple parallel and perpendicular fractures
 - Diaplectic glass- maskelynite
 - Alteration to sercite
- Quartz: 30%, < 1 to 5 mm, anhedral
 - PDFs, multiple parallel and perpendicular fractures
 - Arrays of fluid inclusions
- Biotite: 10%, < 2 mm, subhedral
 - Approximately 5% is altering into chlorite
- K-spar: 30%, 2 to 4 mm, subhedral
 - More is typically seen in hand sample.
- Oxides: 10%, < 0.10 mm, anhedral

Appendix B-4: Ignimbrites

CCMK07013 (S23° 56' 21.0", W068° 15' 35.5")



Hand Sample



Thin Section in PPL

Igneous: Pliocene Ignimbrite**Name:** Fine-grained biotite, plagioclase rhyolitic vitric tuff**Texture:** fine-grained phenocrysts, vesicles present,
glassy matrix with welded texture with discernable ash shards**Color:** fresh surface gray, light tan to tan on weathered surface**Phenocrysts:**Plagioclase: 10%, 0.5 to 2 mm, euhedral-subhedral
Intergrowth between grains.Biotite: 5%, 0.25 to 1 mm, euhedral to subhedral
Pleochroism in thin section, light to medium brownOxides: < 1%, < 0.25 mm, anhedral
Includes magnetite and ilmenites (Electron Microprobe data shows)**Groundmass:**

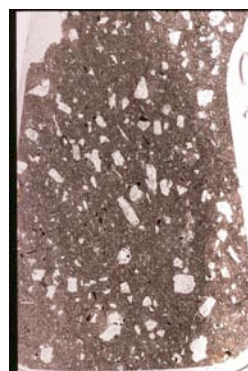
85% glassy matrix

Appendix B-5: Ignimbrites

CCMK07030 (S23° 55' 46.6", W068° 15' 44.5")



Hand Sample



Thin Section in PPL

Igneous: Pliocene Ignimbrite**Name:** Fine-grained biotite, plagioclase rhyolitic vitric tuff**Texture:** fine-grained phenocrysts, vesicles present,
glassy matrix with welded texture with discernable ash shards**Color:** fresh surface gray, light tan to tan on weathered surface**Phenocrysts:**

Plagioclase: 20%, 0.25 to 1.5 mm, euhedral-subhedral

Less intergrowth between grains.

PDFs, multiple parallel and perpendicular fractures.

Biotite: 7%, 0.25 to 1 mm, euhedral to subhedral

Pleochroism in thin section, light to medium brown

Pyroxenes: 1%, \leq 0.25 mm, subhedralOxides: 1%, $<$ 0.05-0.25 mm, anhedral**Groundmass:**

71%, glassy matrix

increased welded texture compared to CCMK07016

Appendix B-6: Ignimbrites

CCMK07034b (S23° 56' 21.0", W068° 15' 35.5")



Hand Sample



Thin Section in PPL

Igneous: Pliocene Ignimbrite**Name:** Medium-grained biotite, plagioclase rhyolitic vitric tuff**Texture:** fine to medium phenocrysts, more vesicles present,**Color:** fresh surface pink, orange weathered surface.**Phenocrysts:**Plagioclase: 7%, 0.5 to 1.75 mm, 8-9 mm, euhedral -subhedral
PDFs, multiple parallel and perpendicular fractures.Biotite: 3%, ≤ 0.50 mm, subhedral

Pleochroism in thin section, light to medium brown

Pyroxenes: 1%, ≤ 0.25 mmOxides: $<1\%$, < 0.20 mm, anhedral

Includes magnetite and ilmenites (Electron Microprobe data shows)

Groundmass:

88% glassy matrix

graduation of melting, increased welding compared to CCMK07016
and CCMK07030

Appendix B-7: Mafic Dikes

CCMK07003 (S23° 55' 43.2", W068° 15' 37.7")



Hand Sample



Thin Section in PPL

Igneous: Mafic Dike**Name:** Olivine-phyric basaltic andesite**Texture:** very fine-grained groundmass with fine-grained phenocrysts**Color:** dark to light gray with greenish hues**Phenocrysts:**

Olivine: 10%, 0.25 to 0.50 mm, euhedral-subhedral

Altered, pockmarked appearance, altering to iddingsite, grain void

Groundmass: 90%, very fine grained, brown oxidationPlagioclase: ≤ 0.25 to 0.50mm, subhedral, inter-granularOxides: < 0.25 to < 0.10 mm, anhedral

Appendix B-8: Mafic Dikes

CCMK07004 (S23° 55' 43.9", W068° 15' 38.3")



Hand Sample



Thin Section in PPL

Igneous: Mafic Dike**Name:** Olivine-phyric basaltic andesite**Texture:** very fine-grained groundmass with fine-grained phenocrysts**Color:** dark to light gray with greenish hues**Phenocrysts:**

Olivine: 10%, 0.5 to 1 mm, euhedral-subhedral

Altered, pockmarked appearance, altering to iddingsite, grain void

Groundmass: 90%, very fine grained, less brown oxidationPlagioclase: ≤ 0.25 to 0.50mm, subhedral, inter-granularOxides: ≤ 0.10 mm, anhedralOlivines: ≤ 0.15 to 0.25 mm, subhedral

Appendix B-9: Mafic Dikes

CCMK07029 (S23° 55' 45.1", W068° 15' 47.1")



Hand Sample



Thin Section in PPL

Igneous: Mafic Dike**Name:** Hornblende-olivine andesite**Texture:** very fine-grained groundmass with fine-grained phenocrysts**Color:** gray fresh surface, weathered brown surface**Phenocrysts:**

Hornblende: 25% 0.25 to 1.5 mm, subhedral

Pleochroism from light green to green.

Olivine: 15%, 0.25 to 0.75 mm, euhedral-subhedral

Plagioclase: 10%, ≤1 mm, euhedral- subhedral

Weathered, grain void

Groundmass: 50%, very fine grained, red brown oxidation along fractures

Plagioclase: ≤ 0.10 mm, subhedral-anhedral,

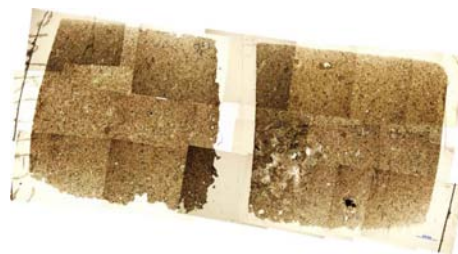
Oxides: ≤ 0.10 mm, anhedral

Appendix B-10: Mafic Dikes

CCMK07035 (S23° 55' 46.7", W068° 15' 40.3")



Hand Sample



Thin Section in PPL

Igneous: Mafic Dike**Name:** Hornblende-olivine andesite**Texture:** very fine-grained groundmass with fine-grained phenocrysts**Color:** gray fresh surface, weathered tan surface**Phenocrysts:**Hornblende: 20% \leq 1 to 2.5 mm, subhedral

Pleochroism from light green to green.

Olivine: 10%, \leq 0.75 mm, euhedral-subhedral

Plagioclase: 10%, 0.5 mm, euhedral- subhedral

Alteration to sercite, original boundary preserved

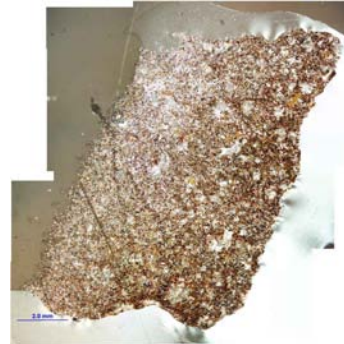
Groundmass: 60%, microcrystalline gray and brown crystalsOxides: \leq 0.10 mm, anhedral

Appendix B-11: Mafic Dikes

CCMK07037 (S23° 55' 46.6", W068° 15' 41.4")



Hand Sample



Thin Section in PPL

Igneous: Mafic Dike**Name:** Olivine-phyric trachy-basalt**Texture:** very fine-grained groundmass with fine phenocrysts**Color:** red with white to yellowish spherules (alterations)**Phenocrysts:**Olivine: 40%, ≤ 0.50 mm, euhedral

Alteration to iddingsite, retain grain boundary

Groundmass: 60%, microcrystalline red, orange, brown, gray crystals
Oxides, microcrystalline

Appendix B-12: Mafic Dikes

CCMK07084 (S23° 55' 35.9", W068° 15' 41.2")



Hand Sample



Thin Section in PPL

Igneous: Mafic Dike**Name:** Plagioclase basaltic andesite**Texture:** very fine-grained groundmass with fine-grained phenocrysts**Color:** red brown**Phenocrysts:**

Plagioclase: 20%, 0.75 to 1 mm, subhedral

Olivine: 5%, 0.5 to 1 mm, euhedral-subhedral

Altered, pockmarked appearance, altering to iddingsite, grain void

Oxides: 5%, ≤ 0.25 mm**Groundmass:** 70%, very fine grained, less brown oxidationPlagioclase: ≤ 0.25 mm, subhedral-anhedral, inter-granular

Appendix B-13: Mafic Dikes

CCMK07085 (S23° 55' 42.2", W068° 15' 49.1")



Hand Sample



Thin Section in PPL

Igneous: Mafic Dike**Name:** Hornblende-olivine andesite**Texture:** very fine-grained groundmass with fine-grained phenocrysts**Color:** gray fresh surface, weathered brown on the surface**Phenocrysts:**

Hornblende: 30% 4 mm, subhedral

Pleochroism from light green to green.

Olivine: 15%, 1 mm, euhedral

alteration

Plagioclase: 10%, ≤ 1 mm, anhedral

Alteration to sercite, original boundary preserved

Groundmass: 45%, microcrystalline gray and brown crystals

Oxides: 0.25 mm, anhedral

Appendix B-14: Impactite

CCMK0700A



Hand Sample



Thin Section in PPL

Impactite: Dark Melt

Name: iron-rich proximal hypocrySTALLINE impact melt rock

Texture: cindery, vesicular, hypocrySTALLINE- angular clasts

Color: dark brown to black

Phenocrysts:

Plagioclase: 20-30%, ≤ 1 mm, subhedral

Spherules: 15-20%, ≤ 1 mm, perfectly spherule to altered shape

Metallic and oxidized, silver in reflected light, black in XPL,
and red to brown (oxidation staining) in PPL

Glass: 50-65% Mostly brown transparent with alteration of red and brown staining. Opaque white patches indicate quartz present in glass composition forming lechatelierite. Schlieren pattern within glass shows lechatelierite mixing incompletely.

Appendix B-15: Impactite

CCMK07045 (S23° 55' 46.4", W068° 15' 40.1")



Hand Sample



Thin Section in PPL

Impactite: Dark Melt**Name:** iron-rich distal hypocrySTALLINE impact melt rock**Texture:** cindery, vesicular, hypocrySTALLINE- angular clasts**Color:** dark brown to black**Phenocrysts:**Plagioclase: 35-40%, ≤ 2 mm, subhedral

PDFs, multiple parallel and perpendicular fractures.

Spherules: 5%, ≤ 10 mm, mostly altered shape, few perfectly spheruleMetallic and oxidized, silver in reflected light, black in XPL,
and red to brown (oxidation staining) in PPL.**Glass:** 55-65% Opaque with patches of transparent light to dark brown oxidation.

Appendix B-16: Impactite

CCMK07082 (S23° 55' 47.1", W068° 15' 36.3")



Hand Sample



Thin Section in PPL

Impactite: Dark Melt**Name:** iron-rich distal hypocrySTALLINE impact melt rock**Texture:** cindery, vesicular, hypocrySTALLINE- angular clasts**Color:** dark brown to black**Phenocrysts:**

Plagioclase: 40%, 0.5 to 1.5 mm, subhedral

PDFs, multiple parallel and perpendicular fractures.

Spherules: ≤10%, ≤ 10 mm, mostly altered shape, few perfectly spherule

Metallic and oxidized, silver in reflected light, black in XPL,
and red to brown (oxidation staining) in PPL.**Glass:** 50-60% Opaque with patches of transparent light to dark brown oxidation.

Appendix B-17: Impactite

CCMK0700B (S23° 55' 46.9", W068° 15' 36")



Hand Sample



Thin Section in PPL

Impactite: Light Melt**Name:** Distal hypocrySTALLINE ignimbrite impact melt rock**Texture:** glassy fluidal surface crust, internally vesicular, angular clasts**Color:** tan to red purple**Phenocrysts:**

Plagioclase: < 10%, 0.25 to 2.5 mm, euhedral-subhedral

Biotite: < 5%, 0.25 to 1 mm, euhedral-subhedral

Glass: 85%:

60% of clear glass mixed with patches of plagioclase grains, < 0.10 mm

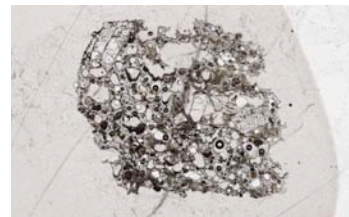
25% of glass has red staining from oxidation

Appendix B-18: Impactite

CCMK07009 (S23° 55' 45.3", W068° 15' 38.8")



Hand Sample



Thin Section in PPL

Impactite: Light Melt**Name:** Proximal hypocrystalline ignimbrite impact melt rock**Texture:** glassy, more vesicular, angular clasts**Color:** tan**Phenocrysts:**

Plagioclase: 20%, 0.5 to 1.5 mm, subhedral

10% of grains altering to clay.

PDFs, multiple parallel and perpendicular fractures.

Glass: 70% clear glass mixed with patches of plagioclase grains, < 0.10 mm.

Appendix B-19: Light Melt

CCMK07046 (S23° 55' 47", W068° 15' 35")



Hand Sample



Thin Section in PPL

Impactite: Light Melt**Name:** Distal hypocrystalline ignimbrite impact melt rock**Texture:** glassy fluidal surface crust, internally vesicular, angular clasts**Color:** tan to red purple**Phenocrysts:**

Plagioclase: 25-30%, 0.25 to 2.5 mm, euhedral-subhedral
 PDFs, multiple parallel and perpendicular fractures.

Biotite: 5-10%, 0.75 to 1 mm, euhedral-subhedral
 Alteration to chlorite.

Glass: 70-60% clear glass mixed with patches of plagioclase grains, < 0.10 mm.
 Glass has red staining from oxidation.

Appendix B-20: Impactite

CCMK07047 (S23° 55' 46.9", W068° 15' 36")



Hand Sample



Thin Section in PPL

Impactite: Light Melt**Name:** Distal hypocrystalline ignimbrite impact melt rock**Texture:** glassy fluidal surface crust, internally vesicular, angular clasts**Color:** tan to red purple**Phenocrysts:**

Plagioclase: 15-20%, 0.5 to 2.5 mm, subhedral

PDFs, multiple parallel and perpendicular fractures.

Biotite: 5-10%, 0.5 to 2 mm, euhedral-subhedral

Alteration to chlorite.

Glass: 70%:

40% clear glass

30% oxidized patches with plagioclase grains, < 0.10 mm, anhedral.

Glass has red staining from oxidation.

APPENDIX C**XRF DATA**

Table C1: X-Ray Fluorescence Data.

	CCMK07016	CCMK07042	CCMK07051	CCMK07013	CCMK07030	CCMK07034b	Bulk Light Melt	CCMK07003	CCMK07004	CCMK07029	CCMK07035	CCMK07037	CCMK07084	CCMK07085
	Granite	Granite	Granite	Ignimbrite	Ignimbrite	Ignimbrite	Impacite	Mafic Dike						
SiO ₂	77.78	75.47	74.61	74.54	74.29	73.70	75.61	52.85	51.99	58.89	59.05	47.73	51.72	58.98
TiO ₂	0.059	0.158	0.149	0.310	0.343	0.342	0.299	1.642	1.811	0.692	0.679	3.022	1.891	0.688
Al ₂ O ₃	12.86	13.61	13.82	13.09	13.25	13.79	12.34	17.24	18.03	18.50	18.56	17.23	17.30	18.45
FeO*	0.75	1.42	1.92	1.31	1.48	1.46	2.04	8.91	8.83	5.94	5.92	10.69	9.50	6.00
MnO	0.040	0.058	0.068	0.050	0.045	0.058	0.103	0.170	0.164	0.142	0.116	0.369	0.165	0.133
MgO	0.14	0.36	0.30	0.67	0.69	0.38	0.42	6.98	6.09	3.79	3.69	5.15	6.42	3.75
CaO	0.26	0.99	2.27	1.02	1.10	1.22	1.22	7.43	6.91	5.37	5.04	8.79	5.66	5.08
Na ₂ O	4.18	4.97	4.12	3.95	3.83	3.65	3.26	3.62	3.05	5.07	4.85	4.19	4.12	5.22
K ₂ O	3.91	2.92	2.70	4.96	4.85	5.32	4.56	0.63	2.58	1.40	1.89	1.85	2.67	1.48
P ₂ O ₅	0.018	0.045	0.041	0.089	0.127	0.075	0.153	0.529	0.554	0.208	0.212	0.967	0.554	0.210
Total	100.00	100.00	100.00	100.00	100.00	100.00	100.00	100.00	100.00	100.00	100.00	100.00	100.00	100.00
Ni	0	0	0	0	0	0	0	134	72	28	28	29	82	26
Cr	2	3	2	0	2	2	2	174	90	24	23	159	105	25
Sc	5	5	5	4	4	3	5	23	22	15	15	16	25	14
V	6	18	23	17	20	16	27	169	188	132	127	171	193	128
Ba	446	718	363	635	700	718	682	162	732	506	531	831	1173	541
Rb	121	95	79	186	191	182	496	15	48	36	54	76	85	38
Sr	48	73	142	97	121	129	181	348	407	512	477	1024	362	500
Zr	57	92	86	230	249	238	204	236	227	102	105	303	219	106
Y	33	18	17	26	25	26	30	31	29	14	14	34	28	14
Nb	12.2	9.4	7.3	18.4	19.6	18.1	18.1	12.3	20.6	3.1	3.2	84.1	12.9	3.1
Ga	9	6	12	15	15	15	13	15	16	16	16	22	14	18
Cu	0	6	0	8	6	5	29	59	45	43	42	27	47	59
Zn	17	45	30	40	40	63	73	93	84	87	68	208	94	74
Pb	21	25	13	13	15	24	33	5	3	7	5	24	6	6
La	19	20	27	47	51	48	47	26	30	15	14	72	29	12
Ce	39	45	52	89	93	89	92	50	56	21	23	137	49	29
Th	14	9	8	30	28	27	28	1	1	0	0	4	0	0
Nd	20	18	17	35	36	33	37	26	30	12	14	60	29	16
U	3	2	2	9	9	8	8	1	3	0	1	5	2	1

Note: Major elements are in wt.%, normalized to 100% on a volatile-free basis, with total iron as FeO. Trace elements are in ppm and un-normalized.

APPENDIX D
ELECTRON MICROPROBE DATA

Table D1: Electron Microprobe Data for biotites in Granite target rock.

	SiO ₂	TiO ₂	Al ₂ O ₃	FeO	MnO	MgO	CaO	Na ₂ O	K ₂ O	P ₂ O ₅	NiO	SO ₃	Cl	F	Total	Cation	Mg-rich	Fe-rich
CCMK07016-3,bio.point 2	25.11	0.06	17.58	23.30	1.36	5.29	0.07	0.02	2.03	0.02	0.03	0.01	0.00	0.01	100.00	16.63	28.80	71.20
CCMK07016-3,bio.point 3	22.74	0.19	16.83	29.19	1.69	5.86	0.13	0.04	0.53	0.06	0.00	0.00	0.02	0.00	100.00	16.96	26.35	73.65
CCMK07016-3,bio.point 4	22.73	0.12	17.08	29.02	1.69	6.22	0.08	0.02	0.37	0.00	0.00	0.01	0.01	0.00	100.00	16.95	27.66	72.34
CCMK07016-3,bio.point 5	23.38	0.15	19.14	24.98	1.24	5.73	0.16	0.05	1.83	0.01	0.00	0.01	0.01	0.01	100.00	16.86	29.03	70.97
CCMK07016-4,bio.point 1	24.61	0.18	20.56	21.95	1.39	4.08	0.02	0.02	2.58	0.02	0.00	0.01	0.01	0.00	100.00	16.53	24.89	75.11
CCMK07016-4,bio.point 2	21.18	0.05	18.24	30.99	2.21	6.14	0.00	0.02	0.02	0.01	0.00	0.01	0.01	0.00	100.00	17.13	26.09	73.91
CCMK07016-4,bio.point 3	21.85	0.04	17.54	30.05	1.99	6.48	0.06	0.00	0.12	0.00	0.02	0.00	0.00	0.00	100.00	17.08	27.76	72.24
CCMK07016-4,bio.point 4	21.61	0.01	18.08	30.62	1.95	5.84	0.04	0.01	0.19	0.02	0.00	0.00	0.01	0.01	100.00	17.08	25.36	74.64
CCMK07016-2,bio.point 1	21.07	0.06	18.84	30.98	1.97	5.45	0.17	0.04	0.23	0.05	0.04	0.00	0.01	0.00	100.00	17.11	23.89	76.11
CCMK07016-2,bio.point 2	23.18	0.06	18.67	27.53	1.54	4.87	0.04	0.00	0.99	0.00	0.00	0.00	0.00	0.00	100.00	16.78	23.98	76.02
CCMK07016-2,bio.point 3	21.30	0.10	18.18	30.64	2.04	6.27	0.03	0.02	0.12	0.03	0.00	0.00	0.01	0.00	100.00	17.12	26.72	73.28
CCMK07016-2,bio.point 4	21.63	0.34	18.13	30.39	1.81	5.73	0.08	0.04	0.32	0.00	0.00	0.00	0.00	0.00	100.00	17.04	25.15	74.85
CCMK07016-2,bio.point 5	22.01	0.08	17.79	29.81	1.88	6.03	0.06	0.03	0.27	0.06	0.00	0.02	0.01	0.00	100.00	17.01	26.49	73.51
CCMK07016-5,bio.point 1	21.95	0.23	18.84	29.22	1.92	5.30	0.04	0.00	0.52	0.01	0.00	0.02	0.00	0.00	100.00	16.94	24.42	75.58
CCMK07016-5,bio.point 2	21.42	0.05	18.25	30.54	2.20	5.96	0.02	0.01	0.10	0.01	0.03	0.00	0.01	0.01	100.00	17.09	25.81	74.19
CCMK07016-5,bio.point 3	21.42	0.08	18.36	30.55	2.06	5.86	0.05	0.02	0.15	0.02	0.00	0.02	0.01	0.00	100.00	17.07	25.47	74.53
CCMK07016-5,bio.point 4	21.51	0.07	18.37	30.45	1.95	5.70	0.03	0.05	0.31	0.05	0.00	0.03	0.01	0.00	100.00	17.07	25.03	74.97
CCMK07016-5,bio.point 5	21.17	0.06	18.41	31.04	2.11	5.74	0.06	0.00	0.14	0.03	0.04	0.05	0.00	0.00	100.00	17.10	24.81	75.19
CCMK07042-1,bio.point 1	22.08	0.13	17.80	26.31	1.40	10.01	0.14	0.00	0.05	0.00	0.00	0.02	0.01	0.00	100.00	17.13	40.42	59.58
CCMK07042-1,bio.point 2	22.24	0.07	18.11	25.87	1.26	10.07	0.06	0.00	0.05	0.02	0.00	0.01	0.00	0.00	100.00	17.09	40.96	59.04
CCMK07042-1,bio.point 4	22.23	0.07	18.00	26.14	1.16	10.05	0.04	0.02	0.03	0.00	0.00	0.02	0.01	0.00	100.00	17.10	40.67	59.33
CCMK07042-1,bio.point 5	22.16	0.10	18.04	25.94	1.30	10.18	0.10	0.00	0.04	0.00	0.00	0.00	0.00	0.00	100.00	17.12	41.16	58.84
CCMK07042-2,bio.point 1	21.94	0.04	18.26	26.56	1.37	9.89	0.00	0.02	0.03	0.00	0.00	0.00	0.00	0.00	100.00	17.13	39.89	60.11
CCMK07042-2,bio.point 2	22.07	0.04	18.17	26.33	1.24	9.94	0.00	0.03	0.01	0.06	0.02	0.01	0.01	0.00	100.00	17.11	40.24	59.76
CCMK07042-2,bio.point 4	22.07	0.03	18.22	26.52	1.31	9.57	0.07	0.07	0.05	0.05	0.00	0.00	0.01	0.00	100.00	17.11	39.15	60.85
CCMK07042-2,bio.point 5	22.02	0.00	18.23	26.51	1.25	9.83	0.07	0.03	0.01	0.03	0.00	0.03	0.00	0.00	100.00	17.11	39.79	60.21
CCMK07042-3,bio.point 1	22.70	0.05	17.72	25.96	1.20	9.15	0.25	0.03	0.24	0.01	0.00	0.00	0.00	0.01	100.00	17.04	38.59	61.41
CCMK07042-3,bio.point 2	21.76	0.11	18.86	26.78	1.32	9.22	0.09	0.02	0.04	0.01	0.04	0.00	0.00	0.00	100.00	17.10	38.03	61.97
CCMK07042-3,bio.point 3	21.97	0.04	18.45	26.63	1.32	9.64	0.01	0.02	0.02	-0.01	0.00	0.00	0.00	0.00	100.00	17.11	39.21	60.79
CCMK07042-3,bio.point 4	21.95	0.04	18.90	26.69	1.35	8.99	0.04	0.00	0.05	0.01	0.00	0.02	0.01	0.00	100.00	17.05	37.50	62.50
CCMK07042-3,bio.point 5	22.14	0.04	18.02	26.42	1.24	9.94	0.03	0.00	0.05	0.01	0.00	0.02	0.00	0.00	100.00	17.10	40.14	59.86
CCMK07042-4,bio.point 1	21.85	0.04	18.16	27.13	1.26	9.56	0.03	0.00	0.04	0.04	0.02	0.04	0.00	0.00	100.00	17.13	38.58	61.42
CCMK07042-4,bio.point 2	22.29	0.07	17.67	26.75	1.20	9.50	0.08	0.00	0.11	-0.03	0.03	0.02	0.00	0.00	100.00	17.10	38.76	61.24
CCMK07042-4,bio.point 3	21.92	0.06	18.15	27.24	1.29	9.28	0.01	0.00	0.04	0.03	0.04	0.00	0.01	0.01	100.00	17.12	37.79	62.21
CCMK07042-4,bio.point 4	22.75	0.33	16.83	26.66	1.04	9.13	0.31	0.02	0.13	0.03	0.00	0.00	0.02	0.01	100.00	17.05	37.92	62.08
CCMK07042-4,bio.point 5	21.80	0.02	18.43	27.32	1.34	9.19	0.07	0.00	0.03	0.00	0.00	0.01	0.00	0.00	100.00	17.12	37.49	62.51
CCMK07051-4,bio.point 1	22.19	0.08	18.59	26.32	1.08	9.34	0.09	0.01	0.10	0.02	0.00	0.00	0.00	0.00	100.00	17.05	38.75	61.25
CCMK07051-4,bio.point 2	22.07	0.09	17.81	26.92	1.12	9.60	0.04	0.03	0.21	0.05	0.02	0.00	0.00	0.00	100.00	17.15	38.86	61.14
CCMK07051-4,bio.point 3	22.03	0.03	18.20	26.92	1.05	9.59	0.00	0.05	0.07	0.00	0.01	0.02	0.01	0.00	100.00	17.13	38.85	61.15
CCMK07051-4,bio.point 4	23.22	0.18	17.73	25.01	1.04	9.07	0.08	0.01	0.41	0.01	0.00	0.00	0.01	0.01	100.00	16.93	39.26	60.74
CCMK07051-3,bio.point 4	22.55	0.09	18.10	25.75	1.09	9.49	0.07	0.02	0.21	0.01	0.04	0.02	0.00	0.00	100.00	17.03	39.66	60.34
CCMK07051-3,bio.point 5	23.24	0.06	18.07	24.96	1.05	8.81	0.09	0.01	0.40	0.03	0.04	0.00	0.00	0.01	100.00	16.90	38.63	61.37
CCMK07051-2,bio.point 2	24.08	0.13	18.41	22.00	0.94	9.32	0.04	0.00	0.97	0.01	0.00	0.04	0.01	0.01	100.00	16.79	43.02	56.98
CCMK07051-2,bio.point 4	26.75	0.12	18.75	17.71	0.64	6.87	0.14	0.02	2.20	0.01	0.04	0.00	0.00	0.00	100.00	16.32	40.89	59.11
CCMK07051-2,bio.point 5	22.55	0.03	18.83	24.49	1.03	9.85	0.05	0.01	0.59	0.02	0.00	0.02	0.02	0.00	100.00	17.05	41.76	58.24
CCMK07051-1,bio.point 1	23.16	0.15	17.55	25.43	1.00	8.91	0.15	0.01	0.45	0.00	0.00	0.05	0.00	0.00	100.00	16.94	38.46	61.54
CCMK07051-1,bio.point 2	22.25	0.08	18.38	26.49	1.02	9.17	0.13	0.00	0.16	0.01	0.00	0.07	0.02	0.01	100.00	17.04	38.15	61.85
CCMK07051-1,bio.point 3	21.92	0.01	18.42	26.64	1.06	9.78	0.06	0.02	0.09	0.05	0.00	0.03	0.01	0.02	100.00	17.14	39.56	60.44
CCMK07051-1,bio.point 4	22.20	0.00	18.14	26.52	1.06	9.68	0.05	0.04	0.15	0.02	0.00	0.00	0.00	0.00	100.00	17.11	39.41	60.59
CCMK07051-1,bio.point 5	22.29	0.04	18.53	25.65	1.23	9.84	0.07	0.00	0.06	0.00	0.00	0.02	0.01	0.00	100.00	17.05	40.61	59.39
granite biotite average	22.37	0.09	18.21	27.00	1.41	8.10	0.07	0.02	0.36	0.02	0.01	0.01	0.01	0.00	100.00			

Table D2: Electron Microprobe Data for feldspar in Granite target rock.

	SiO ₂	TiO ₂	Al ₂ O ₃	FeO	MnO	MgO	CaO	Na ₂ O	K ₂ O	P ₂ O ₅	NiO	SO ₃	Cl	F	Total	Cation	Anorthite	Albite	Orthoclase
CCMK07042-9,plag.point 1	64.48	0.00	18.88	0.01	0.04	0.00	0.01	0.43	16.12	0.01	0.07	0.00	0.00	0.00	100.00	5.00	0.03	3.87	96.09
CCMK07042-9,plag.point 2	64.55	0.00	18.84	0.02	0.00	0.00	0.00	0.46	16.14	0.02	0.00	0.02	0.01	0.00	100.00	5.00	0.01	4.19	95.81
CCMK07042-9,plag.point 3	63.96	0.02	19.48	0.13	0.00	0.01	0.03	0.80	15.55	0.03	0.00	0.00	0.00	0.02	100.00	5.01	0.16	7.21	92.63
CCMK07042-9,plag.point 4	64.30	0.00	19.15	0.07	0.05	0.00	0.00	0.32	16.15	0.02	0.04	0.00	0.00	0.01	100.00	5.00	0.00	2.92	97.08
CCMK07042-9,plag.point 5	64.45	0.00	18.99	0.03	0.02	0.02	0.02	0.23	16.25	0.01	0.00	0.00	0.02	0.00	100.00	5.00	0.09	2.07	97.84
granite orthoclase average	64.35	0.00	19.07	0.05	0.02	0.01	0.01	0.45	16.04	0.02	0.02	0.00	0.00	0.01	100.00				
CCMK07016-9,plag.point 1	66.24	0.01	21.45	0.19	0.00	0.01	0.66	10.89	0.54	0.00	0.04	0.00	0.00	0.01	100.00	5.02	3.15	93.80	3.06
CCMK07016-9,plag.point 2	67.04	0.00	21.06	0.02	0.03	0.02	0.81	10.81	0.16	0.03	0.03	0.00	0.01	0.00	100.00	4.99	3.93	95.16	0.91
CCMK07016-9,plag.point 3	67.37	0.00	20.63	0.06	0.05	0.00	0.64	11.05	0.18	0.01	0.01	0.00	0.01	0.00	100.00	4.99	3.08	95.88	1.04
CCMK07016-9,plag.point 4	67.08	0.00	20.62	0.00	0.04	0.00	0.62	11.49	0.18	0.05	0.00	0.02	0.00	0.02	100.00	5.02	2.86	96.13	1.00
CCMK07016-9,plag.point 5	66.32	0.00	21.28	0.11	0.01	0.03	0.62	10.93	0.65	0.00	0.02	0.03	0.01	0.00	100.00	5.02	2.95	93.42	3.63
CCMK07016-10,plag.point 2	66.78	0.00	21.10	0.00	0.01	0.00	0.70	11.25	0.13	0.04	0.03	0.00	0.00	0.00	100.00	5.01	3.30	95.96	0.75
CCMK07016-10,plag.point 3	66.43	0.03	21.63	0.00	0.00	0.00	0.63	11.18	0.17	0.00	0.00	0.00	0.02	0.00	100.00	5.01	2.99	96.06	0.96
CCMK07016-10,plag.point 4	67.07	0.00	20.76	0.00	0.03	0.02	0.88	11.27	0.13	0.00	0.01	0.00	0.00	0.00	100.00	5.01	3.58	95.70	0.72
CCMK07016-8,plag.point 10	66.51	0.00	21.10	0.05	0.00	0.03	0.70	11.35	0.23	0.02	0.00	0.01	0.00	0.00	100.00	5.02	3.24	95.47	1.29
CCMK07016-8,plag.point 11	67.07	0.00	20.75	0.05	0.02	0.02	0.99	11.01	0.15	0.00	0.00	0.01	0.00	0.00	100.00	5.00	4.68	94.46	0.86
CCMK07016-8,plag.point 12	66.67	0.00	20.95	0.01	0.00	0.01	1.13	11.23	0.09	0.00	0.01	0.00	0.01	0.02	100.00	5.02	5.22	94.30	0.48
CCMK07016-8,plag.point 13	66.78	0.00	20.69	0.02	0.00	0.00	0.78	11.55	0.15	0.00	0.04	0.00	0.00	0.00	100.00	5.03	3.57	95.59	0.84
CCMK07016-8,plag.point 14	67.06	0.03	20.58	0.01	0.00	0.00	0.88	11.32	0.15	0.00	0.00	0.00	0.02	0.01	100.00	5.02	4.07	95.08	0.85
CCMK07016-6,plag.point 1	66.94	0.00	20.56	0.02	0.00	0.00	0.85	11.48	0.12	0.00	0.03	0.04	0.00	0.00	100.00	5.02	3.92	95.43	0.65
CCMK07016-6,plag.point 3	66.38	0.01	21.06	0.19	0.00	0.06	0.68	11.00	0.62	0.01	0.00	0.00	0.01	0.00	100.00	5.02	3.21	93.35	3.44
CCMK07016-6,plag.point 4	67.04	0.01	20.48	0.10	0.00	0.00	0.70	11.57	0.11	0.01	0.00	0.00	0.00	0.01	100.00	5.03	3.23	96.19	0.58
CCMK07016-6,plag.point 5	66.71	0.00	20.97	0.00	0.04	0.01	0.53	11.55	0.16	0.02	0.03	0.01	0.00	0.00	100.00	5.03	2.46	96.66	0.88
CCMK07016-10,plag.point 5	67.08	0.00	20.76	0.00	0.01	0.00	0.82	11.13	0.15	0.00	0.02	0.04	0.00	0.02	100.00	5.00	3.87	95.28	0.85
CCMK07042-8,plag.point 1	67.12	0.00	20.83	0.07	0.01	0.02	0.39	11.36	0.15	0.00	0.01	0.07	0.01	0.01	100.00	5.01	1.84	97.31	0.84
CCMK07042-8,plag.point 2	67.30	0.00	20.46	0.00	0.04	0.00	0.43	11.66	0.13	0.00	0.00	0.00	0.01	0.00	100.00	5.02	1.97	97.29	0.74
CCMK07042-8,plag.point 4	67.98	0.03	20.25	0.01	0.00	0.00	0.36	11.30	0.11	0.02	0.00	0.00	0.03	0.00	100.00	4.99	1.72	97.65	0.64
CCMK07042-8,plag.point 5	67.73	0.00	20.34	0.00	0.00	0.01	0.38	11.47	0.12	0.00	0.00	0.00	0.01	0.00	100.00	5.01	1.78	97.53	0.69
CCMK07042-6,plag.point 3	67.59	0.02	20.45	0.06	0.00	0.01	0.55	11.21	0.12	0.00	0.02	0.00	0.01	0.00	100.00	5.00	2.61	96.72	0.67
CCMK07042-6,plag.point 4	67.06	0.02	20.57	0.05	0.04	0.00	0.59	11.53	0.11	0.03	0.00	0.00	0.01	0.00	100.00	5.02	2.74	96.67	0.59
CCMK07042-6,plag.point 5	67.54	0.00	20.50	0.07	0.00	0.00	0.51	11.28	0.14	0.00	0.00	0.00	0.00	0.00	100.00	5.00	2.40	96.80	0.80
CCMK07042-7,plag.point 1	67.47	0.00	20.27	0.01	0.00	0.00	0.33	11.82	0.10	0.01	0.00	0.03	0.01	0.00	100.00	5.02	1.49	97.99	0.52
CCMK07042-7,plag.point 3	67.73	0.00	20.49	0.01	0.00	0.00	0.28	11.41	0.12	0.00	0.00	0.00	0.02	0.03	100.00	5.00	1.31	97.99	0.69
CCMK07042-7,plag.point 4	67.85	0.00	20.22	0.03	0.00	0.00	0.18	11.64	0.07	0.00	0.00	0.02	0.00	0.03	100.00	5.01	0.86	98.73	0.41
CCMK07042-7,plag.point 5	67.35	0.00	20.56	0.00	0.00	0.00	0.39	11.62	0.11	0.00	0.01	0.02	0.03	0.01	100.00	5.02	1.81	97.58	0.61
CCMK07051-6,plag.point 1	67.38	0.00	20.50	0.04	0.00	0.04	0.35	11.62	0.10	0.00	0.03	0.00	0.00	0.00	100.00	5.02	1.64	97.80	0.56
CCMK07051-6,plag.point 2	67.47	0.04	20.35	0.05	0.00	0.00	0.31	11.64	0.08	0.00	0.05	0.00	0.01	0.00	100.00	5.02	1.45	98.10	0.45
CCMK07051-6,plag.point 3	67.48	0.00	20.11	0.04	0.02	0.00	0.44	11.89	0.12	0.00	0.00	0.00	0.00	0.00	100.00	5.03	1.99	97.37	0.64
CCMK07051-6,plag.point 4	67.60	0.01	20.26	0.00	0.24	0.02	0.24	11.55	0.08	0.01	0.00	0.00	0.01	0.00	100.00	5.01	1.12	98.46	0.42
CCMK07051-6,plag.point 5	67.56	0.00	20.29	0.00	0.00	0.01	0.54	11.54	0.15	0.01	0.00	0.00	0.03	0.00	100.00	5.02	2.49	96.70	0.81
CCMK07051-9,plag.point 1	66.57	0.00	21.09	0.02	0.03	0.00	0.57	11.53	0.13	0.04	0.04	0.00	0.01	0.00	100.00	5.03	2.62	96.67	0.70
CCMK07051-9,plag.point 2	67.47	0.04	20.37	0.00	0.00	0.00	0.36	11.63	0.12	0.02	0.01	0.00	0.01	0.01	100.00	5.02	1.67	97.65	0.68
CCMK07051-9,plag.point 3	66.45	0.00	21.50	0.00	0.00	0.01	0.44	10.94	0.65	0.00	0.03	0.02	0.00	0.00	100.00	5.01	2.09	94.20	3.70
CCMK07051-9,plag.point 4	67.20	0.04	20.64	0.00	0.00	0.01	0.58	11.49	0.12	0.00	0.00	0.00	0.01	0.02	100.00	5.02	2.71	96.64	0.65
CCMK07051-9,plag.point 5	67.91	0.02	20.18	0.00	0.00	0.02	0.12	11.61	0.12	0.00	0.00	0.03	0.00	0.01	100.00	5.01	0.58	98.74	0.68
CCMK07051-8,plag.point 1	67.69	0.00	20.19	0.13	0.00	0.06	0.21	11.61	0.13	0.00	0.00	0.00	0.02	0.00	100.00	5.02	0.97	98.28	0.75
CCMK07051-8,plag.point 2	67.15	0.00	20.49	0.02	0.04	0.00	0.67	11.52	0.11	0.03	0.00	0.00	0.01	0.00	100.00	5.02	3.08	96.31	0.61
CCMK07051-8,plag.point 3	67.74	0.00	20.31	0.05	0.01	0.00	0.42	11.36	0.12	0.00	0.00	0.00	0.00	0.02	100.00	5.00	2.00	97.34	0.66
CCMK07051-8,plag.point 5	67.50	0.00	20.23	0.09	0.00	0.00	0.40	11.80	0.08	0.00	0.00	0.00	0.00	0.00	100.00	5.03	1.83	97.75	0.42
CCMK07051-7,plag.point 3	67.61	0.00	20.26	0.03	0.00	0.00	0.47	11.52	0.10	0.00	0.03	0.00	0.00	0.00	100.00	5.01	2.20	97.24	0.57
CCMK07051-7,plag.point 4	66.94	0.02	21.47	0.05	0.00	0.02	0.33	10.99	0.11	0.06	0.00	0.01	0.00	0.00	100.00	4.99	1.64	97.71	0.66
CCMK07051-7,plag.point 5	66.93	0.00	21.22	0.07	0.01	0.00	0.36	11.29	0.11	0.01	0.00	0.00	0.00	0.00	100.00	5.01	1.70	97.65	0.65
granite albite average	67.17	0.01	20.67	0.04	0.01	0.01	0.54	11.39	0.17	0.01	0.01	0.01	0.01	0.00	100.00				

Table D3: Electron Microprobe Data for hematite in Granite target rock.

	SiO ₂	TiO ₂	Al ₂ O ₃	FeO	MnO	CaO	P ₂ O ₅	NiO	CuO	CoO	Cr ₂ O ₃	SO ₃	Total
CCMK07042 pt 1	4.38	0.03	0.11	94.94	0.00	0.46	0.00	0.02	0.00	0.19	0.00	0.05	100.00
CCMK07042 pt 2	1.80	0.00	0.06	97.43	0.00	0.45	0.00	0.13	0.00	0.23	0.01	0.00	100.00
CCMK07042 pt 3	3.26	0.00	1.27	94.10	0.00	0.56	0.00	0.00	0.67	0.10	0.04	0.15	100.00
CCMK07042 pt 4	4.02	0.00	0.30	94.97	0.00	0.75	0.00	0.00	0.00	0.16	0.01	0.01	100.00
CCMK07042 pt 5	0.33	0.05	0.20	99.09	0.06	0.04	0.08	0.00	0.03	0.09	0.02	0.03	100.00
CCMK07042 pt 6	4.42	0.00	0.18	94.09	0.05	0.30	0.04	0.00	0.62	0.17	0.00	0.17	100.00
CCMK07042 pt 7	3.96	0.00	0.31	94.91	0.00	0.42	0.00	0.00	0.07	0.23	0.05	0.19	100.00
CCMK07042 pt 8	4.30	0.00	0.19	93.85	0.03	0.48	0.04	0.04	0.63	0.21	0.03	0.23	100.00
CCMK07042 pt 9	0.97	0.00	0.53	98.11	0.00	0.40	0.02	0.00	0.00	0.12	0.03	0.01	100.00
CCMK07042 pt 10	4.32	0.03	0.50	93.44	0.01	0.71	0.07	0.40	0.22	0.11	0.01	0.18	100.00
granite hematite average	3.18	0.01	0.37	95.49	0.01	0.46	0.02	0.06	0.22	0.16	0.02	0.10	100.00

Table D4: Electron Microprobe Data for biotites in Ignimbrite target rock.

	SiO ₂	TiO ₂	Al ₂ O ₃	FeO	MnO	MgO	CaO	Na ₂ O	K ₂ O	P ₂ O ₅	NiO	SO ₃	Cl	F	Total	Cation	Mg-rich	Fe-rich
CCMK07013-9,bio.point 1	39.23	4.84	14.76	13.92	0.27	17.12	0.06	70.63	8.81	0.04	0.01	0.05	0.14	0.04	100.00	17.07	68.69	31.31
CCMK07013-9,bio.point 2	39.46	5.27	13.88	13.81	0.27	17.04	0.03	70.83	9.15	0.01	0.00	0.06	0.14	0.03	100.00	17.10	68.74	31.26
CCMK07013-9,bio.point 3	39.12	5.03	14.16	14.11	0.21	17.04	0.01	70.92	9.26	0.04	0.02	0.03	0.15	0.02	100.00	17.14	68.28	31.72
CCMK07013-9,bio.point 4	39.06	5.25	14.08	14.10	0.24	16.66	0.01	70.07	9.57	0.00	0.00	0.10	0.16	0.00	100.00	17.14	67.81	32.19
CCMK07013-9,bio.point 5	39.80	4.95	13.91	13.34	0.18	17.37	0.00	72.38	9.44	0.06	0.01	0.01	0.11	0.01	100.00	17.10	69.88	30.12
CCMK07013-10,bio.point 1	38.88	5.18	13.78	14.56	0.27	16.93	0.24	73.64	9.28	0.08	0.00	0.01	0.16	0.00	100.00	17.14	67.46	32.54
CCMK07013-10,bio.point 2	39.08	5.04	13.41	15.07	0.47	16.51	0.32	72.72	9.09	0.11	0.00	0.03	0.20	0.04	100.00	17.14	66.14	33.86
CCMK07013-10,bio.point 3	39.82	5.05	13.74	13.57	0.21	17.31	0.00	71.46	9.39	0.01	0.00	0.01	0.16	0.01	100.00	17.11	69.45	30.55
CCMK07013-10,bio.point 4	39.64	5.01	14.27	13.53	0.26	16.93	0.15	71.98	9.13	0.02	0.06	0.06	0.17	0.00	100.00	17.05	69.05	30.95
CCMK07013-10,bio.point 5	39.78	5.16	13.81	13.62	0.23	17.14	0.00	71.88	9.29	0.00	0.00	0.06	0.18	0.01	100.00	17.08	69.17	30.83
CCMK07013-7,plag.point 1	38.88	5.21	14.41	14.26	0.24	16.63	0.05	69.69	9.39	0.00	0.00	0.06	0.12	0.03	100.00	17.12	67.52	32.48
CCMK07013-7,plag.point 2	38.65	5.37	14.54	14.26	0.30	16.57	0.03	69.22	9.36	0.00	0.00	0.05	0.15	0.02	100.00	17.13	67.44	32.56
CCMK07013-7,plag.point 3	38.71	5.12	14.40	14.32	0.27	16.64	0.02	69.28	9.40	0.00	0.04	0.05	0.16	0.03	100.00	17.17	67.44	32.56
CCMK07013-7,plag.point 4	39.15	5.15	14.38	14.11	0.25	16.48	0.06	69.82	9.41	0.03	0.03	0.01	0.17	0.00	100.00	17.11	67.56	32.44
CCMK07013-7,plag.point 5	38.98	5.03	14.25	14.54	0.22	16.61	0.03	69.21	9.35	0.03	0.00	0.03	0.16	0.03	100.00	17.15	67.06	32.94
CCMK07013-6,plag.point 1	39.17	4.90	14.42	13.84	0.29	17.02	0.00	71.26	9.37	0.00	0.06	0.02	0.13	0.01	100.00	17.14	68.67	31.33
CCMK07013-6,plag.point 2	38.67	4.78	14.82	14.09	0.20	17.16	0.03	70.85	9.29	0.00	0.00	0.07	0.07	0.01	100.00	17.16	68.46	31.54
CCMK07013-6,plag.point 3	38.99	4.94	14.27	14.05	0.26	17.06	0.21	71.75	9.02	0.17	0.05	0.09	0.10	0.04	100.00	17.10	68.39	31.61
CCMK07013-6,plag.point 4	39.03	4.73	14.56	14.45	0.20	16.79	0.00	69.59	9.30	0.00	0.06	0.06	0.11	0.00	100.00	17.12	67.44	32.56
CCMK07013-6,plag.point 5	38.40	4.79	14.32	14.96	0.18	16.67	0.18	72.49	9.36	0.12	0.05	0.00	0.13	0.03	100.00	17.22	66.50	33.50
CCMK07030-5,bio.point 1	39.26	5.14	13.88	13.86	0.27	17.39	0.08	71.28	9.17	0.02	0.00	0.07	0.19	0.00	100.00	17.12	69.10	30.90
CCMK07030-5,bio.point 2	39.49	5.03	13.52	14.18	0.26	17.32	0.09	70.73	9.05	0.02	0.04	0.03	0.14	0.01	100.00	17.12	68.52	31.48
CCMK07030-5,bio.point 3	39.07	5.27	14.32	13.70	0.21	17.12	0.10	72.21	9.25	0.00	0.00	0.07	0.12	0.02	100.00	17.11	69.01	30.99
CCMK07030-5,bio.point 4	39.34	5.29	14.16	14.00	0.22	17.12	0.13	71.69	8.85	0.00	0.00	0.00	0.16	0.02	100.00	17.06	68.55	31.45
CCMK07030-5,bio.point 5	39.04	5.36	14.06	14.07	0.21	16.95	0.00	70.38	9.27	0.02	0.04	0.08	0.17	0.00	100.00	17.10	68.22	31.78
CCMK07030-9,bio.point 1	40.39	5.22	13.92	13.45	0.20	17.23	0.06	73.24	8.68	0.02	0.00	0.07	0.15	0.00	100.00	16.92	69.55	30.45
CCMK07030-9,bio.point 2	39.72	5.18	13.87	13.73	0.24	17.13	0.01	71.95	9.22	0.00	0.00	0.05	0.17	0.03	100.00	17.08	68.99	31.01
CCMK07030-9,bio.point 3	39.34	5.19	13.98	13.66	0.26	17.07	0.02	71.52	9.57	0.00	0.00	0.03	0.14	0.01	100.00	17.14	69.02	30.98
CCMK07030-9,bio.point 4	39.53	4.90	13.91	13.53	0.28	17.22	0.00	71.61	9.55	0.00	0.09	0.03	0.12	0.01	100.00	17.16	69.42	30.58
CCMK07030-9,bio.point 5	39.29	5.29	14.06	13.53	0.24	17.33	0.01	71.99	9.20	0.04	0.00	0.06	0.15	0.00	100.00	17.10	69.54	30.46
CCMK07030-2,bio.point 1	39.48	5.25	13.83	13.80	0.18	17.05	0.10	71.52	9.29	0.01	0.01	0.06	0.18	0.00	100.00	17.09	68.77	31.23
CCMK07030-2,bio.point 2	40.04	5.19	13.91	13.48	0.27	17.06	0.07	72.61	9.04	0.01	0.00	0.07	0.12	0.03	100.00	17.01	69.29	30.71
CCMK07030-2,bio.point 3	39.76	5.31	14.09	13.58	0.23	16.99	0.04	71.47	9.19	0.00	0.00	0.01	0.13	0.02	100.00	17.03	69.04	30.96
CCMK07030-2,bio.point 4	39.77	5.38	13.94	13.73	0.26	16.92	0.05	71.73	9.00	0.02	0.00	0.07	0.14	0.00	100.00	17.01	68.72	31.28
CCMK07030-2,bio.point 5	39.95	5.24	14.22	13.70	0.25	16.89	0.15	72.69	8.72	0.04	0.00	0.01	0.18	0.00	100.00	16.95	68.73	31.27
CCMK07030-10,bio.point 1	39.35	5.05	13.20	14.41	0.25	17.28	0.06	70.53	9.34	0.00	0.05	0.08	0.15	0.00	100.00	17.16	68.14	31.86
CCMK07030-10,bio.point 2	40.13	5.09	13.79	13.38	0.24	17.50	-0.01	73.24	8.92	0.02	0.00	0.01	0.17	0.03	100.00	17.04	69.98	30.02
CCMK07030-10,bio.point 3	40.15	5.12	13.79	13.32	0.18	17.37	0.05	73.23	9.01	0.00	0.02	0.03	0.19	0.01	100.00	17.04	69.93	30.07
CCMK07034b-2,bio.point 1	39.84	5.20	14.00	13.78	0.28	16.93	0.16	71.48	8.90	0.02	0.00	0.04	0.19	0.01	100.00	17.01	68.66	31.34
CCMK07034b-2,bio.point 2	40.19	5.07	14.03	13.78	0.28	16.32	0.09	71.97	9.28	0.00	0.05	0.04	0.18	0.03	100.00	17.00	67.86	32.14
CCMK07034b-2,bio.point 4	40.11	5.07	13.94	13.60	0.25	17.39	0.09	72.68	8.78	0.00	0.00	0.03	0.16	0.00	100.00	16.98	69.51	30.49
CCMK07034b-2,bio.point 5	40.07	5.20	13.77	13.53	0.25	17.14	0.07	72.44	9.01	0.09	0.00	0.03	0.19	0.01	100.00	17.00	69.31	30.69
CCMK07034b-13,bio.point 1	40.17	5.02	14.60	13.82	0.24	16.90	0.52	76.83	7.93	0.04	0.03	0.05	0.18	0.02	100.00	16.85	68.56	31.44
CCMK07034b-13,bio.point 2	39.33	5.23	14.49	13.94	0.22	16.44	0.04	70.64	9.38	0.03	0.00	0.10	0.16	0.00	100.00	17.04	67.76	32.24
CCMK07034b-13,bio.point 3	38.89	5.22	14.59	14.25	0.24	16.58	0.00	70.84	9.30	0.02	0.00	0.05	0.18	0.02	100.00	17.10	67.47	32.53
CCMK07034b-13,bio.point 4	40.19	5.42	14.04	14.01	0.25	16.93	0.37	72.63	7.99	0.00	0.01	0.07	0.15	0.01	100.00	16.84	68.28	31.72
CCMK07034b-13,bio.point 5	38.77	5.18	14.13	14.25	0.24	15.94	1.09	69.52	8.74	0.71	0.03	0.01	0.17	0.04	100.00	17.00	66.59	33.41
CCMK07034b-5,bio.point 1	39.64	4.94	13.81	13.38	0.31	16.86	0.59	74.15	9.15	0.43	0.00	0.00	0.17	0.01	100.00	17.04	69.20	30.80
CCMK07034b-5,bio.point 2	39.78	5.36	13.95	13.94	0.27	16.38	0.53	73.94	8.90	0.21	0.00	0.03	0.14	0.01	100.00	16.93	67.69	32.31
CCMK07034b-5,bio.point 3	40.19	5.05	13.92	13.40	0.24	17.04	0.03	72.64	9.14	0.00	0.04	0.03	0.13	0.00	100.00	17.02	69.38	30.62
CCMK07034b-5,bio.point 4	40.36	4.98	13.93	13.40	0.25	17.34	0.24	73.56	8.71	0.05	0.00	0.04	0.15	0.01	100.00	16.95	69.76	30.24
CCMK07034b-12,bio.point 1	40.00	5.00	14.01	13.32	0.30	16.73	0.61	74.26	8.91	0.34	0.00	0.08	0.16	0.00	100.00	16.93	69.12	30.88
CCMK07034b-12,bio.point 2	39.82	5.19	14.02	13.99	0.25	17.02	0.34	72.10	8.48	0.09	0.03	0.02	0.14	0.04	100.00	16.96	68.45	31.55
CCMK07034b-12,bio.point 3	40.42	5.15	14.18	13.46	0.20	17.36	0.29	74.20	8.18	0.00	0.00	0.05	0.16	0.00	100.00	16.87	69.69	30.31
CCMK07034b-12,bio.point 4	38.41	5.09	14.02	14.13	0.54	16.08	2.01	73.12	7.85	1.14	0.00	0.09	0.14	0.07	100.00	16.88	66.98	33.02
CCMK07034b-12,bio.point 5	40.02	5.37	13.92	13.81	0.20	16.93	0.12	72.19	8.81	0.00	0.00	0.09	0.13	0.00	100.00	16.95	68.60	31.40
ignimbrite biotite average	39.50	5.13	14.07	13.88	0.25	16.95	0.17	71.83	9.06	0.07	0.01	0.05	0.15	0.01	100.00			

Table D5: Electron Microprobe Data for feldspar in Ignimbrite target rock.

	SiO ₂	TiO ₂	Al ₂ O ₃	FeO	MnO	MgO	CaO	Na ₂ O	K ₂ O	P ₂ O ₅	NiO	SO ₃	Cl	F	Total	Cation	Anorthite	Albite	Orthoclase
CCMK07013-1,plag.point 1	62.52	0.02	23.40	0.25	0.00	0.01	4.20	8.09	1.45	0.00	0.05	0.00	0.01	0.02	100.00	5.00	20.43	71.18	8.38
CCMK07013-1,plag.point 3	58.16	0.00	26.48	0.35	0.01	0.01	7.67	6.71	0.61	0.01	0.00	0.00	0.00	0.02	100.00	5.01	37.34	59.10	3.55
CCMK07013-1,plag.point 5	58.90	0.02	25.96	0.18	0.01	0.00	7.11	7.19	0.73	0.00	0.00	0.00	0.00	0.00	100.00	5.01	33.88	62.00	4.12
CCMK07013-1,plag.point 3	58.70	0.00	25.75	0.31	0.00	0.02	7.28	7.23	0.67	0.00	0.09	0.00	0.00	0.00	100.00	5.02	34.41	61.83	3.76
CCMK07013-2,plag.point 1	58.89	0.00	25.89	0.30	0.01	0.04	6.55	7.54	0.78	0.03	0.00	0.04	0.00	0.01	100.00	5.03	30.99	64.61	4.39
CCMK07013-2,plag.point 3	56.45	0.00	27.95	0.33	0.00	0.06	8.08	6.58	0.53	0.00	0.00	0.02	0.02	0.01	100.00	5.03	39.17	57.79	3.04
CCMK07013-2,plag.point 4	62.86	0.00	22.87	0.27	0.00	0.01	3.86	8.52	1.65	0.01	0.00	0.00	0.00	0.00	100.00	5.02	18.18	72.58	9.24
CCMK07013-3,plag.point 1	62.46	0.02	23.37	0.34	0.00	0.05	4.19	8.04	1.53	0.01	0.00	0.00	0.01	0.02	100.00	5.00	20.38	70.77	8.86
CCMK07013-3,plag.point 1	63.06	0.00	23.02	0.30	0.00	0.01	3.75	8.23	1.65	0.00	0.00	0.05	0.01	0.00	100.00	5.00	18.18	72.26	9.55
CCMK07013-3,plag.point 2	63.31	0.00	22.85	0.28	0.00	0.00	3.76	8.28	1.63	0.01	0.00	0.00	0.00	0.00	100.00	5.00	18.17	72.43	9.40
CCMK07013-3,plag.point 3	60.65	0.05	25.66	0.28	0.00	0.04	3.90	7.82	1.50	0.03	0.03	0.04	0.00	0.02	100.00	5.01	19.67	71.34	8.98
CCMK07013-3,plag.point 4	62.55	0.02	23.39	0.26	0.00	0.03	4.06	8.04	1.63	0.01	0.00	0.00	0.00	0.02	100.00	5.00	19.78	70.80	9.42
CCMK07013-3,plag.point 5	61.62	0.00	23.88	0.30	0.00	0.00	4.90	8.06	1.21	0.00	0.06	0.00	0.00	0.00	100.00	5.01	23.42	69.69	6.88
CCMK07013-4,plag.point 1	59.28	0.03	25.40	0.37	0.00	0.03	6.62	7.43	0.80	0.00	0.05	0.00	0.00	0.03	100.00	5.02	31.52	63.97	4.51
CCMK07013-4,plag.point 2	57.64	0.01	26.57	0.35	0.00	0.00	8.25	6.54	0.56	0.01	0.03	0.05	0.01	0.00	100.00	5.01	39.76	57.00	3.24
CCMK07013-4,plag.point 3	54.87	0.02	28.52	0.34	0.03	0.02	10.09	5.78	0.34	0.02	0.02	0.00	0.00	0.00	100.00	5.03	48.13	49.93	1.94
CCMK07013-4,plag.point 5	60.59	0.03	24.65	0.39	0.03	0.01	5.41	7.89	1.05	0.00	0.00	0.00	0.00	0.00	100.00	5.02	25.83	68.19	5.99
CCMK07013-5,plag.point 1	59.06	0.02	25.57	0.27	0.05	0.02	6.80	7.50	0.72	0.00	0.01	0.00	0.00	0.01	100.00	5.03	32.03	63.93	4.04
CCMK07013-5,plag.point 2	59.73	0.00	25.29	0.34	0.00	0.00	6.43	7.41	0.80	0.00	0.00	0.02	0.00	0.00	100.00	5.01	30.90	64.50	4.60
CCMK07013-5,plag.point 3	55.88	0.00	27.77	0.37	0.01	0.02	9.41	6.15	0.40	0.05	0.00	0.00	0.00	0.01	100.00	5.02	44.77	52.98	2.26
CCMK07013-5,plag.point 4	58.39	0.02	25.87	0.30	0.00	0.02	7.69	7.01	0.63	0.02	0.05	0.00	0.01	0.00	100.00	5.02	36.40	60.08	3.53
CCMK07013-5,plag.point 5	58.80	0.02	25.93	0.28	0.00	0.04	7.02	7.19	0.72	0.00	0.03	0.01	0.00	0.00	100.00	5.01	33.60	62.27	4.13
CCMK07030-4,plag.point 1	61.44	0.00	24.15	0.30	0.00	0.01	4.94	7.96	1.20	0.00	0.00	0.00	0.03	0.03	100.00	5.01	23.76	69.36	6.87
CCMK07030-4,plag.point 2	61.29	0.00	24.10	0.30	0.02	0.03	5.10	7.97	1.17	0.03	0.01	0.00	0.01	0.01	100.00	5.01	24.37	68.95	6.67
CCMK07030-4,plag.point 3	62.06	0.00	23.55	0.31	0.00	0.00	4.68	8.05	1.33	0.04	0.02	0.01	0.00	0.00	100.00	5.00	22.47	69.92	7.60
CCMK07030-4,plag.point 4	62.60	0.01	23.22	0.30	0.00	0.00	4.31	8.14	1.44	0.00	0.00	0.00	0.01	0.00	100.00	5.00	20.75	70.98	8.27
CCMK07030-4,plag.point 5	62.17	0.01	23.60	0.32	0.02	0.00	4.72	7.88	1.27	0.02	0.00	0.01	0.01	0.00	100.00	4.99	23.05	69.59	7.36
CCMK07030-7,plag.point 1	62.71	0.00	23.11	0.33	0.02	0.03	4.14	8.21	1.46	0.00	0.00	0.00	0.00	0.02	100.00	5.00	19.96	71.68	8.36
CCMK07030-7,plag.point 2	60.17	0.00	24.91	0.28	0.02	0.01	6.26	7.47	0.81	0.03	0.01	0.01	0.00	0.02	100.00	5.01	30.15	65.18	4.66
CCMK07030-7,plag.point 3	63.09	0.00	22.78	0.29	0.02	0.01	3.84	8.18	1.77	0.01	0.00	0.01	0.00	0.00	100.00	5.00	18.51	71.32	10.17
CCMK07030-7,plag.point 4	59.74	0.00	25.03	0.25	0.01	0.02	6.45	7.66	0.82	0.03	0.02	0.00	0.00	0.00	100.00	5.02	30.28	65.14	4.58
CCMK07030-7,plag.point 5	62.65	0.03	22.95	0.26	0.01	0.01	3.98	8.35	1.74	0.02	0.00	0.00	0.01	0.00	100.00	5.02	18.79	71.42	9.79
CCMK07030-8,plag.point 1	62.43	0.01	23.08	0.33	0.00	0.02	4.27	8.41	1.41	0.01	0.01	0.01	0.00	0.00	100.00	5.02	20.17	71.89	7.94
CCMK07030-8,plag.point 2	61.68	0.02	23.81	0.28	0.00	0.00	5.05	8.02	1.20	0.00	0.00	0.03	0.01	0.00	100.00	5.01	24.05	69.14	6.81
CCMK07030-8,plag.point 3	62.02	0.00	23.28	0.33	0.03	0.01	4.47	8.50	1.36	0.00	0.06	0.01	0.00	0.00	100.00	5.03	20.83	71.64	7.53
CCMK07030-8,plag.point 4	62.31	0.07	23.15	0.25	0.03	0.02	4.16	8.43	1.61	0.00	0.00	0.00	0.00	0.01	100.00	5.02	19.47	71.52	9.01
CCMK07030-8,plag.point 5	62.31	0.01	23.38	0.27	0.00	0.00	4.36	8.17	1.51	0.00	0.00	0.00	0.01	0.02	100.00	5.01	20.84	70.60	8.57
CCMK07030-1,plag.point 1	57.91	0.00	26.53	0.28	0.00	0.00	8.20	6.61	0.52	0.00	0.00	0.01	0.00	0.01	100.00	5.01	39.45	57.57	2.99
CCMK07030-1,plag.point 2	54.87	0.00	28.77	0.28	0.00	0.01	10.22	5.49	0.36	0.00	0.02	0.01	0.02	0.00	100.00	5.01	49.63	48.29	2.08
CCMK07030-1,plag.point 3	61.22	0.00	24.16	0.30	0.01	0.01	5.22	7.98	1.16	0.00	0.00	0.00	0.00	0.00	100.00	5.01	24.80	68.65	6.55
CCMK07030-1,plag.point 4	62.38	0.02	23.25	0.33	0.03	0.01	4.23	8.31	1.40	0.00	0.03	0.04	0.00	0.00	100.00	5.01	20.19	71.83	7.98
CCMK07030-1,plag.point 5	61.80	0.00	23.83	0.29	0.00	0.03	4.94	8.02	1.13	0.01	0.03	0.00	0.00	0.00	100.00	5.00	23.76	69.79	6.45
CCMK07034b-4,plag.point 1	63.22	0.00	22.93	0.27	0.00	0.01	4.02	7.98	1.58	0.02	0.00	0.02	0.01	0.02	100.00	4.98	19.74	71.03	9.22
CCMK07034b-4,plag.point 2	63.20	0.01	22.93	0.25	0.00	0.01	4.10	8.03	1.52	0.03	0.00	0.00	0.00	0.00	100.00	4.98	20.03	71.12	8.85
CCMK07034b-4,plag.point 3	62.61	0.00	23.45	0.28	0.01	0.02	3.93	8.08	1.60	0.06	0.00	0.00	0.00	0.01	100.00	5.00	19.19	71.49	9.32
CCMK07034b-4,plag.point 4	62.79	0.00	23.06	0.26	0.02	0.00	4.03	8.19	1.63	0.02	0.01	0.00	0.01	0.00	100.00	5.00	19.40	71.28	9.32
CCMK07034b-4,plag.point 5	63.15	0.00	22.97	0.33	0.01	0.03	3.96	7.96	1.56	0.01	0.03	0.02	0.00	0.00	100.00	4.98	19.58	71.25	9.17
CCMK07034b-3,plag.point 1	58.57	0.00	26.25	0.34	0.02	0.00	7.49	6.64	0.66	0.01	0.02	0.02	0.00	0.00	100.00	4.99	36.91	59.21	3.87
CCMK07034b-3,plag.point 2	62.31	0.01	23.45	0.25	0.01	0.02	4.68	8.02	1.25	0.00	0.00	0.03	0.00	0.00	100.00	5.00	22.60	70.18	7.22
CCMK07034b-3,plag.point 3	54.81	0.04	28.61	0.30	0.02	0.02	10.35	5.52	0.33	0.04	0.00	0.02	0.00	0.00	100.00	5.01	49.89	48.20	1.91
CCMK07034b-3,plag.point 4	59.50	0.06	25.31	0.26	0.02	0.01	6.78	7.23	0.76	0.00	0.06	0.00	0.00	0.02	100.00	5.01	32.64	62.99	4.37
CCMK07034b-3,plag.point 5	59.98	0.00	25.11	0.31	0.03	0.03	6.55	7.26	0.78	0.00	0.00	0.03	0.00	0.00	100.00	5.00	31.76	63.71	4.53
CCMK07034b-10,plag.point 1	61.33	0.00	23.97	0.24	0.00	0.01	5.32	8.14	1.10	0.00	0.00	0.00	0.00	0.00	100.00	5.02	24.90	68.98	6.11
CCMK07034b-10,plag.point 2	61.42	0.03	24.13	0.34	0.05	0.01	5.06	7.83	1.13	0.00	0.01	0.00	0.00	0.00	100.00	5.00	24.58	68.90	6.52
CCMK07034b-10,plag.point 4	57.85	0.00	26.68	0.31	0.00	0.02	8.06	6.55	0.60	0.00	0.00	0.00	0.00	0.00	100.00	5.00	39.05	57.48	3.47
CCMK07034b-10,plag.point 5	62.14	0.00	23.42	0.31	0.00	0.01	4.56	8.14	1.41	0.00	0.00	0.05	0.00	0.00	100.00	5.01	21.75	70.25	8.00
CCMK07034b-9,plag.point 1	62.29	0.04	23.16	0.32	0.00	0.00	4.42	8.31	1.46	0.00	0.01	0.02	0.00	0.00	100.00	5.02	20.86	70.96	8.18
CCMK07034b-9,plag.point 2	60.43	0.00	24.68	0.31	0.00	0.02	6.07	7.57	0.89	0.00	0.04	0.02	0.00	0.00	100.00	5.01	29.11	65.78	5.11
CCMK07034b-9,plag.point 3	56.88	0.02	27.86	0.36	0.00	0.02	8.04	6.25	0.59	0.01	0.00	0.00	0.00	0.00	100.00	5.00	40.10	56.39	3.52
CCMK07034b-9,plag.point 4	62.87	0.00	23.09	0.31	0.00	0.02	4.05	8.05	1.56										

Table D6: Electron Microprobe Data for matrix in Ignimbrite target rock.

	SiO ₂	TiO ₂	Al ₂ O ₃	FeO	MnO	MgO	CaO	Na ₂ O	K ₂ O	P ₂ O ₅	NiO	SO ₃	Cl	F	Total
Line 1 CCMK07013-12,3.98um, glass	73.34	0.06	15.00	0.31	0.00	0.13	0.25	3.96	6.97	0.00	0.02	0.00	0.01	0.00	100.00
Line 2 CCMK07013-12,3.98um, glass	70.46	0.09	16.47	0.36	0.03	0.11	0.30	4.49	7.60	0.04	0.05	0.00	0.00	0.00	100.00
Line 3 CCMK07013-12,3.98um, glass	69.62	0.06	16.80	0.35	0.00	0.07	0.28	4.42	8.31	0.03	0.01	0.01	0.03	0.00	100.00
Line 4 CCMK07013-12,3.98um, glass	74.83	0.04	14.12	0.23	0.01	0.11	0.29	2.71	7.65	0.00	0.00	0.02	0.02	0.00	100.00
Line 6 CCMK07013-12,3.98um, glass	66.81	0.06	18.49	0.40	0.03	0.09	0.43	4.74	8.84	0.02	0.03	0.03	0.02	0.00	100.00
Line 7 CCMK07013-12,3.98um, glass	64.83	0.05	19.37	0.41	0.00	0.15	0.37	5.30	9.51	0.00	0.00	0.03	0.00	0.01	100.00
Line 9 CCMK07013-12,3.98um, glass	74.21	0.09	14.33	0.25	0.01	0.27	0.26	3.55	7.07	0.00	0.00	0.00	0.00	0.00	100.00
Line 10 CCMK07013-12,3.98um, glass	68.92	0.04	17.86	0.34	0.00	0.04	0.36	4.57	7.90	0.00	0.00	0.00	0.01	0.00	100.00
Line 1 CCMK07013-13,6.28um,glass	67.24	0.02	18.56	0.39	0.02	0.02	0.32	4.29	9.00	0.04	0.04	0.02	0.05	0.00	100.00
Line 2 CCMK07013-13,6.28um,glass	64.16	0.08	22.72	0.54	0.06	0.25	0.64	4.75	6.63	0.03	0.00	0.06	0.07	0.01	100.00
Line 3 CCMK07013-13,6.28um,glass	72.43	0.11	15.05	0.54	0.01	0.19	0.46	4.25	6.81	0.08	0.00	0.00	0.08	0.00	100.00
Line 6 CCMK07013-13,6.28um,glass	70.34	0.00	16.80	0.31	0.02	0.13	0.32	4.50	7.54	0.02	0.00	0.00	0.06	0.00	100.00
Line 8 CCMK07013-13,6.28um,glass	67.58	0.07	18.44	0.35	0.04	0.00	0.43	4.90	8.14	0.00	0.01	0.00	0.06	0.00	100.00
Line 9 CCMK07013-13,6.28um,glass	66.65	0.10	18.10	0.62	0.05	0.19	0.53	5.17	8.21	0.05	0.07	0.05	0.20	0.00	100.00
Line 1 CCMK07030-13,3.96um,glass	67.20	0.07	18.25	0.48	0.03	0.13	0.39	4.85	8.53	0.04	0.00	0.01	0.04	0.00	100.00
Line 2 CCMK07030-13,3.96um,glass	68.45	0.10	17.65	0.52	0.04	0.25	0.40	4.25	8.18	0.00	0.00	0.06	0.14	0.00	100.00
Line 3 CCMK07030-13,3.96um,glass	69.19	0.13	17.67	0.71	0.00	0.58	0.53	4.32	6.65	0.11	0.00	0.05	0.04	0.01	100.00
Line 4 CCMK07030-13,3.96um,glass	68.26	0.12	19.22	0.54	0.00	0.15	0.50	4.34	6.71	0.08	0.00	0.07	0.03	0.00	100.00
Line 5 CCMK07030-13,3.96um,glass	69.52	0.08	17.03	0.40	0.01	0.01	0.43	4.60	7.80	0.05	0.00	0.00	0.09	0.00	100.00
Line 6 CCMK07030-13,3.96um,glass	70.11	0.15	16.54	0.30	0.00	0.04	0.40	4.60	7.83	0.00	0.05	0.00	0.04	0.00	100.00
Line 7 CCMK07030-13,3.96um,glass	66.23	0.07	18.99	0.44	0.01	0.11	0.51	5.30	8.27	0.03	0.00	0.01	0.03	0.01	100.00
Line 8 CCMK07030-13,3.96um,glass	67.19	0.07	18.35	0.53	0.02	0.04	0.51	5.29	7.74	0.05	0.08	0.00	0.14	0.00	100.00
Line 9 CCMK07030-13,3.96um,glass	67.26	0.13	17.97	0.50	0.05	0.00	0.40	5.40	8.00	0.02	0.00	0.00	0.28	0.00	100.00
Line 10 CCMK07030-13,3.96um,glass	73.65	0.06	14.78	0.31	0.04	0.05	0.28	4.15	6.65	0.01	0.00	0.00	0.05	0.00	100.00
Line 2 CCMK07030-16,5.13um,glass	64.88	0.04	22.15	0.14	0.01	0.07	0.78	5.17	6.69	0.00	0.00	0.03	0.06	0.01	100.00
Line 5 CCMK07030-16,5.13um,glass	72.17	0.05	15.25	0.38	0.04	0.04	0.32	4.15	7.40	0.04	0.01	0.00	0.14	0.01	100.00
Line 6 CCMK07030-16,5.13um,glass	76.36	0.01	13.20	0.26	0.00	0.02	0.31	3.13	6.61	0.01	0.00	0.03	0.09	0.00	100.00
Line 2 CCMK07034b-1,5.49um, glass	71.82	0.21	18.93	0.40	0.03	0.11	0.38	2.43	5.46	0.03	0.00	0.07	0.12	0.01	100.00
Line 3 CCMK07034b-1,5.49um, glass	76.89	0.21	13.09	0.65	0.04	0.07	0.40	2.44	6.10	0.00	0.02	0.00	0.11	0.01	100.00
Line 4 CCMK07034b-1,5.49um, glass	76.59	0.19	12.94	0.80	0.02	0.08	0.43	2.73	6.04	0.01	0.00	0.00	0.15	0.00	100.00
Line 5 CCMK07034b-1,5.49um, glass	76.80	0.22	12.83	0.74	0.06	0.07	0.45	2.62	5.97	0.03	0.03	0.00	0.18	0.00	100.00
Line 6 CCMK07034b-1,5.49um, glass	76.64	0.17	13.07	0.86	0.01	0.10	0.41	2.44	6.09	0.01	0.04	0.00	0.16	0.00	100.00
Line 7 CCMK07034b-1,5.49um, glass	72.00	0.09	18.31	0.76	0.00	0.09	0.54	2.35	5.63	0.04	0.02	0.02	0.13	0.02	100.00
Line 8 CCMK07034b-1,5.49um, glass	76.73	0.18	13.23	0.48	0.04	0.08	0.38	2.39	6.42	0.00	0.00	0.01	0.12	0.00	100.00
ignimbrite matrix average	70.57	0.09	16.81	0.46	0.02	0.11	0.41	4.08	7.32	0.03	0.01	0.02	0.08	0.00	100.00

Table D7: Electron Microprobe Data for magnetite in Ignimbrite target rock.

	SiO ₂	TiO ₂	Al ₂ O ₃	FeO	MnO	CaO	P ₂ O ₅	NiO	CuO	CoO	Cr ₂ O ₃	SO ₃	Total
CCMK07013 pt 1	0.13	9.93	0.79	86.94	2.06	0.12	0.05	0.00	0.00	0.11	0.04	0.00	100.00
CCMK07013 pt 2	0.03	10.99	1.19	86.01	1.64	0.02	0.00	0.00	0.07	0.14	0.04	0.00	100.00
CCMK07013 pt 3	0.19	10.01	1.70	86.33	1.58	0.05	0.05	0.00	0.00	0.12	0.05	0.00	100.00
CCMK07013 pt 4	0.00	4.48	0.71	92.14	2.65	0.03	0.06	0.00	0.00	0.05	0.00	0.00	100.00
CCMK07013 pt 5	0.02	5.90	1.54	91.04	1.37	0.00	0.05	0.02	0.04	0.05	0.01	0.00	100.00
CCMK07013 pt 6	0.07	7.74	1.10	89.33	1.51	0.04	0.05	0.00	0.10	0.10	0.03	0.00	100.00
CCMK07013 pt 8	0.08	8.24	1.33	88.46	1.64	0.01	0.03	0.01	0.00	0.15	0.02	0.03	100.00
CCMK07013 pt 10	0.07	12.50	0.98	83.76	2.42	0.05	0.00	0.00	0.09	0.09	0.12	0.00	100.00
CCMK07030 pt 1	0.08	7.77	1.38	89.50	1.19	0.04	0.00	0.00	0.00	0.13	0.01	0.00	100.00
CCMK07030 pt 2	0.06	8.35	1.40	88.08	1.64	0.21	0.01	0.10	0.00	0.02	0.16	0.00	100.00
CCMK07030 pt 4	0.05	8.57	1.50	87.92	1.80	0.07	0.00	0.03	0.01	0.06	0.01	0.00	100.00
CCMK07030 pt 5	0.09	10.70	1.31	85.80	1.93	0.00	0.00	0.00	0.05	0.10	0.01	0.06	100.00
CCMK07030 pt 6	0.05	8.53	1.19	88.65	1.56	0.00	0.00	0.01	0.00	0.06	0.03	0.00	100.00
CCMK07030 pt 7	0.03	7.96	1.35	89.37	1.25	0.01	0.01	0.00	0.00	0.16	0.03	0.00	100.00
CCMK07030 pt 9	0.04	6.91	1.72	89.62	1.59	0.04	0.01	0.00	0.00	0.07	0.03	0.05	100.00
magnetite average	0.07	8.57	1.28	88.20	1.72	0.04	0.02	0.01	0.02	0.09	0.04	0.01	100.00

Table D8: Electron Microprobe Data for ilmenite in Ignimbrite target rock.

	SiO ₂	TiO ₂	Al ₂ O ₃	FeO	MnO	CaO	P ₂ O ₅	NiO	CuO	CoO	Cr ₂ O ₃	SO ₃	Total
CCMK07013 pt 7	0.02	42.61	0.16	53.28	3.88	0.02	0.02	0.00	0.00	0.05	0.02	0.00	100.00
CCMK07030 pt 3	0.01	43.78	0.46	53.39	2.11	0.04	0.00	0.07	0.07	0.08	0.02	0.00	100.00
CCMK07030 pt 8	0.47	35.21	19.02	43.30	1.63	0.15	0.05	0.01	0.08	0.01	0.00	0.12	100.00
CCMK07030 pt 10	0.37	38.53	12.81	45.99	2.05	0.10	0.00	0.00	0.06	0.00	0.04	0.05	100.00
average ilmenite	0.22	40.03	8.11	48.99	2.41	0.08	0.02	0.02	0.05	0.03	0.02	0.04	100.00

Table D9: Electron Microprobe Data for Light Melt Impactite.

	SiO ₂	TiO ₂	Al ₂ O ₃	FeO	MnO	MgO	CaO	Na ₂ O	K ₂ O	P ₂ O ₅	NiO	SO ₃	Cl	F	Total
1 CCMK07009-9,3.72um,verticalbtw2b	77.61	0.23	12.76	0.84	0.03	0.03	0.21	2.77	5.38	0.04	0.01	0.03	0.06	0.00	100.00
2 CCMK07009-9,3.72um,verticalbtw2b	77.07	0.23	13.56	0.90	0.00	0.05	0.22	2.48	5.44	0.02	0.00	0.00	0.04	0.01	100.00
3 CCMK07009-9,3.72um,verticalbtw2b	78.08	0.22	13.05	0.85	0.02	0.05	0.19	2.31	5.15	0.03	0.00	0.00	0.09	0.00	100.00
4 CCMK07009-9,3.72um,verticalbtw2b	78.18	0.10	12.72	0.89	0.06	0.05	0.27	2.35	5.30	0.01	0.00	0.00	0.09	0.01	100.00
5 CCMK07009-9,3.72um,verticalbtw2b	78.46	0.17	12.84	0.87	0.01	0.03	0.22	2.14	5.22	0.00	0.00	0.01	0.09	0.00	100.00
6 CCMK07009-9,3.72um,verticalbtw2b	78.25	0.17	13.14	0.98	0.07	0.05	0.20	2.00	5.17	0.02	0.00	0.00	0.04	0.00	100.00
7 CCMK07009-9,3.72um,verticalbtw2b	78.19	0.22	13.01	0.88	0.05	0.03	0.24	2.22	5.07	0.00	0.01	0.00	0.06	0.02	100.00
8 CCMK07009-9,3.72um,verticalbtw2b	77.93	0.15	12.81	0.92	0.09	0.04	0.24	2.33	5.40	0.03	0.00	0.00	0.08	0.00	100.00
9 CCMK07009-9,3.72um,verticalbtw2b	77.76	0.24	12.90	0.91	0.02	0.05	0.22	2.53	5.32	0.02	0.00	0.00	0.06	0.00	100.00
10 CCMK07009-9,3.72um,verticalbtw2	78.21	0.21	12.48	0.97	0.04	0.05	0.21	2.41	5.32	-0.01	0.02	0.01	0.09	0.00	100.00
11 CCMK07009-9,3.72um,verticalbtw2	77.69	0.18	12.96	0.88	0.05	0.05	0.22	2.48	5.39	0.03	0.00	0.01	0.08	0.00	100.00
12 CCMK07009-9,3.72um,verticalbtw2	77.91	0.24	12.88	0.94	0.03	0.06	0.23	2.37	5.23	0.02	0.00	0.00	0.07	0.02	100.00
13 CCMK07009-9,3.72um,verticalbtw2	78.23	0.18	12.84	0.94	0.00	0.03	0.26	2.19	5.29	0.00	0.00	0.01	0.07	0.01	100.00
14 CCMK07009-9,3.72um,verticalbtw2	78.00	0.28	13.00	0.92	0.06	0.03	0.20	2.19	5.24	0.05	0.00	0.00	0.07	0.02	100.00
15 CCMK07009-9,3.72um,verticalbtw2	78.24	0.16	12.70	0.90	0.06	0.03	0.21	2.34	5.28	0.00	0.00	0.02	0.08	0.00	100.00
16 CCMK07009-9,3.72um,verticalbtw2	77.82	0.21	12.54	0.90	0.02	0.06	0.24	2.66	5.43	0.01	0.00	0.06	0.06	0.00	100.00
17 CCMK07009-9,3.72um,verticalbtw2	77.89	0.15	12.70	0.95	0.08	0.05	0.22	2.43	5.39	0.03	0.01	0.02	0.09	0.00	100.00
18 CCMK07009-9,3.72um,verticalbtw2	78.01	0.18	12.73	0.92	0.04	0.02	0.24	2.42	5.39	0.01	0.00	0.00	0.10	0.01	100.00
19 CCMK07009-9,3.72um,verticalbtw2	78.10	0.23	12.72	0.98	0.03	0.02	0.24	2.31	5.27	0.01	0.01	0.00	0.09	0.00	100.00
20 CCMK07009-9,3.72um,verticalbtw2	78.14	0.23	12.66	0.97	0.05	0.03	0.19	2.25	5.44	0.00	0.00	0.00	0.08	0.00	100.00
1 CCMK07009-7,6.96um,underlgbubble	77.88	0.11	12.49	0.93	0.04	0.02	0.18	2.81	5.45	0.00	0.00	0.03	0.09	0.00	100.00
2 CCMK07009-7,6.96um,underlgbubble	77.62	0.19	12.74	0.94	0.05	0.05	0.18	2.79	5.37	0.00	0.00	0.02	0.09	0.00	100.00
3 CCMK07009-7,6.96um,underlgbubble	77.32	0.15	12.57	1.04	0.11	0.05	0.24	2.78	5.58	0.03	0.01	0.02	0.09	0.00	100.00
4 CCMK07009-7,6.96um,underlgbubble	77.66	0.15	12.68	0.88	0.06	0.07	0.23	2.74	5.41	0.03	0.03	0.00	0.09	0.01	100.00
5 CCMK07009-7,6.96um,underlgbubble	77.39	0.15	12.73	1.05	0.07	0.05	0.21	2.76	5.46	0.01	0.00	0.01	0.10	0.04	100.00
6 CCMK07009-7,6.96um,underlgbubble	77.36	0.21	12.84	0.88	0.04	0.03	0.22	2.74	5.55	0.00	0.02	0.03	0.11	0.00	100.00
7 CCMK07009-7,6.96um,underlgbubble	77.56	0.12	12.71	0.90	0.06	0.04	0.19	2.85	5.41	0.00	0.00	0.05	0.10	0.00	100.00
8 CCMK07009-7,6.96um,underlgbubble	77.61	0.19	12.81	0.92	0.06	0.03	0.23	2.53	5.47	0.03	0.03	0.00	0.08	0.02	100.00
9 CCMK07009-7,6.96um,underlgbubble	77.59	0.15	12.72	0.95	0.07	0.04	0.22	2.69	5.41	0.01	0.02	0.02	0.09	0.01	100.00
10 CCMK07009-7,6.96um,underlgbubbl	77.71	0.21	12.88	0.97	0.01	0.02	0.18	2.62	5.39	0.00	0.00	0.00	0.06	0.03	100.00
11 CCMK07009-7,6.96um,underlgbubbl	77.76	0.16	12.63	0.91	0.06	0.03	0.23	2.51	5.55	0.00	0.00	0.04	0.12	0.00	100.00
12 CCMK07009-7,6.96um,underlgbubbl	77.80	0.16	12.60	0.80	0.02	0.04	0.22	2.77	5.47	0.00	0.01	0.00	0.12	0.00	100.00
13 CCMK07009-7,6.96um,underlgbubbl	77.40	0.21	12.78	0.94	0.02	0.03	0.21	2.77	5.54	0.00	0.04	0.00	0.11	0.00	100.00
14 CCMK07009-7,6.96um,underlgbubbl	77.38	0.22	12.93	0.86	0.03	0.03	0.19	2.68	5.51	0.01	0.01	0.06	0.09	0.00	100.00
15 CCMK07009-7,6.96um,underlgbubbl	77.43	0.25	12.64	0.97	0.04	0.02	0.21	2.75	5.54	0.00	0.04	0.04	0.07	0.00	100.00
16 CCMK07009-7,6.96um,underlgbubbl	77.65	0.12	12.68	0.92	0.06	0.03	0.19	2.55	5.62	0.01	0.07	0.02	0.09	0.01	100.00
17 CCMK07009-7,6.96um,underlgbubbl	75.95	0.23	14.27	0.90	0.02	0.02	0.27	2.74	5.50	0.04	0.00	0.00	0.09	0.00	100.00
18 CCMK07009-7,6.96um,underlgbubbl	77.81	0.14	12.75	0.81	0.04	0.05	0.21	2.56	5.53	0.00	0.00	0.00	0.10	0.01	100.00
19 CCMK07009-7,6.96um,underlgbubbl	77.65	0.18	12.53	0.97	0.02	0.06	0.22	2.79	5.46	0.03	0.00	0.00	0.09	0.03	100.00
20 CCMK07009-7,6.96um,underlgbubbl	76.47	0.23	13.97	0.81	0.02	0.05	0.22	2.63	5.45	0.05	0.01	0.00	0.08	0.02	100.00
1 CCMK07009-7B,4.06um,diagonalofbu	77.71	0.18	12.81	0.67	0.06	0.03	0.19	2.84	5.43	0.02	0.00	0.06	0.02	0.00	100.00
2 CCMK07009-7B,4.06um,diagonalofbu	77.91	0.25	12.71	0.77	0.04	0.00	0.17	2.70	5.36	0.02	0.01	0.04	0.03	0.01	100.00
3 CCMK07009-7B,4.06um,diagonalofbu	77.69	0.21	12.92	0.72	0.05	0.02	0.26	2.75	5.23	0.04	0.04	0.05	0.03	0.00	100.00
4 CCMK07009-7B,4.06um,diagonalofbu	77.93	0.21	13.06	0.72	0.07	0.03	0.24	2.59	5.19	0.00	0.00	0.00	0.04	0.01	100.00
5 CCMK07009-7B,4.06um,diagonalofbu	78.20	0.19	12.70	0.81	0.02	0.03	0.20	2.55	5.22	0.03	0.00	0.01	0.04	0.00	100.00
6 CCMK07009-7B,4.06um,diagonalofbu	78.72	0.14	12.89	0.71	0.05	0.03	0.15	2.09	5.16	0.00	0.02	0.01	0.05	0.00	100.00
7 CCMK07009-7B,4.06um,diagonalofbu	78.14	0.21	12.72	0.82	0.02	0.03	0.17	2.48	5.39	0.00	0.00	0.00	0.07	0.00	100.00
8 CCMK07009-7B,4.06um,diagonalofbu	78.14	0.14	12.71	0.79	0.01	0.03	0.17	2.52	5.36	0.00	0.02	0.01	0.07	0.01	100.00
9 CCMK07009-7B,4.06um,diagonalofbu	77.87	0.26	12.72	0.81	0.05	0.05	0.21	2.45	5.40	0.05	0.00	0.02	0.09	0.02	100.00
10 CCMK07009-7B,4.06um,diagonalofb	78.14	0.11	12.80	0.80	0.00	0.03	0.17	2.42	5.43	0.03	0.00	0.01	0.09	0.00	100.00
11 CCMK07009-7B,4.06um,diagonalofb	78.26	0.20	12.69	0.90	0.05	0.03	0.18	2.24	5.33	0.01	0.02	0.01	0.08	0.01	100.00
12 CCMK07009-7B,4.06um,diagonalofb	78.35	0.24	12.78	0.99	0.06	0.04	0.19	2.08	5.16	0.00	0.01	0.01	0.08	0.00	100.00
13 CCMK07009-7B,4.06um,diagonalofb	77.90	0.12	12.70	0.91	0.02	0.05	0.18	2.53	5.51	0.03	0.00	0.00	0.07	0.00	100.00
14 CCMK07009-7B,4.06um,diagonalofb	77.77	0.17	12.60	0.92	0.05	0.05	0.19	2.74	5.38	0.00	0.01	0.04	0.08	0.00	100.00
15 CCMK07009-7B,4.06um,diagonalofb	77.56	0.17	12.92	0.97	0.06	0.03	0.19	2.60	5.36	0.02	0.00	0.03	0.10	0.00	100.00
16 CCMK07009-7B,4.06um,diagonalofb	77.98	0.21	12.89	0.99	0.11	0.06	0.27	2.05	5.26	0.02	0.00	0.05	0.11	0.00	100.00
17 CCMK07009-7B,4.06um,diagonalofb	77.94	0.25	12.61	0.91	0.06	0.05	0.20	2.45	5.48	0.00	0.00	0.01	0.09	0.02	100.00
18 CCMK07009-7B,4.06um,diagonalofb	78.35	0.24	12.68	0.98	0.00	0.02	0.20	2.12	5.27	0.04	0.03	0.00	0.08	0.00	100.00
19 CCMK07009-7B,4.06um,diagonalofb	77.40	0.14	13.56	0.94	0.02	0.04	0.26	2.31	5.29	0.03	0.00	0.00	0.07	0.00	100.00
20 CCMK07009-7B,4.06um,diagonalofb	77.43	0.22	12.70	0.86	0.05	0.05	0.26	2.83	5.38	0.05	0.04	0.03	0.12	0.00	100.00

Table D9: Continued.

	SiO ₂	TiO ₂	Al ₂ O ₃	FeO	MnO	MgO	CaO	Na ₂ O	K ₂ O	P ₂ O ₅	NiO	SO ₃	Cl	F	Total
1 CCMK07046-7,3.24um,abovedoublebu	76.33	0.14	12.50	1.16	0.00	0.03	0.25	2.68	6.88	0.02	0.00	0.00	0.04	0.00	100.00
3 CCMK07046-7,3.24um,abovedoublebu	76.77	0.19	12.32	0.98	0.02	0.04	0.21	2.81	6.56	0.03	0.07	0.01	0.00	0.00	100.00
5 CCMK07046-7,3.24um,abovedoublebu	76.88	0.21	12.83	0.99	0.00	0.04	0.23	2.66	6.13	0.01	0.01	0.00	0.05	0.02	100.00
7 CCMK07046-7,3.24um,abovedoublebu	77.02	0.24	12.35	1.01	0.01	0.04	0.23	2.81	6.18	0.00	0.05	0.01	0.04	0.02	100.00
9 CCMK07046-7,3.24um,abovedoublebu	77.03	0.17	12.33	0.88	0.09	0.03	0.27	2.86	6.30	0.00	0.00	0.01	0.05	0.01	100.00
11 CCMK07046-7,3.24um,abovedoubleb	76.89	0.17	12.81	0.95	0.04	0.05	0.26	2.79	5.95	0.00	0.02	0.00	0.06	0.01	100.00
13 CCMK07046-7,3.24um,abovedoubleb	75.84	0.21	13.39	0.97	0.05	0.06	0.27	2.77	6.27	0.02	0.03	0.04	0.07	0.00	100.00
15 CCMK07046-7,3.24um,abovedoubleb	76.48	0.20	13.25	0.94	0.04	0.05	0.29	2.65	6.00	0.00	0.04	0.03	0.05	0.00	100.00
17 CCMK07046-7,3.24um,abovedoubleb	76.65	0.24	12.72	0.95	0.05	0.06	0.25	2.89	5.99	0.04	0.10	0.00	0.08	0.00	100.00
19 CCMK07046-7,3.24um,abovedoubleb	75.99	0.20	13.74	0.93	0.06	0.07	0.26	2.78	5.85	0.02	0.00	0.04	0.09	0.00	100.00
1 CCMK07046-8,2.15um,nextlgbubble	77.06	0.26	12.87	0.88	0.01	0.05	0.30	2.64	5.75	-0.01	0.00	0.00	0.25	0.00	100.00
3 CCMK07046-8,2.15um,nextlgbubble	76.71	0.18	13.13	0.94	0.07	0.04	0.34	2.52	5.84	-0.03	0.00	0.03	0.24	0.00	100.00
5 CCMK07046-8,2.15um,nextlgbubble	77.26	0.14	12.79	0.91	0.05	0.08	0.32	2.44	5.68	0.03	0.02	0.00	0.28	0.00	100.00
7 CCMK07046-8,2.15um,nextlgbubble	77.47	0.27	12.61	0.94	0.07	0.05	0.34	2.39	5.58	0.05	0.01	0.00	0.23	0.00	100.00
9 CCMK07046-8,2.15um,nextlgbubble	77.97	0.19	12.76	1.02	0.03	0.05	0.29	2.01	5.41	0.04	0.00	0.03	0.23	0.00	100.00
11 CCMK07046-8,2.15um,nextlgbubble	77.53	0.17	12.63	0.94	0.09	0.08	0.32	2.42	5.61	0.00	0.01	0.00	0.23	0.00	100.00
13 CCMK07046-8,2.15um,nextlgbubble	77.43	0.19	12.41	0.94	0.04	0.08	0.31	2.60	5.62	0.07	0.03	0.01	0.25	0.00	100.00
15 CCMK07046-8,2.15um,nextlgbubble	77.34	0.18	12.59	0.97	0.05	0.06	0.31	2.47	5.72	0.00	0.02	0.02	0.28	0.00	100.00
17 CCMK07046-8,2.15um,nextlgbubble	77.26	0.15	12.89	0.92	0.06	0.04	0.37	2.33	5.67	0.04	0.00	0.00	0.27	0.00	100.00
1 CCMK07047-11,2.89um,aroundbubble	77.78	0.15	12.32	0.89	0.04	0.05	0.25	2.72	5.77	0.00	0.00	0.02	0.06	0.00	100.00
13 CCMK07047-11,2.89um,aroundbubbl	78.83	0.20	11.69	1.13	0.00	0.06	0.33	1.90	5.76	0.02	0.02	0.01	0.06	0.00	100.00
17 CCMK07047-11,2.89um,aroundbubbl	76.86	0.14	12.49	0.95	0.04	0.04	0.25	2.74	6.47	0.00	0.00	0.00	0.08	0.00	100.00
19 CCMK07047-11,2.89um,aroundbubbl	77.14	0.19	12.56	0.86	0.03	0.05	0.23	2.67	6.17	0.00	0.03	0.00	0.09	0.00	100.00
light melt average	77.60	0.19	12.80	0.91	0.04	0.04	0.23	2.53	5.54	0.02	0.01	0.01	0.09	0.00	100.00

Table D10: Electron Microprobe Data for Melted Minerals.

	SiO ₂	TiO ₂	Al ₂ O ₃	FeO	MnO	MgO	CaO	Na ₂ O	K ₂ O	P ₂ O ₅	NiO	SO ₃	Cl	F	Total	Mixture group
1 CCMK07A-17.2.35um.acrossdarkspot	90.56	0.04	3.96	3.02	0.02	0.23	0.67	0.44	0.87	0.01	0.08	0.07	0.03	0.00	100.00	lechatelierite
2 CCMK07A-17.2.35um.acrossdarkspot	94.73	0.05	2.27	1.61	0.00	0.12	0.35	0.26	0.53	0.00	0.04	0.02	0.02	0.00	100.00	lechatelierite
3 CCMK07A-17.2.35um.acrossdarkspot	95.54	0.06	2.07	1.26	0.00	0.10	0.30	0.25	0.37	0.03	0.02	0.01	0.01	0.01	100.00	lechatelierite
1 CCMK07082-3.4.85um,underwhitevie	99.81	0.00	0.03	0.14	0.00	0.00	0.02	0.00	0.03	0.00	0.03	0.00	0.01	0.00	100.00	lechatelierite
3 CCMK07082-3.4.85um,underwhitevie	99.67	0.06	0.03	0.20	0.00	0.01	0.02	0.01	0.03	0.00	0.02	0.00	0.01	0.00	100.00	lechatelierite
5 CCMK07082-3.4.85um,underwhitevie	99.82	0.00	0.01	0.09	0.01	0.00	0.02	0.01	0.02	0.01	0.00	0.02	0.00	0.00	100.00	lechatelierite
7 CCMK07082-3.4.85um,underwhitevie	99.67	0.00	0.04	0.13	0.04	0.02	0.05	0.00	0.01	0.04	0.00	0.01	0.00	0.01	100.00	lechatelierite
9 CCMK07082-3.4.85um,underwhitevie	99.53	0.00	0.08	0.14	0.03	0.00	0.04	0.02	0.01	0.01	0.11	0.02	0.00	0.00	100.00	lechatelierite
11 CCMK07082-3.4.85um,underwhitevi	99.60	0.04	0.01	0.17	0.02	0.01	0.01	0.00	0.04	0.02	0.08	0.00	0.01	0.01	100.00	lechatelierite
13 CCMK07082-3.4.85um,underwhitevi	98.56	0.00	0.99	0.21	0.00	0.03	0.06	0.02	0.03	0.07	0.00	0.06	0.00	0.02	100.00	lechatelierite
15 CCMK07082-3.4.85um,underwhitevi	99.72	0.00	0.02	0.17	0.03	0.00	0.01	0.03	0.04	0.00	0.04	0.00	0.00	0.00	100.00	lechatelierite
17 CCMK07082-3.4.85um,underwhitevi	99.48	0.04	0.01	0.26	0.03	0.01	0.02	0.03	0.03	0.02	0.09	0.00	0.00	0.00	100.00	lechatelierite
19 CCMK07082-3.4.85um,underwhitevi	99.45	0.00	0.01	0.41	0.00	0.00	0.03	0.01	0.02	0.01	0.11	0.01	0.00	0.01	100.00	lechatelierite
1 CCMK07082-3A,3.78um,below3	99.00	0.01	0.21	0.47	0.03	0.01	0.00	0.08	0.13	0.00	0.06	0.00	0.02	0.00	100.00	lechatelierite
3 CCMK07082-3A,3.78um,below3	99.37	0.03	0.02	0.44	0.00	0.00	0.02	0.03	0.03	0.01	0.00	0.02	0.01	0.01	100.00	lechatelierite
5 CCMK07082-3A,3.78um,below3	99.05	0.00	0.07	0.68	0.01	0.01	0.04	0.06	0.07	0.01	0.02	0.02	0.02	0.00	100.00	lechatelierite
9 CCMK07082-3A,3.78um,below3	96.08	0.03	1.00	1.84	0.00	0.10	0.27	0.28	0.30	0.00	0.08	0.05	0.00	0.01	100.00	lechatelierite
11 CCMK07082-3A,3.78um,below3	96.58	0.01	0.68	1.82	0.04	0.09	0.15	0.35	0.29	0.00	0.01	0.00	0.00	0.00	100.00	lechatelierite
17 CCMK07082-3A,3.78um,below3	99.03	0.05	0.34	0.38	0.04	0.02	0.02	0.01	0.05	0.00	0.07	0.00	0.02	0.00	100.00	lechatelierite
19 CCMK07082-3A,3.78um,below3	98.57	0.00	0.31	0.79	0.00	0.07	0.09	0.10	0.14	0.00	0.00	0.02	0.01	0.01	100.00	lechatelierite
6 CCMK07A-17.2.35um.acrossdarkspot	73.12	0.16	14.60	4.47	0.03	0.51	1.66	1.81	3.54	0.05	0.00	0.05	0.00	0.00	100.00	maskelynite
13 CCMK07045-6.2.52um,dark/light	77.57	0.01	10.93	4.55	0.00	0.20	0.88	1.60	4.21	0.00	0.03	0.03	0.00	0.00	100.00	maskelynite
14 CCMK07045-6.2.52um,dark/light	73.74	0.00	15.16	2.80	0.02	0.14	0.68	2.18	5.39	0.01	0.00	0.00	0.00	0.02	100.00	maskelynite
15 CCMK07045-6.2.52um,dark/light	72.47	0.00	16.44	2.14	0.00	0.12	0.70	2.46	5.64	0.04	0.04	0.00	0.00	0.00	100.00	maskelynite
16 CCMK07045-6.2.52um,dark/light	70.57	0.00	18.18	1.94	0.00	0.11	0.65	2.76	5.74	0.03	0.05	0.00	0.01	0.00	100.00	maskelynite
17 CCMK07045-6.2.52um,dark/light	68.64	0.00	19.67	2.17	0.00	0.10	0.72	2.71	5.98	0.01	0.00	0.00	0.00	0.02	100.00	maskelynite
18 CCMK07045-6.2.52um,dark/light	66.86	0.05	20.23	2.55	0.05	0.12	0.79	3.32	5.99	0.00	0.00	0.06	0.01	0.00	100.00	maskelynite
19 CCMK07045-6.2.52um,dark/light	66.23	0.08	20.64	3.20	0.01	0.20	0.95	2.77	5.92	0.01	0.01	0.01	0.00	0.00	100.00	maskelynite
20 CCMK07045-6.2.52um,dark/light	66.69	0.11	20.61	2.88	0.01	0.16	0.94	2.79	5.78	0.03	0.03	0.00	0.00	0.00	100.00	maskelynite
4 CCMK07A-17.2.35um.acrossdarkspot	84.67	0.08	6.94	4.68	0.01	0.30	0.90	0.79	1.10	0.08	0.45	0.01	0.00	0.00	100.00	melted mineral mix
5 CCMK07A-17.2.35um.acrossdarkspot	72.88	0.08	13.46	6.36	0.04	0.44	1.36	1.67	2.88	0.06	0.65	0.04	0.04	0.04	100.00	melted mineral mix
7 CCMK07A-17.2.35um.acrossdarkspot	69.50	0.31	15.04	6.63	0.03	0.79	2.34	2.65	2.53	0.05	0.06	0.06	0.01	0.01	100.00	melted mineral mix
8 CCMK07A-17.2.35um.acrossdarkspot	70.00	0.19	14.22	6.92	0.07	0.78	2.58	2.42	2.64	0.07	0.02	0.05	0.02	0.00	100.00	melted mineral mix
9 CCMK07A-17.2.35um.acrossdarkspot	70.75	0.25	13.96	6.20	0.04	0.74	2.87	2.18	2.92	0.03	0.00	0.06	0.01	0.01	100.00	melted mineral mix
10 CCMK07A-17.2.35um.acrossdarkspo	63.65	0.20	16.91	8.49	0.09	1.03	3.55	1.87	3.99	0.08	0.01	0.12	0.01	0.01	100.00	melted mineral mix
11 CCMK07A-17.2.35um.acrossdarkspo	67.31	0.16	14.98	7.43	0.10	0.96	3.28	1.66	3.93	0.01	0.07	0.11	0.00	0.02	100.00	melted mineral mix
12 CCMK07A-17.2.35um.acrossdarkspo	69.73	0.17	14.31	6.68	0.03	0.78	2.89	1.75	3.56	0.01	0.02	0.07	0.00	0.00	100.00	melted mineral mix
13 CCMK07A-17.2.35um.acrossdarkspo	62.95	0.18	17.83	8.13	0.07	0.80	3.54	2.11	4.24	0.05	0.04	0.06	0.01	0.00	100.00	melted mineral mix
14 CCMK07A-17.2.35um.acrossdarkspo	61.88	0.21	18.65	9.45	0.09	0.90	3.67	1.30	3.65	0.06	0.01	0.10	0.04	0.00	100.00	melted mineral mix
15 CCMK07A-17.2.35um.acrossdarkspo	63.71	0.23	17.57	9.67	0.09	0.98	3.48	1.42	2.51	0.10	0.07	0.13	0.02	0.01	100.00	melted mineral mix
16 CCMK07A-17.2.35um.acrossdarkspo	62.77	0.26	17.16	10.27	0.12	1.00	3.59	2.44	2.19	0.04	0.02	0.13	0.00	0.02	100.00	melted mineral mix
17 CCMK07A-17.2.35um.acrossdarkspo	60.38	0.26	17.32	11.41	0.06	0.97	4.20	3.06	2.12	0.05	0.00	0.20	0.00	0.00	100.00	melted mineral mix
18 CCMK07A-17.2.35um.acrossdarkspo	59.22	0.23	17.40	11.85	0.12	0.99	4.36	3.32	2.29	0.03	0.07	0.12	0.00	0.00	100.00	melted mineral mix
19 CCMK07A-17.2.35um.acrossdarkspo	57.97	0.23	18.26	10.94	0.12	0.95	5.19	4.16	2.02	0.03	0.00	0.13	0.02	0.00	100.00	melted mineral mix
20 CCMK07A-17.2.35um.acrossdarkspo	56.27	0.25	17.27	14.38	0.07	1.17	4.38	3.95	1.99	0.00	0.19	0.10	0.00	0.01	100.00	melted mineral mix
2 CCMK07045-6.2.52um,dark/light	47.57	0.52	12.58	27.16	0.10	2.16	5.32	1.39	2.79	0.12	0.06	0.24	0.02	0.00	100.00	melted mineral mix
11 CCMK07045-6.2.52um,dark/light	53.87	0.46	13.21	21.73	0.10	1.25	4.38	1.46	3.01	0.09	0.05	0.38	0.01	0.01	100.00	melted mineral mix
12 CCMK07045-6.2.52um,dark/light	62.75	0.22	13.41	13.98	0.01	0.58	3.13	1.73	3.96	0.16	0.00	0.11	0.00	0.01	100.00	melted mineral mix
1 CCMK07045-7.2.86um,dark/light	48.40	0.09	14.01	31.29	0.12	2.00	0.63	2.03	0.32	0.04	0.93	0.05	0.05	0.03	100.00	melted mineral mix
2 CCMK07045-7.2.86um,dark/light	56.73	0.09	13.60	21.67	0.09	1.99	0.53	2.47	0.39	0.01	2.34	0.06	0.02	0.01	100.00	melted mineral mix
3 CCMK07045-7.2.86um,dark/light	54.00	0.11	13.22	21.85	0.13	2.26	0.47	2.39	0.28	0.00	5.22	0.06	0.01	0.00	100.00	melted mineral mix
4 CCMK07045-7.2.86um,dark/light	54.04	0.12	13.64	24.04	0.07	1.97	0.59	2.78	0.27	0.00	2.41	0.05	0.00	0.01	100.00	melted mineral mix
5 CCMK07045-7.2.86um,dark/light	54.10	0.14	16.21	24.19	0.07	1.66	0.65	2.44	0.40	0.02	0.09	0.02	0.00	0.01	100.00	melted mineral mix
6 CCMK07045-7.2.86um,dark/light	51.53	0.16	16.56	25.92	0.13	1.73	0.81	2.53	0.54	0.03	0.00	0.05	0.01	0.02	100.00	melted mineral mix
7 CCMK07045-7.2.86um,dark/light	56.97	0.18	15.08	21.65	0.08	1.67	1.15	2.48	0.66	0.02	0.02	0.01	0.01	0.01	100.00	melted mineral mix
9 CCMK07045-7.2.86um,dark/light	51.92	0.40	13.26	24.60	0.06	1.70	2.75	2.74	2.24	0.03	0.07	0.20	0.00	0.03	100.00	melted mineral mix
10 CCMK07045-7.2.86um,dark/light	47.26	0.48	12.52	28.09	0.06	1.43	3.61	2.96	3.11	0.13	0.00	0.38	0.00	0.01	100.00	melted mineral mix
11 CCMK07045-7.2.86um,dark/light	50.04	0.41	12.27	25.07	0.07	1.45	5.50	1.97	2.58	0.17	0.09	0.39	0.00	0.01	100.00	melted mineral mix
12 CCMK07045-7.2.86um,dark/light	53.08	0.48	12.81	22.68	0.08	1.21	5.07	1.81	2.18	0.18	0.00	0.48	0.00	0.00	100.00	melted mineral mix
13 CCMK07045-7.2.86um,dark/light	52.41	0.43	12.66	24.53	0.07	1.61	4.01	1.52	2.18	0.21	0.00	0.38	0.00	0.01	100.00	melted mineral mix
18 CCMK07045-7.2.86um,dark/light	52.47	0.36	12.97	24.19	0.09	1.00	3.94	1.33	2.20	0.75	0.12	0.51	0.00	0.07	100.00	melted mineral mix
19 CCMK07045-7.2.86um,dark/light	53.35	0.35	11.88	23.93	0.07	1.46	3.73	1.46	2.44	0.80	0.05	0.47	0.01	0.02	100.00	melted mineral mix
20 CCMK07045-7.2.86um,dark/light	54.20	0.36	12.09	22.95	0.07	1.86	3.02	1.55	2.51	0.92	0.08	0.35	0.01	0.04	100.00	melted mineral mix
20 CCMK07045-9.1.89um,thrudarkclou	45.35	0.39	15.61	27.61	0.09	1.53	4.07	1.91	3.04	0.04	0.00	0.42	0.01	0.00	100.00	melted mineral mix
7 CCMK07082-3A,3.78um,below3	81.86	0.21	6.04	7.37	0.00	0.50	1.44	1.17	1.13	0.00	0.04	0.25	0.02	0.00	100.00	melted mineral mix
13 CCMK07082-3A,3.78um,below3	79.41	0.29	5.77	8.81	0.01	0.63	1.60	1.64	1.55	0.03	0.01	0.19	0.02	0.04	100.00	melted mineral mix
15 CCMK07082-3A,3.78um,below3	77.90	0.19	6.33	9.53	0.05	0.68	1.87	1.67	1.52	0.00	0.03	0.23	0.02	0.01	100.00	melted mineral mix
15 CCMK07082-10.6.71um,inbtvbubble	47.58	0.35	11.02	29.50	0.10	1.68	3.17									

Table D11: Electron Microprobe Data for Dark Melt Group 1.

	SiO ₂	TiO ₂	Al ₂ O ₃	FeO	MnO	MgO	CaO	Na ₂ O	K ₂ O	P ₂ O ₅	NiO	SO ₃	Cl	F	Total
1 CCMK07045-6,2.52um,dark/light	51.31	0.46	12.95	24.11	0.13	2.80	3.72	1.65	2.51	0.17	0.00	0.23	0.01	0.02	100.00
3 CCMK07045-6,2.52um,dark/light	51.13	0.57	12.14	25.06	0.14	1.93	4.78	1.27	2.51	0.15	0.04	0.29	0.00	0.00	100.00
4 CCMK07045-6,2.52um,dark/light	51.01	0.51	12.44	24.74	0.08	1.88	4.59	1.45	2.68	0.14	0.07	0.37	0.00	0.03	100.00
5 CCMK07045-6,2.52um,dark/light	51.30	0.54	12.50	24.88	0.04	1.79	4.54	1.41	2.38	0.13	0.03	0.46	0.00	0.00	100.00
6 CCMK07045-6,2.52um,dark/light	51.10	0.45	12.25	25.14	0.10	2.38	4.33	1.35	2.33	0.18	0.05	0.33	0.00	0.02	100.00
7 CCMK07045-6,2.52um,dark/light	51.18	0.48	11.91	25.32	0.12	2.18	4.46	1.15	2.38	0.15	0.22	0.42	0.03	0.00	100.00
8 CCMK07045-6,2.52um,dark/light	51.17	0.50	12.47	24.83	0.11	1.42	5.06	1.38	2.45	0.15	0.02	0.42	0.00	0.01	100.00
9 CCMK07045-6,2.52um,dark/light	50.91	0.45	13.29	24.55	0.09	1.90	4.47	1.28	2.60	0.12	0.00	0.31	0.01	0.01	100.00
10 CCMK07045-6,2.52um,dark/light	51.61	0.46	13.18	23.82	0.09	1.68	4.32	1.43	2.78	0.16	0.05	0.42	0.00	0.00	100.00
1 CCMK07045-8A,4.44um,acrossgrain	50.46	0.42	11.59	25.85	0.10	1.59	4.09	2.45	2.30	0.19	0.43	0.51	0.02	0.00	100.00
2 CCMK07045-8A,4.44um,acrossgrain	50.51	0.41	11.91	26.03	0.07	1.45	4.31	2.37	2.35	0.18	0.00	0.41	0.00	0.00	100.00
3 CCMK07045-8A,4.44um,acrossgrain	51.32	0.43	12.13	25.01	0.09	1.46	4.29	2.39	2.35	0.11	0.01	0.40	0.01	0.00	100.00
4 CCMK07045-8A,4.44um,acrossgrain	50.97	0.43	12.08	25.47	0.07	1.55	4.33	2.28	2.26	0.11	0.05	0.40	0.01	0.01	100.00
5 CCMK07045-8A,4.44um,acrossgrain	50.88	0.47	12.00	25.36	0.09	1.61	4.55	2.26	2.25	0.09	0.05	0.37	0.00	0.03	100.00
6 CCMK07045-8A,4.44um,acrossgrain	50.51	0.47	12.24	25.44	0.06	1.32	4.65	2.25	2.28	0.17	0.15	0.44	0.02	0.01	100.00
7 CCMK07045-8A,4.44um,acrossgrain	50.45	0.43	12.34	25.12	0.11	1.69	4.33	2.46	2.36	0.18	0.11	0.41	0.00	0.01	100.00
8 CCMK07045-8A,4.44um,acrossgrain	50.44	0.43	12.38	25.49	0.05	1.76	4.06	2.43	2.34	0.18	0.04	0.40	0.00	0.00	100.00
9 CCMK07045-8A,4.44um,acrossgrain	50.54	0.46	12.50	25.75	0.11	1.72	3.95	2.18	2.25	0.17	0.01	0.34	0.00	0.02	100.00
10 CCMK07045-8A,4.44um,acrossgrain	49.38	0.53	12.99	26.09	0.08	1.62	4.10	2.20	2.23	0.17	0.10	0.48	0.01	0.00	100.00
1 CCMK07082-9,2.85um,acrossgrain	51.03	0.42	12.70	25.08	0.07	1.39	3.85	2.56	2.35	0.03	0.02	0.47	0.02	0.00	100.00
3 CCMK07082-9,2.85um,acrossgrain	51.24	0.48	13.16	24.41	0.05	1.04	4.59	2.26	2.31	0.01	0.00	0.49	0.00	0.00	100.00
5 CCMK07082-9,2.85um,acrossgrain	51.46	0.47	12.82	24.76	0.05	1.28	4.16	2.09	2.23	0.00	0.05	0.60	0.02	0.00	100.00
7 CCMK07082-9,2.85um,acrossgrain	50.65	0.43	12.97	25.30	0.06	1.22	4.14	2.39	2.11	0.03	0.12	0.58	0.00	0.00	100.00
9 CCMK07082-9,2.85um,acrossgrain	50.25	0.45	13.01	25.76	0.03	1.31	3.89	2.41	2.11	0.07	0.13	0.56	0.01	0.01	100.00
11 CCMK07082-9,2.85um,acrossgrain	49.91	0.41	12.25	27.20	0.04	1.91	3.29	2.37	2.12	0.05	0.07	0.33	0.01	0.02	100.00
13 CCMK07082-9,2.85um,acrossgrain	50.17	0.48	12.66	26.34	0.04	1.52	3.69	2.52	2.15	0.05	0.00	0.43	0.01	0.01	100.00
15 CCMK07082-9,2.85um,acrossgrain	50.24	0.35	12.47	26.82	0.03	1.81	3.29	2.42	2.14	0.05	0.00	0.38	0.00	0.00	100.00
17 CCMK07082-9,2.85um,acrossgrain	50.94	0.38	12.65	25.78	0.04	1.84	3.20	2.57	2.23	0.00	0.03	0.37	0.00	0.00	100.00
19 CCMK07082-9,2.85um,acrossgrain	50.58	0.44	12.38	26.52	0.11	1.92	3.08	2.43	2.16	0.00	0.04	0.34	0.01	0.01	100.00
Group 1 Average	50.78	0.46	12.50	25.38	0.08	1.69	4.14	2.06	2.33	0.11	0.07	0.41	0.01	0.01	100.00

Table D12: Electron Microprobe Data for Dark Melt Group 2.

	SiO ₂	TiO ₂	Al ₂ O ₃	FeO	MnO	MgO	CaO	Na ₂ O	K ₂ O	P ₂ O ₅	NiO	SO ₃	Cl	F	Total
1 CCMK07A-13, 17.42um,toptobottomo	56.16	0.44	13.78	18.83	0.15	1.62	3.73	2.43	2.54	0.00	0.05	0.28	0.00	0.01	100.00
2 CCMK07A-13, 17.42um,toptobottomo	55.73	0.49	13.81	19.12	0.10	1.52	4.06	2.24	2.61	0.00	0.00	0.33	0.01	0.00	100.00
3 CCMK07A-13, 17.42um,toptobottomo	55.62	0.47	13.70	19.28	0.04	1.58	3.98	2.44	2.51	0.00	0.00	0.39	0.01	0.00	100.00
4 CCMK07A-13, 17.42um,toptobottomo	55.89	0.51	13.68	19.17	0.08	1.59	4.01	2.24	2.52	0.00	0.00	0.35	0.01	0.00	100.00
5 CCMK07A-13, 17.42um,toptobottomo	55.76	0.47	14.04	18.94	0.05	1.47	3.80	2.46	2.62	0.03	0.04	0.30	0.01	0.00	100.00
6 CCMK07A-13, 17.42um,toptobottomo	56.01	0.53	13.83	18.65	0.06	1.48	3.89	2.60	2.68	0.03	0.00	0.27	0.00	0.01	100.00
7 CCMK07A-13, 17.42um,toptobottomo	54.72	0.50	13.95	19.79	0.08	1.57	4.12	2.34	2.58	0.05	0.00	0.29	0.00	0.00	100.00
8 CCMK07A-13, 17.42um,toptobottomo	56.02	0.35	13.79	19.07	0.08	1.52	3.89	2.45	2.67	0.01	0.00	0.20	0.01	0.01	100.00
9 CCMK07A-13, 17.42um,toptobottomo	56.09	0.41	13.68	19.07	0.07	1.51	3.93	2.39	2.65	0.02	0.01	0.20	0.00	0.00	100.00
10 CCMK07A-13, 17.42um,toptobottomo	55.75	0.48	13.73	19.01	0.06	1.59	3.99	2.54	2.62	0.02	0.00	0.24	0.01	0.02	100.00
11 CCMK07A-13, 17.42um,toptobottomo	56.07	0.49	13.65	19.10	0.06	1.49	3.91	2.28	2.73	0.03	0.00	0.24	0.01	0.01	100.00
12 CCMK07A-13, 17.42um,toptobottomo	55.96	0.41	13.63	19.00	0.06	1.48	3.81	2.56	2.72	0.02	0.00	0.35	0.00	0.00	100.00
13 CCMK07A-13, 17.42um,toptobottomo	55.98	0.44	13.61	19.00	0.03	1.53	3.91	2.36	2.75	0.00	0.09	0.29	0.02	0.00	100.00
14 CCMK07A-13, 17.42um,toptobottomo	55.72	0.44	13.79	19.16	0.04	1.53	4.03	2.44	2.66	0.00	0.00	0.24	0.00	0.00	100.00
15 CCMK07A-13, 17.42um,toptobottomo	55.49	0.42	13.82	18.85	0.09	1.55	3.95	2.73	2.68	0.06	0.03	0.32	0.00	0.01	100.00
16 CCMK07A-13, 17.42um,toptobottomo	55.48	0.47	13.88	19.10	0.11	1.51	3.88	2.61	2.68	0.03	0.00	0.25	0.01	0.00	100.00
17 CCMK07A-13, 17.42um,toptobottomo	55.73	0.36	13.65	18.98	0.04	1.47	3.91	2.73	2.78	0.03	0.00	0.31	0.01	0.00	100.00
18 CCMK07A-13, 17.42um,toptobottomo	55.57	0.47	13.70	19.36	0.09	1.58	3.91	2.51	2.56	0.00	0.00	0.27	0.00	0.00	100.00
19 CCMK07A-13, 17.42um,toptobottomo	55.59	0.40	13.59	19.39	0.05	1.56	3.96	2.56	2.59	0.02	0.00	0.30	0.01	0.01	100.00
20 CCMK07A-13, 17.42um,toptobottomo	55.54	0.44	13.77	19.32	0.08	1.52	3.89	2.56	2.64	0.00	0.00	0.26	0.00	0.01	100.00
1 CCMK07A-14,11.40um,diagonalgrain	55.96	0.49	14.05	18.95	0.07	1.31	3.54	2.66	2.73	0.00	0.04	0.20	0.00	0.01	100.00
2 CCMK07A-14,11.40um,diagonalgrain	55.85	0.39	14.02	18.68	0.06	1.34	3.68	2.76	2.81	0.07	0.02	0.32	0.01	0.01	100.00
3 CCMK07A-14,11.40um,diagonalgrain	55.02	0.39	14.20	19.34	0.04	1.44	3.77	2.67	2.76	0.03	0.03	0.28	0.02	0.01	100.00
4 CCMK07A-14,11.40um,diagonalgrain	55.32	0.45	13.91	19.53	0.07	1.46	3.68	2.52	2.69	0.00	0.07	0.33	0.00	0.00	100.00
5 CCMK07A-14,11.40um,diagonalgrain	54.99	0.39	13.93	19.89	0.08	1.45	3.82	2.50	2.62	0.00	0.02	0.28	0.00	0.02	100.00
6 CCMK07A-14,11.40um,diagonalgrain	54.90	0.40	13.89	19.76	0.10	1.46	3.84	2.64	2.71	0.05	0.00	0.26	0.01	0.03	100.00
7 CCMK07A-14,11.40um,diagonalgrain	54.86	0.42	14.04	19.58	0.10	1.41	3.76	2.76	2.76	0.01	0.00	0.30	0.00	0.02	100.00
8 CCMK07A-14,11.40um,diagonalgrain	54.99	0.45	13.98	19.49	0.12	1.43	3.89	2.54	2.78	0.00	0.03	0.26	0.01	0.02	100.00
9 CCMK07A-14,11.40um,diagonalgrain	55.14	0.46	13.86	19.55	0.05	1.44	3.91	2.53	2.73	0.05	0.03	0.25	0.01	0.00	100.00
10 CCMK07A-14,11.40um,diagonalgrai	55.64	0.40	13.79	19.47	0.09	1.38	3.82	2.31	2.79	0.05	0.00	0.28	0.00	0.00	100.00
11 CCMK07A-14,11.40um,diagonalgrai	54.98	0.45	13.88	19.74	0.13	1.41	3.83	2.63	2.70	0.03	0.00	0.23	0.01	0.01	100.00
12 CCMK07A-14,11.40um,diagonalgrai	54.89	0.45	14.06	19.54	0.06	1.40	3.97	2.63	2.75	0.06	0.00	0.22	0.00	0.00	100.00
13 CCMK07A-14,11.40um,diagonalgrai	54.84	0.41	13.98	19.61	0.06	1.50	3.98	2.59	2.77	0.02	0.00	0.30	0.00	0.00	100.00
14 CCMK07A-14,11.40um,diagonalgrai	55.37	0.34	13.79	19.62	0.04	1.32	4.08	2.34	2.81	0.01	0.00	0.28	0.00	0.00	100.00
15 CCMK07A-14,11.40um,diagonalgrai	55.31	0.39	13.81	19.56	0.08	1.31	4.02	2.59	2.63	0.03	0.00	0.27	0.00	0.00	100.00
16 CCMK07A-14,11.40um,diagonalgrai	54.19	0.36	13.83	20.50	0.06	1.42	4.36	2.42	2.56	0.06	0.00	0.25	0.02	0.00	100.00
17 CCMK07A-14,11.40um,diagonalgrai	54.47	0.39	13.66	20.23	0.11	1.49	4.27	2.44	2.64	0.00	0.00	0.30	0.00	0.00	100.00
18 CCMK07A-14,11.40um,diagonalgrai	55.31	0.44	13.85	19.43	0.07	1.36	4.03	2.37	2.77	0.01	0.03	0.31	0.00	0.01	100.00
19 CCMK07A-14,11.40um,diagonalgrai	55.24	0.39	13.79	19.41	0.07	1.36	4.05	2.49	2.78	0.05	0.10	0.28	0.01	0.00	100.00
20 CCMK07A-14,11.40um,diagonalgrai	55.25	0.40	13.72	19.55	0.04	1.31	4.06	2.56	2.77	0.01	0.03	0.25	0.01	0.03	100.00

Table D12: Continued.

	SiO ₂	TiO ₂	Al ₂ O ₃	FeO	MnO	MgO	CaO	Na ₂ O	K ₂ O	P ₂ O ₅	NiO	SO ₃	Cl	F	Total
1 CCMK07A-16,13.17um,acrossgrain	55.20	0.41	13.87	19.91	0.00	1.43	3.63	2.60	2.58	0.04	0.01	0.30	0.01	0.01	100.00
2 CCMK07A-16,13.17um,acrossgrain	55.52	0.40	13.76	19.52	0.08	1.46	3.69	2.56	2.66	0.02	0.04	0.27	0.01	0.01	100.00
3 CCMK07A-16,13.17um,acrossgrain	55.54	0.36	13.95	19.52	0.08	1.40	3.57	2.61	2.78	0.04	0.00	0.23	0.00	0.00	100.00
4 CCMK07A-16,13.17um,acrossgrain	55.09	0.45	13.77	19.96	0.09	1.38	3.70	2.55	2.72	0.03	0.00	0.28	0.00	0.00	100.00
5 CCMK07A-16,13.17um,acrossgrain	55.07	0.39	13.76	20.11	0.04	1.45	3.65	2.51	2.77	0.00	0.00	0.25	0.00	0.03	100.00
6 CCMK07A-16,13.17um,acrossgrain	55.83	0.42	13.63	19.64	0.06	1.48	3.56	2.58	2.62	0.02	0.00	0.23	0.00	0.00	100.00
7 CCMK07A-16,13.17um,acrossgrain	55.83	0.36	13.77	19.45	0.08	1.50	3.66	2.36	2.75	0.03	0.00	0.26	0.01	0.00	100.00
8 CCMK07A-16,13.17um,acrossgrain	55.50	0.39	13.81	19.59	0.04	1.43	3.64	2.58	2.72	0.03	0.00	0.26	0.01	0.02	100.00
9 CCMK07A-16,13.17um,acrossgrain	55.65	0.45	13.75	19.58	0.05	1.38	3.66	2.60	2.70	0.00	0.00	0.22	0.00	0.00	100.00
10 CCMK07A-16,13.17um,acrossgrain	55.43	0.40	13.91	19.55	0.06	1.40	3.53	2.71	2.73	0.03	0.00	0.26	0.00	0.00	100.00
11 CCMK07A-16,13.17um,acrossgrain	55.66	0.44	13.82	19.56	0.05	1.39	3.68	2.60	2.63	0.02	0.00	0.23	0.01	0.00	100.00
12 CCMK07A-16,13.17um,acrossgrain	55.38	0.48	13.83	19.46	0.09	1.41	3.74	2.48	2.80	-0.01	0.09	0.27	0.00	0.00	100.00
13 CCMK07A-16,13.17um,acrossgrain	56.17	0.43	13.99	19.36	0.05	1.51	3.79	1.65	2.74	-0.01	0.04	0.30	0.00	0.00	100.00
14 CCMK07A-16,13.17um,acrossgrain	55.47	0.35	13.92	19.36	0.06	1.30	3.57	2.55	2.71	0.01	0.31	0.39	0.00	0.01	100.00
15 CCMK07A-16,13.17um,acrossgrain	55.90	0.47	13.82	18.97	0.07	1.38	3.81	2.49	2.77	0.05	0.03	0.23	0.01	0.00	100.00
16 CCMK07A-16,13.17um,acrossgrain	55.68	0.42	13.83	19.51	0.05	1.45	3.70	2.38	2.72	0.01	0.00	0.33	0.01	0.00	100.00
17 CCMK07A-16,13.17um,acrossgrain	55.25	0.43	13.71	19.62	0.09	1.45	3.77	2.63	2.75	0.02	0.02	0.26	0.00	0.00	100.00
18 CCMK07A-16,13.17um,acrossgrain	55.30	0.41	13.81	19.67	0.08	1.52	3.83	2.42	2.57	0.06	0.06	0.27	0.01	0.00	100.00
19 CCMK07A-16,13.17um,acrossgrain	55.61	0.40	13.87	19.53	0.06	1.38	3.84	2.47	2.52	0.05	-0.03	0.30	0.01	0.00	100.00
20 CCMK07A-16,13.17um,acrossgrain	55.55	0.36	13.94	19.89	0.08	1.44	3.83	2.11	2.41	0.05	0.03	0.31	0.00	0.01	100.00
1 CCMK07045-9,1.89um,thrudarkcloud	57.75	0.38	13.40	19.20	0.06	1.36	3.71	1.59	2.31	0.04	0.00	0.24	0.00	0.01	100.00
2 CCMK07045-9,1.89um,thrudarkcloud	58.70	0.41	13.32	19.49	0.12	1.41	3.72	0.72	1.81	0.00	0.06	0.25	0.00	0.00	100.00
3 CCMK07045-9,1.89um,thrudarkcloud	58.54	0.31	13.08	19.80	0.05	1.37	3.75	0.95	2.03	0.00	0.00	0.19	0.00	0.01	100.00
4 CCMK07045-9,1.89um,thrudarkcloud	58.75	0.38	13.06	19.59	0.03	1.33	3.69	0.86	1.97	0.01	0.05	0.30	0.00	0.00	100.00
5 CCMK07045-9,1.89um,thrudarkcloud	58.65	0.40	13.22	19.89	0.06	1.28	3.60	0.75	1.87	0.03	0.00	0.24	0.00	0.04	100.00
6 CCMK07045-9,1.89um,thrudarkcloud	59.16	0.41	13.27	19.80	0.07	1.33	3.59	0.52	1.62	0.00	0.00	0.21	0.01	0.02	100.00
7 CCMK07045-9,1.89um,thrudarkcloud	59.04	0.41	13.39	19.57	0.06	1.28	3.59	0.71	1.62	0.02	0.05	0.25	0.02	0.00	100.00
8 CCMK07045-9,1.89um,thrudarkcloud	59.53	0.45	13.59	19.16	0.08	1.23	3.37	0.66	1.71	0.05	0.00	0.21	0.00	0.00	100.00
9 CCMK07045-9,1.89um,thrudarkcloud	60.23	0.33	13.24	18.75	0.06	1.18	3.34	0.84	1.72	0.05	0.00	0.30	0.01	0.00	100.00
10 CCMK07045-9,1.89um,thrudarkcloud	59.63	0.43	13.50	19.08	0.01	1.27	3.48	0.71	1.65	0.05	0.00	0.23	0.00	0.00	100.00
11 CCMK07045-9,1.89um,thrudarkcloud	59.67	0.34	13.26	19.26	0.09	1.25	3.50	0.65	1.66	0.04	0.03	0.23	0.02	0.01	100.00
12 CCMK07045-9,1.89um,thrudarkcloud	57.42	0.40	12.89	20.64	0.05	1.43	3.82	0.94	2.10	0.07	0.04	0.15	0.03	0.00	100.00
13 CCMK07045-9,1.89um,thrudarkcloud	56.30	0.43	13.09	21.41	0.05	1.50	3.94	1.01	2.03	0.03	0.00	0.25	0.00	0.01	100.00
14 CCMK07045-9,1.89um,thrudarkcloud	56.03	0.47	13.31	21.49	0.08	1.56	3.96	0.91	1.97	0.00	0.00	0.33	0.00	0.00	100.00
15 CCMK07045-9,1.89um,thrudarkcloud	55.95	0.43	13.62	21.63	0.07	1.60	3.94	0.69	1.75	0.03	0.00	0.31	0.00	0.00	100.00
16 CCMK07045-9,1.89um,thrudarkcloud	55.23	0.43	13.60	21.81	0.11	1.45	4.07	0.85	2.06	0.05	0.06	0.27	0.00	0.00	100.00
17 CCMK07045-9,1.89um,thrudarkcloud	55.07	0.42	13.84	20.94	0.09	1.30	4.04	1.41	2.51	0.02	0.03	0.32	0.02	0.00	100.00
18 CCMK07045-9,1.89um,thrudarkcloud	55.11	0.39	13.73	20.56	0.08	1.40	4.15	1.67	2.60	0.05	0.02	0.24	0.01	0.00	100.00
19 CCMK07045-9,1.89um,thrudarkcloud	55.25	0.45	13.75	20.27	0.13	1.43	4.01	1.81	2.57	0.04	0.06	0.23	0.00	0.01	100.00
1 CCMK07082-10,6.71um,inbtwbubbles	54.89	0.31	12.32	20.63	0.07	1.18	4.67	2.15	2.78	0.17	0.43	0.39	0.00	0.01	100.00
3 CCMK07082-10,6.71um,inbtwbubbles	55.03	0.41	12.04	20.80	0.12	1.04	4.14	2.38	2.83	0.13	0.88	0.21	0.00	0.00	100.00
5 CCMK07082-10,6.71um,inbtwbubbles	54.75	0.34	11.88	21.81	0.07	1.28	3.46	2.66	2.81	0.10	0.54	0.30	0.00	0.00	100.00
7 CCMK07082-10,6.71um,inbtwbubbles	55.45	0.34	11.99	20.98	0.04	1.09	4.19	2.42	2.76	0.06	0.58	0.07	0.01	0.00	100.00
9 CCMK07082-10,6.71um,inbtwbubbles	54.85	0.30	11.97	21.32	0.10	1.05	3.94	2.54	2.70	0.13	0.93	0.15	0.02	0.01	100.00
11 CCMK07082-10,6.71um,inbtwbubble	54.76	0.35	12.02	20.63	0.08	1.00	5.04	2.15	2.58	0.26	0.63	0.52	0.00	0.00	100.00
13 CCMK07082-10,6.71um,inbtwbubble	53.68	0.29	12.25	22.13	0.05	0.97	4.41	2.19	2.47	0.25	0.77	0.51	0.00	0.04	100.00
19 CCMK07082-10,6.71um,inbtwbubble	54.45	0.36	12.51	20.83	0.09	0.80	4.34	2.39	2.60	0.43	0.53	0.64	0.01	0.02	100.00
Group 2 Average	55.88	0.41	13.57	19.73	0.07	1.40	3.86	2.15	2.53	0.04	0.08	0.28	0.00	0.01	100.00

Table D13: Electron Microprobe Data for meteorite standards, meteorite and hematite samples.

	Si	Ti	Al	Fe	Mn	Ca	P	Ni	Cu	Co	Cr	S	Total
Iron Meteorite:													
Canyon Diablo pt 1	0.00	0.00	0.00	93.00	0.00	0.04	0.09	6.13	0.00	0.79	0.00	0.01	100.00
Canyon Diablo pt 2	0.00	0.00	0.04	92.51	0.00	0.00	0.05	6.72	0.08	0.69	0.00	0.02	100.00
Canyon Diablo pt 3	0.01	0.00	0.05	92.66	0.00	0.00	0.09	6.50	0.03	0.71	0.01	0.00	100.00
Canyon Diablo pt 4	0.00	0.02	0.03	92.53	0.03	0.02	0.11	6.76	0.00	0.59	0.00	0.00	100.00
Canyon Diablo pt 5	0.00	0.02	0.02	92.65	0.00	0.00	0.10	6.58	0.01	0.69	0.00	0.01	100.00
Canyon Diablo pt 6	0.01	0.03	0.02	93.69	0.00	0.02	0.04	5.47	0.04	0.66	0.01	0.02	100.00
Canyon Diablo pt 7	0.01	0.01	0.00	92.45	0.00	0.01	0.11	6.84	0.00	0.57	0.00	0.03	100.00
CD average	0.00	0.01	0.02	92.78	0.00	0.01	0.08	6.43	0.02	0.67	0.00	0.01	100.00
Iron Meteorite:													
Nantan pt 1	0.01	0.00	0.11	92.41	0.00	0.01	0.07	6.73	0.01	0.68	0.02	0.00	100.00
Nantan pt 2	0.00	0.00	0.17	92.52	0.00	0.02	0.08	6.57	0.04	0.66	0.00	0.00	100.00
Nantan pt 3	0.00	0.00	0.04	92.11	0.01	0.03	0.08	7.11	0.02	0.64	0.01	0.00	100.00
Nantan pt 4	0.00	0.00	0.02	92.45	0.00	0.00	0.07	6.90	0.03	0.56	0.03	0.01	100.00
Nantan pt 5	0.09	0.00	0.12	97.63	0.02	0.08	0.07	1.78	0.00	0.21	0.00	0.03	100.00
Nantan pt 6	0.04	0.00	0.02	98.15	0.00	0.03	0.02	1.51	0.00	0.22	0.04	0.03	100.00
NA average	0.02	0.00	0.08	94.21	0.01	0.03	0.07	5.10	0.02	0.49	0.02	0.01	100.00
092 pt 5	0.01	0.00	0.00	93.84	0.00	0.01	0.03	5.56	0.00	0.59	0.00	0.00	100.00
092 pt 9	0.65	0.00	0.35	91.69	0.00	0.14	0.14	6.59	0.04	0.49	0.04	0.00	100.00
093 pt 6	0.09	0.02	0.10	90.75	0.00	0.17	0.85	7.35	0.05	0.58	0.01	0.04	100.00
093 pt 7	0.13	0.00	0.19	90.31	0.03	0.19	0.91	7.51	0.03	0.68	0.01	0.05	100.00
093 pt 8	0.01	0.01	0.00	91.75	0.00	0.00	0.15	7.59	0.00	0.47	0.00	0.02	100.00
iron shale average	0.18	0.01	0.13	91.67	0.01	0.10	0.42	6.92	0.02	0.56	0.01	0.02	100.00
CCMK07007 pt 1	1.28	0.00	9.82	88.56	0.03	0.17	0.11	0.00	0.00	0.11	0.00	0.08	100.00
CCMK07007 pt 2	0.31	0.00	0.57	98.63	0.00	0.21	0.04	0.00	0.10	0.18	0.00	0.00	100.00
CCMK07007 pt 5	0.46	0.01	0.28	99.07	0.03	0.07	0.00	0.00	0.00	0.12	0.01	0.01	100.00
CCMK07007 pt 6	0.12	0.09	0.44	99.15	0.00	0.07	0.03	0.00	0.11	0.09	0.01	0.00	100.00
CCMK07007 pt 7	1.05	0.02	0.40	98.21	0.01	0.20	0.02	0.05	0.00	0.08	0.00	0.00	100.00
CCMK07007 pt 8	2.19	0.02	0.64	96.86	0.05	0.14	0.00	0.00	0.01	0.10	0.02	0.03	100.00
CCMK07022 pt 1	0.57	0.01	0.57	98.35	0.17	0.08	0.07	0.00	0.04	0.20	0.00	0.02	100.00
CCMK07022 pt 2	0.41	0.01	5.84	93.50	0.02	0.02	0.03	0.00	0.00	0.27	0.00	0.02	100.00
CCMK07022 pt 3	0.00	0.03	0.04	99.64	0.00	0.03	0.01	0.08	0.10	0.06	0.04	0.00	100.00
CCMK07022 pt 4	0.01	0.00	0.11	99.87	0.00	0.02	0.02	0.00	0.00	0.10	0.00	0.01	100.00
CCMK07022 pt 5	0.02	0.00	0.22	99.88	0.01	0.00	0.00	0.00	0.00	0.14	0.00	0.00	100.00
CCMK07022 pt 6	0.11	0.04	1.60	98.18	0.00	0.03	0.01	0.01	0.00	0.01	0.00	0.04	100.00
CCMK07022 pt 8	0.00	0.00	0.07	99.90	0.00	0.00	0.00	0.00	0.01	0.08	0.00	0.01	100.00
CCMK07086 pt 1	1.30	0.06	0.93	97.28	0.00	0.21	0.02	0.01	0.10	0.13	0.00	0.00	100.00
CCMK07086 pt 2	2.30	0.00	0.29	97.04	0.05	0.30	0.00	0.00	0.00	0.10	0.00	0.04	100.00
CCMK07086 pt 5	3.20	0.06	3.25	92.82	0.24	0.36	0.02	0.00	0.02	-0.04	0.00	0.09	100.00
CCMK07086 pt 7	0.56	0.00	0.13	99.17	0.00	0.12	0.00	0.00	0.03	0.07	0.00	0.03	100.00
CCMK07086 pt 8	9.45	0.00	0.99	88.70	0.02	0.78	0.00	0.00	0.00	0.13	0.07	0.01	100.00
CCMK07086 pt 9	0.52	0.00	0.06	99.13	0.03	0.04	0.02	0.00	0.00	0.28	0.00	0.00	100.00
CCMK07086 pt 10	0.32	0.00	0.06	99.54	0.00	0.06	0.01	0.00	0.00	0.16	0.00	0.02	100.00
hematite average	1.21	0.02	1.32	97.17	0.03	0.15	0.02	0.01	0.03	0.12	0.01	0.02	100.00

Table D14: Electron Microprobe Data for metallic spherules.

	Si	Ti	Al	Fe	Mn	Ca	P	Cu	Ni	Co	Cr	S	Total	Width	Shape/Comment
CCMK07045 pt 002	0.03	0.03	0.08	70.05	0.00	0.00	0.03	0.06	28.06	1.68	0.00	0.01	100.00	10	TAIL
CCMK07045 pt 007	0.00	0.00	0.02	72.59	0.00	0.05	0.12	0.13	25.25	1.88	0.00	0.01	100.00	30	PARTIAL
CCMK07045 pt 008	0.02	0.03	0.02	74.37	0.00	0.05	0.01	0.05	23.65	1.80	0.01	0.01	100.00	10	WHOLE
CCMK07045 pt 011	0.03	0.00	0.09	50.95	0.02	0.03	0.03	0.17	46.43	2.28	0.01	0.00	100.00	10	TINY TAIL
CCMK07045 pt 012	0.04	0.01	0.07	64.87	0.00	0.09	0.16	0.04	32.76	2.00	0.00	0.00	100.00	10	
CCMK07045 pt 015	0.01	0.00	0.00	69.10	0.00	0.06	0.92	0.04	28.11	1.80	0.00	0.01	100.00	20	WHOLE
CCMK07045 pt 016	0.00	0.00	0.03	68.56	0.00	0.04	0.56	0.13	28.94	1.77	0.01	0.02	100.00	50	ALTERED WITHIN
CCMK07045 pt 022	0.00	0.00	0.09	60.38	0.00	0.06	0.15	0.12	37.13	2.04	0.01	0.05	100.00	20	
CCMK07045 pt 024	1.01	0.01	0.01	88.00	0.00	0.02	0.35	0.05	9.17	0.69	0.03	0.71	100.00	60	ALTERED WITHIN AND SHAPE
CCMK07045 pt 030	0.00	0.00	0.04	68.87	0.00	0.08	0.00	0.02	28.88	2.13	0.00	0.01	100.00	15	TINY TAIL
CCMK07045 pt 032	0.05	0.00	0.07	54.94	0.00	0.10	0.00	0.11	42.65	2.14	0.01	0.01	100.00	10	
CCMK07045 pt 035	0.11	0.02	0.24	54.33	0.02	0.07	0.00	0.09	42.80	2.34	0.00	0.00	100.00	10	
CCMK07045 pt 036	0.01	0.01	0.05	62.93	0.00	0.05	0.04	0.12	34.52	2.29	0.02	0.00	100.00	20	
CCMK07045 pt 037	0.00	0.00	0.03	64.65	0.00	0.02	0.02	0.08	33.30	1.92	0.03	0.00	100.00	20	TAIL
CCMK07045 pt 038	0.00	0.00	0.05	64.58	0.00	0.04	0.05	0.06	33.12	2.08	0.05	0.03	100.00	20	VERY TINY TAIL
CCMK07045 pt 039	0.01	0.00	0.06	61.69	0.00	0.05	0.01	0.07	35.97	2.15	0.00	0.02	100.00	20	ALTERATED AROUND RIM
CCMK07045 pt 041	0.02	0.01	0.04	68.54	0.00	0.04	0.11	0.11	29.33	1.80	0.00	0.00	100.00	30	TWO TINY TAILS
CCMK07045 pt 042	0.01	0.00	0.04	65.73	0.00	0.02	0.18	0.04	31.94	2.04	0.01	0.03	100.00	25	ALTERED SHAPE
CCMK07045 pt 043	0.01	0.01	0.01	56.10	0.00	0.05	0.01	0.03	40.99	2.77	0.00	0.05	100.00	15	ELONGATE
CCMK07045 pt 044	0.05	0.00	0.78	54.55	0.01	0.05	0.09	0.17	41.88	2.10	0.00	0.34	100.00	10	ALTERED SHAPE
CCMK07045 pt 046	0.05	0.03	0.15	59.86	0.00	0.12	0.00	0.10	36.64	2.66	0.00	0.40	100.00	10	
CCMK07045 pt 048	0.00	0.00	0.04	70.74	0.00	0.06	0.15	0.10	27.09	1.84	0.02	0.02	100.00	10	VERY ALTERED SHAPE
CCMK07045 pt 049	0.01	0.00	0.01	70.14	0.01	0.02	0.30	0.07	27.76	1.69	0.00	0.02	100.00	40	TINY TAIL, ALTERED SHAPE
CCMK07045 pt 050	0.01	0.04	0.06	64.81	0.00	0.06	0.01	0.12	32.93	1.93	0.00	0.05	100.00	15	ALTERED SHAPE
CCMK07045 pt 054	0.01	0.00	0.03	79.43	0.00	0.06	0.38	0.05	17.74	1.55	0.02	0.75	100.00	15	ALTERED SHAPE
CCMK07045 pt 055	0.02	0.00	0.04	62.81	0.00	0.07	0.04	0.00	34.96	2.14	0.00	0.00	100.00	15	ALTERED SHAPE
CCMK07045 pt 056	0.03	0.00	0.05	60.81	0.04	0.05	0.15	0.07	36.77	2.03	0.00	0.02	100.00	15	ALTERED SHAPE
CCMK07045 pt 057	0.01	0.00	0.03	77.23	0.00	0.03	0.29	0.05	20.87	1.51	0.00	0.06	100.00	30	
CCMK07045 pt 058	0.00	0.00	0.08	61.42	0.00	0.05	0.15	0.06	36.32	1.99	0.00	0.02	100.00	20	
CCMK07045 pt 060	0.02	0.00	0.02	66.10	0.00	0.07	0.32	0.14	31.20	2.16	0.04	0.00	100.00	15	
CCMK07045 pt 061	0.01	0.01	0.11	63.93	0.00	0.06	0.13	0.12	33.42	2.23	0.01	0.00	100.00	20	
CCMK07045 pt 062	0.00	0.00	0.02	68.58	0.02	0.00	0.35	0.06	29.16	1.81	0.00	0.03	100.00	40	TAIL
CCMK07045 pt 063	0.01	0.03	0.06	64.65	0.03	0.04	0.00	0.11	32.96	2.06	0.01	0.04	100.00	30	VERY ALTERED SHAPE
CCMK07045 pt 064	0.00	0.00	0.00	79.78	0.00	0.03	0.35	-0.02	18.38	1.50	0.01	0.02	100.00	20	
CCMK07045 pt 065	0.00	0.00	0.04	81.38	0.00	0.05	0.34	0.03	17.00	1.20	0.00	0.01	100.00	40	VERY ALTERED WITHIN
CCMK07045 pt 066	0.01	0.02	0.12	67.29	0.00	0.03	0.25	-0.02	30.63	1.66	0.00	0.02	100.00	100	BUBBLE?
CCMK07045 pt 067	0.01	0.00	0.03	63.17	0.01	0.03	0.44	0.17	33.94	2.17	0.01	0.03	100.00	30	
CCMK07045 pt 073	0.01	0.00	0.05	72.24	0.00	0.04	0.02	0.14	25.80	1.71	0.01	0.01	100.00	70	SLIGHT ELONGATION, VERY ALTERED WITHIN
CCMK07045 pt 075	0.01	0.03	0.02	66.05	0.00	0.06	0.21	0.13	31.33	2.17	0.01	0.02	100.00	25	TAIL
CCMK07045 pt 076	0.00	0.01	0.04	63.52	0.00	0.03	0.34	0.05	33.99	2.06	0.01	0.01	100.00	15	VERY ALTERED SHAPE
CCMK07045 pt 079	0.05	0.00	0.04	70.37	0.02	0.01	0.33	0.08	27.36	1.71	0.02	0.01	100.00	55	VERY ALTERED SHAPE, WITHIN
CCMK07045 pt 081	0.01	0.00	0.01	67.87	0.00	0.04	0.12	0.03	30.14	1.84	0.00	0.02	100.00	55	ALTERED WITH TAIL
CCMK07045 pt 082	0.00	0.00	0.01	64.55	0.00	0.03	0.29	0.05	32.96	2.17	0.00	0.02	100.00	20	ALTERED SHAPE
CCMK07045 pt 083	0.01	0.00	0.00	67.22	0.00	0.06	0.09	0.07	30.67	1.93	0.01	0.01	100.00	20	TINY TAIL
CCMK07045 pt 086	0.02	0.01	0.00	82.10	0.00	0.06	0.05	0.15	16.36	1.26	0.00	0.01	100.00	10	CORE
CCMK07045 pt 087	0.00	0.00	0.03	63.75	0.00	0.03	0.43	0.01	33.78	1.99	0.01	0.03	100.00	40	RIM
CCMK07045 pt 088	0.01	0.00	0.05	65.23	0.00	0.02	0.15	0.15	32.52	1.87	0.00	0.03	100.00	50	ELONGATE, ALTERED SHAPE, SLIGHT TAIL
CCMK07045 pt 089	0.02	0.02	0.00	84.10	0.00	0.00	0.04	0.03	14.69	1.19	0.00	0.00	100.00	30	ALTERATED AROUND RIM
CCMK07045 pt 091	0.02	0.00	0.06	48.81	0.00	0.03	0.02	0.13	49.01	1.91	0.00	0.02	100.00	20	ALTERED SHAPE
CCMK07045 pt 092	0.03	0.00	0.03	66.81	0.00	0.09	0.01	0.00	31.16	1.92	0.00	0.01	100.00	10	ELONGATE, ALTERED WITHIN
CCMK07045 pt 093	0.04	0.06	0.05	73.04	0.01	0.10	0.06	0.10	24.70	1.72	0.04	0.10	100.00	15	ALTERED SHAPE
CCMK07045 pt 094	0.00	0.04	0.15	62.05	0.05	0.01	0.08	0.21	35.24	2.12	0.06	0.00	100.00	35	ALTERED WITHIN AND SHAPE
CCMK07045 pt 098	0.03	0.04	0.10	59.66	0.00	0.04	0.00	0.17	37.76	2.23	0.00	0.04	100.00	20	TAIL, ALTERED WITHIN

Table D14: Continued.

	Si	Ti	Al	Fe	Mn	Ca	P	Cu	Ni	Co	Cr	S	Total	Width	Shape/Comment
CCMK07A pt 004	0.03	0.03	0.11	78.01	0.02	0.08	0.35	0.08	19.81	1.48	0.00	0.02	100.00	10	
CCMK07A pt 005	0.04	0.02	0.02	81.58	0.03	0.08	0.38	0.13	13.00	0.81	0.06	3.85	100.00	10	SLIGHT ELONGATION
CCMK07A pt 006	0.02	0.04	0.00	82.98	0.00	0.06	0.27	0.02	15.49	1.18	0.00	0.03	100.00	20	ALTERED AROUND RIM
CCMK07A pt 007	0.06	0.02	0.00	85.18	0.00	0.13	0.37	0.00	13.19	0.93	0.00	0.16	100.00	10	
CCMK07A pt 008	0.03	0.01	0.02	86.85	0.00	0.05	0.60	0.04	11.46	0.89	0.00	0.11	100.00	10	SLIGHTLY ALTERED WITHIN
CCMK07A pt 009	0.00	0.00	0.03	87.57	0.00	0.04	0.48	0.00	10.96	0.88	0.04	0.06	100.00	15	
CCMK07A pt 012	0.00	0.00	0.10	84.37	0.00	0.03	0.77	0.03	12.77	0.81	0.01	1.16	100.00	30	SLIGHTLY ALTERED WITHIN
CCMK07A pt 015	0.00	0.04	0.02	88.33	0.03	0.05	0.35	0.04	10.29	0.73	0.00	0.11	100.00	20	SLIGHTLY ALTERED WITHIN
CCMK07A pt 018	0.03	0.00	0.02	75.19	0.00	0.09	0.23	0.08	22.85	1.56	0.00	0.03	100.00	10	SLIGHTLY ALTERED WITHIN
CCMK07A pt 019	0.01	0.03	0.00	85.55	0.00	0.07	0.28	0.08	12.93	1.03	0.02	0.03	100.00	10	SLIGHTLY ALTERED WITHIN
CCMK07A pt 020	0.02	0.00	0.02	86.73	0.01	0.04	0.73	0.05	11.36	0.85	0.00	0.22	100.00	25	SLIGHTLY ALTERED WITHIN
CCMK07A pt 022	0.02	0.01	0.00	88.98	0.00	0.10	0.06	0.12	9.82	0.85	0.02	0.04	100.00	10	SLIGHTLY ALTERED WITHIN, SLIGHT ELONGATION
CCMK07A pt 023	0.02	0.02	0.02	84.29	0.00	0.05	0.50	0.03	13.93	1.15	0.00	0.02	100.00	20	SLIGHTLY ALTERED WITHIN
CCMK07A pt 024	0.02	0.00	0.01	85.24	0.03	0.07	0.07	0.08	13.54	0.93	0.01	0.01	100.00	20	SLIGHTLY ALTERED WITHIN, SLIGHT ELONGATION
CCMK07A pt 028	0.00	0.01	0.01	81.86	0.00	0.03	0.53	0.10	13.26	0.92	0.00	3.29	100.00	25	SLIGHTLY ALTERED WITHIN
CCMK07A pt 031	0.04	0.01	0.03	83.28	0.00	0.07	0.47	0.09	14.91	1.11	0.00	0.01	100.00	20	SLIGHTLY ALTERED WITHIN
CCMK07A pt 032	0.01	0.00	0.04	86.04	0.00	0.06	0.12	0.08	11.51	0.93	0.00	1.29	100.00	20	SLIGHTLY ALTERED WITHIN
CCMK07A pt 038	0.01	0.01	0.04	82.76	0.00	0.06	0.29	0.00	15.72	1.15	0.01	0.01	100.00	15	SLIGHTLY ALTERED WITHIN
CCMK07A pt 043	0.00	0.00	0.02	85.12	0.00	0.09	0.44	0.00	13.41	0.96	0.00	0.01	100.00	15	SLIGHTLY ALTERED WITHIN
CCMK07A pt 045	0.02	0.00	0.05	85.60	0.00	0.06	0.26	0.03	12.56	0.99	0.00	0.48	100.00	15	SLIGHTLY ALTERED WITHIN
CCMK07A pt 046	0.04	0.05	0.01	84.26	0.01	0.04	0.43	0.03	12.73	0.93	0.00	1.48	100.00	15	SLIGHTLY ALTERED WITHIN
CCMK07A pt 047	0.01	0.00	0.02	88.56	0.00	0.04	0.41	0.00	10.20	0.77	0.00	0.07	100.00	25	SLIGHTLY ALTERED WITHIN
CCMK07A pt 049	0.02	0.00	0.03	86.93	0.03	0.06	0.42	0.00	11.62	0.87	0.00	0.07	100.00	10	SLIGHTLY ALTERED WITHIN
CCMK07A pt 054	0.02	0.00	0.03	85.53	0.02	0.10	0.34	0.03	12.89	1.00	0.03	0.02	100.00	15	SLIGHTLY ALTERED WITHIN
CCMK07A pt 058	0.01	0.00	0.01	87.45	0.00	0.02	0.51	0.01	11.14	0.89	0.00	0.04	100.00	30	SLIGHTLY ALTERED WITHIN AND SHAPE
CCMK07A pt 059	0.00	0.00	0.04	77.96	0.00	0.04	0.06	0.06	20.37	1.47	0.01	0.03	100.00	15	SLIGHTLY ALTERED WITHIN
CCMK07A pt 060	0.02	0.00	0.03	79.38	0.00	0.04	0.38	0.00	18.17	1.17	0.00	0.87	100.00	20	SLIGHTLY ALTERED WITHIN
CCMK07A pt 061	0.02	0.00	0.00	87.10	0.00	0.06	0.31	0.04	11.59	0.91	0.03	0.00	100.00	25	SLIGHTLY ALTERED WITHIN
CCMK07A pt 063	0.03	0.00	0.09	88.55	0.00	0.09	0.34	0.02	10.06	0.83	0.02	0.01	100.00	10	SLIGHTLY ALTERED WITHIN
CCMK07A pt 066	0.00	0.00	0.01	87.99	0.00	0.05	0.45	0.00	10.53	0.98	0.02	0.04	100.00	35	SLIGHTLY ALTERED WITHIN
CCMK07A pt 067	0.00	0.01	0.02	85.87	0.00	0.02	0.51	0.12	12.64	0.87	0.00	0.00	100.00	25	ALTERED AROUND RIM
CCMK07A pt 068	0.01	0.03	0.03	86.70	0.00	0.05	0.30	0.04	11.93	0.93	0.00	0.02	100.00	20	SLIGHTLY ALTERED WITHIN
CCMK07A pt 069	0.02	0.00	0.01	86.06	0.00	0.06	0.38	0.00	12.47	1.01	0.01	0.02	100.00	15	SLIGHTLY ALTERED WITHIN
CCMK07A pt 070	0.04	0.04	0.01	82.46	0.00	0.06	0.45	0.09	15.81	1.04	0.00	0.02	100.00	10	SLIGHTLY ALTERED WITHIN
CCMK07A pt 072	0.02	0.00	0.20	87.30	0.00	0.02	0.58	0.07	10.92	0.84	0.02	0.04	100.00	30	ALTERED AROUND RIM AND WITHIN
CCMK07A pt 073	0.02	0.00	0.03	85.08	0.00	0.06	0.44	0.00	13.33	1.08	0.00	0.03	100.00	25	SLIGHTLY ALTERED WITHIN
CCMK07A pt 074	0.00	0.03	0.02	86.92	0.00	0.03	0.30	0.09	11.58	1.01	0.00	0.03	100.00	20	SLIGHTLY ALTERED WITHIN
CCMK07A pt 075	0.03	0.00	0.02	85.39	0.00	0.03	0.46	0.04	12.43	1.12	0.01	0.53	100.00	20	SLIGHTLY ALTERED WITHIN
CCMK07A pt 077	0.02	0.00	0.02	81.17	0.00	0.09	0.20	0.01	17.10	1.42	0.00	0.00	100.00	10	SLIGHTLY ALTERED WITHIN
CCMK07A pt 080	0.00	0.05	0.03	84.03	0.00	0.05	0.47	0.00	14.46	1.05	0.00	0.00	100.00	20	SLIGHTLY ALTERED WITHIN
CCMK07A pt 081	0.04	0.00	0.07	86.08	0.00	0.03	0.36	0.01	12.26	1.02	0.00	0.17	100.00	20	SLIGHTLY ALTERED WITHIN
CCMK07A pt 088	0.07	0.05	0.04	87.95	0.00	0.06	0.40	0.02	10.51	0.91	0.00	0.03	100.00	15	ALTERED SHAPE, SLIGHTLY ALTERED WITHIN
CCMK07A pt 089	0.02	0.02	0.03	84.26	0.00	0.07	0.39	0.08	12.68	0.88	0.02	1.61	100.00	25	ALTERED SHAPE, SLIGHTLY ALTERED WITHIN
CCMK07A pt 092	0.00	0.00	0.01	88.09	0.00	0.00	0.41	0.12	10.47	0.81	0.04	0.05	100.00	45	ALTERED WITHIN
CCMK07A pt 093	0.00	0.00	0.02	87.24	0.00	0.03	0.36	0.00	11.52	0.89	0.01	0.01	100.00	25	ALTERED SHAPE, SLIGHTLY ALTERED WITHIN
CCMK07A pt 096	0.01	0.02	0.01	87.51	-0.03	0.05	0.37	0.00	11.07	0.96	0.02	0.05	100.00	10	SLIGHTLY ALTERED WITHIN
CCMK07A pt 097	0.02	0.00	0.06	85.92	0.00	0.04	0.30	0.06	12.55	1.05	0.02	0.00	100.00	25	SLIGHTLY ALTERED WITHIN
CCMK07A pt 098	0.22	0.00	0.03	86.70	0.00	0.13	0.43	0.05	11.43	0.95	0.03	0.05	100.00	10	SLIGHTLY ALTERED WITHIN
CCMK07A pt 099	0.01	0.01	0.01	85.52	0.03	0.05	0.20	0.03	12.98	1.12	0.02	0.02	100.00	25	VERY ALTERED SHAPE, SLIGHTLY ALTERED WITHIN
CCMK07A pt 100	0.01	0.06	0.00	84.91	0.00	0.04	0.45	0.00	13.54	0.97	0.02	0.04	100.00	25	SLIGHTLY ALTERED WITHIN
CCMK07A pt 101	0.02	0.01	0.04	89.24	0.00	0.05	0.32	0.00	9.71	0.68	0.01	0.01	100.00	15	SLIGHTLY ALTERED WITHIN
CCMK07A pt 106	0.03	0.00	0.03	82.68	0.03	0.08	0.29	0.03	15.67	1.16	0.00	0.03	100.00	10	SLIGHTLY ALTERED WITHIN
CCMK07A pt 107	0.00	0.02	0.02	87.30	0.00	0.02	0.44	0.00	11.26	1.00	0.03	0.00	100.00	25	SLIGHTLY ALTERED WITHIN
CCMK07A pt 109	0.01	0.00	0.01	84.18	0.00	0.03	0.58	0.05	12.81	0.96	0.01	1.46	100.00	15	SLIGHTLY ALTERED WITHIN
CCMK07A pt 110	0.05	0.02	0.06	83.87	0.00	0.09	0.41	0.04	14.14	1.10	0.00	0.24	100.00	10	SLIGHTLY ALTERED WITHIN
spherule average	0.03	0.01	0.05	76.08	0.00	0.05	0.28	0.06	21.83	1.45	0.01	0.20	100.00		